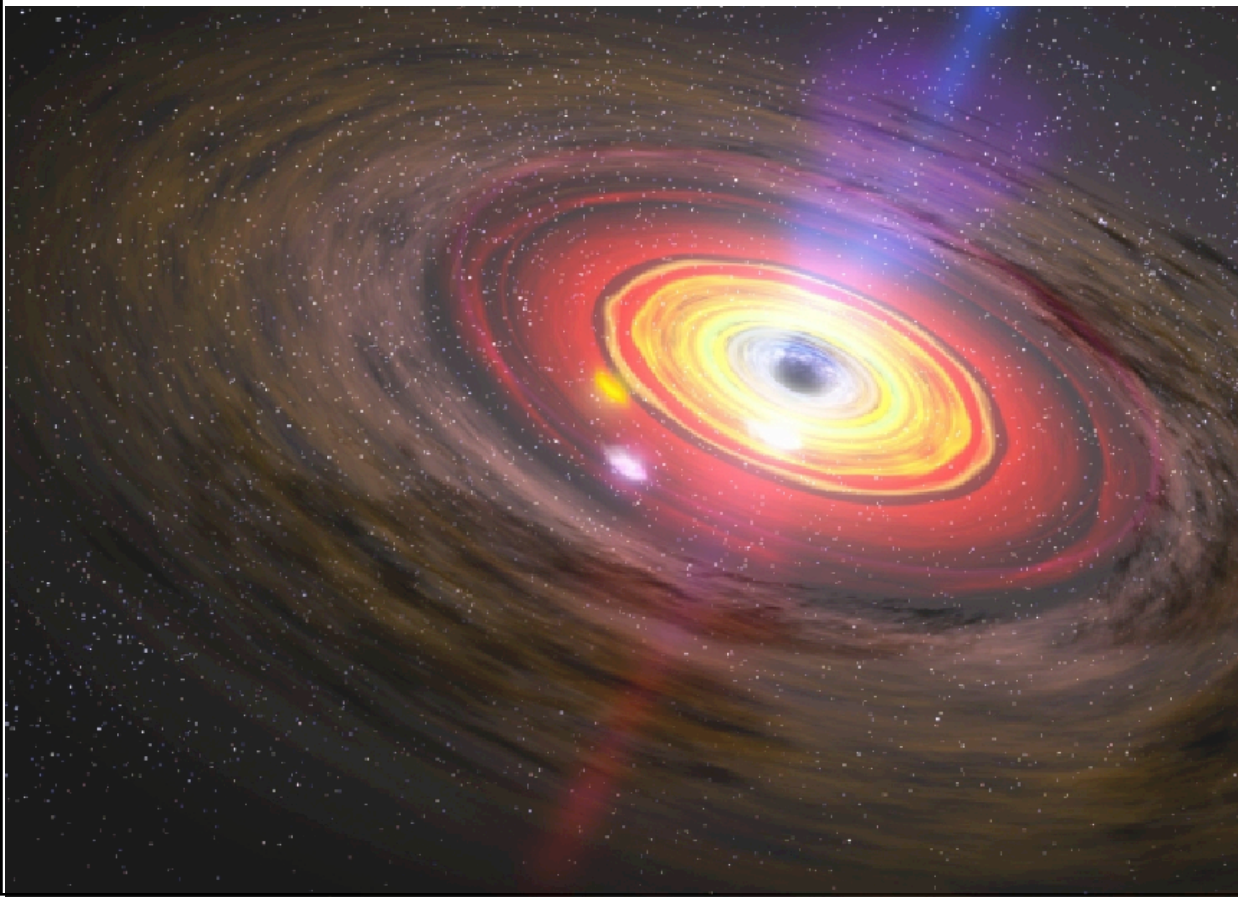


Dissertation

Co-Evolution Of Galaxies And Black Holes

vorgelegt von
Michaela Hirschmann



CO-EVOLUTION OF GALAXIES AND BLACK HOLES

Dissertation

PhD thesis

zur Erlangung der Doktorwürde

for the degree of Doctor of natural science

an der Fakultät für Physik

at the Faculty for Physics

der Ludwig-Maximilians-Universität (LMU), München

of the Ludwig-Maximilians-University (LMU) of Munich

vorgelegt von

presented by

Dipl.-Phys. Michaela Hirschmann

aus Nürnberg, Deutschland

from Nürnberg, Germany

München, 12. Mai 2011

LUDWIG MAXIMILIANS UNIVERSITY OF MUNICH



Erster Gutachter: Prof. Dr. Andreas Burkert (USM, LMU)
First advisor

Zweiter Gutachter: Prof. Dr. Joseph Mohr (USM, LMU)
Second advisor

Tag der mündlichen Prüfung: 17.6.2011
Day of oral exam

"Zwei Dinge erfüllen das Gemüt mit immer neuer zunehmender Bewunderung und Ehrfurcht, je öfter und anhaltender sich das Nachdenken damit beschäftigt: Der bestirnte Himmel über mir und das moralische Prinzip in mir. "

Immanuel Kant, deutscher Philosoph, 1724-1804

Zusammenfassung

Beobachtungen zeigen, dass die Massen schwarzer Löcher und die Eigenschaften ihrer Heimatgalaxien (“Hostgalaxie”) deutlich korreliert sind, was als Nachweis für eine gemeinsame Entwicklung zwischen Galaxien und ihren schwarzen Löchern angesehen werden kann. Dies impliziert, dass schwarze Löcher zum einen das Wachstum der Galaxien regulieren und zum anderen Galaxien die Entwicklung der schwarzen Löcher selbst beeinflussen. Ein umfassendes Verständnis dafür fehlt allerdings bis heute. Daher untersuche ich in dieser Arbeit verschiedene Aspekte, wie sich Galaxien und schwarze Löcher entwickeln, z.B. die Korrelationen zwischen schwarzen Löchern und Galaxien bei hohen Rotverschiebungen und das antihierarchische Wachstum von schwarzen Löchern. Um die Entwicklung von Galaxien und das damit zusammenhängende Wachstum von schwarzen Löchern zu modellieren und insbesondere, um eine grosse Anzahl von Galaxien mit schwarzen Löchern zu generieren, sind analytische oder semianalytische Modelle (SAMs) die am besten geeigneten Methoden.

Im ersten Teil meiner Arbeit wird gezeigt wie Galaxien- und Schwarzloch-Wachstum allein durch Verschmelzungsprozesse die Korrelation zwischen schwarzen Löchern und Galaxien bei hohen Rotverschiebungen und die intrinsische Streuung in der Masse des schwarzen Lochs beeinflussen. Im einfachen Fall von zufälligem Verschmelzen von schwarzen Löchern und Galaxien nimmt die Streuung in der Schwarzlochmasse bei gegebener Galaxienmasse mit zunehmender Anzahl von Verschmelzungsprozessen, Zeit und Masse des schwarzen Loches ab, wie es von dem Zentralen Grenzwertsatz in der Statistik vorhergesagt wird. Generell kann die Streuung durch $\sigma_{\text{merg}}(m) \approx \sigma_{\text{ini}} \times (m + 1)^{-a/2}$ mit $0 < a < 1$ abgeschätzt werden. Kosmologisches Verschmelzen basierend auf Verschmelzungsbäumen dunkler Materie von kosmologischen N-body Simulationen zeigt eine ähnliche Abnahme der Streuung mit $a = 0.3$ für $m \approx 50$. Das herausragende Fazit dieses Kapitels ist, dass die Ergebnisse, unter der Annahme einer heutigen Streuung von 0.3 dex in der Masse des schwarzen Loches, eine Streuung von 0.6 dex bei einer Rotverschiebung von $z = 3$ implizieren. Dies stellt damit ein mögliches Szenario dar, in dem schwarze Löcher bei hohen Rotverschiebungen, die vornehmlich oberhalb bzw. unterhalb der heutigen Korrelation zwischen schwarzen Löchern und Galaxienmassen liegen, die Folge einer grösseren Streuung bei hohen Rotverschiebungen sein könnten. In anderen Worten, “übermassive” bzw. “untermassive” schwarze Löcher bei hohen Rotverschiebungen könnten lediglich durch statistische Verschmelzungsprozesse erklärt werden, ohne dass das Wachstum von schwarzen Löchern und Galaxien durch gas-physikalische Prozesse verknüpft sein muss.

Trotz der Wichtigkeit von Verschmelzungsereignissen repräsentiert jedoch die Akkretion von Gas auf schwarze Löcher einen bedeutenden Beitrag zum Gesamtwachstum von schwarzen Löchern. Dies ist insbesondere relevant, um das rätselhafte, beobachtete antihierarchische Verhalten im Wachstum von schwarzen Löchern verstehen zu können, was das Thema des zweiten Teils meiner Arbeit darstellt. Antihierarchisches Wachstum von schwarzen Löchern bedeutet, dass leuchtkräftige, aktive galaktische Kerne (AGN) bereits sehr früh im Universum vorhanden sind, wohingegen weniger leuchtkräftige

AGN vornehmlich zu späteren Zeiten auftreten. Verknüpft man die Leuchtkraft einer aktiven Galaxie mit der Schwarzschild-Masse würde dies im Konflikt zu momentan favorisierten, hierarchischen Strukturmodellen stehen, in denen sich zuerst kleinskalige Strukturen bilden, welche sich mit fortschreitender Zeit zu immer Grösseren akkumulieren. Aufgrund der Komplexität der gas-physikalischen Prozesse verwende ich für diese Untersuchung semianalytische Modelle (SAMs), welche eine Näherung für die wichtigsten Prozesse in Galaxienentstehung und für das Wachstum schwarzer Löcher beinhalten. Die SAMs basieren auf einer der momentan grössten numerischen Simulationen von dunkler Materie, der Millennium-Simulation (Boxlänge: 500 Mpc, Teilchenzahl: 10^{10}). Dabei scheinen Akkretion auf schwarze Löcher aufgrund von Scheibeninstabilitäten, eine “sub-Eddington” Grenze für Gasakkretion, welche von Masse und Rotverschiebung abhängt, und massive, anfängliche schwarze Löcher wichtige “Schlüssel”-Prozesse darzustellen um den antihierarchischen Trend erklären zu können. Darüberhinaus, kann eine rotverschiebungsabhängige Staubverschleierung zusätzlich als wichtiges Puzzleteil für das Verständnis des antihierarchischen Verhaltens angesehen werden. Das “best-fit” Modell dieser Arbeit, welches die oben erwähnten Prozesse beinhaltet, zeichnet sich dadurch aus, dass es die beobachtete, heutige Schwarzschild-Massenfunktion und die heutige Galaxien-Halomassen Relation reproduzieren kann genauso wie es die bolometrische AGN Leuchtkraftfunktion und diejenige im harten Röntgenbereich korrekt vorherzusagen vermag.

Allerdings besteht ein entscheidender Nachteil von SAMs in einem höheren Grad an analytischen Näherungen (grosser Parameterraum) als in hydrodynamischen Simulationen. Im letzten Teil meiner Arbeit vergleiche ich daher die kosmische Entwicklung der baryonischen Komponente in Galaxien und deren Unterteilung in eine stellare Komponente, in heisses und in kaltes Gas in 48 kosmologischen “zoom” Simulationen mit bislang unerreichter Auflösung und in SAMs, die auf derselben Verschmelzungshistorie von dunkler Materie basieren. Die Simulationen beinhalten Kühlen durch He & H, Photoionization, Sternentstehung und energetische Supernova Rückkopplung. Beinhalten SAMs dieselben physikalischen Prozesse wie die Simulationen, reproduzieren sie den baryonischen Anteil in Halos besser als 20% verglichen mit Simulationen. Die bemerkenswertesten Unterschiede zwischen den beiden Modellen sind allerdings die folgenden: Simulationen haben eine wesentlich grössere Sternentstehungseffizienz bei hohen Rotverschiebungen als SAMs. Ausserdem dominiert in SAMs “insitu” Sternentstehung bei allen Rotverschiebungen, wohingegen in Simulationen die Akkretion von Sternen der dominierende Prozess bei niedrigeren Rotverschiebungen wird. Zuletzt überschätzen die SAMs den Anteil von “heisser” relativ zu “kalter” Akkretion verglichen mit Simulationen. Der Grund für diese Diskrepanzen besteht in vereinfachten und/oder fehlenden physikalischen Prozessen in SAMs. Ein wichtiger, zukünftiger Aspekt könnte demnach darin bestehen, SAMs zu verbessern und auszuweiten, motiviert durch kosmologische Simulationen, insbesondere um die Auswirkung auf die Entwicklung der AGN Galaxien zu untersuchen.

Summary

Observationally, there exist strong correlations between black hole masses and properties of the host galaxies, which may be seen as an evidence for a co-evolution between galaxies and their residing black holes. This implies that black holes are responsible for regulating the growth of galaxies and vice versa. However, a full understanding of self-regulated black hole growth and how it is exactly connected to spheroid formation of the host galaxy is still missing. In this thesis I focus on different aspects of how galaxies and black holes are co-evolving, such as the black hole scaling relations at high redshifts and the origin of the anti-hierarchical black hole growth. In order to model galaxy formation and the connected black hole growth and in particular to facilitate the construction of large, statistical samples of galaxies with black holes, a highly successful approach is provided by 'analytic' and 'semi-analytic' tools.

In the first part of my thesis, it is demonstrated how merger-driven growth affects the correlations between black hole mass and host bulge mass and the evolution of the intrinsic scatter in black hole mass. In the simple case of random merging of galaxies and black holes, it is found that the scatter in black hole mass σ decreases with increasing merging number m , time and black hole mass as predicted by the Central-limit-theorem. Generally, the scatter can be approximated by $\sigma_{\text{merg}}(m) \approx \sigma_{\text{ini}} \times (m + 1)^{-a/2}$ with $0 < a < 1$. Cosmological merging based on halo merger trees of cosmological N-body simulations reveal a similar decrease of the scatter with $a = 0.3$ for $m \approx 50$. The striking result of this work is that assuming a present-day scatter of 0.3 dex in black hole mass, the analysis implies a scatter of 0.6 dex at $z = 3$ and thus, a possible scenario, in which over- and under-massive black holes at high redshift are the consequence *only* of a larger scatter in black hole mass at high redshift. This way, an explanation for observed over- and under-massive black holes in scaling relations at high redshift might be given *solely by 'statistical' merging* without considering a connected growth of black holes and galaxies by gas-physical processes.

However, despite of the importance of the merger events, gas accretion onto black holes represents a significant contribution to the over-all mass growth of black holes. This will be particularly relevant for understanding the puzzle of the observed downsizing trend in black hole growth, which is the topic of the second part of my thesis. I use a more complex modeling tool, such as a semi-analytic model (SAM). Downsizing or anti-hierarchical black hole growth means that luminous active galactic nuclei (AGN) are observationally found to be already in place very early in the Universe, whereas moderately luminous AGN predominantly occur at later times. Relating the luminosity directly to the black hole mass, this would be in contrast to the currently favored hierarchical clustering scenarios, where first small structures (galaxies) are assumed to form growing into larger ones with evolving time. Applying the semi-analytic model to one of the currently largest dark matter simulations, the Millennium-simulation (500 Mpc box-length and 10^{10} particles), I find that an accretion channel onto the black hole due to disk instabilities, a sub-Eddington limit, which is dependent on mass and redshift, as well as a heavy black hole seeding scenario may represent important key

mechanisms for explaining the anti-hierarchical trend. Moreover, a redshift dependent dust obscuration may additionally be seen as a further, fundamental “puzzle piece” in understanding the observed downsizing. The great success of the best-fit SAM, including the outlined ingredients, can be demonstrated by a good reproduction of the observed present-day black hole mass function and the present-day galaxy-halo mass relation as well as the bolometric and hard X-ray luminosity function within a large redshift range $0 < z < 5$.

The primary disadvantage of semi-analytic modeling consists in a greater degree of approximation (parameter space) than in hydrodynamical simulations. Therefore, in the last part of my thesis, I perform a direct comparison of the cosmic evolution of the baryon content in galaxies and its division into stars, cold and hot gas in a large set of about 48 cosmological zoom simulations with unprecedented resolution for a sample this large and in SAMs based on the same dark matter merging history. The simulations include H&He cooling, Photo-ionization, star formation and thermal SN feedback. I find that SAMs that include the same physical processes as the simulations reproduce the total baryon fraction in halos and the fraction of cold gas plus stars in the central galaxy to better than 20%. However, the most striking discrepancies of this study are the following: simulations have a much larger star formation efficiency at high redshifts than SAMs. In SAMs, in-situ star formation is always the dominating process, whereas in simulations, accretion of stars becomes more important than in-situ star formation at low redshift. Finally, SAMs overestimate the fraction of “hot” relative to “cold” accretion compared to simulations. The reason for these discrepancies may consist in simplified or missing physical processes in SAMs, which should be refined or included. Therefore, for future models it might be an important aspect to extend and improve SAMs - motivated by detailed high-resolution cosmological simulations, in particular to focus on the effect on the evolution of the AGN population.

Meinen Eltern

Contents

1	Motivation for this thesis	1
2	A framework for galaxy formation and black hole growth	3
2.1	A brief history of extragalactic astrophysics	3
2.1.1	Towards modern cosmology	4
2.2	Formation and evolution of large-scale structures in the Universe	5
2.2.1	The homogeneous Universe	6
2.2.2	The mass content of the Universe	9
2.2.3	The linear growth of perturbation and spherical collapse model .	9
2.2.4	Modeling dark matter	11
2.3	Current picture of the joint evolution of galaxies and black holes	14
2.3.1	Evolution of baryonic matter	14
2.3.2	Observational evidence for supermassive black holes	15
2.3.3	Current picture of co-evolving galaxies and black holes	17
2.3.4	Modeling galaxy formation and black hole growth	21
3	The intrinsic scatter in black hole mass scaling relations	25
3.1	Black hole mass relations in the present-day universe	26
3.2	Black hole mass relations at higher redshifts	27
3.3	Models for random merging	30
3.3.1	Initial conditions	30
3.3.2	Depletion scenario	33
3.3.3	Replenishment scenario	41
3.4	Comparison to merging in Λ CDM-Simulations	47
3.4.1	Simulation setup	47
3.4.2	Merger tree algorithm	47
3.4.3	Evolution of the relation between black hole and galaxy mass .	48
3.4.4	Quantifying the scatter in the black hole mass relation	53
3.4.5	Evolution of the black hole mass function	53
3.5	Discussion and conclusions	56

4	Origin of the anti-hierarchical growth of black holes	61
4.1	Motivation and observational evidence for downsizing	62
4.2	Previous studies	64
4.3	The semi-analytic model	66
4.3.1	Merging history from the Millennium simulation	66
4.3.2	Galaxy formation	66
4.3.3	Models for black hole growth in the quasar phase	70
4.4	Properties of nearby galaxies and black holes	77
4.4.1	Black hole mass function	77
4.4.2	Black hole-bulge mass relation	79
4.4.3	Galaxy-dark matter halo mass relation	80
4.5	Galaxy and black hole properties at higher redshift	81
4.5.1	Black hole mass function	81
4.5.2	Galaxy-dark matter halo relation	83
4.6	Number density evolution of AGN	84
4.7	The AGN luminosity function	90
4.7.1	Bolometric luminosities	90
4.7.2	Hard X-ray luminosities	92
4.8	Eddington-ratio distributions	95
4.9	Luminosity-black hole mass-relation	97
4.10	Discussion and conclusion	99
5	Galaxy formation in semi-analytic models and zoom simulations	105
5.1	Different approaches for modeling galaxy formation	106
5.2	Previous comparison studies	109
5.3	The simulation and merger tree construction	111
5.3.1	Simulation setup	111
5.3.2	Merger trees	113
5.4	The semi-analytic model	114
5.5	Redshift evolution of galaxy properties	115
5.5.1	Baryon fraction	115
5.5.2	Cold gas and stars	117
5.5.3	Hot halo gas	127
5.6	Comparison to observations	131
5.7	Discussion and conclusions	135
6	Conclusion and Outlook	141
6.1	Summary	141
6.2	Next steps	146
A	Appendix	151
A.1	Dark matter component	151
A.2	Baryonic components	151

Curriculum Vitae	187
List of publications	189
Danksagung	191
Erklärung	193

Motivation for this thesis

It is now well established that the dark energy dominated dark matter paradigm (Λ CDM) provides a successful basis for understanding and simulating galaxy formation. In this picture, it is now widely believed that most spheroid-dominated galaxies host a supermassive black hole in their center at the present time. In addition, there exist strong correlations between black hole masses and properties of the host galaxies as the luminosity, mass and velocity dispersion of the stellar spheroidal component (e.g. Häring & Rix, 2004). These correlations may be seen as an evidence for a co-evolution between galaxies and their residing black holes implying that black holes are responsible for regulating the growth of galaxies and vice versa. However, a full understanding of self-regulated black hole growth and how it is exactly connected to spheroid formation of the host galaxy is still missing. Therefore, in the current picture of galaxy formation and black hole growth, there exist a number of interesting, unanswered questions, as e.g.:

- Which trigger mechanisms are responsible for bringing gas into the host galaxy for black hole accretion?
- How strong is the influence of black hole feedback on the host galaxy?
- How do black holes accrete their gas, i.e. how is cold gas transported to the accretion disk?
- How do seed black holes form and how massive are they?
- What is the origin of the observed black hole mass scaling relations?
- Are black hole mass scaling relations also valid at higher redshifts or do they evolve with cosmic time?
- What is the origin of the observed anti-hierarchical black hole growth?

Numerical, hydrodynamical simulations of isolated galaxies or galaxy mergers modeling detailed gas dynamical accretion processes in the vicinity of a black hole are necessary in order to get a deeper understanding for exact growth mechanisms and the connected effect of feedback on the host galaxy. However, due to a lack in current computational power for coevally resolving a large range of scales, in particular in *cosmological simulations*, a further highly successful approach is provided by '*semi-analytic*' *galaxy formation modeling*, which is computationally inexpensive compared to hydrodynamical simulations. This facilitates the construction of samples of galaxies orders of magnitude larger than possible with N-body simulations. This is especially important for studying statistical properties of galaxies and black holes. However, a major disadvantage of semi-analytical methods is the large degree of approximation due the large parameter space, whereas hydrodynamical simulations represent a more precise approach as gas-dynamical equations are explicitly solved. Therefore, it is of particular importance to compare directly galaxy formation in semi-analytic models and in cosmological 'zoom-simulations' based on the same dark matter evolution, in order to understand their differences, and in particular, in order to reveal limitations of both approaches.

In this PhD thesis, I mainly focused on two statistical problems of the above outlined puzzling questions, namely the black hole mass scaling relations at higher redshifts as well as the anti-hierarchical growth of black holes. In order to be able to generate large samples of galaxies providing sufficiently large statistics, I worked with analytical and semi-analytical methods based on the merging histories of cosmological dark matter simulations. The outline of my thesis is the following: In Chapter 2, I will give a brief theoretical framework of cosmology, structure formation and the joint evolution of galaxies and black holes, which is the basis for further understanding of the following investigations in this work. In Chapter 3, I will concentrate on the black hole mass scaling relations at higher redshift, in particular on explaining the observed over- and under-massive black holes at high redshifts by studying the intrinsic scatter in black hole mass scaling relations using analytical methods. Chapter 4 deals with the origin of the observed anti-hierarchical (or downsizing) trend in black hole growth, which is at first glance in disagreement with currently favored hierarchical structure formation models. To understand, which physical processes might be causing the observed downsizing trend, I use semi-analytic models. However, in order to reveal the limitations of semi-analytics, in Chapter 5 a detailed comparison of the evolution of the baryonic component in semi-analytic models and in cosmological zoom simulations is performed based on the same dark matter merging history. Finally in Chapter 6, the most striking results of this thesis will be briefly summarized and some future prospects will be given, which might be important steps towards a better understanding of the complex but exciting co-evolution of galaxies and the black holes residing at their centers over cosmic times.

A framework for galaxy formation and black hole growth

2.1 A brief history of extragalactic astrophysics

Within living memory, the extraordinary beauty of the night sky was always of fascinating and impressing nature for human beings and had historically a strong impact on culture as well as on religious beliefs. From the ancient Greek term *'κυκλος γαλακτικός'* the name 'galaxy' (= Milky Way) is derived for its appearance in the sky. This originates from Greek mythology, where Zeus places his son born by a mortal woman, the infant Heracles, on Hera's breast while she is asleep so that the baby will drink her divine milk and will thus become immortal. But Hera wakes up while breastfeeding and realizes an unknown baby: she pushes the baby away and a jet of milk sprays the night sky, producing the faint band of light known as the Milky Way. With a more academic attempt, the Greek philosopher Democritus (450-370 BC) already proposed that the Milky Way might consist of distant stars, what was finally proven by Galileo Galilei about 2000 years later (1610 AD). The earliest recorded observation for a distinction of stars of our Galaxy to other nebulae is made in the 10th century by the Persian astronomer, Abd al-Rahman al-Sufi (known in the West as Azophi), describing the Andromeda Galaxy as a "small cloud". The earliest cosmologies of the modern era were of very speculative nature, as e.g. the 'island' universe model of Rene Descartes (1636 AD) or the 'New Hypothesis of the Universe' of Thomas Wright (1750 AD), in which the sun was one of many stars which orbit about the 'Divine Center' of the star system. At the end of the eighteenth century, William Herschel was the first astronomer, who defined the distribution of stars in the Universe in some detail on basis of careful consideration. By the end of the nineteenth century, a large amount of astronomical objects was discovered that differ from stars as they were fuzzy and not point-like. These objects were collectively referred to as 'nebulae'. E.g. Charles Messier (1784 AD) was among the first who have catalogued bright nebulae. However, for many years after their discovery, the nature of these nebulae was still unclear. There

were two different explanations: On the one hand, nebulae were assumed to be objects within our Milky Way, on the other hand nebulae were thought to be extragalactic objects - individual 'island universes' like the Milky Way itself. The controversy remained unsolved until 1925, when Edwin Hubble used distances estimated from Cepheid variables to demonstrate conclusively that some of the nebulae are indeed *extragalactic*, individual galaxies comparable to our Milky Way in size and luminosity. Hubble's discovery was the *beginning of the extragalactic astronomy*. During the 1930s, high-quality photographic images allowed to classify galaxies according to their different morphological types (Ellipticals, Spirals, Irregulars).

2.1.1 Towards modern cosmology

Only four years after the discovery that the 'nebulae' are really extragalactic objects, Hubble made the second main discovery: he demonstrated that our Universe is expanding (the velocities of galaxies are linearly related to their distances (Hubble, 1929; Hubble & Humason, 1931). This revolutionized the picture of our Universe profoundly. Some years earlier, the construction of mathematical models had started to explain the large-scale evolution of the Universe in a self-consistent way, mainly based on the general relativity of Albert Einstein and a few basic assumptions (cosmological principles). According to solutions of the field equations, an expanding or contracting Universe would be the natural consequence. Alexander Friedmann (1922) and George Lemaitre (1927, Lemaître, 1927) found independently the same solution for an expanding or static Universe. In the late 1940s George Gamow suggested that the Universe must have been denser and perhaps also hotter at earlier times, as the Universe is expanding leading to the Hot Big Bang model. He also realized that, as a consequence of a hotter Universe at early times, the residual heat should still be visible in the present-day Universe as a background of thermal radiation with a few degrees of kelvin - the first prediction for the cosmic microwave background. Therefore, the 1965 discovery of the cosmic microwave background by Penzias & Wilson (1965) and Dicke et al. (1965) was a great success for the Hot Big Bang model and firmly established it as the standard model of cosmology. They found the cosmic microwave background to be isotropic and to have a temperature of $2.7K$, exactly in the range expected in the Hot Big Bang model. However, due to several shortcomings of the Hot Big Bang theory, in 1981, Alan Guth (Guth, 1981) proposed that the Universe might have experienced an early phase of exponential expansion ('inflation') driven by the vacuum energy of a quantum field. This original model was later-on revised by Linde (1982) and by Albrecht & Steinhardt (1982). In this scenario, different parts of the Universe could have been in causal contact before inflation started, important for the principle of isotropy and homogeneity. Another basic prediction of inflation is that the present-day Universe should appear to have a flat geometry. Furthermore, in the 1980s, it was realized that quantum fluctuations of a scalar field (inflaton) can generate density perturbations close to the ones predicted by Harrison-Zel'dovich, which was found to be the only

possible scaling set-up in the Big Bang theory being consistent with galaxy formation at early times. (Hawking, 1982; Guth & Pi, 1982; Bardeen et al., 1983).

In the meanwhile, a large amount of further conclusive evidences have been accumulated that the visible matter is only a small fraction and that the majority of the mass in the Universe consists of a still unknown dark matter component. The first hint can be traced back to 1933, when Zwicky studied the velocities of galaxies in the Coma cluster and concluded that the total mass required for a cluster to be stable is about 400 times larger than the luminous mass in stars. However, it took more than 40 years that the existence of dark matter was generally accepted. E.g. Ostriker et al. (1974) and Einasto et al. (1974) claimed that massive halos around our Milky Way are required in order to explain the motion of satellite galaxies. This hypothesis was confirmed by measurements of spiral galaxy rotation curves (Roberts & Rots, 1973; Rubin et al., 1978). Dark matter particles have been discussed to be neutrinos (electron neutrino in the 1960s and 70s, e.g. Reines et al., 1980). However, in 1984, White (1984) showed that simulations assuming a neutrino-dominated Universe (hot dark matter) result in a stronger clustering of galaxies than is observed. Therefore, alternative models suggest that e.g. dark matter might be a kind of weakly interacting massive particle (WIMP) referred to as cold dark matter (Peebles, 1982; Blumenthal et al., 1982). Cold dark matter results in the 'bottom-up' scenario, originally proposed by Peebles, 1965, which are nowadays favored over the top-down scenario (= hot dark matter). This means that smaller structures collapse first and are later assembled in larger collapsing structures. Dark matter particles can decouple from radiation at earlier times than baryonic matter so that the perturbation in density can also start to grow at earlier times. After baryons decouple from radiation they fall into the potential wells of dark matter (Davis et al., 1985). However, in the early 90s measurements of galaxy clustering showed that the CDM model predicts less clustering than observed (Maddox et al., 1990; Efstathiou et al., 1990). Thus, several alternative models have been discussed with a final model assuming a flat geometry and adding a cosmological constant (= dark energy component) resulting in the Λ CDM model. This was verified, when it was shown by SNIa measurements (Perlmutter et al., 1999) that the Universe is accelerating and that it is flat (CMB measurements by de Bernardis et al., 2000).

Altogether, the Λ CDM model has now established itself firmly as the standard paradigm for structure formation and is the basis for the evolution and formation of galaxies.

2.2 Formation and evolution of large-scale structures in the Universe

How large-scale structures form and evolve within the current framework of our cosmological understanding will be subject of this section, in particular with respect to a more precise mathematical prescription than in the last Section where a short historical

overview was given.

2.2.1 The homogeneous Universe

One of the fundamental assumptions in cosmology is that the Universe is on large-scales approximately homogeneous and isotropic. Out of this basic cosmological principle and the theory of general relativity, the space-time metric of the Universe is given by the Robertson-Walker metric (Peacock, 1999):

$$ds^2 = (cdt)^2 - a(t)^2 \left[\frac{dr^2}{1 - Kr^2} + r^2(d\theta^2 + \sin^2\theta d\phi^2) \right], \quad (2.1)$$

where r , θ and ϕ are spherical comoving coordinates, and t is the proper time. The growth of the spatial expansion can be parameterized with the function $a(t) := R(t)/R_0$, which is called expansion factor, and by definition is $a_0 = a(t_0) = R(t_0)/R_0 \equiv 1$ at the present time. The information of the curvature of the space-time is given by the parameter K , which can have values $1, 0, -1$, corresponding to a open (hyperbolic), flat (euclidean) or closed (spherical) geometry of the space-time. Using the Robertson-Walker metric, Einstein's field equations simplify into the Friedmann equations:

$$\frac{\ddot{a}}{a} = -\frac{4\pi G}{3} \left(\rho + \frac{3p}{c^2} \right) + \frac{\Lambda c^2}{3} \quad (2.2)$$

$$\left(\frac{\dot{a}}{a} \right)^2 = \frac{8\pi G}{3} \rho - \frac{Kc^2}{a^2} + \frac{\Lambda c^2}{3}, \quad (2.3)$$

where p represents the pressure and Λ the cosmological constant, corresponding to an energy density of the vacuum:

$$\rho_v c^2 = \frac{\Lambda c^4}{8\pi G} \quad (2.4)$$

For the density ρ , which appears in Eq. 2.3, one distinguishes between a non-relativistic matter component, a radiation component and a vacuum energy (cosmological constant) component. At the present time, they are denoted as $\rho_{M,0}$, $\rho_{r,0}$ and $\rho_{\Lambda,0}$, respectively. The Hubble parameter, that represents the expansion rate of the Universe, is related to the scale-factor by the equation:

$$H(a) = \frac{\dot{a}}{a} \quad (2.5)$$

In order to solve the above equations, the time dependence of p and ρ has to be specified, i.e. by defining an equation of state, which depends obviously on the ratio of energy (radiation) to matter. In the early Universe the energy is dominated by relativistic particles and radiation; hence, the equation of state is given by $p = \rho/3$ and the density scales with a^{-4} . As the Universe expands, the energy density decays

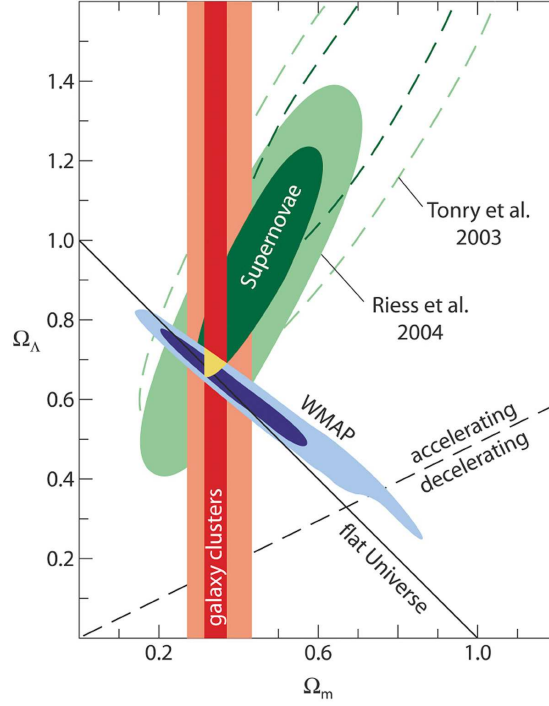


Figure 2.1: *Cosmological constraints in the $\Omega_m - \Omega_\Lambda$ plane. Three data sets are shown based on supernovae, CMB and galaxy cluster measurements, which provide independent methods to determine the cosmological parameters (<http://www.eso.org/public/images/eso0419d>).*

and the Universe enters a matter-dominated phase, non-relativistic matter is assumed to be pressure-less and its energy density scales with a^{-3} .

It is convenient to define the today's critical density of the Universe as

$$\rho_{\text{cr}} = \frac{3H_0^2}{8\pi G}, \quad (2.6)$$

where H_0 is the Hubble constant at the present time. Moreover, it is useful to define the following dimensionless density parameters:

$$\Omega_{M,0} = \frac{\rho_{M,0}}{\rho_{\text{cr}}}, \quad \Omega_{\Lambda,0} = \frac{\Lambda c^2}{3H_0^2}, \quad \Omega_{r,0} = -\frac{Kc^2}{a_0^2 H_0^2} \quad (2.7)$$

where $\Omega_{M,0}$ is the non-relativistic matter density parameter, $\Omega_{\Lambda,0}$ the dark energy density parameter and $\Omega_{r,0}$ the relativistic matter density parameter at the *present* time. Thereby, whether the total density parameter $\Omega_0 := \Omega_{M,0} + \Omega_{\Lambda,0} + \Omega_{r,0}$ is smaller, equal or larger than unity $< 1, = 1, > 1$ is equivalent to $K = -1, 0, 1$ distinguishing between an open, flat or closed geometry. With these definitions, Eq. 2.2 becomes

$q_0 = 1/2\Omega_{M,0} - \Omega_{\Lambda,0}$ with $q_0 := -(\ddot{a}a/\dot{a}^2)_{t_0}$ (= rate, at which the Universe is accelerating) and Eq. 2.3 becomes $\Omega_{M,0} + \Omega_{r,0} + \Omega_{\Lambda,0} = 1$, again at the *present time*.

In order to measure and to quantify today's cosmological parameters, different methods have been used, illustrated by Fig. 2.1 showing the $\Omega_{M,0} - \Omega_{\Lambda,0}$ plane. The different colored regions depict the favored parameter ranges resulting from different measurements. Cluster of galaxies provide a powerful diagnostic for the measurement of $\Omega_{M,0}$ (see red area in Fig. 2.1) as the number density of cluster at a given mass at varying redshift is strongly dependent on $\Omega_{M,0}$. Supernova of type Ia (SNIa) are considered as excellent standard candles because of the constancy of their luminosity at maximum brightness. Since SNIa are relatively luminous objects, they can be observed out to high redshift, and thus, they provide a powerful tool for the determination of the geometry and matter content of the Universe (Perlmutter et al., 1999, see green area in Fig. 2.1). Finally, a very strong observational constraint originates from the measurement of the temperature fluctuations in the cosmic microwave background (CMB), most exactly with WMAP (Spergel et al., 2007; Komatsu et al., 2009). Decomposing the temperature fluctuations in spherical harmonics, it is possible to recover the underlying fluctuation spectrum (see blue area in Fig. 2.1). Altogether, observational data seem to converge towards a concordance model with a low-density, vacuum-dominated Universe ($\Omega_{M,0} \sim 0.27 \pm 0.05$, $\Omega_{\Lambda,0} \sim 0.75 \pm 0.02$ and $\Omega_{r,0} \sim 4.2 \times 10^{-5} \pm 0.02$). The Hubble constant at the present time is found to be $H_0 = 72 \pm 5 \text{ km s}^{-1} \text{ Mpc}^{-1}$.

By putting the definitions of Eq. 2.7 into the second Friedmann equation 2.3 one obtains the evolution of the Hubble parameter with cosmic time:

$$H(z) = \frac{\dot{a}}{a}(z) = H_0 E(z), \quad \text{with} \quad (2.8)$$

$$E(z) = \sqrt{\Omega_{r,0}(1+z)^4 + \Omega_M(1+z)^3 + (1-\Omega_0)(1+z)^2 + \Omega_{\Lambda,0}} \quad (2.9)$$

Here, z is the cosmological redshift, which is directly related to the scale factor $a(t)$:

$$1+z = \frac{a(t_0)}{a(t_e)} \quad (2.10)$$

This quantity z can be understood as the Doppler shift of its emitted light due to the expansion of the Universe:

$$z = \frac{\lambda_{\text{obs}} - \lambda_{\text{emitted}}}{\lambda_{\text{emitted}}}. \quad (2.11)$$

For small distances $z \approx v/c = d/D_H$ is valid, where v is the velocity of the object and $D_H = c/H_0$ represents the Hubble distance. The redshift z is directly measurable from the spectra and is related to both the distance of the objects and the epoch of emission of the light and thus, is often used as a time variable. Note that light emitted

from objects gets additionally Doppler-shifted due to their peculiar velocities besides the global expansion of the Universe:

$$1 + z_{\text{pec}} = \sqrt{\frac{1 + v_{\text{pec}}/c}{1 - v_{\text{pec}}/c}}. \quad (2.12)$$

This means that the observed redshift of any object consists of a contribution due to the universal expansion and one due to its peculiar velocity along the light-of-sight. Therefore, the observed redshift for the relativistic case is given by $1 + z_{\text{obs}} = (1 + z_{\text{pec}})(1 + z)$, and for the non-relativistic case ($z_{\text{pec}} = v_{\text{pec}}/c$) it can be calculated by $z_{\text{obs}} = z + v_{\text{pec}}/c \cdot (1 + z)$.

2.2.2 The mass content of the Universe

Observations show that ordinary matter (baryonic component) can only account for $\sim 15 - 20\%$ of the total matter content (CMB constraints, rotation curves of spiral galaxies). Principally, non-baryonic particles are classified as relativistic and hot or non-relativistic and cold dark matter particles. However, at present time, the best agreement with observational studies is given by the *cold* dark matter paradigm, in the form of *Weakly Interacting Massive Particles* (WIMPs), which naturally arise in supersymmetric extensions of the standard model in particle physics. Dark matter, which only interacts via weak and gravitational forces, is assumed to behave as a collisionless fluid for most of the history of the Universe. As the number of particles is assumed to be large, two-body interactions can be neglected, and the system can be described by a distribution function in phase-space. Its evolution is given by the collisionless Boltzmann equation (also called Vlasov equation):

$$\frac{df}{dt} = \frac{\partial f}{\partial t} + \mathbf{v} \frac{df}{d\mathbf{r}} - \frac{d\Phi}{d\mathbf{r}} \frac{df}{d\mathbf{v}}, \quad (2.13)$$

where the potential is given by the Poisson equation:

$$\Delta\Phi(\mathbf{r}, t) = 4\pi G\rho(\mathbf{r}, t). \quad (2.14)$$

2.2.3 The linear growth of perturbation and spherical collapse model

The currently favored theories of structure formation assume that structure grows out of primordial quantum fluctuations which get amplified during a phase of rapid expansion ($\Delta t \approx 10^{-33}s$), what is called inflation (Guth, 1981). The statistical properties of the density field $\delta(\mathbf{x}, t)$ can be characterized by a Fourier transformation of its two-point correlation function, which is called power spectrum:

$$P(\mathbf{k}, t) = \langle |\delta(\mathbf{k}, t)|^2 \rangle \text{ with} \quad (2.15)$$

$$\delta(\mathbf{k}, t) = \frac{1}{(2\pi)^2} \int d\mathbf{x} \delta(\mathbf{x}, t) e^{-i\mathbf{k}\mathbf{x}} \text{ and } \delta(\mathbf{x}, t) = \frac{\rho(\mathbf{x}, t) - \bar{\rho}}{\bar{\rho}}, \quad (2.16)$$

where $\bar{\rho}$ is the background density of the Universe. The latest measurements from the CMB are consistent with a Gaussian scale free Harrison-Zeldovich initial fluctuation spectrum, i.e. $P_{\text{initial}}(k) \propto k^n$ with $n = 1$. Perturbations in cold dark matter begin already to grow after the radiation-matter equality ($\rho_{\text{matter}} = \rho_{\text{radiation}}$) so that by the time of decoupling (i.e. “recombination” of H and He nuclei with electrons) dark matter density fluctuations have already grown by a factor $20 \times \Omega_{\text{m},0}$ with respect to the perturbations in the photon-baryon fluid, i.e. cold dark matter can accumulate before baryonic matter. After recombination, baryonic matter can follow the evolution of dark matter by collapsing into the dark matter potential wells and mass is assembled following hierarchical clustering (bottom-up scenario). The density fluctuations grow by self-gravitation, and as long as these inhomogeneities are small, the growth of structure can be approximated with the linear perturbation theory. Based on the Euler equation and the continuity equation, which are given by

$$\frac{\partial \rho}{\partial t} + \nabla \cdot (\rho \cdot \mathbf{v}) = 0 \text{ (Continuity : mass conservation) and} \quad (2.17)$$

$$\frac{\partial \mathbf{v}}{\partial t} + (\mathbf{v} \cdot \nabla) \cdot \mathbf{v} + \frac{1}{\rho} \nabla p = -\nabla \Phi \text{ (Euler : momentum conservation),} \quad (2.18)$$

and the Poisson equation (Eq. 2.14) one can derive the growth of the perturbations in the linear regime:

$$\ddot{\delta} + 2\frac{\dot{a}}{a}\dot{\delta} = 4\pi G\bar{\rho}\delta \quad (2.19)$$

Note that the equation has two solutions, a growing mode and a decaying mode. However, the decaying solution will become negligible after some time and solely the growing mode is the relevant solution for structure formation.

After some time the density contrast of a given perturbation becomes comparable to unity and the linear perturbation theory will no longer represent a valid approximation. At a certain point, the perturbation will start to decouple from the background expansion as due to the self-gravity an over-dense region will expand at a slower rate compared to the background Universe. This will increase the density contrast and at some point, the over-dense region will collapse under its own self-gravity, forming a bound system. In the spherical collapse model, it can be shown that the perturbation decouples from the background expansion and collapses when it reaches a critical overdensity of $\delta_{\text{c}} \approx 1.68$. However, in reality, the sphere of matter does not collapse into one point. As a collisionless system can not dissipate its energy, the gravitational potential energy during the collapse has to be converted into kinetic energy of the particles according to the virial theorem. Moreover, due to the collapse, a rapid change of the gravitational potential occurs, a process called violent relaxation, which causes particle mixing in binding energy and let the particles get virialized (equilibrium state). The over-density at virialization can be computed using the virial theorem yielding $\delta_{\text{vir}} = 18\pi^2 \approx 180$ for $\Omega_{\text{m},0} = 1$ (resulting in M_{200}, r_{200}). Assuming $\Omega_{\text{m},0} \neq 1$ and $\Lambda \neq 0$

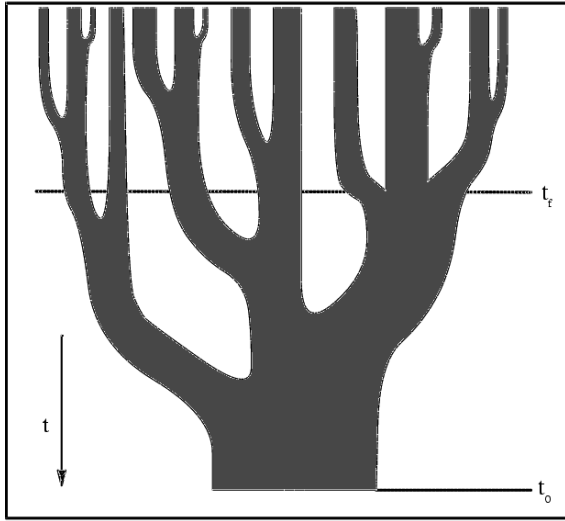


Figure 2.2: Schematic illustration of a merger tree, depicting the evolution of dark matter in a bottom-up scenario (Mo et al., 2010).

leads to more complex expression, namely a dependence of the virial over-density δ_{vir} on the matter density at the time of virialization $\Omega_{\text{m}}(t_{\text{vir}})$.

2.2.4 Modeling dark matter

For modeling the structure formation in the dark matter component, current methods consist either in using analytical techniques based on the Press-Schechter formalism or in performing numerical N-body simulations. Within the framework of a spherical collapse model, Press & Schechter (1974) realized that although small-scale modes have become non-linear, large-scale modes may still follow the linear theory. Therefore, using a filtering density function, they obtain a smoothed, linearly extrapolated density field (with no density fluctuation smaller than of a certain size). Therefore it is possible to determine if a given region in the space belongs to a collapsed object (when the linearly extrapolated density becomes ≈ 1.7). Thus, the PS formalism can be used to determine the mass function:

$$n(M)dM = - \left(\frac{2}{\pi} \right)^{1/2} \frac{\bar{\rho}}{M} \frac{\delta_{\text{crit}}}{\sigma^2} \frac{d\sigma}{dM} \exp \left(- \frac{\delta_{\text{crit}}^2}{2\sigma^2} \right) dM \quad (2.20)$$

where σ^2 is the variance of the linear density field smoothed over a mass scale M . Note that extending the PS formalism (EPS) by assuming a ellipsoidal collapse seems to fit simulation results better. Based on PS or EPS formalisms one can derive conditional mass functions for finding progenitors of dark matter halos (using Monte-Carlo-techniques) and thus, also construct merger trees for dark matter halos, which are

often used as input for semi-analytical models (e.g. Kauffmann et al., 1993; Sheth & Lemson, 1999; Somerville & Primack, 1999a). Fig. 2.2 shows a merger tree, depicting the growth of dark matter halos as a result of mergers. Time increases from top to bottom. A horizontal slice through the tree gives the distribution of the masses of the progenitors at a given time (Lacey & Cole, 1993).

Even if linear theory together with the spherical collapse model provides a useful tool for describing the growth of structure in the early universe, it can not account completely for the non-linear processes which are occurring in hierarchical structure formation. Therefore, a more accurate method for calculating the evolution of dark matter is by performing numerical N-body simulations. In these simulations, the phase-space distribution function is replaced by a set of N collisionless particles which are assumed to evolve only under self-gravity. Therefore, the following equations of motion have to be solved for a particle i :

$$\frac{d\mathbf{r}_i}{dt} = \mathbf{v}_i \quad (2.21)$$

$$\frac{d\mathbf{v}_i}{dt} = \mathbf{F}_i = -\nabla\Phi|_i, \quad (2.22)$$

where \mathbf{F}_i is the gravitational force on the particle i determined by the gravitational potential Φ (Equation 2.14). As in cosmological simulations the background space is uniformly expanding with time, it is convenient to use *comoving* coordinates, $\mathbf{r} \rightarrow \mathbf{x} = \mathbf{r}/a$, where a is the scale factor, and to re-write the above equations of motion 2.21 and 2.22. In order to calculate the gravitational force on a particle there exist several algorithms (PP, Tree, PM, P³M algorithms), with the aim to significantly reduce the computational time. The most straight forward way to calculate the gravitational force on a particle is given by direct summation of particle-particle interactions (PP), but this is combined with huge computational costs. Instead, particularly the *treecode* algorithm has led to substantial progress in this field by reducing the calculating time. In the tree-algorithm, particles are arranged in a hierarchy of groups (e.g. Barnes & Hut, 1986) and the gravitational field for each particle is calculated by a summation over the multipole expansion of the gravitational field of these groups, where higher order terms die off faster with increasing distance. Note that the N-body simulations I will use in this thesis have always been performed with the treecode GADGET (Springel et al., 2005a, see Sections 3.4.1, 4.3.1 and 5.3.1), partly combined with high-resolution techniques. Fig. 2.3 shows a part of the density distribution of dark matter in the Millennium simulation at redshift $z = 5$ (upper panel) and at $z = 0$ (lower panel, Springel et al., 2005c). It illustrates nicely the growth of large-scale structures in the Universe. Using halofinder single dark matter halos can be identified at different time steps and this way, merger trees can also be constructed based on simulations, which is, however, more demanding than the EPS based techniques (see 3.4.2 and 5.3.2).

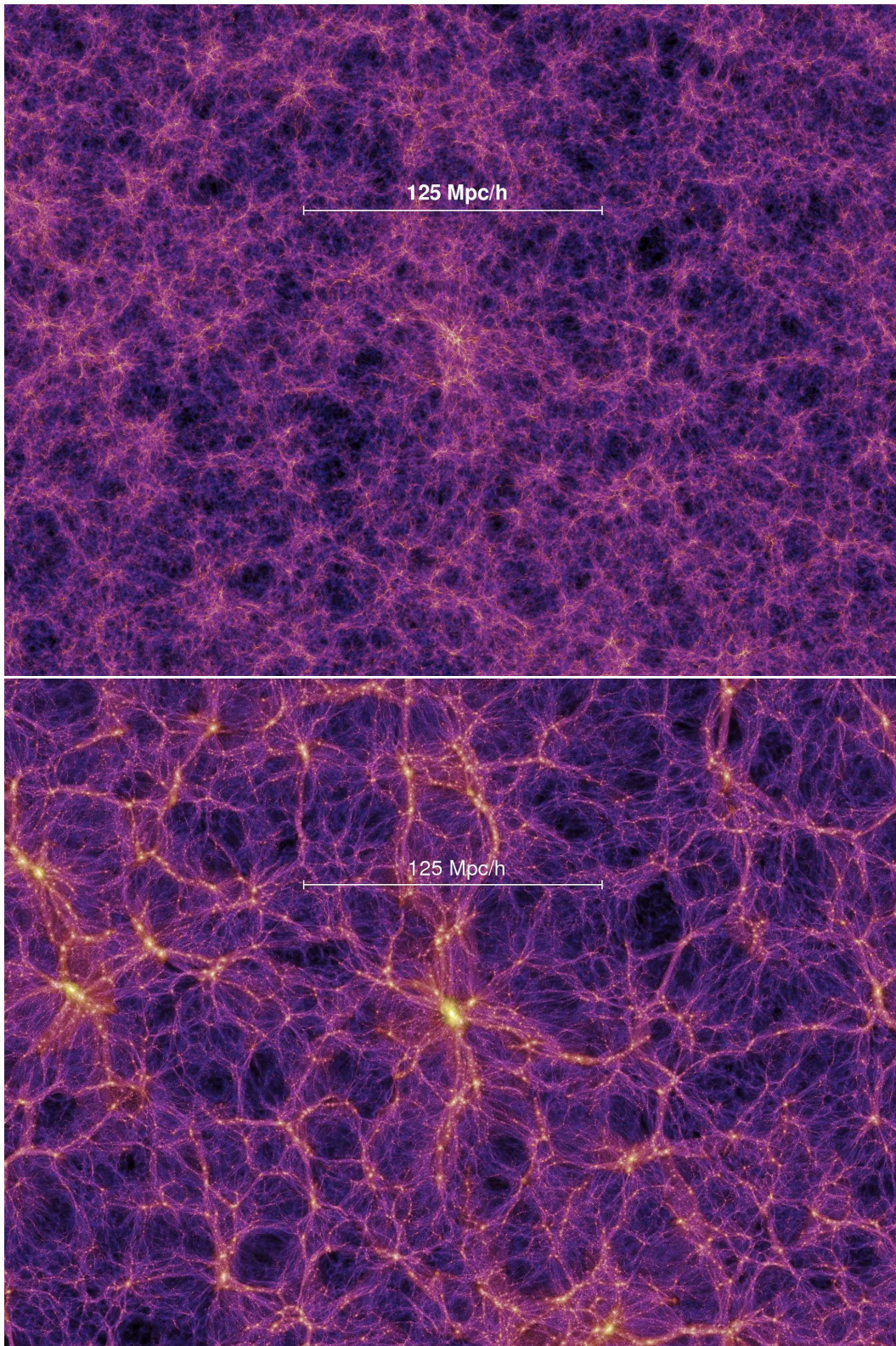


Figure 2.3: *Density distribution of dark matter in the Millennium simulation at $z = 5$ (upper panel) and at $z = 0$ (lower panel) (Springel et al., 2005c).*

2.3 Current picture of the joint evolution of galaxies and black holes

2.3.1 Evolution of baryonic matter

Due to gravitational interaction, the evolution of the baryonic component is primarily based on the structure formation of cold dark matter - as described in the last Section (Section 2.2). However, because of additional gas-dynamical and radiative processes the treatment of baryonic matter is much more complicated. Gas is believed to get trapped in the potential wells of dark matter halos and subsequently cools and condenses (radiative cooling, Silk, 1977; Rees & Ostriker, 1977; Binney, 1977) in their centers. Different cooling processes can affect the gas depending on its temperature and density. E.g. for $T > 10^7$ K, gas is fully ionized and cools mainly through bremsstrahlung emission from free electrons. At lower temperatures 10^4 K $< T < 10^6$ K, many excitation and deexcitation processes play a role (depending strongly on the chemical composition of the gas). However, when the temperature is smaller than $T = 10^4$ K, gas is mainly neutral and thus, cooling gets suppressed (only heavy elements or/and molecules allow further cooling). Cold, dense gas clouds may fragment due to self-gravity into small, high-density cores that may then eventually form stars. As a consequence, dying stars (SN explosions) can produce an enormous amount of energy which may heat or re-heat the surrounding gas or even blow a fraction of gas out of the galaxy (winds). Moreover, in the hierarchical evolution of galaxies, merging processes are found to play an important role for the growth processes. Minor mergers can be seen as kind of smooth accretion, but might be important for the size evolution of elliptical galaxies. In contrast, in major mergers, violent relaxation transforms orbital energy of the progenitors into internal binding energy of the remnant so that any hot gas associated with the progenitors gets shock-heated during the merger accompanied by strong star formation if the merging galaxies contain cold gas. Mergers are also influencing the shape of the galaxies significantly and thus, they are important for reproducing the observed different morphologies (spirals and ellipticals, e.g. Toomre & Toomre, 1972). Fig. 2.4 illustrates very schematically and simplified the relevant processes for galaxy formation. The dashed box represents the galaxy containing a hot and cold gas and a stellar component. Gas can cool and cold gas can form stars. Dying stars can inject energy, mass and metals into the surrounding gas. Note that a galaxy is not a closed box, so significant gas inflow and outflow can happen. However, besides all these processes, it is generally accepted that galaxies contain a supermassive black hole (SMBH) in their center, which might power active galactic nuclei (AGN), a very important phase in the process of galaxy formation. Active galaxies (AGN) can be divided into a variety of galaxies, e.g. Quasars, Radio galaxies, Seyfert galaxies, Blazars and BL Lacertae objects. However, common properties of AGN are that they have a very *bright and compact nuclear region* often much brighter than the host galaxy, they emit *non-stellar (thus, non-thermal) continuum emission* (from radio to the hard X-ray range) and show *strong emission lines*. By Salpeter (1964); Zel'Dovich (1964);

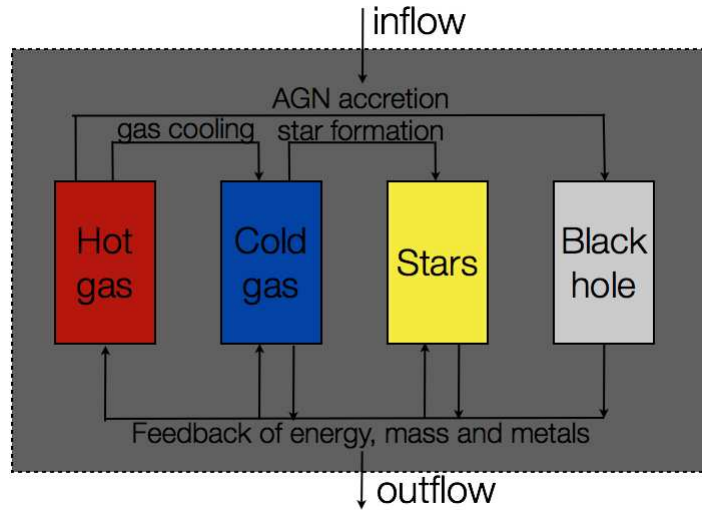


Figure 2.4: Schematic picture for the relevant processes in galaxy formation (Mo et al., 2010). The dashed box represents the galaxy containing a hot and cold gas and a stellar component as well as a black hole. Gas can cool and cold gas can form stars. Dying stars as well as heavily accreting black holes can inject energy, mass and metals into the surrounding gas. Note that the box is 'open', i.e. one can have gas infall (maybe driven by merger events or smooth gas accretion) and also gas outflows, e.g. SN-driven winds.

Lynden-Bell (1969) it was originally proposed that the central energy source of an AGN is gravitational in nature and thus, might be related to a SMBH. Until today, the only reasonable explanation for AGN behavior is the paradigm that a gravitational singularity is responsible for converting infalling matter into energy (Rees, 1984). During such active phases, black holes can influence the evolutionary processes of the galaxies significantly as large amounts of energy are released heating up the gas component. Therefore, in this Section I will briefly describe the interplay between the evolution of galaxies and the growth of black holes in more detail starting with a brief review of observational evidence for SMBHs.

2.3.2 Observational evidence for supermassive black holes

Observational evidence for black holes (see a summary in Colpi et al., 2006) - in particular, the supermassive variety - was very difficult to state, despite of the fact that the theoretical basis was already in place immediately following the 1915 publication of Albert Einstein's theory of general relativity. Karl Schwarzschild's 1916 solution of Einstein's field equations led to the conclusion that for a star of given mass, there exists a finite, critical radius at which light cannot escape anymore, and thus, reaches an

infinite time dilation. That real stars can indeed achieve such a critical radius was later demonstrated in a series of papers (Chandrasekhar, 1931; Landau, 1938; Oppenheimer & Serber, 1938). The first stellar mass black hole was detected in the rapidly variable X-ray source Cygnus X-1 (e.g. Brucato et al., 1972; Bolton, 1972), a strong confirmation of the theoretical work. In contrast, the common acceptance of supermassive black holes (SMBHs) in galaxies - not several masses in size, but rather millions of solar masses - was driven by an increasing amount of observational evidence. Although many of the present-day SMBH detections are in quiescent or weakly active galaxies, historically the SMBH paradigm evolved in the context of AGN. The first hint was found by Carl Seyfert's identification (early 1940s) of galaxies with 'unusual nuclei'. Fifty years later, one of Seyfert's original galaxy, NGC4258, was the first, for which the existence of a SMBH was conclusively demonstrated (Miyoshi et al., 1995). The most obvious evidence was found for M87 and Cygnus A (bright radio sources). In both cases the presence of radio lobes and of a bright optical narrow jet suggested that the radio emission might be due to relativistic particles ejected from the nucleus.

Although galaxies with AGN are the obvious places to look for evidence for the existence of SMBHs, the fact that quasars were more numerous at $z = 2$ than today suggests that 'dead quasar engines' should be hiding in many nearby, quiescent galaxies. Modeling the kinematics of stars in galactic nuclei provides a proper method for constraining the central potential and thus the mass of the central object. In particular in the Galactic Center, kinematics can be studied on much smaller scales revealing a black hole with a mass $M_{\bullet} = 3 \times 10^6 M_{\odot}$ (Genzel et al., 2000; Schödel et al., 2003; Ghez et al., 2005). However, for $cz \approx 10,000$ km/s SMBH estimates become unfeasible. While a way to measure black hole masses in more distant quiescent galaxies has yet to be devised, for type-1 AGN and quasars an alternative method already exists, the 'reverberation mapping' (Blandford & McKee, 1982; Peterson, 1993). Note that type-1 AGN refer to a orientation based distinction, and here, the observer has a direct view onto the nucleus (in contrast to type-2 AGN, which are observed through an obscuring torus). In the current picture of black holes, the central black hole and the accretion disk are surrounded by a dusty torus and one distinguishes between broad-line region (BLR) close to the black hole and a narrow-line regions (NLR) surrounding the torus. Therefore, the difference for type-1 and type-2 AGN depends on whether the inner region, the BLR can be detected or not. The size of the BLR can be probed by the time delay τ between variations in the ionizing continuum and in the flux of each velocity component of the line emissions: $r \sim c\tau$. Meanwhile, the emission line width reflects the velocity dispersion of the emission-line clouds in the gravitational potential which is dominated by the black hole. Thus, the mass can be derived from the virial theorem ($M_{\bullet} = fr\sigma^2/G$, where r is the radius, f is a dimensionless parameter depending on the kinematics, the geometry and inclination of the AGN and σ is the mean velocity dispersion). Reverberation mass measurements are consistent with other mass estimates within a factor of a few (Bentz et al., 2009).

2.3.3 Current picture of co-evolving galaxies and black holes

Providing the pure existence of the supermassive black holes in galactic centers powering AGN, is, however, only a first step towards a complete understanding of galaxy formation. In a second step, observational evidence was found that the black hole masses are tightly correlated to properties of their host galaxies. Kormendy & Richstone (1995) were the first, who noticed that SMBHs correlate with the luminosity of the surrounding stellar component. That is the bulge of spiral galaxies or the entire galaxy in case of ellipticals. Further detections of SMBHs have confirmed the existence of the $M_{\bullet} - M_{\text{bulge}}$ -correlation (e.g. Magorrian et al., 1998; Ferrarese & Merritt, 2000; McLure & Dunlop, 2001; Marconi & Hunt, 2003; Häring & Rix, 2004). The left panel of Fig. 2.5 shows the relation between black hole mass and bulge mass ($M_{\bullet} \sim 10^{-3} M_{\text{bulge}}$). Bulge magnitudes and velocity dispersions are connected through the Faber-Jackson

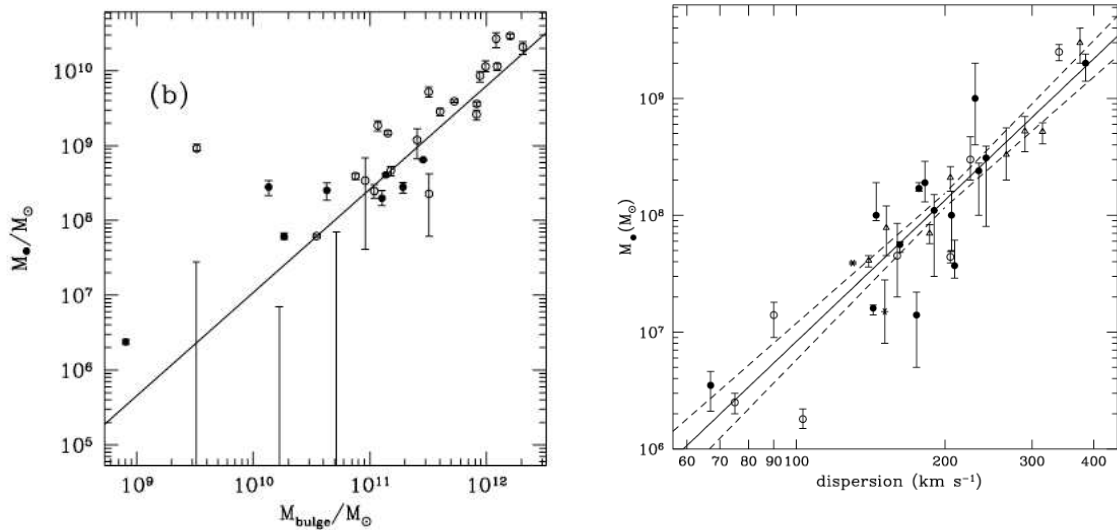


Figure 2.5: *Left panel: relation between black hole and bulge mass in the present-day universe according to Magorrian et al. (1998) Right panel: relation between black hole mass and velocity dispersion in the present-day universe according to Tremaine et al. (2002)*

relation, what directly implies that black holes are also connected with the velocity dispersion. Indeed, observational studies found that an even tighter correlation exists between the black hole mass and the velocity dispersion of the spheroid (Gebhardt et al., 2000; Ferrarese & Merritt, 2000; Tremaine et al., 2002). The right panel of Fig. 2.5 shows the relation: $M_{\bullet} \propto \sigma_{ve}^{\gamma}$, with $\gamma \sim 3.7 - 4.8$. Moreover, in a very recent study, Burkert & Tremaine (2010) showed that there exists even a tight correlation between black hole mass and the number of globular clusters. Whether black holes are also correlated with the dark matter halo mass is subject of ongoing debate: Ferrarese (2002) showed indirectly the existence of such a relation, however, in a very recent study of Kormendy & Bender (2011) they claim that there is *no* correlation between black hole

and halo mass, at least at the low mass end. Nevertheless, these observations strongly suggest that the formation of SMBHs is tightly linked with that of the (spheroidal component of) its host galaxy. That means the growth of black holes might not only be understood in the general framework of galaxy formation (where the evolutionary state of a galaxy governs black hole growth), but black holes themselves can also have significant impact on the formation and evolution of their host galaxies.

In the following, a few basic equations, which are important for describing black hole growth, will be given: An important approximation for an upper limit of the accretion rate onto a black hole of mass M_{\bullet} is resulting from a simple spherical model with a central source of a certain luminosity surrounded by gas. Considering the balance between an (outwards directed) radiation pressure and the (inwards directed) force of gravity defines a maximum luminosity, the *Eddington* luminosity L_{edd} . The gravity force is given by:

$$F_{\text{grav}} = \frac{GM_{\bullet}m_p}{r^2}, \quad (2.23)$$

and the force of radiation pressure can be expressed with:

$$F_{\text{rad}} = \sigma_T \frac{L}{4\pi r^2 c}, \quad (2.24)$$

where m_p is the proton mass and σ_T is the Thomson cross-section. With the condition $F_{\text{rad}} = F_{\text{grav}}$ and solving for the luminosity, one obtains (Mo et al., 2010):

$$L_{\text{edd}} = \frac{4\pi GM_{\bullet}m_p c}{\sigma_T} \approx 1.3 \times 10^{46} \left(\frac{M_{\bullet}}{10^8 M_{\odot}} \right) \text{ erg/s} \quad (2.25)$$

Above the Eddington luminosity, the source is unable to maintain steady spherical accretion. The Eddington luminosity corresponds to a mass accretion rate, which is the *highest possible* accretion rate within the simple spherical model:

$$\dot{M}_{\text{edd}} = \frac{L_{\text{edd}}}{\epsilon c^2}, \quad (2.26)$$

where ϵ is the radiative efficiency at which the mass of accreted material is converted into radiation. The Eddington ratio f_{edd} is defined as the ratio of the actual luminosity of the AGN and the Eddington luminosity (the largest possible luminosity for given black hole mass):

$$f_{\text{edd}} := \frac{L}{L_{\text{edd}}} \quad (2.27)$$

Observationally, bright Quasars and Seyfert galaxies are believed to be mostly connected with black holes accreting at large Eddington-ratios, whereas Radio galaxies are mainly assumed to be linked to black holes accreting only at a small fraction of the

Eddington rate.

An important growth channel for black holes is gas accretion (besides merger events). In the picture of *radiative* accretion, the black hole growth rate \dot{M}_\bullet ($= (1 - \epsilon)\dot{M}_{\text{acc}}$, i.e. the fraction ϵ of accreted mass is converted into radiation and escapes the black hole) is given by (Mo et al. (2010)):

$$\dot{M}_\bullet = \frac{1 - \epsilon}{\epsilon} \frac{L}{c^2} = \frac{1 - \epsilon}{\epsilon} \frac{L}{L_{\text{edd}}} \frac{M_\bullet}{t_{\text{salp}}} = \frac{1 - \epsilon}{\epsilon} f_{\text{edd}} \frac{M_\bullet}{t_{\text{salp}}}, \quad (2.28)$$

where L is the Luminosity of the AGN and $t_{\text{salp}} \sim 4.5 \times 10^8 \text{yr}$ is the Salpeter timescale. Thus, the mass evolution of the black hole can be described by an exponential increase:

$$M_\bullet(t) = M_{0,\bullet} \exp\left(\frac{1 - \epsilon}{\epsilon} f_{\text{edd}} \frac{t}{t_{\text{salp}}}\right) \quad (2.29)$$

When black holes grow through gas accretion, a considerable amount of cold gas is required in the host galaxy to be funneled into the center. Major mergers can be possible scenarios for driving gas into the center (e.g. Di Matteo et al., 2005; Hopkins et al., 2008c), and moreover, also bar instabilities in disks might lead to a significant gas inflow. Another source for cold gas accretion might be provided by stellar mass loss from evolved intermediate mass stars (Ciotti & Ostriker, 2007). One prediction of the merger scenario is that bright AGN should preferentially be found in interacting systems (what could not have been verified observationally at low redshifts). Moreover, as starbursts are a further consequence of merger events, nuclear activity is often associated with an increase in star formation. However, even if there is mainly *hot* gas present in the host galaxy (in particular in massive, early-type galaxies at low redshifts), a black hole can still accrete some gas through Bondi-accretion (Bondi, 1952). This is a spherical accretion onto an object and occurs when the gravitational potential of the black hole overcomes the specific thermal energy of the gas:

$$\dot{M}_\bullet \sim 4\pi r_A^2 \rho_A c_s(r_A) \quad (2.30)$$

where $r_A \sim GM_\bullet/c_s^2$ is the accretion radius, c_s is the sound speed of the hot gas and ρ_A the gas density. In this phase, black holes are accreting extremely below the corresponding Eddington limit and thus, they are radiatively very inefficient.

An important consequence of the gas accretion onto the black hole is, that AGN can release a huge amount of energy during their lifetime. The power of its energy output may be expressed as

$$\frac{dE}{dt} = (\epsilon_r + \epsilon_m) \dot{M}_\bullet c^2, \quad (2.31)$$

where ϵ_r and ϵ_m is the radiative and mechanical efficiency, respectively. Comparing the energetic feedback from an AGN to the binding energy of its host galaxy reveals the significant impact of AGN feedback. Broadly speaking, there are three different possible processes which can release energy from the AGN into its surrounding gas:

- Radiative processes: Interaction of photons with gas particles
- Mechanical processes: Particle-particle interaction
- Energetic particles (cosmic rays)

Radiative feedback is mainly connected with high-accretion phases and one distinguishes between radiation pressure (momentum-driven winds) and radiative heating (energy transfer). In contrast, mechanical feedback is mainly believed to occur in low-accretion AGN in form of radio jets or lobes releasing kinetic energy. Again one distinguishes between momentum-driven winds and energetic transfer. Through gas heating and expelling the gas out of the host galaxy, AGN feedback has a profound influence on the further evolution of the galaxy: cooling might be suppressed and thus, further star formation might be quenched. Additionally, also further gas accretion onto the black hole might be quenched leading to a self-regulation in black hole growth.

Unanswered, open questions

However, in this picture, there still exists a number of unanswered questions about how the co-evolution of black holes and galaxies actually works. E.g. *How does the gas get into galaxies and how is it transported afterwards to the inner accretion disk surrounding the black hole? How strong is the effect of the AGN feedback onto the host galaxy evolution? Is the AGN phase only a once-a-lifetime event in the life of a galaxy or is it more an intermittent process? What is the origin of the black hole mass scaling relations and do they show a redshift evolution? What is the origin of the observed anti-hierarchical black hole growth?* In this thesis, I will especially focus on the latter two ‘mysteries’.

Currently, there exist different ways for explaining the emergence of the present-day black hole scaling relations. One possibility is that they occur due to a connected growth of black holes and galaxies, as outlined above, as e.g. rapid cold gas accretion during gas-rich major mergers (e.g. Naab et al., 2006b; Robertson et al., 2006a; Hopkins et al., 2008c; Johansson et al., 2009b) and/or AGN feedback for regulating black hole growth and star formation (Granato et al., 2004; Di Matteo et al., 2005; Croton, 2006). However, it is still not understood which of the black hole mass scaling relations is the fundamental one. Hopkins et al. (2007c) claim that there is a “black hole fundamental plane” relation between black hole mass, the galaxy effective radius, the dynamical mass and the velocity dispersion. In contrast, a complete alternative attempt for explaining the black hole mass scaling relations is purely based on statistical merging of objects without any need for a physically coupled growth of black holes and host galaxies. Peng (2007) and Jahnke & Maccio (2010) show that for merging scenarios (either based on random or cosmological merging of galaxies and black holes) a relation between black hole and bulge emerges automatically even if the objects are totally uncorrelated in the beginning. This is mainly a consequence of the

statistical Central-Limit-Theorem. Moreover, there are claims that the relationship between galaxy mass and black hole mass may be evolving with cosmic time due to observations of 'over-massive' and 'under-massive' black holes at high redshifts (Peng et al., 2006; Salviander et al., 2007; Woo et al., 2008), i.e. black holes which are lying above or below the present-day relation between black hole and bulge mass and even outside the $1\text{-}\sigma$ -range of the present-day scatter. E.g. Hopkins et al. (2007c); Croton (2006); Robertson et al. (2006a) explain this by a shifted relation towards larger black hole masses at high redshifts compared to the present-day relation. In their scenarios, this is again due to gas accretion processes and thus, due to the underlying connected growth of galaxies and black holes. However, solely considering the statistics in merging scenarios might give a complete alternative explanation, what will be the subject of investigations in Chapter 3.

Besides, the cosmic evolution of differently luminous AGN is a further subject of current, intense debate. Observations reveal that bright quasars start to form already at $z > 6$, have an activation peak at around $z \sim 2 - 3$ and decline rapidly at lower redshifts. Here the question emerges what determines such a redshift-dependence of the activation rate. As the number density of dark matter halos with $M_{\text{halo}} = 10^{12.5} M_{\odot}$ increases rapidly with time at $z > 3$, the increase of the quasar number density might eventually be connected directly to the increase of massive halos. At $z < 3$ on the other hand, the number density of dark matter halos keeps increasing constantly with increasing time, implying that other processes might be necessary. If quasar activity is mainly triggered by galaxy interactions, the decline of the quasar number density might reflect the decline of the major merger rate. In addition to the drop of the merger rate further physical processes as the availability of cold gas in the host galaxy as well as the AGN feedback processes might state other plausible effects in order to reduce the activity in bright quasars at low redshifts. Interestingly, less luminous AGN are observationally found to peak at smaller redshift compared to bright quasars. This indicates the 'downsizing' or 'anti-hierarchical' trend, i.e. it seems as if more massive black holes have been in place already very early in the cosmic history whereas less massive black holes seem to preferentially form only at lower redshift. At first sight, this seems to be in clear contrast to currently favored hierarchical clustering scenarios. Possible mechanisms, which may account for the observed downsizing trend, will be discussed in Chapter 4.

2.3.4 Modeling galaxy formation and black hole growth

In order to model galaxy formation and black hole growth, there exist currently different methods, which are all based on the large-scale structure formation of cold dark matter either modeled using the analytical EPS theory or numerical N-body simulations (see Section 2.2):

1. Analytical methods, e.g. *halo occupation distribution models* (HOD) (see Section 3.4.3)

2. *Semi-analytical models* (see Section 4.3.2)
3. *Hydrodynamical simulations* (see Section 5.3)

In halo occupation distribution models, dark matter halos at a given mass and redshift are populated with a number of galaxies with a certain mass/luminosity. The dark matter halo distributions are calculated either analytically using the EPS theory or numerically with N-body simulations. They are connected with observed luminosity/galaxy mass functions (e.g. van den Bosch et al. (2003, 2007); Mandelbaum et al. (2006); Wechsler et al. (2006); Zheng et al. (2007); Conroy & Wechsler (2009); Guo & White (2009); Moster et al. (2010); Zehavi et al. (2010); Behroozi et al. (2010); Wake et al. (2011)). Formally, the connection between the luminosity function $\Phi(L, z)$ and the dark matter halo distribution $n(M, z)$ can be written as:

$$\Phi(L, z)dL = dL \int \Phi(L|M, z)n(M, z)dM, \quad (2.32)$$

where $\Phi(L|M, z)dL$ is the conditional luminosity function at z , which specifies the average number of galaxies with luminosities in the range $L \pm dL/2$, that reside in a halo of mass M at redshift z . The simplest assumption about the galaxy-halo relation is that the total luminosity of a galaxy is directly proportional to its halo mass M . This, however, results in a wrong shape of the luminosity function compared to the observed one as at the low mass end supernova winds and at the high mass AGN feedback become important, non-negligible processes for suppressing cooling and thus, for quenching star formation.

However, in contrast to halo occupation models, semi-analytic models and hydrodynamical simulations represent a more thorough approach in an 'ab initio' way for modeling galaxy formation. In semi-analytical models (e.g. White & Frenk, 1991; Kauffmann et al., 1993; Cole et al., 1994; Somerville & Primack, 1999b; Kauffmann et al., 1999; Cole et al., 2000; Springel et al., 2001a; Hatton et al., 2003; Kang et al., 2005; Baugh et al., 2005; Khochfar & Silk, 2006a; Croton, 2006; Bower et al., 2006; De Lucia & Blaizot, 2007; Somerville et al., 2008b; Font et al., 2008; Guo & White, 2009; Weinmann et al., 2009), complicated and tightly connected physical processes for the formation of galaxies are modeled as a set of simplified recipes and prescription assuming a spherical halo geometry and carrying a large number of free parameters. Within a dark matter halo, one distinguishes between three different baryonic components, cold disk gas, hot halo gas and stars assuming simple prescriptions for conversion rates between these baryonic components. With a stellar population synthesis model, star-formation history and metallicity can be converted into luminosity and color of the stellar population. Dynamical friction calculations are important for the treatment of merger processes. The free parameters in semi-analytic models are mainly set in order to reproduce observations of the present-day Universe. However, partly they can also be motivated by detailed hydrodynamical simulations. The main advantage of semi-analytic modeling is that one can easily generate large samples of model galaxies, what

is especially useful for investigating statistical properties of galaxies. Semi-analytic models have been successful in reproducing the luminosity function, the Tully-Fisher and Faber-Jackson relations, star formation histories, morphology, and color distributions. Thus, despite of some unresolved problems (e.g. over-prediction of the fraction of red satellite galaxies), the overall agreement between predictions of semi-analytic and observations is encouraging and suggest that the main physical processes are considered. However, as a number of physical processes are still poorly understood and are thus not treated accurately from first principles, many recipes are too simplified and thus, the semi-analytic models are far from being complete (see Mo et al., 2010).

In contrast, in cosmological hydrodynamical simulations, the evolution of the initial density field is followed explicitly by solving the gravitational and hydrodynamical equations (see Equations 2.14, 2.17 and 2.18) numerically. This can be sampled either using a large spatial grid (Eulerian approach) or by a large number of particles (Lagrangian approach). Note that in this work the latter approach will be used, the smoothed particles hydrodynamics (SPH) method. As the technique is particle based, it can follow the motion of individual mass elements (coordinates are comoving with the fluid element) (Springel et al., 2001a). The main advantage of hydrodynamical simulations compared to semi-analytics is that they can follow the evolution of gas without relying on simplified approximations in a more self-consistent manner. However, simulations are still limited by numerical resolution, why some of the processes have to be modeled on a subgrid level (e.g. Cen & Ostriker, 1993; Davé et al., 2001; Springel & Hernquist, 2003; Maller & Bullock, 2004; Nagamine et al., 2005; Kereš et al., 2005; Navarro et al., 2009; Schaye et al., 2010a), with recipes not so different from semi-analytics. But it is still difficult with current computational power to have both large statistics (large cosmological box) and a high resolution. In recent years, many different implementations for star formation (e.g. the multi-phase model for the interstellar medium as proposed by Springel & Hernquist, 2003), feedback from supernovae, supernova-driven winds as well as AGN feedback have been proposed (e.g. Di Matteo et al., 2005; Cattaneo et al., 2005; Sijacki et al., 2007; Oppenheimer & Davé, 2008; Booth & Schaye, 2009; Scannapieco et al., 2009; Governato et al., 2010; Schaye et al., 2010b; Sawala et al., 2010). For example, it has been demonstrated that star formation can effectively be quenched after an initial burst (due to a merger event) by AGN/SN driven outflows, producing massive red galaxies. One can conclude that hydrodynamical simulations provide a very promising way to study galaxy formation *self-consistently* in a cosmological context. However, numerical resolution is clearly insufficient and thus, many processes are still implemented in a very crude and ad-hoc way (see Mo et al., 2010).

As both methods, SAMs and hydrodynamical simulations, have their pros and cons, it is of utmost importance to compare directly how galaxies form in these different approaches. It might be extremely helpful in order to reveal limitations of both approaches and in particular to test often very simplified recipes assumed for galaxy

formation processes in SAMs. The investigation of the robustness and reliability of semi-analytic models will be the main topic in Chapter 5.

THE INTRINSIC SCATTER IN BLACK HOLE MASS SCALING RELATIONS

In this Chapter, I present results on the evolution of the intrinsic scatter of black hole masses considering different implementations of a model in which black holes only grow via mergers. It is demonstrated how merger driven growth affects the correlations between black hole mass and host bulge mass. The simple case of an initially lognormal distributed scatter in black hole and bulge masses combined with random merging within the galaxy population results in a decreasing scatter with merging generation/number as predicted by the central-limit theorem. In general, it is found that the decrease in scatter σ is well approximated by $\sigma_{\text{merg}}(m) \approx \sigma_{\text{ini}} \times (m + 1)^{-a/2}$ with $a = 0.42$ for a range of mean number of mergers $m < 50$. For a large mean number of mergers ($m > 100$), there is a convergence to $a = 0.61$. This is valid for a wide range of different initial distributions, refill-scenarios or merger mass ratios. Growth scenarios based on halo merger trees of cosmological N-body simulations show a similar behavior with a scatter decrease of $a = 0.30$ with typical number of mergers $m < 50$ consistent with random merging (best matching model: $a = 0.34$). Assuming a present-day scatter of 0.3 dex in black hole mass and a mean number of mergers not exceeding $m = 50$ the results imply a scatter of 0.6 dex at $z = 3$ and thus, a possible scenario in which over-massive (and under-massive) black holes at high redshift are the consequence of a larger intrinsic scatter in black hole mass. A simple toy model connecting the growth of black holes to the growth of haloes via mergers, neglecting any contribution from accretion, yields a consistent $M_{\bullet} - M_{\text{Bulge}}$ relation at $z = 0$, if the correct initial relation is assumed. This study is published by MNRAS (Hirschmann et al., 2010)

3.1 Black hole mass relations in the present-day universe

Observationally, there exists a strong correlation between black hole masses and properties of the host galaxy, e.g. the host bulge mass, the bulge velocity dispersion and the number of globular clusters (Håring & Rix, 2004, Ferrarese & Merritt, 2000, Gebhardt et al., 2000, Tremaine et al., 2002, Gültekin et al., 2009, Burkert & Tremaine, 2010) and possibly the host halo (Ferrarese, 2002) in nearby galaxies. Håring & Rix (2004) find the relation between black hole mass M_{\bullet} and bulge mass M_{bulge} to be:

$$\log(M_{\bullet}/M_{\odot}) = 8.20 + 1.12 \times \log(M_{\text{bulge}}/10^{11}M_{\odot}). \quad (3.1)$$

The correlation between black hole mass M_{\bullet} and velocity dispersion σ_{*} can be written as

$$\log(M_{\bullet}/M_{\odot}) = a \log(\sigma_{*}/200\text{kms}^{-1}) + b, \quad (3.2)$$

where a is the slope and b is the zero point. In the literature the values for the slope vary between $a = 3.68$ and $a = 4.86$. For example Ferrarese & Merritt (2000) give values for the zero point $b = -2.9$ and the slope $a = 4.80$. Gebhardt et al. (2000) claim a smaller slope of $a = 3.75$, Tremaine et al. (2002) find $a = 4.02$ and more recently Ferrarese & Ford (2005) estimated a slope of 4.86 and Graham (2008b) one of 3.68 for barless galaxies. Concerning the intrinsic scatter σ in black-hole mass, $\log M_{\bullet}$, most studies agree that the scatter is not larger than 0.3 dex (Gebhardt et al., 2000; Tremaine et al., 2002; Novak et al., 2006; Graham, 2008b). Note, that with σ_{*} I describe the central velocity dispersion of a galaxy, whereas the intrinsic scatter is characterized as σ . In contrast to Gebhardt et al. (2000) and Tremaine et al. (2002), a recent study by Gültekin et al. (2009) obtains for Eq. 3.2 a slope $a = 4.24$ and an intrinsic scatter in black hole mass of $\sigma = 0.44$ dex for a sample of 49 M_{\bullet} -measurements. For a subsample of early-type galaxies they find a smaller slope as well as a smaller scatter ($a = 3.96, \sigma = 0.31$ dex) than for the full sample. For non-elliptical galaxies the intrinsic scatter is larger with $\sigma = 0.53$ dex. Additionally, Graham (2008a) find a reduced intrinsic scatter by removing barred galaxies from their sample ($\sigma_{\text{all}} = 0.27$ dex, $\sigma_{\text{barless}} = 0.17$ dex). In the following the scatter σ will always be given in dex. The existence of these tight correlations strongly suggests a co-evolution of the black hole and the bulge component of the host galaxy. However, the origin of these relations is uncertain and a subject of current research (e.g. Volonteri & Natarajan, 2009; Peng, 2007; Burkert & Silk, 2001; Springel et al., 2005a; Johansson et al., 2009b). Apparently, the origin of these relations can be connected to the gas dynamics in major galaxy mergers (Mihos & Hernquist, 1996, Naab et al., 2006a, Robertson et al., 2006b, Hopkins et al., 2008b). In this scenario, the black holes grow significantly in gas rich mergers of disk galaxies and the remnants appear on the observed scaling relations. Subsequent, possibly gas poor, major and minor merging (Khochfar & Burkert, 2003, Naab et al., 2006b, Khochfar & Silk, 2009, Naab et al., 2009) conserves the relation (Sesana et al., 2004, Robertson et al., 2006b, Peng, 2007, Hopkins et al., 2007a, Hopkins et al., 2007b, Springel et al.,

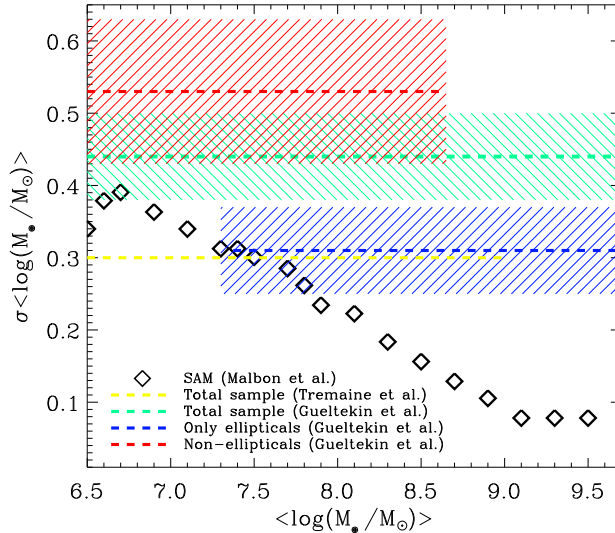


Figure 3.1: Comparison of the intrinsic scatter from observations (Tremaine et al., 2002, Gültekin et al., 2009) and theoretical predictions (Malbon et al., 2007). From the 10-90 percentile spread in the model the corresponding theoretical scatter was calculated. The shaded areas illustrate the error on the observationally estimated intrinsic scatter.

2005a, Johansson et al., 2009b). Moreover, AGN feedback plays an important role in regulating the black hole growth as well as influencing the host galaxy evolution by quenching further cooling and star formation (Di Matteo et al., 2005; Croton, 2006; Robertson et al., 2006a).

However, a completely different approach, in order to explain the origin of the black hole scaling relations at redshift $z = 0$, was made by Peng (2007) and Jahnke & Maccio (2010). In these studies they show that the emergence of a relation can be derived from pure statistics in merging scenarios *without* directly connecting the growth of black holes and the host galaxies by gas physical processes, as e.g. AGN feedback. They show either in random merging (Peng, 2007) or in cosmological merging scenarios (Jahnke & Maccio, 2010) that a relation between black hole and bulge mass can be established even if the objects are completely uncorrelated in the beginning. They claim this is mainly a consequence of the Central-limit-theorem and the corresponding convergence against a normal distribution independent of the initial distribution.

3.2 Black hole mass relations at higher redshifts

Observationally the black hole mass relations are well constrained only in the nearby Universe and it is unclear, if and how they evolve with cosmic time. Several authors

have found evidence that galaxies at higher redshift have a higher black hole to bulge mass ratio $M_{\bullet}/M_{\text{bulge}}$ than ellipticals today (McLure et al., 2006; Treu et al., 2007; Woo et al., 2008; Walter et al., 2004; Schramm et al., 2008; Peng et al., 2006; Greene et al., 2010; Natarajan & Treister, 2009; Salviander et al., 2007; Shields et al., 2006). For a sample of Seyfert galaxies at moderate redshifts $z < 0.1$ the black holes are more massive by $\Delta \log M_{\bullet} \sim 0.5$ dex compared to the local black hole-bulge mass relation (Treu et al., 2007, Woo et al., 2008). Salviander et al. (2007) find at redshift $z \approx 1$ an evolution of the M_{\bullet} - σ_{*} -relation by 0.2 dex in black hole mass. At higher redshifts of $z \sim 2$ McLure et al. (2006) observe black holes 8 times more massive than expected and Peng et al. (2006) show that for $z \geq 2$ the $M_{\bullet}/M_{\text{bulge}}$ -ratio is 3–6 times larger than today. This has been confirmed by Greene et al. (2010) based on a lensed quasar sample. Schramm et al. (2008) find evidence for an excess in $M_{\bullet}/M_{\text{bulge}}$ at $z \sim 3$ of a factor of ~ 10 . At redshifts $4 < z < 6$ Shields et al. (2006) obtain for black hole masses in the range of $8 < \log(M_{\bullet}/M_{\odot}) < 10$ a deviation from the present-day M_{\bullet} - M_{bulge} -relation of $\Delta \log(M_{\bullet}) \sim 2$ dex. Walter et al. (2004) report an even higher redshift object, a quasar at $z = 6$, whose black hole is about 20 times more massive than expected. Considering a present-day scatter according to Tremaine et al. (2002) ($\sigma = 0.3$) or according to Gültekin et al. (2009) ($\sigma = 0.31$ for ellipticals) all observed black holes at $z \geq 2$ are outside the $2 - \sigma$ range of the present-day scatter. Furthermore, recent observations (Alexander et al., 2008; Shapiro et al., 2009) show also the existence of under-massive black holes at high redshifts. Alexander et al. (2008) find black hole masses, which are 3 times smaller than those found in comparable massive galaxies in the local Universe. The results in Shapiro et al. (2009) show that black hole masses at $z = 2$ are an order of magnitude lower than those predicted by local scaling relations.

The most obvious explanation for the over-massive black holes at high redshifts are possible selection effects. It is more likely to detect the most luminous and most massive black holes at high redshift than less luminous ones. However, the probability for finding a massive black hole in the mass range $10^9 - 10^{10} M_{\odot}$ in the observed volume at $z = 3$ (e.g. Schramm et al., 2008) is extremely low as estimates of the local SMBH mass function from SDSS (Benson et al., 2007) would predict no high mass black holes to be found in a similar volume even assuming no evolution in the SMBH mass function. Cosmic variance is very unlikely to be an explanation for the observed, massive black holes. Lauer et al. (2007) point out that there is an additional bias which is due to different selection effects for high-redshift (e.g. black holes in high- z galaxies selected by nuclear activity) and local samples (e.g. black holes in local galaxies selected by luminosity or velocity dispersion). They deduce that because of this bias M_{\bullet} will typically appear to be too large in a distant sample for a given luminosity or velocity dispersion. Some authors (e.g. Croton, 2006) explain observed, over-massive black holes at high redshift with a shifted relation towards higher black hole masses for a given bulge mass. He uses the Millennium Λ CDM-simulation (Springel et al., 2001b) coupled with a model of galaxy formation, where galaxy mergers are the primary drivers for black hole and galaxy growth and explore an additional growth channel through which only

bulges gain mass, e.g. the disruption of stellar galactic disks in major disk mergers. He argues, that if the bulge growth rate from such disrupted disks is not constant with time, an evolution in the M_{\bullet} - M_{bulge} -relation can occur. Furthermore, Robertson et al. (2006c) find from simulations of galaxy mergers, that the M_{\bullet} - σ_* -relation shows a slight redshift evolution towards higher black hole masses for a given σ_* at higher redshifts, but they predict no evolution for the M_{\bullet} - M_{bulge} -relation. However, Hopkins et al. (2007c) using again simulations of major galaxy mergers show that high redshift black holes will be more massive at a fixed bulge mass than expected from the present-day relation. They find an evolution towards lower black hole to bulge mass ratios with cosmic time which is driven by the fact that disks (merger progenitors) have characteristically larger gas fractions at high redshifts. It should be pointed out that these studies (Croton, 2006; Robertson et al., 2006c; Hopkins et al., 2007c) are consistent with each other, they are only focusing on different aspects of the evolution of the relation. However, these methods do not provide a sufficient explanation for the observed under-massive black hole masses at high redshifts, since these methods find to have black holes mainly lying above the median M_{\bullet} - M_{bulge} -relation at high redshift evolving towards the relation with decreasing redshift. However, they also predict that the black holes go through a rapid growth phase before they end up above the relation; these objects might be under-massive. Furthermore, if a black hole at high z is already above the median M_{\bullet} - M_{bulge} -relation it will not end below the median relation at $z=0$ if only assuming merging and not gas accretion. Therefore, an alternative explanation for the observed high *and* low $M_{\bullet}/M_{\text{bulge}}$ -ratios at high redshifts could be the existence of a larger intrinsic scatter in black hole mass, even assuming no evolution of the mean relation with cosmic time, what would be in agreement with Lauer et al. (2007). This would be consistent with a study from Shankar et al. (2010), where they find empirically - using the Soltan argument and quasar clustering - that the scatter in the L - M_{\bullet} -relation must be large at redshifts $0.4 < z < 2.5$.

In this Chapter, the question is addressed: how does the intrinsic scatter in black hole mass evolve and change with time assuming that black holes grow only via mergers? An answer to this question is also important with respect to similarities and differences between the observed scatter of black hole masses and predictions from theoretical models. Malbon et al. (2007), using semi-analytic modeling, find that the present day scatter in black hole mass decreases significantly with increasing black hole mass. This is in contrast to observations using the full samples of e.g. Gebhardt et al. (2000), Tremaine et al. (2002), and Gültekin et al. (2009). Here, the scatter appears to be independent of black hole mass. In particular at the high mass end the observed scatter is much larger than the model predictions (see Fig. 3.1). However, Gültekin et al. (2009) demonstrate that the scatter for non-elliptical galaxies (typically at lower masses) is larger than for elliptical galaxies. This is, at least qualitatively, in agreement with the predictions from Malbon et al. (2007).

So far the time evolution of the scatter in black hole mass has not been investi-

gated in detail. Peng (2007) deals with the evolution of the scatter, but he mainly focuses on the aspect of how the present day M_{\bullet} - M_{bulge} -relation can form in a simple model applying random merging of galaxies. He claims that the relation develops even if black holes and bulges are uncorrelated or wrongly correlated in the beginning. This behavior is supposed to result from an initially exponentially decreasing SMBH mass function where minor mergers drive the objects towards the observed correlation. Furthermore, the scatter in black hole mass decreases with increasing merger number, and according to his results the decrease in scatter is dominated by major mergers. However, a quantitative study of the scatter evolution was not presented, which is the main subject of this Chapter. A further major difference between this work and that of Peng (2007) is that - besides Monte-Carlo generated random merging scenarios - merging as it is found for dark matter haloes in large scale *cosmological* simulations is included.

In the following, the evolution of the intrinsic scatter is investigated assuming:

- Simple random merging (Section 3.3.2)
- Modified random merging (Section 3.3.3)
- Merging in Λ CDM-simulations (Section 3.4)

It should be pointed out that random merging does not describe a full physical evolution process according to currently favored structure formation models. In principle, the model follows dry merging of galaxies and therefore is limited to high mass galaxies, since merging at the high mass end is assumed to be almost dry, so that gas physics and star formation do not play an important role and can be neglected in the growth processes. However, an advantage of using a simple model such as random merging is that separate effects on the scatter evolution can be studied, e.g. the influence of the initial mass distribution, of the merger mass-ratio or different refill-scenarios. Then these results are compared to merging according to currently favored structure formation models based on dark matter Λ CDM-simulations. Since it is known that a significant contribution to black hole growth is caused by accretion, this issue will be discussed in Section 5.7.

3.3 Models for random merging

3.3.1 Initial conditions

In the following, two different initial distributions of bulges are described including black holes as a starting point for random merging: a log-normal distribution and a Schechter distribution of bulges.

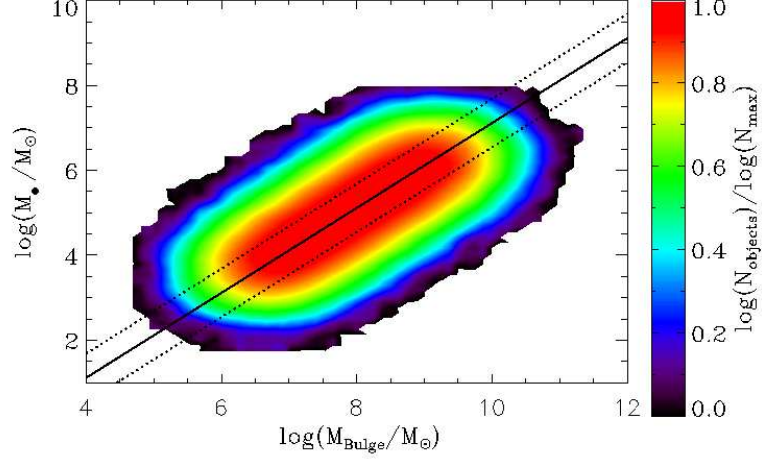


Figure 3.2: Normalized 2D-histogram of the initial distribution with the same, log-normal distributed scatter ($\sigma_{\text{ini}} = 0.6$) in bulge and black hole mass. The observed relation is shown by the black, solid line. The black dotted lines indicate the $1\text{-}\sigma$ range of the initially applied scatter in the model.

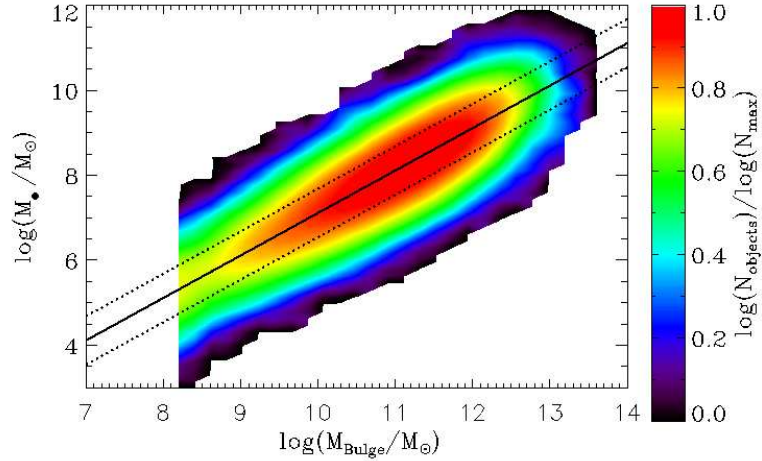


Figure 3.3: Initial distribution based on the Schechter-fit for early-type galaxies at $z \sim 2$. An initial scatter is only applied to the black hole mass ($\sigma_{\text{ini}} = 0.6$)

Initial log-normal distribution

The initial log-normal distribution was constructed by taking a uniform distribution (in the log) of bulge masses with black hole masses according to Häring & Rix (2004). Then I applied to the bulge as well as black hole masses a log-normal distributed scatter with a value of $\sigma = 0.5$. Having set this scatter to bulge *as well as* to black hole masses results in a larger scatter in black hole and bulge masses with a value of ~ 0.6 . This scatter is larger than the observed, present-day one specified by Tremaine et al. (2002) and Gültekin et al. (2009). I have chosen this fiducial value a posteriori as in the most realistic Λ CDM-simulation this results in a final observed scatter value of $\sigma \sim 0.32$ (see Section 3.4). However, the scatter evolution is independent of the choice of the initial scatter value (see Section 3.3.2). I start with an initial distribution of 580,000 bulges with black holes. The black hole masses range from $2.0 < \log(M_{\bullet}/M_{\odot}) < 8.0$ with a mean of $\langle \log(M_{\bullet}/M_{\odot}) \rangle = 5.0$ and the bulges have masses of $4.7 < \log(M_{\text{bulge}}/M_{\odot}) < 11.1$ with a mean of $\langle \log(M_{\text{bulge}}/M_{\odot}) \rangle = 7.9$. The resulting distribution of bulges including black holes is depicted in the 2-D histogram in Fig. 3.2. In this plot the number of objects N_{objects} is normalized to the maximum number of objects N_{max} found in a black hole-bulge mass bin. The observed M_{\bullet} - M_{bulge} -relation according to Häring & Rix (2004) is plotted together with the $1\text{-}\sigma$ -range of the applied scatter (solid and dashed black lines).

Initial Schechter distribution

Observationally, it is known that the mass function of bulges follows a Schechter function (e.g. Bell et al., 2003) rather than a log-normal distribution. Therefore, the scatter evolution of a Schechter-shaped initial distribution of bulge masses is studied. I use a fit to the measured luminosity function (K-band magnitude) for red galaxies at redshift $z \sim 2$ according to Cirasuolo et al. (2007) to construct the initial galaxy sample,

$$\Phi(M_k) = 0.4 \ln(10) \cdot \Phi^* \cdot 10^{-0.4\Delta M_k(\alpha+1)} \cdot \exp(10^{-0.4\Delta M_k}), \quad (3.3)$$

with the fitting parameters

$$\begin{aligned} \alpha &= -0.1 \\ M_k^* &= -23.04 \\ \Phi(10^{-3}\text{Mpc}^{-3}) &= 0.2 \end{aligned}$$

where M_k are the absolute magnitudes in K-band. The luminosity function is converted into a mass function using the mass-to-light ratios as function of the K-band magnitude according to Cappellari et al., 2006:

$$\begin{aligned} \frac{M}{L} &= 1.88 \cdot \left(\frac{L_k}{10^{10} \cdot L_{k,\odot}} \right) \quad \text{with} \\ M_k &= -2.5 \log L_k + 3.28 \end{aligned} \quad (3.4)$$

These mass-to-light ratios were measured for a population of ellipticals at $z = 0$ and for simplicity no evolution with redshift is assumed. A consequence of this assumption is, that I obtain quite massive galaxies at $z = 2$, although the stellar population was not evolved completely at this time. Probably, the mass-to-light ratio was smaller at higher z than the present-day value leading to smaller galaxy masses. However, for this work it is sufficient to see the evolution of statistical properties, which are independent of the exact choice of the mass-to-light ratio. The resulting mass distribution is scaled to a volume of $(500\text{Mpc})^3$ and the evolution of $\sim 100,000$ bulges with black holes is studied, considering only bulge masses larger than $1.6 \times 10^8 M_\odot$ ($\hat{=} \log(M_{\text{bulge}}/M_\odot) > 8.2$). To keep the Schechter-distribution for the bulge masses, a log-normal scatter of $\sigma = 0.6$ was only applied to the black hole masses (see Fig. 3.3).

3.3.2 Depletion scenario

For the fiducial random merging scenario (depletion case, i.e. without refilling the initial distribution with new galaxies), either the initial log-normal or Schechter distribution is used as described above. From the initial pool two objects are selected randomly, are merged by adding their black hole and bulge masses and the merged object is put back into the pool. In the next step, again, two objects are merged randomly, but now from the new rearranged pool. This procedure is repeated iteratively until, on average, every object has had one merger, i.e. only half of the initial objects are left over. At this point one merging generation is defined to be completed. Then all remaining objects are considered as the initial pool for the next generation. Therefore, after the first generation, $N(1) = N_{\text{ini}}/2$ objects are remaining and after the n -th generation the pool is reduced to $N(n) = N_{\text{ini}}/2^n$ objects. Note that in one generation some objects can have merged several times while others have not merged at all. Here and in the following, if not stated otherwise, the number of mergers is defined by counting all mergers that occur for galaxies $> 10^{4.7} M_\odot$ independent of their mass ratio.

Evolution of the black hole-bulge mass relation

If the galaxies are merged randomly from the initial log-normal or Schechter distribution in Fig. 3.2 and 3.3, an important consequence of the model is, as already pointed out by Peng (2007), that the sample behaves according to the *central-limit-theorem* (CLT). This theorem states that the mean of a sufficiently large number of independent random variables, each with finite mean and variance, will be approximately normally distributed. Therefore, for this case the theorem predicts that, independent of the initial distribution, the resulting distribution always converges towards a Gaussian distribution. This trend can already be seen after only one merging generation.

In Fig. 3.4, the evolution in the black hole-bulge mass plane of the log-normal distributed sample for merger generations $n = 1 - 8$ is shown. Again, the black solid line

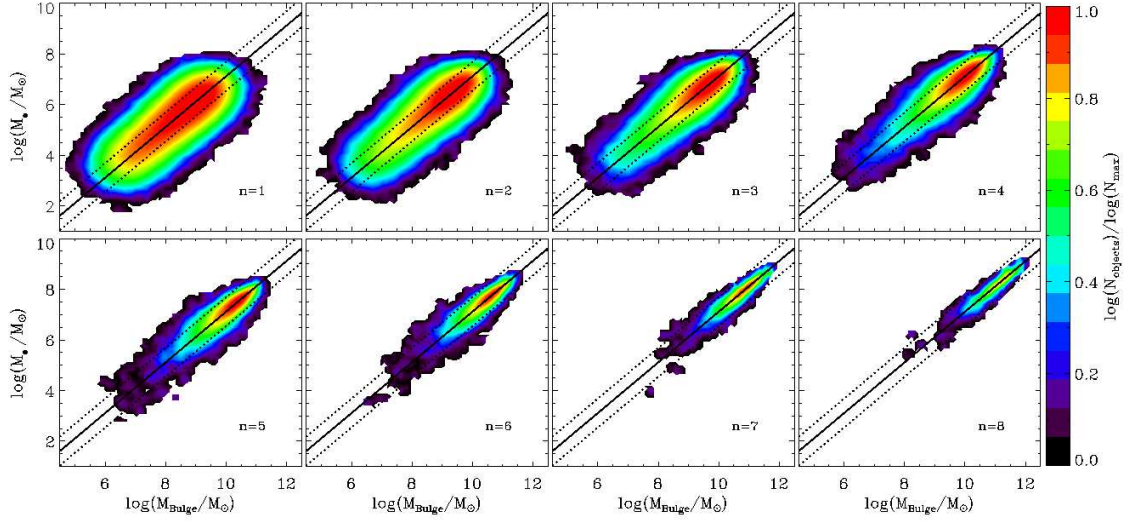


Figure 3.4: Normalized 2D-histograms for the random merging generations 1 – 8 on the basis of an initial log-normal distribution, as shown in Fig. 3.2 (depletion case). The fit to the observed relation is illustrated by the black, solid line; the black dotted lines show the $1 - \sigma$ range of the initially applied scatter.

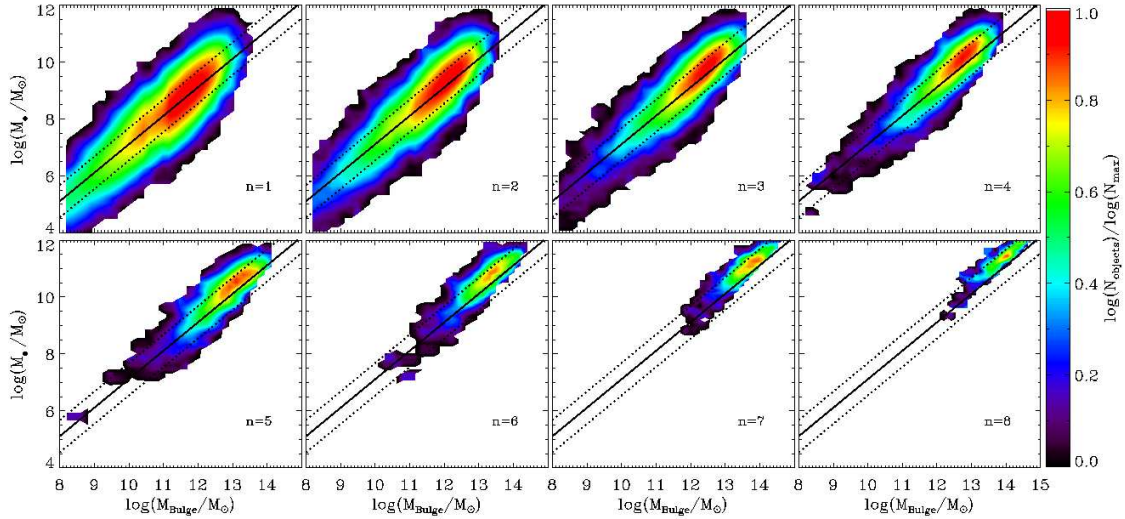


Figure 3.5: Same as Fig. 3.4, but for random merging with an initial Schechter-distribution resembling $z \sim 2$ red galaxies.

shows the observed, present day, M_{\bullet} - M_{bulge} -relation with the $1\text{-}\sigma$ range of the assumed $\sigma_{\text{ini}} = 0.6$ initial scatter. The relation is conserved during all merging generations. Note, however, that here the *same* initial scatter in black hole and bulge masses is used. In addition, the overall scatter decreases significantly with increasing merger generation. The low mass end of the distribution is depleted by merging whereas the high mass end is populated. Moreover, there is a clear trend that the scatter decreases more for more massive black holes and bulges than low mass systems.

The evolution of a randomly merging initial Schechter-distribution of bulges is shown in Fig. 3.5. In this case the overall slope increases for small merger generations. For high merger generations, when the low mass end is depopulated, the slope again becomes similar to the initial slope and the relation is shifted towards larger black hole masses. The reason for the change in tilt as well as the shift is the different initial scatter in black hole and bulge masses. The shift towards larger black hole masses shows that having such initial conditions of a larger scatter in black hole masses than in bulge masses is quite unlikely in order to explain the over-massive black holes at high redshift. However, qualitatively the scatter evolution is similar to the previous case. The scatter decreases with increasing merging generation and a quantitative scatter estimate is presented in the next Section 3.3.2. Note that the initially Schechter distributed bulges evolve into a log-normal distribution for massive systems as a consequence of the CLT. Still, this might not be a bad approximation for massive galaxies as, in principle, the Schechter distribution is a superposition of multiple Gaussians (Blanton et al., 2003).

Quantifying the scatter in the black hole mass relation

The scatter is characterized as the σ in a log-normal-like distribution:

$$f(x) = \frac{1}{\sigma\sqrt{2\pi}} \cdot e^{-\frac{(x-\mu)^2}{2\sigma^2}} \quad (3.5)$$

$$\text{with } x = \log(M_{\bullet}) \quad \text{and} \quad \mu = \langle \log(M_{\bullet}) \rangle.$$

Note that here the logarithm in base 10 'log' is used instead of the natural logarithm 'ln'. This, however, only changes the normalization. The 'log(M)' representation is chosen to be consistent with the observations (e.g. Tremaine et al., 2002, Gültekin et al., 2009). To estimate the scatter σ for the black hole mass in the evolution of the M_{\bullet} - M_{bulge} -relation (Fig. 3.4) I use the following method. For each merging generation the bulges are divided into different mass bins. Then for each bin black hole mass histograms are constructed which resemble normal distributions which are fitted with Eq. 3.5 to derive the scatter σ . This method is consistent with the scatter determination in observations (Gültekin et al., 2009). The fit is performed with a Levenberg-Marquardt-algorithm which interpolates between the Gauss-Newton algorithm and the method of gradient descent and searches iteratively for the best fit.

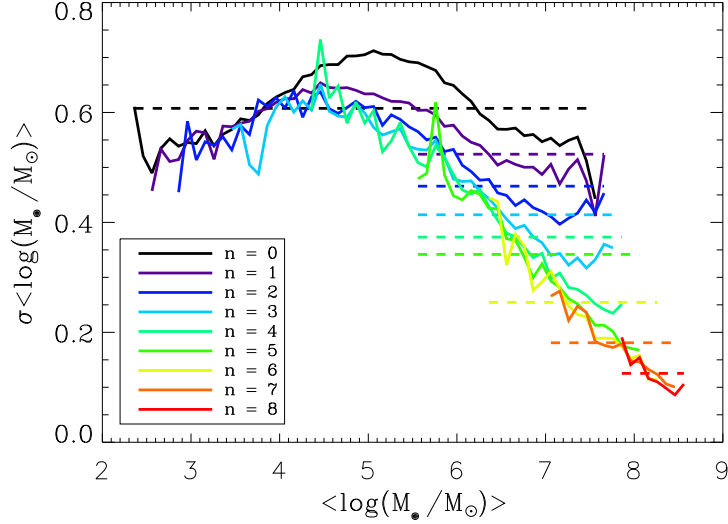


Figure 3.6: Scatter σ vs. mean black hole mass $\langle \log(M_{\bullet}/M_{\odot}) \rangle$ per bin for different merging generations n in the random merging model (depletion case, initial log-normal distribution). $n = 0$ is the initial distribution. The average values of σ for black hole masses higher than $10^5 M_{\odot}$ within one merging generation are shown by dotted lines. This shows a continuous decline in scatter with merger generation.

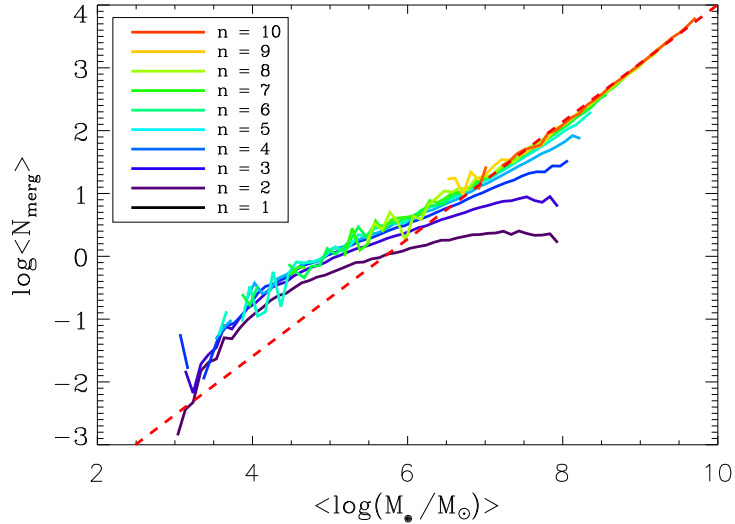


Figure 3.7: Black hole mass $\langle \log(M_{\bullet}/M_{\odot}) \rangle$ as a function of the mean number of merger $\langle N_{\text{merg}} \rangle$ for different merging generations n (depletion case, initial log-normal distribution). For higher generations n , $\log \langle N_{\text{merg}} \rangle$ correlates with $\langle \log(M_{\bullet}/M_{\odot}) \rangle$. The linear fit is shown by the dashed, red line.

Fig. 3.6 shows the scatter σ as a function of mean black hole mass $\langle \log(M_{\bullet}) \rangle$ per bin for the initial log-normal distribution ($n = 0$) and the eight subsequent merging generations ($n = 1..8$) indicated by different colors. For the initial distribution the scatter on average is $\sigma = 0.6$. However, it is not constant with mass as a log-normal distributed scatter has been applied to the bulge masses as well as the black hole masses. Higher merger generations show a decreasing average scatter for black hole masses larger than $10^5 M_{\odot}$ (indicated by the dashed lines) as well as a decrease in scatter for larger black hole masses within one merging generation. This indicates a strong correlation between the scatter, the black hole mass, and the merging generation.

In Fig. 3.7 the dependence of the mean number of mergers $\langle N_{\text{merg}} \rangle$ on the black hole mass $\langle \log(M_{\bullet}) \rangle$ is shown for the 8 different merging generations indicated by the colored lines. At the high mass end and for merger generations $n \geq 7$ there is a convergence towards a linear relation between black hole mass and mean number of mergers. The linear relation in Fig. 3.7 (red, dashed line) is given by:

$$\begin{aligned} \log \langle N_{\text{merg}} \rangle &= a \cdot \langle \log(M_{\bullet}/M_{\odot}) \rangle + b \\ \text{with } a &= 0.93 \quad \text{and} \quad b = -5.32. \end{aligned} \quad (3.6)$$

This relation suggests that after several merging generations n , it can be predicted, how many mergers a black hole of a certain mass must have experienced on average. E.g. a typical supermassive black hole of $10^8 M_{\odot}$ had about 100 mergers, taking into account all mergers which an object has had during its evolution (i.e. not only mergers in the main branch, but all progenitors in the tree since the first merging generation). Most importantly, in Fig. 3.8 the scatter σ is plotted versus the mean number of mergers $\langle N_{\text{merg}} \rangle$ within one bulge mass bin for the different merging generations (indicated by different colors). The decrease in the scatter with increasing merger number is an important consequence of the CLT. Hence, an analytic expression for the scatter decrease can be derived from the CLT for an initial normal distribution as a function of the merging generation n (Peng, 2007):

$$\sigma_{\text{merg}}(n) \approx \sigma_{\text{ini}} \cdot 2^{-n/2}, \quad (3.7)$$

where n is the generation number and σ_{ini} is the initial scatter applied to black hole and bulge masses. The mean number of mergers m of objects within one merging generation as a function of the generation number n can be written as

$$m = 2^n - 1, \quad (3.8)$$

Note, that for the calculation of the mean number of mergers all merger events are considered, which galaxies had undergone until this merging generation. With help of Eq. 3.8, Eq. 3.7 can be rewritten to get the scatter σ as a function of the mean number of mergers m :

$$\sigma_{\text{merg}}(m) \approx \sigma_{\text{ini}} \cdot (m + 1)^{-1/2}. \quad (3.9)$$

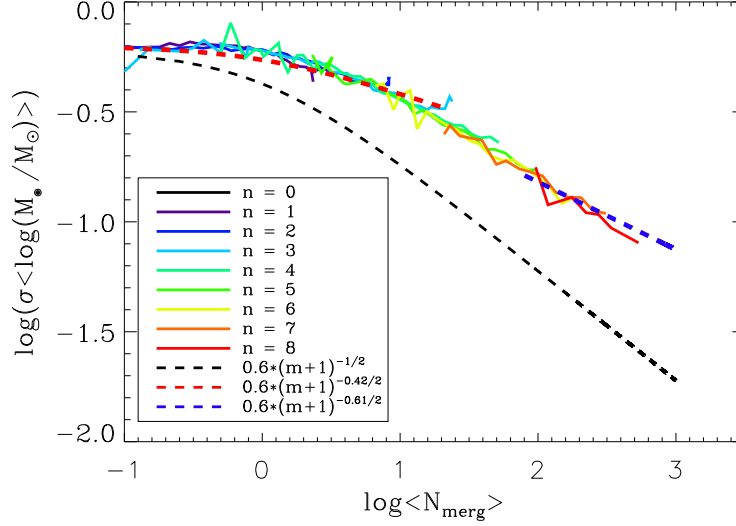


Figure 3.8: Scatter $\log(\sigma)$ vs. mean number of mergers $\log(\langle N_{\text{merg}} \rangle)$ for different merging generations n (depletion case, initial log-normal distribution). The black dashed line shows the analytic solution according to the CLT for an initial normal distribution. The blue dashed line is a fit to the scatter for $\langle N_{\text{merg}} \rangle > 100$, the blue one for $\langle N_{\text{merg}} \rangle < 10$.

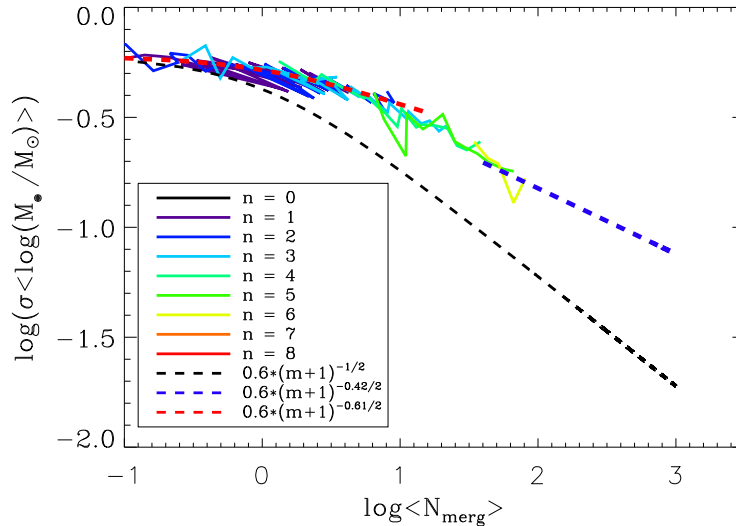


Figure 3.9: Same as in Fig. 3.8, but based on the initial Schechter-distribution at $z \sim 2$.

This analytic expression is depicted in Fig. 3.8 by the black dashed line. Thereby the assumption has been made that m (= mean number of mergers *per generation*) $\approx \langle N_{merg} \rangle$ (= mean number of mergers *per bulge mass bin* for one generation), which is a good approximation especially for high-mass objects. Note, that therefore it will not be distinguished between m and $\langle N_{merg} \rangle$. In comparison to merger results, the analytic solution exhibits a stronger decrease in scatter. This is due to the fact that the CLT makes predictions for the sum of *independent* random numbers, while, in this study, the pool is continuously changed by removing the merging objects and by adding the merged object. This means that the added black hole and bulge masses are not completely independent anymore leading to a violation of the CLT principle. Note that for merging using an unchanged pool, the scatter decrease of the distribution of merged objects does exactly follow the CLT prediction, resulting in a stronger scatter decrease. The red and blue dashed lines in Fig. 3.8 are a fit to the random merging data assuming a fitting formula similar to Eq. 3.9 with the exponent a as a free parameter,

$$\sigma_{merg}(m) \approx \sigma_{ini} \cdot (m + 1)^{-a/2}. \quad (3.10)$$

For the mass range of convergence, $\sim m > 100$, $a = 0.61 \pm 0.02$ (blue dashed line). The exponent a can therefore be used as a measure for the strength of the scatter decrease. For small merger numbers ($0 < m < 20$) a weaker scatter decrease is obtained with a value of $a = 0.42 \pm 0.02$ (red dashed line). This qualitatively different behavior of the scatter decrease depending on the merger number range will be explained in Section 3.3.2. If the initial scatter in black hole and bulge mass is varied, the same strength of scatter decrease is obtained within the errors, i.e. a remains unchanged. This was tested for two different initial scatter values $\sigma_{ini} = 0.40$ and 0.83 . Even if the value to which the scatter converges varies, the strength of the scatter decrease is the same ($a \sim 0.60 \pm 0.02$) in the limit of large m .

In Fig. 3.9 the same scatter quantification is presented for a more realistic initial Schechter distribution. Assuming convergence for $\sim m > 50$ or the region with merger numbers between $0 < m < 10$, a similar value for the exponent as for an initial log-normal distribution is obtained ($a = 0.61 \pm 0.02$ or $a = 0.42 \pm 0.02$, see Eq. 3.10). This indicates that the strength of the scatter decrease is only *weakly* dependent on the exact choice of the initial distribution. Again, varying the initial scatter in black hole and bulge mass does not influence the value a in the exponent for large m .

Difference between major and minor mergers

According to Peng (2007) there is a difference for objects with only major or only minor mergers. He claims that major mergers exhibit a stronger central-limit tendency leading to a stronger decrease of the scatter whereas minor mergers are mainly responsible for evolving a linear relation between bulge and black hole masses even if they are uncorrelated in the beginning. Going beyond the qualitative estimates in Peng (2007), here, a quantitative analysis of the scatter evolution is presented for major and minor

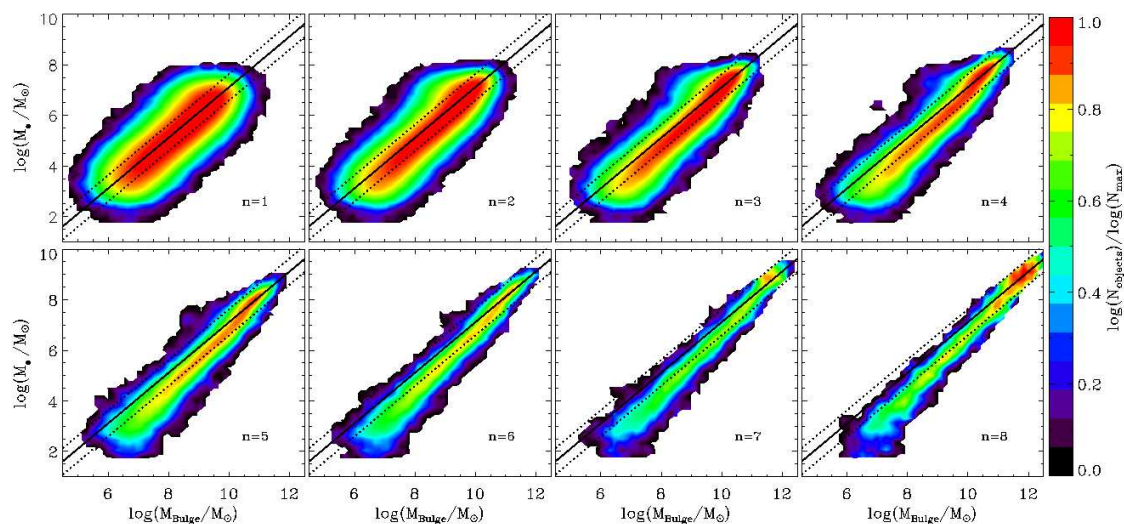


Figure 3.10: Same as Fig. 3.4, but galaxies had undergone only major mergers in the random merging model (depletion case).

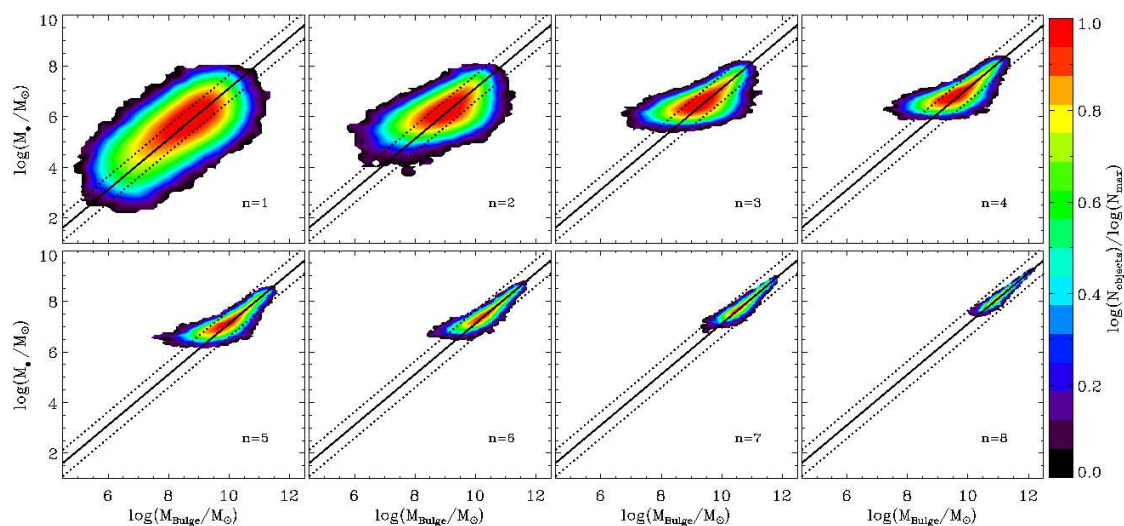


Figure 3.11: Same as Fig. 3.4, but galaxies had undergone only minor mergers in the random merging model (depletion case).

mergers. The following definitions are used:

$$\text{Major merger: } M_1/M_2 \leq 4, \quad M_1 > M_2 \quad (3.11)$$

$$\text{Minor merger: } M_1/M_2 \geq 10, \quad M_1 > M_2 \quad (3.12)$$

The definition for major mergers is consistent with Peng (2007). In Figs. 3.10 and 3.11 the evolution of the black hole-bulge mass relation is shown if only major or minor galaxy mergers are allowed, respectively, for an initial log-normal distribution. In both cases the relation is conserved, however, by construction, for minor mergers the low and intermediate mass range is depleted. The corresponding scatter quantification is shown in Fig. 3.12. Indeed, there is a difference between major and minor mergers; but in contrast to the results of Peng (2007) in the depletion case, a stronger decrease of the scatter for minor mergers ($a = 0.66$) is obtained than for major mergers ($a = 0.39$). However, Peng (2007) never calculated the quantitative scatter evolution, as it is done in this study, but showed for some exemplary objects, which had undergone many major mergers, that they seem to lie closer to the black hole-bulge mass relation than objects with less major mergers. This might explain the different statements of Peng's work and this one. This result, which is found in this chapter, at first glance seems to contradict the expectations of the CLT. However, it is important to note that here the change of the scatter of black hole masses is considered within individual bulge mass bins, and not over the whole population of bulge masses. During a merger generation a bulge mass bin has a constant influx and outflux of bulges due to mergers, which modifies the scatter behavior with respect to the CLT. Here, the scatter behavior for major and minor mergers was investigated in the over-all distribution of bulges. I find that when forcing galaxies to undergo only major mergers the scatter even *increases*, whereas for minor mergers, again, a scatter decrease is obtained as expected from the CLT. This shows that major mergers are a very strong constraint leading to a strong violation of the CLT principle and causing the slower scatter decrease in smaller mass bins. With this behavior an explanation can be deduced for the weak scatter decrease in the small merger number range and the stronger decrease in the limit of large merger number: the probability for having minor mergers is higher at the high mass end than for the low mass end, where major mergers dominate.

3.3.3 Replenishment scenario

From observations as well as from simulations it is known that new galaxies form during the structure formation process. To make the simple model more realistic different replenishment scenarios are now considered. Again, a certain initial number of objects N_{ini} is assumed with a log-normal or a Schechter distribution and the same iterative random merging procedure is performed as described in Section 3.3.2. However, the pool is now refilled after merger events with new objects from an external unchanged reservoir. The refill-ratio $N_{\text{new}}/N_{\text{event}}$ is defined to be the number of objects added from the refill pool N_{new} per number of merger events N_{event} within one merging generation. The definition of one merging generation is the same as before but after the n -th

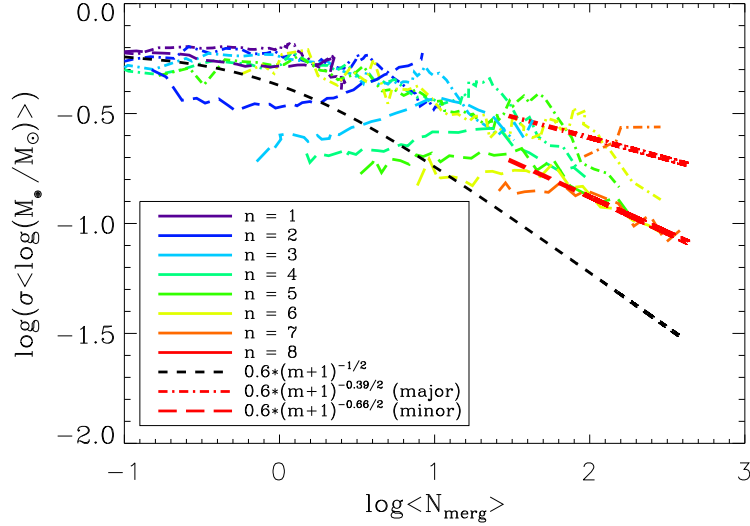


Figure 3.12: Scatter evolution for the depletion case as a function of mean number of merger for galaxies, which had either only major (dotted-dashed lines) or only minor mergers (dashed lines).

merging generation the sample always contains more than $N(n) = N_{ini}/2^n$ objects depending on the refill-ratio N_{new}/N_{event} . At first, a refill-ratio of $N_{new}/N_{event} = 1$ is assumed, i.e. for each merger event one new object is added randomly from the refill pool and the total number of objects in the sample stays constant. Moreover, also a refill-ratio of $N_{new}/N_{event} = 1/3$ is considered, i.e. one new object for every *three* events, motivated by Λ CDM simulations (see Section 3.4).

For the initial log-normal distribution, a refill pool is considered identical to the initial distribution as well as a pool of smaller mass galaxies with mean black hole masses $\langle \log(M_{\bullet}/M_{\odot}) \rangle \sim 3.3$ and the same initial scatter. For the initial Schechter distribution, either the initial Schechter distribution itself is used as a refill-pool or the Schechter distribution containing only bulges at the low mass end with $m_{bulge} = 1.58 \times 10^8 - 1.58 \times 10^{10} M_{\odot}$. The cases with smaller refill pools (lower galaxy masses) allow a more realistic comparison to the Λ CDM-simulations presented in Section 3.4. In total there are four different refill-scenarios which will be investigated in the following:

1. Refill-ratio 1:3 & initial mean (*Ini 1:3*)
2. Refill-ratio 1:3 & small mean (*Small 1:3*)
3. Refill-ratio 1:1 & initial mean (*Ini 1:1*)
4. Refill-ratio 1:1 & small mean (*Small 1:1*)

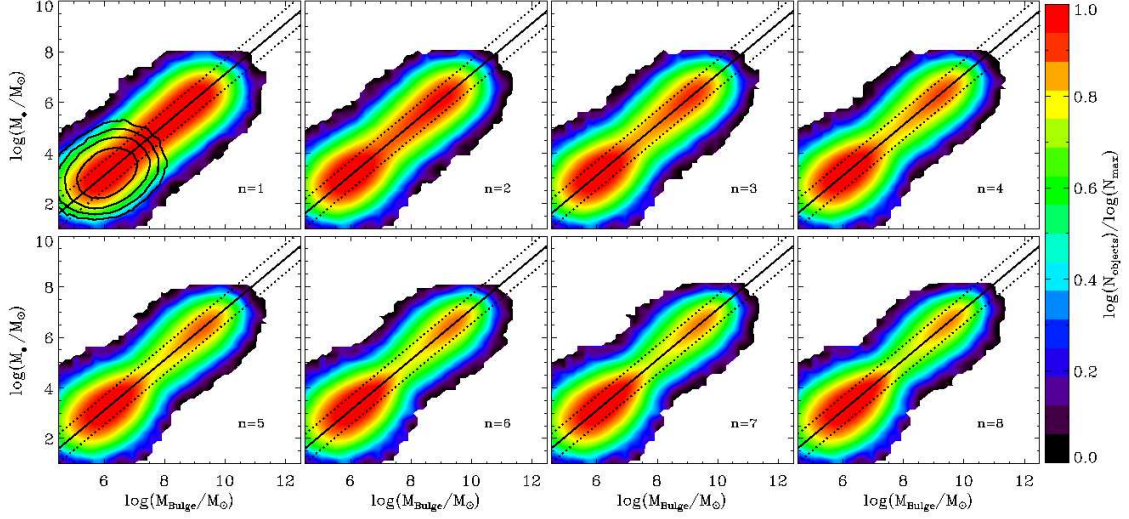


Figure 3.13: Same as Fig. 3.4, but for random merging (using an initial log-normal distribution) in the replenishment scenario with a refill-ratio of 1:1 and a low mass refill pool. The black contours in the first merging generation indicate the distribution of the unchanged refill-pool.

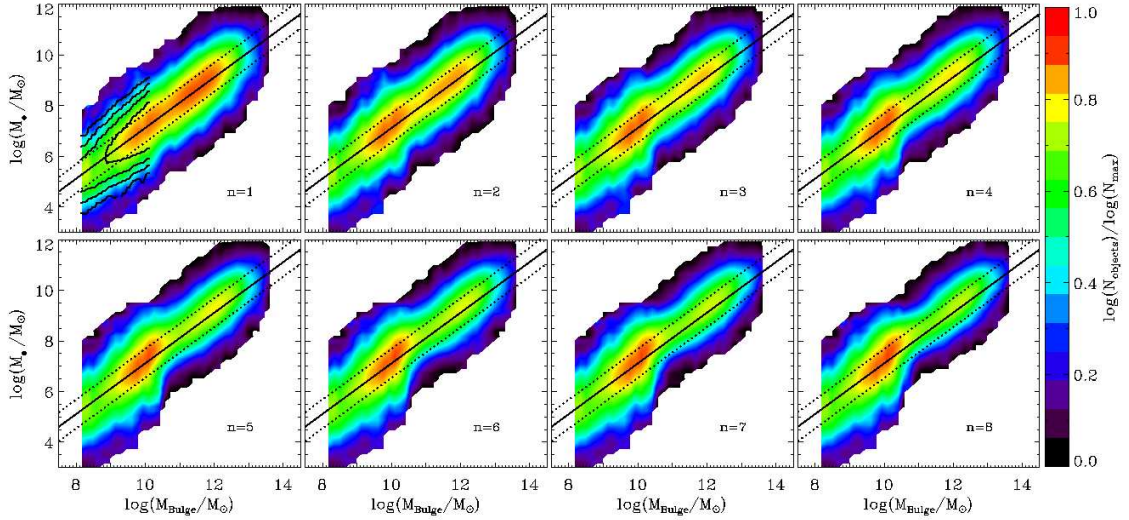


Figure 3.14: Same as Fig. 3.13, but for random merging (using an initial Schechter distribution) in the replenishment scenario with a refill-ratio of 1:1 and a refill pool of bulges with masses $10^8 M_\odot < M_{\text{bulge}} < 10^{10} M_\odot$. The black contours in the first merging generation indicate the distribution of the refill-pool.

Table 3.1: Values of the fit parameter a for the scatter decrease in different random merging models for a Schechter and a log-normal initial distribution in the limit of small ($0 < m < 20$) and large merger number ($100 < m$).

Ini. distr.	Depl.	Ini 1:3	Small 1:3	Ini 1:1	Small 1:1
Log-norm					
high m	0.61	0.60	0.51	0.55	0.31
small m	0.42	0.38	0.34	0.33	0.53
Schechter					
high m	0.61	0.56	0.50	0.56	0.32
small m	0.42	0.38	0.36	0.34	0.54

Evolution of the black hole-bulge mass relation

A general feature of all replenishment models is that the scatter in the M_{\bullet} - M_{bulge} -relation is again reduced with increasing merger number. However, compared to the depletion scenario, more merger generations are needed to reduce the scatter by the same amount. In other words, for the same merger generation the scatter decrease is weaker as new objects with a larger initial scatter are added. For small refill pools and large refill-ratios an interesting feature is found. Fig. 3.13 and Fig. 3.14 show the evolution of the relation for a refill-ratio of one and the small (low mass) refill pools (*Small 1:1*) for an initial log-normal and a Schechter distribution. The contours in the plot of the first random merging generation illustrate the distribution of the unchanged refill-pool. In both cases a double peak structure emerges. This is a consequence of using a low mass refill pool and a high refill-ratio. The low-mass peak reflects the appearance of new objects chosen from refill-distribution whereas the high mass peak evolves through merging from the initial distribution, similar to the simple case (Section 3.3.2). This behavior will be discussed in Section 3.4 in more detail.

Quantifying the scatter in black hole relations

In contrast to the depletion scenario, the replenishment models lead to a slower decrease of the scatter in black hole mass. The scatter quantification for the evolution of the M_{\bullet} - M_{bulge} -relation in Figs. 3.13 and 3.14 (refill-ratio 1, small mean and initial log-normal distribution or Schechter distribution) is shown in Figs. 3.15 and 3.16. The decrease of the scatter at low merger numbers originates from merging of new objects from the refill-pool mainly dominated by minor mergers whereas the decrease of the scatter at high merger numbers reflects merging at the high mass end (see Section 3.3.2), mainly dominated by major mergers. A stronger scatter decrease for small merger numbers ($a = 0.53$, red dashed line) is obtained than for the large merger numbers ($a = 0.31$, blue dashed line), since the probability for having minor mergers is higher at the small merger number end.

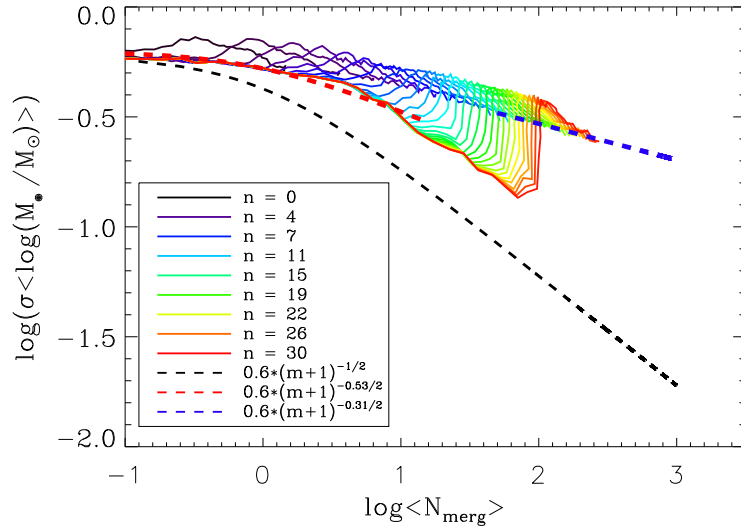


Figure 3.15: Same as in Fig. 3.8, but for a replenishment scenario with a refill-ratio of 1, a refill-pool with a small mean and an initial log-normal distribution. The 'spike' near $\log \langle N_{\text{merg}} \rangle = 2$ is due to the bimodality as discussed in the text.

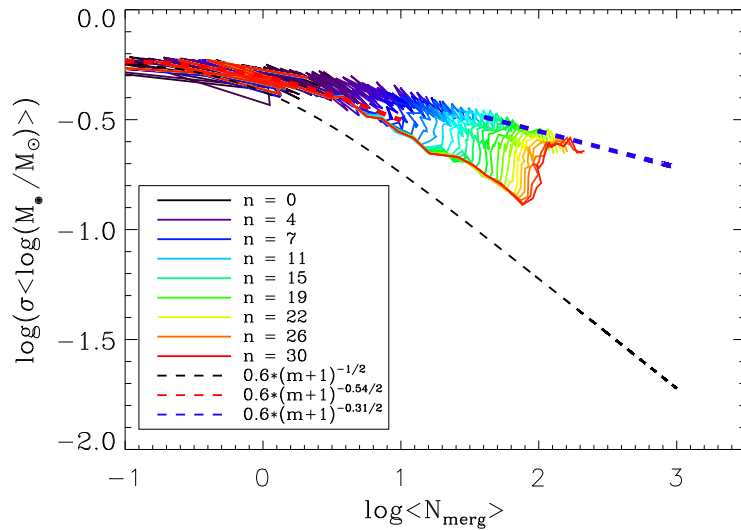


Figure 3.16: Same as in Fig. 3.15, but for a replenishment scenario with a refill-ratio of 1, a refill-pool with a small mean and an initial Schechter distribution.

Table 3.2: Values of the fit parameter a for scatter decrease in different random merging models for either only major or only minor mergers based on an initially log-normal distribution in the limit of large merger numbers ($m > 100$).

	Depl.	Ini 1:3	Small 1:3	Ini 1:1	Small 1:1
Major	0.39	0.50	0.43	0.54	0.15
Minor	0.66	0.65	0.59	0.59	0.30
All	0.61	0.60	0.50	0.55	0.30

The influence of refill-ratio and refill-pool is analysed and the scatter evolution resulting from the four different replenishment models is summarized in table 3.1 for an initial log-normal and an initial Schechter distribution. The typical errors are ± 0.02 . The larger the refill-ratio, the more slowly the scatter decreases. Keeping in mind that a larger refill-ratio corresponds to a larger number of new objects added per merger generation, this behavior can be explained as follows. New objects from the refill-pool have a large *initial* scatter in black hole mass, in contrast to objects after several merging generations, whose scatter has already decreased. Therefore, the more objects are added to the sample, the less the scatter decreases with merging generation. In addition, the lower the typical mass of objects in the refill pool, the more slowly the scatter decreases in the limit of large merger numbers. That means that for large merger numbers, the probability for having major mergers gets higher when using a low mass refill-pool. However, for low merger numbers the scatter decreases more rapidly with a low mass refill-pool. In this range, minor mergers become more likely because of the low-mass refill-pool, leading to a stronger scatter decrease than in the major merger dominated region (i.e. convergence region of large merger numbers). Altogether, a small-mass refill-pool leads to a higher probability of having minor mergers in the small merger number region than at the limit of large merger numbers, where major mergers dominate. Furthermore, as shown in table 3.1, the choice of the initial distribution does not change the scatter decrease a (for small as well as large m). This is expected from the CLT as the distribution quickly evolves into a normal distribution no matter which initial distribution is used.

Difference between major and minor mergers

Since Peng (2007) considered in his study a replenishment scenario with a refill ratio of $N_{\text{new}}/N_{\text{event}} = 1$ using the initial distribution as the refill pool, I will also investigate the difference between major and minor mergers for different replenishment models. The fitted slopes for the scatter evolution for major and minor mergers are summarized in table 3.2 with an error of about ± 0.02 . Note that for the case of a refill-ratio of 1 : 1 with a low-mass refill-pool, a larger error of about ± 0.05 is obtained, since here the black hole mass histograms are not fitted well by a Gaussian function anymore. As in

the depletion case (see Section 3.3.2) a stronger scatter decrease for galaxies undergoing only minor mergers can be seen than for major mergers. One can argue as above that this deviation from the CLT is most likely due to dividing the bulge masses in different mass bins which suffer a constant influx and outflux from bulges during each merger generation. And furthermore, forcing galaxies to undergo only major mergers is a very strong constraint leading to a violation of the CLT.

3.4 Comparison to merging in Λ CDM-Simulations

So far, the influence of different idealized random merging models on the evolution of the M_{\bullet} - M_{bulge} -relation and the corresponding scatter in black hole mass has been discussed. In this Section, a more complex and astrophysically motivated model is investigated based on merger trees from dark matter simulations following structure formation in a Λ CDM universe.

3.4.1 Simulation setup

Here, a simulated, comoving periodic box with $L = 100$ Mpc box length and 512^3 particles is used performed with the GADGET2 code (Springel et al., 2005a). For this simulation a Λ CDM cosmology was assumed based on the WMAP3 (see e.g. Spergel et al. (2003)) measurements with $\sigma_8 = 0.77$, $\Omega_m = 0.26$, $\Omega_{\Lambda} = 0.74$, and $h = H_0/(100 \text{ kms}^{-1}) = 0.72$ (see also Moster et al. (2010) for a first analysis of this simulation). The simulation was started at $z = 43$ and run until $z = 0$ with a fixed comoving softening length of $2.52 h^{-1}\text{kpc}$. Starting at an expansion factor of $a = 0.06$ there exist halo catalogues for 94 snapshots until $z = 0$ separated by $\Delta a = 0.01$ in time. The mass of one dark matter particle is $2 \times 10^8 M_{\odot}/h$.

3.4.2 Merger tree algorithm

The merger trees of the dark matter component are constructed as follows: For every snapshot, one has to identify the different dark matter haloes. In a first step Friends-of-Friends (FOF) groups are defined using a FOF algorithm with a linking length of $b = 0.2$ ($\approx 28\text{kpc}$, Davis et al., 1985). In a second step, subhaloes of every FOF group are extracted using the SUBFIND algorithm (Springel et al., 2001b). This halofinder identifies over-dense regions and removes gravitationally unbound particles. This way, the FOF group is split into a main or host halo and its satellite halos. In most cases, 90% of the total mass is located in the main halo.

The sizes and virial masses of the main halos (i.e. the most massive SUBFIND halos) are determined with a spherical over-density criterion. The minimum halo mass is set to 20 particles ($4 \times 10^9 M_{\odot}/h$). In the following, *isolated* merger trees are used which are constructed only for the the main halos, i.e. the central objects of one FOF group identified by SUBFIND. The dark matter mass of a central object is defined by the dark matter mass within the virial radius. The over-density approximation in the spherical

collapse model is used according to Bryan & Norman (1998). The algorithm to connect the dark matter halos between the snapshots is described in detail in Maubetsch et al. (2007). The branches of the trees for $z = 0$ halos are constructed by connecting the halos to their most massive progenitors (MMP) at previous snapshots. Thereby, halo j with n_j particles at redshift z_j with the maximum probability $p(i, j)$ is chosen to be a MMP of halo i containing n_i particles at redshift z_i (where $j < i$ and $z_j > z_i$). The probability $p(i, j)$ is defined as

$$p(i, j) = \frac{n_{ov}(i, j)}{n_{max}(i, j)} \quad \text{with} \quad (3.13)$$

$$n_{ov} = n_i(z_i) \cap n_j(z_j) \quad \text{and}$$

$$n_{max}(i, j) = \max(n_i(z_i), n_j(z_j))$$

Here, n_{ov} is the number of particles found in both halos and n_{max} is the particle number of the larger halo. 'Fake' haloes are removed which exist only within one time-step and have no connection to any branch (close to the resolution limit). The low redshift ends of the branches are then checked for mergers. A halo j is assumed to merge into halo i , if at least 50% of the particles of halo j are found in halo i . In case of a merger the branches are connected. For a proper connection, the 'split'-algorithm (Genel et al., 2009) is applied to prevent double or multiple counting of merger events within a tree. The 'split' algorithm was shown to produce more reliable merger rates which is also important for this work.

3.4.3 Evolution of the relation between black hole and galaxy mass

Two different possibilities are considered in order to populate dark matter haloes with black holes and bulges. Either black hole masses or bulge masses are directly applied to dark matter halos and the corresponding missing quantity is calculated using the the black hole-bulge mass relation in Häring & Rix (2004).

Using a M_\bullet - M_{DM} -relation

Ferrarese (2002) proposed a relation between the mass of the central black hole M_\bullet and the mass of the dark matter halo M_{DM} of the form

$$\frac{M_\bullet}{10^8 M_\odot} \sim 0.1 \cdot \left(\frac{M_{DM}}{10^{12} M_\odot} \right)^{1.65}. \quad (3.14)$$

I want to point out that only the M_\bullet - M_{bulge} -relation is directly observable and therefore, assumed to be more fundamental than the M_\bullet - M_{DM} -relation. Furthermore, in a very recent study of Kormendy & Bender (2011), they showed observationally that the black holes seem not to correlate with dark matter halos, in particular at the low mass end. However, the M_\bullet - M_{DM} -relation has been supported by e.g. recent results of Booth

& Schaye (2009), where the authors obtain a similar relation between black hole and dark matter halo mass using numerical simulations (GADGET III) with self-consistent black hole growth, which are tuned to match the relations between black hole mass and galaxy stellar properties. Furthermore there are observations from Croom et al. (2007); Yu & Lu (2008) and White et al. (2008), which confirm the existence of a relation between black hole and dark matter halo mass, what may justify the use of this controversial relation in this Chapter. However, this relation is only valid for $z = 0$. Since here the black holes are seeded at higher redshift, expression Eq. 3.14 is modified in order to maintain the relation at $z = 0$. The same derivation is assumed as it is described in Ferrarese (2002). Therefore, first the virial velocities v_{vir} are assumed from the simulations calculated by SUBFIND. This way v_{vir} can be obtained as a function of M_{DM} and redshift z . Assuming that $v_{vir} \approx v_c$ then the relation between circular velocity v_c and velocity dispersion σ_c is used and the one between velocity dispersion σ_c and black hole mass M_\bullet . So equation 3.14 can be rewritten:

$$M_\bullet = 3.12 \times \left(\frac{v_c(M_{DM}, z)^{1.19}}{200 \text{ km/s}} \right)^{4.58} 10^5 M_\odot \quad (3.15)$$

Note, that the relation between circular velocity v_c and velocity dispersion σ_c is derived from observations of spiral galaxies at $z = 0$. Presumably at higher redshifts dissipation of baryons has a higher influence than for $z = 0$. This could lead to larger velocity dispersions and therefore also to larger black hole masses. According to relation 3.15 halos can be populated with masses extracted from the dark matter simulations with central supermassive black holes. As massive galaxies are of major interest, where gas physics is assumed to be less important (at least at low redshifts e.g. Dekel & Birnboim, 2008; Naab et al., 2006b; Khochfar & Silk, 2009), only merger trees have been investigated starting at $z = 3$ for halos more massive than $10^{12} M_\odot$ at $z = 0$. At the high redshift end of every branch starting at $z = 3$ the most massive progenitors of the selected $z = 0$ halos are populated with black holes according to Eq. 3.15. Additionally, a log-normal distributed scatter is added to the black hole masses with $\sigma_{ini} = 0.6$ (see Section 3.3). For the subsequent growth of the black holes, only dark matter halo mergers and the corresponding mergers of their black holes are taken into account.

To allow for a comparison with the random merging cases shown previously, the evolution of the $M_\bullet - M_{bulge}$ -relation is shown in Fig. 3.17. Black holes in dark matter haloes have been chosen according to Eq. 3.15 and then corresponding bulge masses have been calculated by taking the median relation of Häring & Rix (2004). Once the dark halos have been populated with these bulge masses, a scatter of $\sigma = 0.6$ has been applied to the black hole masses for each bulge mass. Again, the growth process is followed only via merger events. The high mass end of the relation is shifted towards larger black hole masses as only an initial scatter to black hole masses has been applied but not to the bulge masses. Similar to the simple models investigated before again the scatter decreases with time. Moreover, a double peak structure can be seen at low redshifts $z < 0.4$ similar to the replenishment random merging model with a low mass

refill pool (Section 3.3.3). This is a consequence of the conditional mass function. Only halos were investigated under the condition that they merged into $z = 0$ halos with masses larger than $10^{12}M_{\odot}$ (see e.g. Somerville et al., 2000).

Using a galaxy population model

Alternatively, to populate dark matter halos with black holes, a fitting function can be used that relates host dark halo masses to stellar masses of galaxies to assign to every dark matter halo mass a galaxy stellar mass. There exist many studies which link the distribution of galaxies to that of dark matter halos (van den Bosch et al., 2003, 2007; Mandelbaum et al., 2006; Moster et al., 2010; Guo & White, 2009). Here, the fitting formula from Moster et al. (2010) is taken. They assume that every host halo contains exactly one central galaxy and - as a constraint from the observed galaxy mass function - that the stellar mass to dark matter halo mass ratio M_*/M_{DM} first increases with increasing mass, reaches a maximum and then decreases again. Hence Moster et al. (2010) adopt the following parametrization, similar to the one used in Yang et al. (2003):

$$\frac{M_*(M_{DM})}{M_{DM}} = 2 \left(\frac{M_*}{M_{DM}} \right)_0 \left(\left(\frac{M_{DM}}{M_1} \right)^{-\beta} + \left(\frac{M_{DM}}{M_1} \right)^{\gamma} \right)^{-1} \quad (3.16)$$

Basically, this parametrization is set to reproduce many observations, as the galaxy mass function or clustering. Choosing a redshift parametrization for each of the parameters in Eq. 3.16, they can predict the galaxy to dark matter mass ratio at any redshift:

$$\log M_1(z) = \log M_0 \cdot (z + 1)^{\mu} \quad (3.17)$$

$$\left(\frac{M_*}{M_{DM}} \right)_0(z) = \left(\frac{M_*}{M_{DM}} \right)_{z=0} \cdot (z + 1)^{\nu} \quad (3.18)$$

$$\gamma(z) = \gamma_0 \cdot (z + 1)^{\gamma_1} \quad (3.19)$$

$$\beta(z) = \beta_1 \cdot z + \beta_0 \quad (3.20)$$

with $\log M_0 = 11.88$, $\mu = 0.019$, $(M_*/M_{DM})_{z=0} = 0.0282$, $\nu = -0.72$, $\gamma_0 = 0.556$, $\gamma_1 = -0.26$, $\beta_0 = 1.06$ and $\beta_1 = 0.17$.

To populate the galaxies with black holes, it is assumed for simplicity that all stars are in the spheroidal component of the galaxy ($M_* \approx M_{\text{bulge}}$). Using the M_{\bullet} - M_{bulge} -relation (Häring & Rix, 2004), to each galaxy mass a black hole mass is applied with the same initial scatter as already used before ($\sigma = 0.6$). If then the growth of black holes and galaxies is taken into account through merging according to the Λ CDM-simulations, an evolution of the M_{\bullet} - M_{bulge} -relation is obtained as shown in Fig. 3.18. Again, the same effect can be seen as already described in Section 3.4.3: a decreasing scatter with time together with an evolving double peak structure.

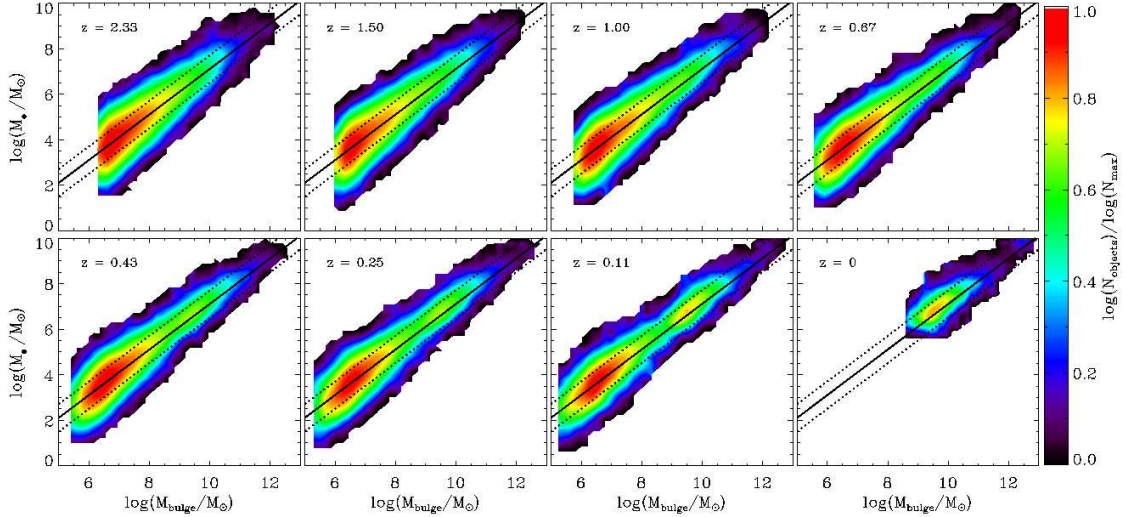


Figure 3.17: Evolution of the M_{\bullet} - M_{bulge} -relation through merging only in Λ CDM-simulations using M_{\bullet} - M_{DM} -relation.

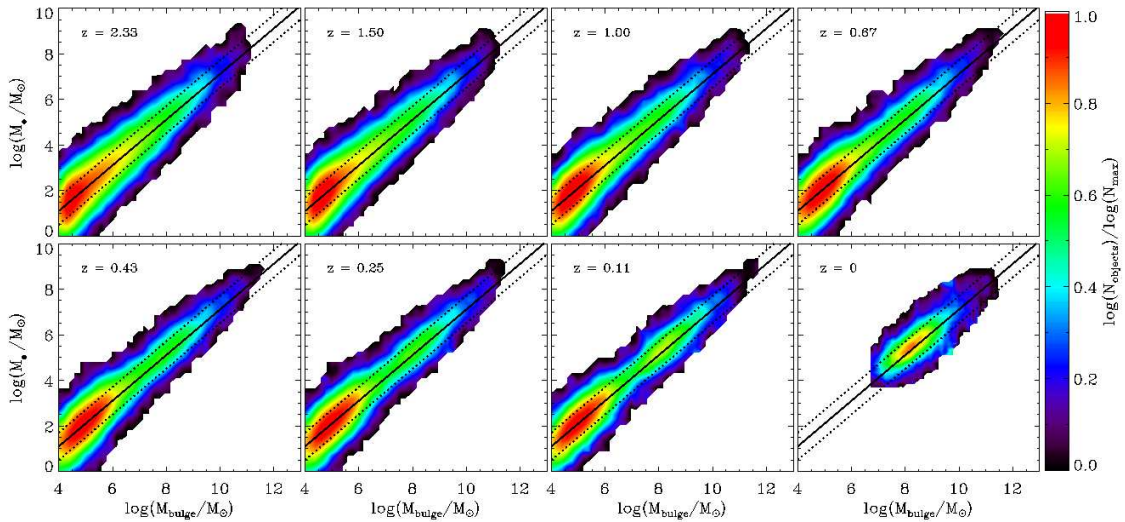


Figure 3.18: Evolution of the M_{\bullet} - M_{bulge} -relation through merging only in Λ CDM-simulations using a galaxy population model (Moster et al., 2010).

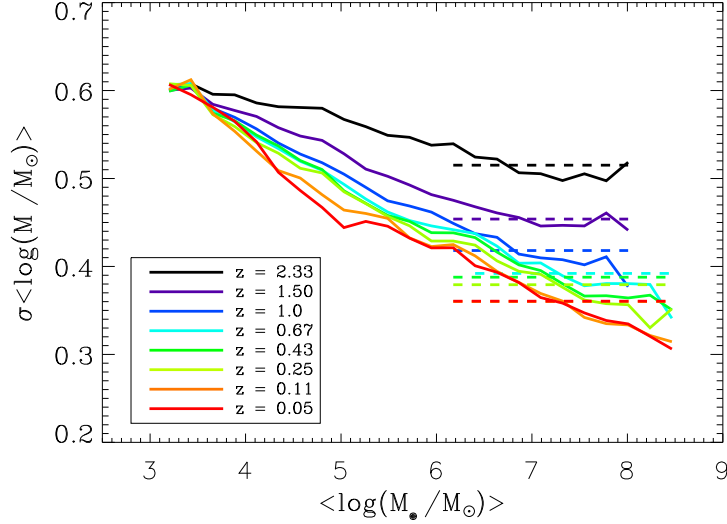


Figure 3.19: Scatter in black hole mass versus mean black hole mass $\langle \log(M_{\bullet}/M_{\odot}) \rangle$ at different redshifts (different colors) in the Λ CDM-simulation assuming black hole seeding according to the M_{\bullet} - M_{DM} -relation. The horizontal lines indicate the average scatter for black holes more massive than $\approx 10^6 M_{\odot}$. The scatter for massive black holes continuously decreases towards lower redshifts.

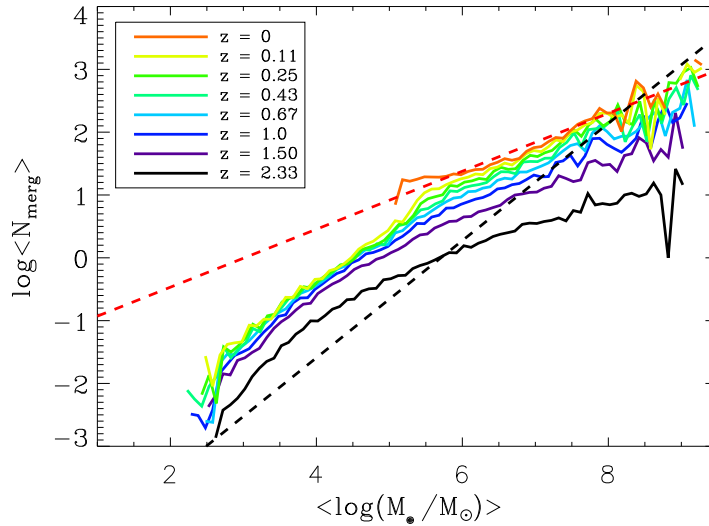


Figure 3.20: Relation between mean black hole mass $\langle \log(M_{\bullet}/M_{\odot}) \rangle$ and mean number of mergers $\log \langle N_{\text{merg}} \rangle$ at different redshifts (different colors) in the Λ CDM-simulation assuming black hole seeding according to the M_{\bullet} - M_{DM} -relation. The best fit at $z=0.05$ is indicated by the red dashed line. For comparison the dashed black line indicates the best fit for the random merging depletion model (Fig. 3.7).

3.4.4 Quantifying the scatter in the black hole mass relation

For the evolution of the M_{\bullet} - M_{bulge} -relation shown in Fig. 3.17 (the model based on the relation between dark halo mass and black hole mass) the same scatter quantification was performed as before for the different random merging models. Fig. 3.19 shows the evolution of the scatter in black hole mass. At the high mass end, which I am focusing on here, the scatter decreases towards lower redshift. Furthermore - similarly to random merging - in Fig. 3.20 there is a convergence towards a linear relation between the logarithm of the mean number of mergers and the logarithm of black hole mass at low redshift. This relation is fitted according to

$$\log\langle N_{\text{merg}}\rangle = a \cdot \langle \log(M_{\bullet}/M_{\odot})\rangle + b \quad (3.21)$$

with $a = 0.46$ and $b = -1.39$.

shown by the red dashed line in Fig. 3.20. For comparison the dashed black line illustrates the random merging case (depletion). As expected lower mass black holes ($M_{\bullet} < 10^8 M_{\odot}$) experience more mergers than predicted for the simple depletion case, whereas at the high mass end galaxies undergo less mergers than in the depletion model.

Finally the scatter σ is plotted as a function of the mean number of mergers $\langle N_{\text{merg}}\rangle$ in Fig. 3.21. The same qualitative behavior is found as for all random merging models. The scatter decreases with increasing number of merger events. However, the scatter decrease in Λ CDM-merging is weaker. The fit parameter $a = 0.30 \pm 0.03$ is smaller than for most of the random merging models at the limit of large merger numbers. Note that for the case where black holes are assigned to dark matter halos using the galaxy population model, as described in Section 3.4.3, the same qualitative scatter behavior is obtained. The only difference is that because there are fewer objects at the high mass end, the resulting scatter value is connected with a larger error than for the black hole population described in Section 3.4.3. In comparison to the best-matching random merging scenario - a refill-ratio of 1/3 and a low-mass refill-pool - Λ CDM-merging leads to a clear difference in the scatter decrease ($a = 0.51 \pm 0.02$). However, in the case of Λ CDM-merging there is only a maximum number of mergers of ~ 60 . Therefore, the scatter decrease in CDM-merging is consistent with the best-matching random merging model only in the low merger range ($a = 0.34 \pm 0.02$), indicated by the blue, dashed line. This shows that the scatter evolution in Λ CDM-merging can be well approximated - quantitatively and qualitatively - by the simple model of random merging without any structure formation model.

3.4.5 Evolution of the black hole mass function

In this Section, the evolution of the black hole mass function is investigated in the merger-driven model to test, if merging as only growth channel provides an adequate description for black hole formation. Fig. 3.22 shows the black hole mass function for different redshifts (different colors) assuming an initial log-normal scatter in black

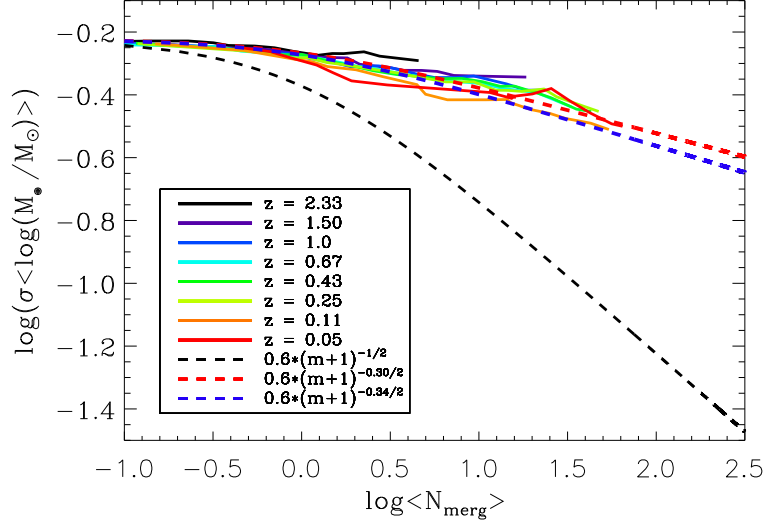


Figure 3.21: Scatter $\log(\sigma)$ as a function of mean number of mergers $\log\langle N_{\text{merg}}\rangle$ at different redshifts in the Λ CDM-simulation assuming black hole seeding according to the M_{\bullet} - M_{DM} -relation. The red dashed line corresponds to the fit to the scatter for Λ CDM merging. The blue dashed line shows the fit to the best-matching random merging model (refill-ratio 1/3 and low-mass refill-pool), the black dashed line illustrates the analytic case.

hole mass at $z = 3$ and a growth of black holes only via mergers. The solid lines indicate the evolution of the black hole mass function assuming seeding according to the M_{\bullet} - M_{DM} -relation (Ferrarese, 2002) and the dashed lines show the black hole mass function based on the galaxy population model of Moster et al. (2010). In the left panel the local observed black hole mass function (black triangles) is shown derived from correlations between black hole mass and bulge luminosity or stellar velocity dispersion (Marconi et al., 2004). This is in disagreement with the $z = 0$ model prediction (red line), since black hole masses are underestimated. This implies that growth by gas accretion might be an important contribution to the overall formation process of black holes and should not be neglected. Furthermore, if we seed the black holes only at $z = 1$, the disagreement with observations is - as expected - less pronounced than for $z = 3$ -seeding. But again, the black holes are not massive enough to reproduce the observations. This shows that even from $z = 1$ till $z = 0$ merging only seems to be an insufficient description for black hole growth. However, it should be pointed out most importantly that in this Chapter it is *not* the primary aim to fit the present-day black hole mass function. In fact it shall be shown how the scatter evolution in black hole mass would be affected by merger events only. The possible influence of additional gas physics will be discussed in the next Section.

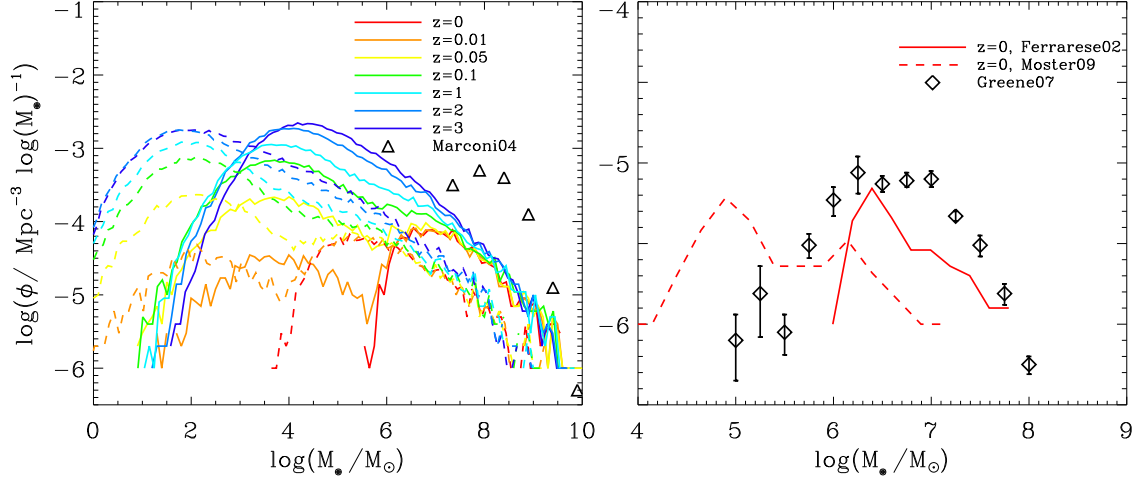


Figure 3.22: *Left: Evolution of the black hole mass function through Λ CDM-merging using the M_\bullet - M_{DM} -relation (solid lines) and using the galaxy population model (dashed lines). The triangles correspond to the local black hole mass function according to Marconi et al. (2004). Right: Same as in the left panel, but only for $z = 0$. However, only objects are considered, that had undergone a merger event within the last 100×10^6 yrs with a merger ratio smaller than 1 : 10. The diamonds show the observed, present-day black hole mass function for active galaxies (Greene & Ho, 2007).*

The right panel of Fig. 3.22 shows the black hole mass function for the two different seeding mechanisms only at $z = 0$. However, here only galaxies have been considered that have undergone a merger with a merger ratio smaller than 1 : 10 in the last 100×10^6 yrs. Therefore, they can be assumed to be in the active phase during this time. These results deviate from observed values of the present-day black hole mass function for a sample of active galaxies (8500 objects from SDSS DR4, Greene & Ho, 2007). On the one hand, this could be a consequence of under-predicting the overall black hole mass function as shown by the left panel, assuming the correct number of merger events. Alternatively, it might imply that merger events are not frequent enough to give an explanation for observed active galaxies and accretion is needed even without any merger event. However, assuming that also lower mass ratios ($< 1 : 100$) can trigger the activity of galaxies, a good agreement can be obtained with observations. Also raising the time for one duty cycle would lead to a better consistence with observations. This could be justified by the fact that within the assumed time for one duty cycle there could exist more active objects if *galaxy* mergers would be considered, which happen later in time than mergers of isolated dark matter halos (which are taken into account in this study).

3.5 Discussion and conclusions

In this Chapter, the evolution of the intrinsic scatter in black hole mass was investigated under the assumption that the black holes only grow by mergers with other black holes during galaxy mergers. For many different idealized random merging models with (replenishment) and without (depletion) refilling from an external galaxy pool, the following general results can be stated:

1. The evolution of the black hole distribution can be well described within the framework of the central limit theorem (CLT). Independent of the initial distributions, e.g. log-normal or Schechter, of black holes the distribution always evolves into a normal distribution after a few merger generations. All mergers are considered independent of the mass merger ratio that galaxies with masses $> 10^{4.7} M_{\odot}$ experience.
2. For all random merging models a decreasing scatter σ was found with increasing merging generation n and with increasing merger number m . As a consequence of the mass built-up during the merger events the scatter also decreases with increasing black hole mass. Motivated by the CLT, the scatter dependence on the mean number of mergers can be approximated by

$$\sigma_{\text{merg}}(m) \approx \sigma_{\text{ini}} \cdot (m + 1)^{-a/2}. \quad (3.22)$$

Here, the exponent a is a measure of the strength of the scatter decrease. For the different random merging models I find $0.30 < a < 0.61$ for a large number of mergers ($m > 100$) independent of the initial scatter applied to black hole and bulge masses. In general, replenishment models show a weaker scatter decrease.

3. Considering either only major or only minor mergers for galaxy growth, minor mergers are found to lead to a much stronger scatter decrease than major mergers; hence the smaller the mass ratio of merger events, the more rapidly the scatter decreases. This is in contrast to findings of Peng (2007) because they have not investigated the scatter decrease in black hole explicitly and quantitatively as in this chapter.
4. For different replenishment models, the higher the refill-ratio and the smaller the typical mass of black holes in the refill-pool is, the more slowly the scatter decreases.

Studying the effect of merging according to current structure formation models in Λ CDM-simulations, a qualitatively similar behavior is found. The scatter decreases with the number of mergers ($a = 0.3$), and as a consequence it also decreases with cosmic time. This finding is quantitatively consistent with the best-matching random merging model (refill-ratio 1/3 and low mass refill-pool) at least for the limit of the low merger number range ($a = 0.34$), since in Λ CDM-merging the most massive galaxies

experience only $\sim 50 - 60$ merger events. Therefore, the scatter evolution in Λ CDM-merging can be well approximated by a simple model assuming random merging of galaxies.

From the above results, some implications can be drawn about recent observations of high redshift black holes:

- For a simple merger driven growth of black holes it can be predicted that the scatter in black hole mass must have been larger at higher redshift. Assuming an initial scatter of 0.6 at $z = 3$ the over-massive black holes investigated by Schramm et al. (2008), Peng et al. (2006) and McLure et al. (2006) would be within the $2 - \sigma$ range of this large initial scatter. If these objects had on average $50 - 60$ dry merger events then the present-day scatter value of ~ 0.31 can also be obtained for massive ellipticals (Gültekin et al., 2009). This shows that the observations of over-massive black holes at high redshifts are consistent with a population of galaxies that has a large scatter in black hole mass (~ 0.6) at high redshifts being reduced through subsequent merging.
- A further important advantage of this model is that not only over-massive black holes at high redshifts can be explained, but it can be also accounted for the observed under-massive black holes at $z = 2$ (Alexander et al., 2008; Shapiro et al., 2009). These objects would be lying within the $2 - \sigma$ range of the scatter at $z = 2$ ($\sigma \approx 0.5$) assuming an initial scatter of 0.6 at $z = 3$. Here, I want to point out, that models assuming an evolution of the $M_{\bullet} - M_{\text{bulge}}$ relation (from higher towards lower black hole masses with decreasing redshift) can be an explanation for over-massive black holes at high redshifts, but *not* for the observed under-massive ones.
- The scatter evolution of model predictions from GALFORM (Malbon et al., 2007) can be explained: the decreasing scatter with increasing black hole mass (see Fig. 3.1). This is the consequence of the merger driven growth of black holes. More massive objects have undergone more merger events than less massive ones; this higher merger number leads to a stronger decrease in scatter. However, observations show a larger scatter in black hole masses, especially at the high mass end (Tremaine et al., 2002, Gültekin et al., 2009). That might indicate that in the model of Malbon et al. (2007) either the number of merger events for massive objects was overestimated (unlikely) or that they started with a too small scatter in black hole mass at high redshift.
- The finding of a decreasing scatter with increasing black hole mass as a consequence of subsequent merging are also consistent with the results of Gültekin et al. (2009), who distinguish between two subsamples of ellipticals and non-ellipticals. For ellipticals they find a smaller scatter in black hole masses than for non-ellipticals. Referring elliptical galaxies mainly to the high-mass end and non-elliptical ones mainly to low-mass end, these observations are also consistent

with the results presented in this Chapter. Furthermore, ellipticals presumably had more mergers.

The aim of this Chapter was to investigate the scatter evolution of supermassive black hole for dry merger driven growth. Despite the interesting insights other important physical growth mechanisms have been neglected, the accretion of gas onto black holes. The importance of an additional growth mechanism is also confirmed by the comparison of the black hole mass function resulting from merging only with observations at $z = 0$: the masses of black holes are under-estimated. Furthermore, if only active galaxies are considered that have undergone a merger event in the last $100 \cdot 10^6$ yrs with a merger ratio smaller than 1 : 10, there is again a deviation from observations, which could be a consequence of under-predicting the over-all black hole mass function. Alternatively, it might indicate that merger events are not frequent enough to be an explanation for the observed active galaxies. This implies that there has to be additional gas accretion even if no merger event happened.

Furthermore, according to the Soltan argument (Soltan, 1982) accretion onto massive black holes is the dominant source of energy produced by quasars ($L \sim \dot{M}_\bullet c^2$), which presumably indicates that the mass in black holes is mainly generated by accretion of gas. This gas accretion might be triggered by galaxy mergers and their ability to drive large amounts of gas to the centers of the galaxies and possibly feed a black hole (Springel et al., 2005a; Di Matteo et al., 2005; Johansson et al., 2009b; Hopkins et al., 2008c). It was shown in hydrodynamical galaxy-galaxy merger simulations with self-regulated black hole growth that after the active phase of the quasar, star formation and black hole growth are quenched by gas heating through energy release by the active quasar. Following the merger, the quasar host becomes a red and dead, massive elliptical galaxy without any further black hole growth through gas accretion (Johansson et al., 2009b). For these galaxies the further evolution of their black holes is mainly dominated by dry merger events. However, gas-rich mergers and cold accretion flows seem to be the dominant growth mode for massive high redshift black holes, as the galaxies are more gas rich (Khochfar & Silk, 2006b, 2009). The quasar activity peaks at $z \approx 2 - 3$ (e.g. Hasinger et al., 2005; Ueda, 2006). Therefore, this phase is most likely to be responsible for the scatter in black holes at this redshift (corresponding to the initial scatter in the models). According to Hasinger et al. (2005) the emissivity of the high luminosity objects ($\log(L/L_\odot) \geq 45$) drops by $\sim 10^2 \text{ erg s}^{-1} \text{ Mpc}^{-3}$ between $z \sim 2$ and $z \sim 0$. Therefore, the subsequent evolution, at least for these massive black holes, might be driven mainly by dry mergers as investigated in this Chapter. In addition, there is theoretical evidence that for $z \leq 2$ gas is more efficiently heated by accretion shocks associated with gravitational heating in massive ($M_{\text{DM}} \geq 10^{12} M_\odot$) galaxy halos (Khochfar & Ostriker, 2008; Dekel & Birnboim, 2008; Naab & Ostriker, 2009; Birnboim et al., 2007), suppressing further gas cooling and star formation as well as accretion onto the central supermassive black hole. Thus, 'red and dead' massive spheroids evolve starting at $z \sim 1$, where again merging may dominate the further growth of these black holes (Dekel & Birnboim, 2006; Khochfar & Silk, 2009). From disk galaxy merger sim-

ulations in Johansson et al. (2009a), it is known that over-massive black holes lying above the black hole-bulge relation do not evolve onto the relation considering only gas accretion driven growth. A solution for this problem could be that the evolution of over-massive black holes onto the relation might be caused mainly by growth through merger events leading to a scatter decrease in black hole mass as shown in this Chapter. That would also indicate, that gas accretion may not play the most important role in the evolution process of over-massive black holes, at least at late stages, where dry merging is the dominating process.

Intentionally, in this Chapter the physics was kept very simple and was focused only on the growth through merging in order to understand the influence of *merging* on the evolution of the scatter in black hole mass. However, gas accretion is - even for $z < 2$ - an important growth channel. The impact of gas accretion on the evolution of the scatter in the $M_{\bullet} - M_{\text{bulge}}$ relation is complicated and so far not easy to assess. To get an idea for such an influence, I refer the reader to Johansson et al. (2009a). Using merger simulations of disk galaxies with gas ($3 \cdot 10^9 M_{\odot} < M_{\text{bulge}} < 10^{10} M_{\odot}$) they show two possible scenarios: Starting with galaxies on the relation leads to an increase of the scatter which gets even larger for higher gas fractions. However, considering initially galaxies below and above the relation causes a decrease of the scatter. The decrease seems to get stronger for lower gas fractions. In order to really understand the effect of gas physics we definitely need further investigations of this process in a statistical sense.

ORIGIN OF THE ANTI-HIERARCHICAL GROWTH OF BLACK HOLES

In this Chapter, different mechanisms are presented influencing the co-evolution of galaxies and black holes, which can provide an explanation of for the observed anti-hierarchical trend of black hole growth within hierarchical clustering scenarios. Observational studies (e.g. Ueda et al., 2003; Hasinger et al., 2005) have shown that the number densities of luminous AGN peak at higher redshifts than the ones of less luminous AGN, implying that massive black holes seem to have predominantly formed before lower mass black holes. For the investigation presented here, the semi-analytic code of Somerville et al. (2008b) is used based on the merging history of the Millennium-simulation. The fiducial model includes a very sophisticated prescription for black hole growth following the light curve parametrizations from a large set of merger simulation (Hopkins et al., 2006a). It is found for the fiducial model that the maximum number densities of AGN in different luminosity bins can match the ones of the observations. However, the fiducial model fails to reproduce the correct number densities of AGN in different luminosity bins at low ($z < 2$) and high ($z > 4$) redshifts. Additional modifications, such as a sub-Eddington limit for gas accretion dependent on mass and redshift, an additional accretion channel onto the black holes due to disk instabilities and a 'heavy' black hole seeding scenario seem to be key mechanisms for reproducing the observed downsizing, i.e. the bolometric as well as the hard X-ray AGN luminosity functions. The picture can be confirmed that disk instabilities are the main driver for moderately luminous Seyfert galaxies, whereas major merger events are mostly triggering very luminous quasars. Moreover, it is shown that, when gravitational heating is additionally assumed, the best-fit model can simultaneously predict the black hole mass function and the galaxy-halo mass relation at $z = 0$.

4.1 Motivation and observational evidence for downsizing

As pointed out in the last Chapter, Section 5.7, besides merging of black holes, cold gas accretion onto black holes represents a significant contribution to the over-all evolution of black holes, in particular for high-redshift and low-mass galaxies where a large fraction of cold gas is present. During phases of strong gas accretion, it is generally accepted that black holes are powering luminous active galactic nuclei (AGN) (Salpeter, 1964; Zel'Dovich, 1964; Lynden-Bell, 1969). Moreover, by estimating the total energy radiated by AGN during their whole life, it can be shown that nearly all the mass in black holes has been accumulated during periods of bright AGN activity (Soltan, 1982). The large amounts of released energy arising from accretion onto black holes (AGN feedback) is a very important ingredient in order to understand the joint evolution of galaxies and black holes. On the one hand, feedback is assumed to cause a self-regulated black hole growth and on the other hand it is thought to influence the evolution of the host galaxy by quenching further cooling and suppressing star formation. In order to investigate this complex scenario, several models have been developed based on either purely analytic (Efsthathiou & Rees, 1988; Haehnelt & Rees, 1993; Haiman & Loeb, 1998; Hopkins et al., 2007b) or semi-analytic approximations (e.g. Kauffmann & Haehnelt, 2000; Volonteri et al., 2003; Granato et al., 2004; Croton, 2006; Somerville et al., 2008b). In recent years, numerical models have also become available (Springel et al., 2005b; Hopkins et al., 2006a; Di Matteo et al., 2005; Robertson et al., 2006a; Li et al., 2007; Sijacki et al., 2007), which clearly demonstrate the important influence of AGN feedback.

From the observational point of view with respect to AGN, one can state the following picture for black hole growth: Early surveys of quasars in the optical demonstrated that quasars undergo significant evolution from $z = 0$ up to $z \approx 2 - 2.5$ (Schmidt & Green, 1983; Boyle et al., 1988; Hewett et al., 1994; Boyle et al., 2000). Beyond $z = 2$ the space density starts to decline (Warren et al., 1994; Schmidt et al., 1995). Studies of Fan et al. (2000, 2001) find very bright quasars with black hole masses of the order of $10^9 M_\odot$ at $z \approx 6$. Recent progress in detecting faint and obscured AGN was achieved by analysing data from X-ray surveys (XMM-Newton, Chandra, ROSAT, ASCA, e.g. Miyaji et al., 2000; La Franca et al., 2002; Cowie et al., 2003; Fiore et al., 2003; Barger et al., 2003; Ueda et al., 2003; Hasinger et al., 2005; Barger & Cowie, 2005; Sazonov & Revnivtsev, 2004; Nandra et al., 2005; Aird et al., 2010). Because AGN are typically far more X-ray luminous than even actively star-forming galaxies, such deep X-ray surveys provide the most efficient means of AGN selection and a wider range of AGN luminosity can be probed than in the optical. This allows to study the evolution of a wide variety of different AGN types in addition to quasars (e.g. Seyfert galaxies). All of these studies in the hard and soft X-ray range find a strong evolution of bright AGN with redshift: the space density of bright AGN is peaking at higher redshifts ($z \approx 2$) than that of faint AGN ($z < 1$). Making the simplified assumption that black holes

are accreting at the Eddington rate (i.e. $L \propto M_{\bullet}$) would imply that very massive black holes seem to be in place already very early in the universe, whereas less massive black holes seem to evolve predominantly at lower redshifts. This behavior is called 'downsizing' or 'anti-hierarchical' growth of black holes. The downsizing trend is not only found in observations in the soft and hard X-ray bands, but also in the optical range (Cristiani et al., 2004; Croom et al., 2004; Fan et al., 2004; Hunt et al., 2004; Richards et al., 2006; Wolf et al., 2003) and the NIR (e.g. Matute et al., 2006). Thus, putting all observations from different wavebands and redshift ranges together, reveals again an anti-hierarchical trend as shown in a compilation of Hopkins et al. (2007c) (see Section 4.6). At first sight, these observations seem to be in contraction with currently favored hierarchical structure formation models, where one would expect less massive objects to form at early times with a subsequent hierarchical clustering of more massive objects only at later times in the Universe. However, in our current picture, the connection of AGN luminosity to the over-all mass assembly of black holes is pretty complex because of the following reasons: The AGN luminosity is mainly governed by the different accretion mechanisms and phases black holes are experiencing during their life-time and the corresponding accretion efficiencies. This means that e.g. a very massive black hole might accrete at low Eddington-ratios leading to a small luminosity. If quasar activity would be mainly triggered by galaxy interactions, the observed decline in the quasar number density at $z < 2$ might reflect the decrease of the major merger rate with decreasing redshifts. Also the smaller amount of cold gas, which can be accreted onto the black hole together with AGN feedback processes might state other plausible effects for reducing the quasar number density. For low luminous AGN, however, additional trigger mechanisms besides merger events might become important as e.g. gas accretion onto the black hole due to stellar mass loss or disk instabilities.

Therefore, the aim of this Chapter will be to provide a better understanding for the mechanisms triggering AGN activity and for the accretion efficiencies during the active phases of black holes which might be causing the observed downsizing. Moreover, I want to reproduce the AGN number density evolution in a quantitative way by simulatenuously satisfying observational constraints of the present-day universe. For such an investigation, simple models based only purely merging scenario, as they were used in the previous Chapter, are certainly not sufficient anymore, and tools for a more thorough approach for modeling the gas physics in galaxy formation are needed. There exist several studies using semi-analytical models ('MUNICH', 'GALFORM' or 'MORGANA' models), where they try to give different explanations for the downsizing trend (Fontanot et al., 2006; Malbon et al., 2007; Marulli et al., 2008; Bonoli et al., 2009; Fanidakis et al., 2010). They will be discussed in more detail in the next Section. However, in contrast to these previous studies, in this thesis I am using a differently developed semi-analytic model according to Somerville et al. (2008b) (S08), which includes a sophisticated prescription for black hole accretion in the 'bright' quasar mode. Following the large set of merger simulations (Springel et al., 2005b; Robertson et al., 2006a,c; Cox et al., 2006; Hopkins et al., 2007a) typical light curve models for

quasars are adopted in this model. Moreover, the effect of several modifications and extensions is discussed - based on the fiducial model - such as:

- a sub-Eddington limit for Eddington-ratios dependent on redshift and black hole mass
- secular evolution processes triggering AGN activity, e.g. disk instabilities
- a 'heavy' black hole seeding scenario combined with a large scatter in the accreted gas mass onto the black hole at high redshifts.

In the course of this Chapter, first the results of previous studies (Section 4.2) are summarized with respect to the downsizing trend in black hole growth. Section 4.3 gives a brief overview of the semi-analytic model used in this study and the different modifications and extensions for black hole growth which will be considered. In Sections 4.4 and 4.5 properties of present-day and high-redshift galaxies and their black holes are investigated in comparison to observations. The AGN number density evolution is studied in Section 4.6, considering the influence of the different model modifications. Section 4.7 shows a comparison of the evolution of the observed bolometric and hard X-ray luminosity function with the model output. Moreover, the evolution of the Eddington-ratio distributions and of the relation between black hole mass and luminosity is discussed in Sections 4.8 and 4.9. Finally, in Section 4.10, the main results summarized and compared to previous studies.

4.2 Previous studies

In the last few years, several studies were trying to understand the observed anti-hierarchical trend using the 'GALFORM' (Durham)- (Bower et al., 2006), the 'MUNICH'- (De Lucia & Blaizot, 2007) or the 'MORGANA' semi-analytic model (Monaco & Fontanot, 2005; Fontanot et al., 2006). The first two models are applied to the dark matter merger trees of the Millennium-simulation, whereas the latter uses merger trees from the PINOCCHIO tool. All models distinguish between black hole accretion in the bright quasar mode and the low-Eddington ratio radio-mode. However, while in the 'GALFORM' model, the quasar mode is triggered by merger events *and* secular evolution processes as disk instabilities (note that the contribution to the total baryons in black holes is dominated by disk instabilities), the 'MUNICH'- and the 'MORGANA'-model assume quasar phases to be *only* a consequence of merger events. The black hole accretion rate in the 'GALFORM'-model is proportional to the produced stellar mass during a starburst, whereas in the 'MUNICH'-model the accretion rate is dependent on the cold gas content in the galaxy. Similarly, the 'MORGANA'-model assumes black holes growth to be proportional to a cold gas reservoir of the galaxy.

Fontanot et al. (2006) show the predictions of their 'MORGANA' model for the AGN number density compared to luminosity functions of AGNs in the optical, soft and hard

X-ray bands. They claim that downsizing within the hierarchical Λ CDM cosmogony can be reproduced and that this is most likely to be caused by stellar kinetic feedback that arises in star-forming bulges leading to a removal of cold gas in small elliptical galaxies. To obtain a good match to the amount of bright quasars they require quasar-triggered galactic winds, which self-limit the accretion onto black holes.

In a theoretical study, Malbon et al. (2007) find - using the 'GALFORM' semi-analytic code - that the direct accretion of cold gas during starbursts is an important growth mechanism for lower mass black holes and at high redshift. On the other hand, the reassembly of pre-existing black hole mass into larger units via merging dominates the growth of more massive black holes at low redshift. Therefore, they claim that as redshift decreases progressively less massive black holes have the highest growth rates, in agreement with downsizing. Their model output reproduces the evolution of the optical luminosity function of quasars, however, they do not show a quantitative comparison for the X-ray and/or bolometric AGN luminosity.

In a very recent work, Fanidakis et al. (2010), again based on the 'GALFORM'-model, present a quantitative comparison of their model output to the observed quasar luminosity function at different redshifts. In contrast to previous SAMs, they calculate their bolometric AGN luminosity from the accretion rates during their quasar phases *and* from radio-mode, low *cold* accretion dominated regimes according to the advective dominated accretion flow model (ADAFs: no radiation occurs since cooling happens through advection). At high redshift, they do not limit their accretion to the Eddington rate, but assume super-Eddington accretion. Therefore, they claim that super-Eddington accretion is responsible for very luminous AGN at high redshifts, whereas the high number density of low luminous AGN at low redshift can be explained by the luminosity derived from the ADAF model. They attribute the observed downsizing trend mainly to dust obscuration of low luminous AGN at high redshift.

Marulli et al. (2008), based on the 'MUNICH'-model, investigate different modifications for black hole growth in the quasar mode and compare the results directly to the observed bolometric quasar luminosity function. For their best-fit model they find that quasar light curve parametrizations (increasing the amount of low luminous AGN at low z) and accretion rates dependent on mass and redshift seem to be important (larger accretion rates at high redshift). Finally, in a study of Bonoli et al. (2009), the follow-up work from Marulli et al. (2008), they assume that the amount of cold gas accreted on the black hole depends linearly on redshift and is weighted with the merger ratio. However, they are still not able to reproduce a sufficiently large amount of high-luminous objects at high z and the one of low-luminous objects at low z . In the course of this work, these previous results will be discussed by comparing them to the ones presented in this Chapter.

4.3 The semi-analytic model

In this work, the semi-analytic code from S08 is used as the fiducial model. At this point, a short overview of the physical recipes for galaxy formation is given and the reader is referred to S08 for more details. Moreover, different, additional modifications for black hole growth are presented based on the fiducial model in order to explain the origin of the observed downsizing.

4.3.1 Merging history from the Millennium simulation

The SAM is applied to the merging history of the Millennium simulation (Springel et al., 2005a) in order to have sufficiently large statistics. The Millennium simulation is a cosmological N-body simulation performed with GADGET. It contains 2160^3 particles with masses of $8.6 \times 10^8 h^{-1} M_\odot$, has a comoving box length of $500 h^{-1} \text{Mpc}$ and generates 64 output times from $z = 127$ to $z = 0$. As cosmological parameters they use $\Omega_m = 0.25$, $\Omega_\Lambda = 0.75$, $\Omega_b = 0.045$, $h = 0.73$ and $\sigma_8 = 0.9$. The structure identification in each snapshot was done using first a friends-of-friends (FOF) algorithm (Davis et al., 1985) followed by the algorithm SUBFIND (Springel et al., 2001a), where a spherical overdensity criterium is chosen to identify substructures (subhalos within a FOF group). The merger trees are constructed from the subhalos by finding a single descendant for each subhalo at the following snapshot (see Fig. 2.3 for a visualisation of a part of the dark matter density distribution in the Millennium simulation at $z = 0$ and $z = 5$).

4.3.2 Galaxy formation

In order to model the formation and evolution of galaxies on top of the dark matter structure evolution, the SAM code includes physical prescriptions for gas cooling, re-ionization, star formation, supernova feedback, metal evolution, black hole growth and AGN feedback. In the following, the implementations of the different mechanisms are briefly summarized. In table 4.1, a summary of the different galaxy formation parameters is provided.

1. **Radiative cooling** The rate of gas condensation via atomic cooling is computed based on the model proposed by White & Frenk (1991). At each radius the cooling time can be computed according to

$$t_{\text{cool}} = \frac{3/2 \mu m_p k T}{\rho_g(r) \Lambda(T, Z_h)}. \quad (4.1)$$

Here, T is the virial temperature, μm_p is the mean molecular mass, $\rho_g(r)$ is the radial density profile of the gas and $\Lambda(T, Z_h)$ is the cooling function (temperature and metallicity dependent). The cooling time is the time required for the gas to radiate away all its energy starting at the virial temperature. The gas density

profile $\rho_g(r)$ is assumed to follow an isothermal sphere: $\rho_g(r) = m_{\text{hot}}/(4\pi r_{\text{vir}} r^2)$. Putting this expression in Eq. 4.1 one can solve for a cooling radius r_{cool} . Within the cooling radius all gas can cool within the cooling time t_{cool} . The cooling rate for the mass within r_{cool} is

$$\frac{dm_{\text{cool}}}{dt} = \frac{1}{2} m_{\text{hot}} \frac{r_{\text{cool}}}{r_{\text{vir}}} \frac{1}{t_{\text{cool}}}. \quad (4.2)$$

Following Springel et al. (2001a) and Croton (2006), it is assumed that the cooling time is equal to the halo dynamical time $t_{\text{cool}} = t_{\text{dyn}} = r_{\text{vir}}/V_{\text{vir}}$. In order to account for cold gas flows and hot gas accretion as found by simulations, two different modes of accretion are distinguished: the rapid and the slow cooling regime (= cold and hot mode cooling). In the rapid cooling regime, where the cooling radius is larger than the virial radius $r_{\text{cool}} > r_{\text{vir}}$, the cooling rate is equal to the gas accretion rate, governed by the mass accretion history. Slow mode cooling occurs, whenever the cooling radius is smaller than the virial radius $r_{\text{cool}} < r_{\text{vir}}$. Here, the cooling rate is calculated according to equation 4.2.

2. **Photo-ionization** Photo-ionization heating causes halos below a certain, critical filtering mass M_F to have a lower baryon fraction than the universal average. The collapsed baryon fraction as a function of redshift and halo mass is parameterized by the expression:

$$f_{\text{b,coll}}(z, M_{\text{vir}}) = \frac{f_b}{[1 + 0.26 M_F(z)/M_{\text{vir}}]^3}, \quad (4.3)$$

where f_b is the universal baryon fraction. The filtering mass is a function of redshift and depends on the re-ionization history of the universe.

3. **Star formation** The SAM distinguishes between quiescent star formation and merger-driven starbursts. The quiescent star formation is based on the empirical Schmidt-Kennicutt relation (Kennicutt, 1989, 1998). The star formation rate surface density Σ_{SFR} is calculated according to

$$\Sigma_{\text{SFR}} = A_{\text{KS}} \Sigma_{\text{gas}}^{N_K} \quad (4.4)$$

with $A_{\text{KS}} = 1.67 \times 10^{-4}$, $N_K = 1.4$, and Σ_{gas} is the surface density of cold gas in the disk. The normalisation is tuned for a Chabrier IMF (Chabrier, 2003). The gas follows an exponential disk (proportional to the scale-length of the stellar disk) and only gas above a critical surface density threshold Σ_{crit} ($= 6M_{\odot}/pc^2$) is available for star formation. Computing the radius r_{crit} within which the gas density exceeds the critical value the total star formation rate is

$$\dot{m}_* = \int_0^{r_{\text{crit}}} \Sigma_{\text{SFR}} 2\pi r dr. \quad (4.5)$$

Star formation during starbursts is driven by merger events. The star formation rate is assumed to be a function of the mass ratio and the combined cold gas content of the merging galaxies, the bulge to total stellar component and burst timescale (exponential decline). The burst continues until the cold gas reservoir is exhausted and the burst SFR will decline exponentially. In the case that a merger occurs, whenever a starburst from a former merger is still going on, the new cold gas is added to the current fuel reservoir.

4. **Supernova feedback** Cold gas is reheated through the energy release from supernovae explosions and the cold gas may be ejected from the galaxy by supernova-driven winds. The heating rate of the cold gas is calculated with

$$\dot{m}_{\text{rh}} = \epsilon_0^{\text{SN}} \left(\frac{V_{\text{disk}}}{200 \text{km/s}} \right)^{\alpha_{\text{rh}}} \dot{m}_*, \quad (4.6)$$

where ϵ_0^{SN} and α_{rh} are free parameters. The circular velocity V_{disk} is assumed to be the maximum rotation velocity of the dark matter halo, V_{max} . The heated gas can either stay within the dark matter halo as hot gas, or, if the supernova-driven winds are strong enough, it can be ejected from the halo into the intergalactic medium (IGM). The fraction of reheated gas, which is ejected from the halo, is given by

$$f_{\text{eject}}(V_{\text{vir}}) = \left[1 + \left(\frac{V_{\text{vir}}}{V_{\text{eject}}} \right)^{\alpha_{\text{eject}}} \right]^{-1}, \quad (4.7)$$

with $\alpha_{\text{eject}} = 6$ and V_{eject} is a free parameter ($\approx 100 - 150 \text{km/s}$). This ejected heated gas can re-collapse onto the halo at later times and then is available for cooling. As in Springel et al. (2001a) and De Lucia & Blaizot (2007) the rate of reinfall of rejected gas is given by

$$\dot{m}_{\text{reinfall}} = \chi_{\text{reinfall}} \left(\frac{m_{\text{eject}}}{t_{\text{dyn}}} \right). \quad (4.8)$$

Here, χ_{reinfall} is a free parameter, m_{eject} is the mass of the ejected gas outside of the halo and $t_{\text{dyn}} = r_{\text{vir}}/V_{\text{vir}}$ is the dynamical time of the halo.

5. **Metal enrichment** To track the production of metals, it is assumed that, together with a parcel of new stars dm_* , a certain mass of metals $dM_Z = y dm_*$ is created and instantaneously mixed with the cold gas in the disc. The yield is assumed to be constant $y = 1.5$ and is treated as a free parameter. Whenever new stars are formed, they are assumed to have the metallicity of the cold gas at this time step. When metals are ejected from the disc due to SN-winds, either the metals are mixed with the hot gas or ejected from the halo into the 'diffuse' IGM in the same proportion as reheated cold gas. Note that only metal enrichment due to Supernovae TypeII is tracked.

6. Black hole growth with AGN-driven winds and Radio-mode feedback

Black holes form at the centers of the galaxies and are thought to grow by two channels: quasar mode and radio mode. The quasar mode is the bright mode of black hole growth observed as optical or X-ray bright AGN radiating at a significant fraction of their Eddington limit ($L \approx (0.1 - 1)L_{\text{Edd}}$; Vestergaard, 2004; Kollmeier et al., 2006). Such bright AGN are believed to be fed by optically thick, geometrically thin accretion disks (Shakura & Sunyaev, 1973). In the next Section, the physical processes during the quasar mode and the corresponding implementations in the code will be discussed in more detail. In contrast, AGN activity in the radio-mode is much less dramatic. A large fraction of massive galaxies are detected at radio wavelengths (Best et al., 2007) without showing characteristic emission lines of classical optical or X-ray bright quasars (Kauffmann et al., 2008). Their accretion rates are believed to be a small fraction of the Eddington rate and they are radiatively extremely inefficient. Even if AGN spend most of their time in the radio-mode, they gain most of their mass during the short, Eddington limited episodes of quasar phases which in the model are assumed to be triggered by merger events. The energy being released during the rapid growth of the black holes can drive powerful galactic scale winds. By relating the momentum of the radiative energy from the accreting black hole with the momentum of the outflowing wind, the following expression for the mass outflow rate can be obtained:

$$\frac{dM_{\text{out}}}{dt} = \epsilon_{\text{wind}} \eta_{\text{rad}} \frac{c}{v_{\text{esc}}} \dot{m}_{\text{acc}}, \quad (4.9)$$

where ϵ_{wind} is the effective coupling efficiency, η_{rad} is the conversion efficiency of matter into radiation, M_{out} is the ejected gas mass and v_{esc} is the escape velocity.

In contrast to the quasar mode, the radio mode has low-Eddington ratio accretion rates and thus, is radiatively inefficient and associated with efficient production of radio jets that can heat gas in a quasi-hydrostatic hot halo solving the overcooling problem of massive galaxies at low redshifts. Assuming Bondi-Hoyle accretion combined with an isothermal cooling flow solution (Nulsen & Fabian, 2000) the accretion rate in the radio mode can be calculated by the following formula:

$$\dot{m}_{\text{radio}} = \kappa_{\text{radio}} \left[\frac{kT}{\Lambda(T, Z_h)} \right] \left(\frac{M_{\bullet}}{10^8 M_{\odot}} \right). \quad (4.10)$$

Thereby, κ_{radio} is a free parameter, namely the efficiency for gas accretion in the radio mode. Note that the central black hole accretes at this rate whenever hot halo gas is present (hot 'cooling' mode, $r_{\text{cool}} > r_{\text{vir}}$). The energy that effectively couples to and heats the hot gas is given by $L_{\text{heat}} = \kappa_{\text{heat}} \eta_{\text{rad}} \dot{m}_{\text{radio}} c^2$. Assuming that all the hot gas is at the virial temperature of the halo, the rate of the heated gas mass is given by

$$\dot{m}_{\text{heat}} = \frac{L_{\text{heat}}}{3/4 v_{\text{vir}}^2}. \quad (4.11)$$

The net cooling rate is then the usual cooling rate minus the heating rate from the radio-mode.

4.3.3 Models for black hole growth in the quasar phase

The most important physical recipe for the investigation of AGN luminosities is the prescription of how black holes grow during their 'bright' and short quasar episodes. Besides the fiducial implementation, three different extensions are considered based on the fiducial calculations. They will be described in the following:

1. **Fiducial model:** The quasar phase is triggered by galaxy merger events with a mass ratio of $\mu > 0.1$. It is adopted that, whenever the two progenitor galaxies merge, their black holes merge also instantaneously and form a new black hole according to mass conservation. For modeling the gas accretion onto the black hole a large set of numerical merger simulations are considered (Springel et al., 2005b; Robertson et al., 2006a,c; Cox et al., 2006; Hopkins et al., 2006a, 2007a), where they draw the following evolutionary picture of AGN activity and the different phases: Major merger events are leading to an infall of large amounts of cold gas providing the fuel for the central black hole and are also triggering a starburst event. In this first coalescence phase, the starburst dominates the luminosity (ULIRG), whereas the AGN is surrounded by a dusty torus and thus, can be only observed in the X-ray range. The black hole is growing very rapidly in this phase with accretion rates near the Eddington limit. Afterwards, the black hole enters the blow-out phase, where the remaining dust and gas is expelled due to feedback processes from the gas accretion and the AGN can be observed as a traditional quasar in the optical range. Due to lacking further gas supply and an emerging hot halo, the quasar luminosity fades rapidly, the accretion rate decreases and further star formation is suppressed resulting in a 'read and dead' elliptical mainly growing by dry merger events. Moreover, they find that AGN spend most of their time in the 'decaying' phase, *not* accreting at the Eddington-limit. To summarize, in isolated merger simulations typical light curves for quasars can be extracted, consisting of an obscured heavy accretion phase and a subsequent blow-out phase.

Therefore, in this model, the final black hole mass $M_{\bullet,\text{final}}$ is calculated in the beginning of each quasar phase using a parametrization according to (Hopkins et al., 2006b):

$$M_{\bullet,\text{final}} = f_{\text{BH,final}} \times 0.158 \left(\frac{M_{\text{sph}}}{100M_{\odot}} \right)^{1.12} \times \Gamma(z), \quad (4.12)$$

where M_{sph} is the final spheroid mass after the merger, $f_{\text{BH,final}}$ an adjustable parameter and $\Gamma(z)$ is a parameter, which describes the evolution of the black hole-

Table 4.1: Summary of the galaxy formation parameters in the fiducial model according to S08.

Parameter	Description	Fiducial value
<i>Quiescent star formation</i>		
A_{KS}	Normalization of Kennicutt law	1.67×10^{-4}
N_K	Power-law index in Kennicutt law	1.4
Σ_{crit}	Critical surface density	$6 M_{\odot} \text{pc}^{-2}$
<i>Burst star formation</i>		
μ_{crit}	Critical mass ratio for burst activity	0.1
<i>SN feedback</i>		
ϵ_{SN}^0	Normalization of reheating fct	1.3
α_{rh}	Power-law slope of reheating fct	2.0
V_{eject}	Velocity scale for ejecting gas	120 km s^{-1}
$\chi_{\text{re-infall}}$	Time-scale for re-infall of ejected gas	0.1
<i>Chemical evolution</i>		
y	Chemical yield	1.5
<i>Black hole growth</i>		
η_{rad}	Efficiency of conversion of rest mass to radiation	0.1
M_{seed}	Mass of seed black hole	$100 M_{\odot}$
$f_{\text{BH,final}}$	Scaling factor for BH mass after merger	0.8
$f_{\text{BH,crit}}$	Scaling factor for critical BH mass	0.4
<i>AGN-driven winds</i>		
ϵ_{wind}	Coupling factor for AGN-driven winds	0.5
<i>Radio-mode feedback</i>		
κ_{radio}	Normalization of 'radio mode' accretion rate	2×10^{-3}
κ_{heat}	Coupling efficiency of radio jets with hot gas	1.0

bulge mass relation with time (Hopkins et al., 2006b). Following the merger simulations, additionally a Gaussian distributed scatter with a value of $\sigma_{\bullet} = 0.3$ dex is applied to the accreted gas mass when the final black hole mass is calculated. When the black hole mass has reached this final value, the quasar mode is switched off. During the quasar phase, the light curve models describe mainly two different growth regimes: an Eddington-limited and a power-law decline phase of accretion. In the first regime, the black hole accretes at the Eddington rate until it reaches a certain critical black hole mass $M_{\bullet,\text{crit}}$:

$$M_{\bullet,\text{crit}} = f_{\text{BH,crit}} \times 1.07 (M_{\bullet,\text{final}})^{1.1}. \quad (4.13)$$

Here, the parameter $f_{\text{BH,crit}}$ is set according to the merger simulations, which determines how much of the black hole growth occurs in the Eddington-limited versus power-law decline phase. The growth of the black hole during the first regime can be modeled by an exponential increase of mass:

$$M_{\bullet,\text{new}}(t) = M_{\bullet} \exp\left(\frac{1-\epsilon}{\epsilon} f_{\text{edd}} \frac{t}{t_{\text{salp}}}\right), \quad (4.14)$$

where $\epsilon = 0.1$ is the accretion efficiency factor and $t_{\text{salp}} \approx 0.45$ Gyr the Salpeter timescale. No strong observational constraints are available for ϵ and if or how it evolves with redshift. However, some observations at $z = 0$ indicate that $0.04 < \epsilon < 0.16$ (Marconi et al., 2004). For simplicity in this study a constant mean value for the accretion efficiency of $\epsilon = 0.1$ is taken at all redshifts. f_{edd} in Eq. 4.14 is the Eddington ratio defined by the ratio of bolometric luminosity to the Eddington luminosity:

$$f_{\text{edd}} := L_{\text{bol}}/L_{\text{edd}}. \quad (4.15)$$

The Eddington luminosity L_{edd} (assuming a hydrostatic equilibrium between the inward gravitational force and the outward radiation pressure) is given by:

$$L_{\text{edd}} = \frac{4\pi G M_{\bullet} m_P c}{\sigma_T} = 1.4 \times 10^{46} \left(\frac{M_{\bullet}}{10^8 M_{\odot}}\right) \text{erg/s}, \quad (4.16)$$

where σ_T is the Thomson cross section for an electron and m_P the mass of a proton. Combining eq. 4.14, 4.15 and 4.16 and the relation $L_{\text{bol}} = \epsilon/(1-\epsilon)\dot{M}c^2$ The corresponding accretion rate in the first regime can be calculated by:

$$\dot{M}_{\bullet,I}(t) = 1.26 \times 10^{38} \text{erg/s} \frac{1-\epsilon}{\epsilon} \frac{f_{\text{edd}}}{c^2} M_{\bullet,\text{new}}(t). \quad (4.17)$$

Note that in the fiducial model it is always assumed an accretion at the Eddington rate, i.e. a constant Eddington ratio of $f_{\text{edd}} = 1$.

Exceeding the critical mass $M_{\bullet,\text{crit}}$ in Eq. 4.13, the black hole enters the second regime, the 'blow-out' phase, which is described by a power-law decline in the

accretion rate. Fitting the light curves in merger simulations from Hopkins et al. (2006a) gives the following parametrization for $\dot{M}_{\bullet,II}$:

$$\dot{M}_{\bullet,II}(t) = \frac{\dot{M}_{\bullet,peak}}{1 + (t/t_Q)^\beta} \quad (4.18)$$

where $t_Q \propto t_{\text{salp}}$ is the e-folding time, $\dot{M}_{\bullet,peak}$ is the peak accretion rate and β is a parameterized function of the peak accretion rate. In the case that the initial black hole mass is already larger than the calculated critical mass, the black hole is not allowed to accrete at the Eddington rate at all and goes immediately into the blow-out phase. If the initial black hole is even larger than the calculated final mass, no quasar phase occurs at all. Note that for calculating the bolometric luminosity only the accretion rates during the quasar phases are taken into account (thus ignoring the contribution from the radio mode accretion):

$$L_{\text{bol}} = \frac{\epsilon}{1 - \epsilon} \dot{M}_{\bullet,\text{QSO}} c^2. \quad (4.19)$$

Thereby, $\dot{M}_{\bullet,\text{QSO}} = \dot{M}_{\bullet,I/II}$ is the accretion rate from regime I or II.

2. **Sub-Eddington limit for the Eddington-ratios:** Observational studies show that the peak in the Eddington-ratio distributions is not constant with time, instead, it is found to be dependent on redshift as well as on black hole mass (Padovani, 1989; Vestergaard, 2003; Shankar et al., 2004; Kollmeier et al., 2006; Netzer & Trakhtenbrot, 2007; Hickox et al., 2009; Schulze & Wisotzki, 2010). Moreover, in particular at low redshifts, there seems to exist a *sub-Eddington* limit for black hole accretion which is also dependent on black hole mass and redshift (e.g. Netzer & Trakhtenbrot, 2007; Steinhardt & Elvis, 2010). In this thesis, observations of a sample of type-1 AGNs ($0 < z < 0.75$) are closely followed as shown in Netzer & Trakhtenbrot (2007). In this study they find that the median of the Eddington-ratio distribution as well as the upper limit of Eddington-ratios decreases with decreasing redshift and increasing black hole mass. This can be parameterized by the following expression:

$$f_{\text{Edd}} \propto z^{\gamma(M_\bullet)}, \quad (4.20)$$

where γ is a parameter varying with black hole mass. In Netzer & Trakhtenbrot (2007) they derive different values for γ from fitting their observations for different black hole mass bins. Therefore, instead of assuming an accretion at the Eddington rate *below* the critical black hole mass $M_{\bullet,\text{crit}}$ (= first regime of accretion) at all redshifts and for all black hole masses, a parametrization for the sub-Eddington limits is assumed in the model motivated by the observations

from Netzer & Trakhtenbrot (2007):

$$1. \quad M_{\bullet} < 3 \times 10^8 M_{\odot} : \quad (4.21)$$

$$f_{\text{Edd}}(z) = \begin{cases} 1, & z > 1 \\ 0.99 \cdot z + 0.01, & z < 1 \end{cases}$$

$$2. \quad M_{\bullet} > 3 \times 10^8 M_{\odot} : \quad (4.22)$$

$$f_{\text{Edd}}(z) = \begin{cases} 1, & z > 1.5 \\ 0.39 \cdot z^{2.3}, & z < 1.5 \end{cases}$$

Again I want to emphasize that this parametrization is only implemented for the *first* regime of black hole accretion resulting in a *decreasing upper limit* of the Eddington-ratios with decreasing redshift and increasing black hole mass. In the subsequent power-law decline phase, black holes are accreting at even smaller Eddington-ratios. The corresponding distribution and its evolution with redshift will be discussed in Section 4.5.

3. **Additional accretion onto the black hole due to disk instabilities:** So far, AGN activity is assumed to be only triggered by major merger processes in the model used in this study. However, different observational studies suggest that moderately luminous AGN are typically not major-merger driven, at least at $z < 1$ (Cisternas et al., 2010; Georgakakis et al., 2009; Pierce et al., 2007; Grogin et al., 2005), as they do *not* find more morphological distortions for AGN host galaxies than for inactive galaxies. Thus, the current consensus suggests that most AGN at $z < 1 - 1.5$ are undergoing a 'main sequence' secular growth, e.g. the activity might be additionally driven by disk instabilities. Thus, in this thesis at low redshift ($z \leq 2$), a study of Efstathiou et al. (1982) is considered, where they investigate the global stability of disk galaxies by numerical N-body simulations. They find that the disk gets unstable if the ratio of dark matter mass to disk mass becomes too low and give the following parameterization for the onset of disk instabilities:

$$M_{\text{disk,crit}} = \frac{v_{\text{max}}^2 R_{\text{disk}}}{G \epsilon}, \quad (4.23)$$

where $M_{\text{disk,crit}}$ is the critical disk mass, above which the disk is assumed to get unstable, v_{max} is the maximum circular velocity, R_{disk} the exponential disk length and ϵ the stability parameter, where a slightly smaller value is used than proposed in Efstathiou et al. (1982) ($\epsilon = 0.75$). Therefore, in this model it is assumed that, whenever the disk mass exceeds the critical disk mass, the bulge component is enlarged by this difference in 'excess' stellar mass $\Delta M_{\text{disk}} = M_{\text{disk}} - M_{\text{disk,crit}}$ so that the disk becomes stable again. Moreover, it is assume that a certain amount

of cold gas (proportional to the excess disk mass) is additionally accreted onto the black hole triggering an active phase:

$$M_{\bullet, \text{disknew}} = M_{\bullet} + f_{\text{BH,disk}} \times \Delta M_{\text{disk}}. \quad (4.24)$$

$f_{\text{BH,disk}} = 10^{-3}$ is used, motivated by the local black hole-bulge mass relation. Assuming an Eddington-ratio of $f_{\text{edd}} = 0.01$ (motivated by observations, personal conversation with D. Alexander), the accretion rate is calculated by:

$$\dot{M}_{\bullet, \text{diskinst}} = 1.26 \times 10^{38} \text{erg/s} \frac{1 - \epsilon f_{\text{edd}}}{\epsilon c^2} M_{\bullet, \text{disknew}} \quad (4.25)$$

and obtain the bolometric luminosity for disk instabilities using $L_{\text{bol}} = \epsilon/(1 - \epsilon)\dot{M}c^2$. For the total bolometric luminosity, the bolometric luminosities from the major-merger driven quasar phase (equation 4.19) and the ones from disk instabilities are summed up:

$$L_{\text{bol}} = \frac{\epsilon}{1 - \epsilon} \left(\dot{M}_{\bullet, \text{QSO}} + \dot{M}_{\bullet, \text{diskinst}} \right) c^2. \quad (4.26)$$

Note that in the studies using the MUNICH model (Marulli et al., 2008; Bonoli et al., 2009) no disk instabilities for calculating the AGN bolometric luminosity are considered. However, in the GALFORM model disk instabilities are assumed to destroy the *whole* disk, which is added completely to the bulge component and they are believed to trigger quasar activity. In their model, disk instabilities are found to be the *major* contribution for black hole growth at all redshifts (Bower et al., 2006; Fanidakis et al., 2010).

4. **'Heavy' seeding scenario and a larger scatter at high z :** The origin of the first massive black holes is still subject of intense debate. Currently, there exist two favored seeding mechanisms (Haiman, 2010; Volonteri, 2010): either black hole seeds could form out of the remnants of Pop III stars (e.g. Madau & Rees, 2001; Heger & Woosley, 2002) or during a direct core-collapse of a low-angular momentum gas cloud (e.g. Loeb & Rasio, 1994; Koushiappas et al., 2004). In the first case the seeds would have masses of $M_{\text{seed}} \approx 100 - 600 M_{\odot}$ ('light' seeding), while in the latter case, more massive seeds between $M_{\text{seed}} \approx 10^4 - 10^6 M_{\odot}$ ('heavy' seeding) would be expected. The detailed physical processes, in particular of the direct core-collapse, are widely unknown. Unfortunately, observational constraints of the high-redshift universe are too weak in order to favor one of these models. However, future observations of gravitational waves (LISA, Sesana et al., 2005; Koushiappas & Zentner, 2006) or planned X-ray missions (WFXT: Sivakoff et al., 2010; Gilli et al., 2010; IXO), will have technical capabilities to detect accreting black holes at $z > 6$, will test these models of first black holes. Moreover, due to an exponential growth of the black holes during accretion, it is

also very difficult to use the local population of massive halos to recover information about their original masses before the onset of accretion. For instance, in theoretical studies of Volonteri et al. (2008), and Volonteri (2010), the different seeding mechanisms are investigated by following the mass assembly using Monte-Carlo merger trees to the present time. They find that both models can fit observational constraints at $z = 0$ (e.g. the black hole mass-velocity dispersion relation or the black hole mass function), when light seeds form already at very early times ($z = 20$), or when heavy seeds evolve later on ($z = 5 - 10$). In our fiducial model, seed black hole masses of $100M_{\odot}$ have been assumed so far, however, as there hardly happens seeding before $z \approx 10$, now the heavy seeding scenario is adopted with $M_{\bullet, \text{seed}} = 10^5 M_{\odot}$. I want to stress that different seeding mechanisms will not affect the $z = 0$ black hole mass population, as initial seed masses are compensated by gas accretion growth processes. Only the black hole distribution at high redshifts will be influenced by this modification (see Section 4.5.1).

Moreover, many observations (e.g. Walter et al., 2004; Peng et al., 2006; McLure et al., 2006; Schramm et al., 2008) suggest that the black hole-to-bulge mass ratio was larger at higher redshifts than expected from the local black hole-bulge mass relation what was discussed a great detail in Chapter 3. This eventually implies that black holes were accreting more gas and thus, growing faster than the corresponding bulges at high redshifts than at lower ones. Therefore, besides assuming an evolving black hole-bulge mass relation (see the z -dependent Γ parameter in eq. 4.12) it is additionally adopted a larger scatter $\sigma_{\bullet, \text{accr}}$ for the accreted mass onto the black hole at high redshifts. This means that, when calculating the final black hole mass $M_{\bullet, \text{final}}$, a larger Gaussian distributed scatter is applied with a value of $\sigma_{\bullet, \text{accr}} = 0.8$ for $z > 5$. At redshift $z < 5$ the original scatter value $\sigma_{\bullet, \text{accr}} = 0.3$ is considered. This additional assumption might also be justified, as it was shown in the last Chapter and by Hirschmann et al. (2010) that a large scatter in black hole mass ($\sigma = 0.6$ dex) at high redshift ($z = 3$) will decrease with subsequent merging towards the observed present-day value (see also Chapter 3).

In the course of this Chapter, the effects of the outlined modifications on the AGN/black hole evolution are investigated. Thus, besides the fiducial model, the three additional models are considered including the different extensions in a cumulative way:

- **FID:** Fiducial model, point 1
- **VE:** Varying sub-Eddington limit for the Eddington-ratios f_{edd} , points 2
- **VEDI:** Varying sub-Eddington limit & Disk Instabilities, points 2+3

- **VEDIS**: Best-fit model including a **V**arying sub-**E**ddington limit, **D**isk **I**nstabilities & a heavy **S**eeding mechanism, points 2+3+4

4.4 Properties of nearby galaxies and black holes

As shown in S08, the fiducial semi-analytic model was mainly tuned to match observational galaxy properties at $z = 0$. Therefore, in this Section the black hole properties at $z = 0$ and the influence of the different extensions applied to the three modified models are investigated. The $M_{\text{galaxy}}-M_{\text{DM}}$ -relation, the black hole mass function and the $M_{\bullet}-M_{\text{bulge}}$ -relation will be shown, where the FID and the VEDIS models are compared to the $z = 0$ -observations. Note that the VE and VEDI models do not result in a stronger deviation from the FID model than the VEDIS model.

4.4.1 Black hole mass function

The present-day black hole mass function is depicted in Fig. 4.1. The blue, solid line visualizes the FID model, whereas the black solid line together with the grey shaded area represents observations from Shankar et al. (2004) and the black dashed line with the open triangles corresponds to an observational study from Marconi et al. (2004). One can find a good agreement of the FID model predictions with the observations for black holes with masses $M_{\bullet} < 10^{8.5} M_{\odot}$. At the high mass end, however, the FID model significantly over-predicts the number density of black holes by more than one order of magnitude (for $M_{\bullet} \approx 10^{10} M_{\odot}$). This excess of massive black holes can be seen in many different SAM studies (e.g. Fontanot et al., 2006; Malbon et al., 2007; Marulli et al., 2008; Fanidakis et al., 2010). However, I find that this is predominantly due to very efficient growth of black holes during the radio-mode, which mainly contributes to the growth of massive black holes at low redshifts (Croton, 2006, S08). When no accretion onto the black hole during the radio-mode is assumed in the FID model, then a much better agreement with the observations can be obtained for the whole mass range. This implies that the radio-mode accretion is significantly over-estimated in most of the current SAMs, as it was already shown in a recent study of Fontanot et al. (2011), where they compared different semi-analytic models to observations. However, in order to obtain in addition a sufficiently large suppression of gas cooling and thus, of star formation for reproducing the luminosity function (in particular the bright end), one *does need* the amount of feedback (note that the heating rate in the radio-mode is proportional to the radio-mode accretion). This suggests that SAMs might need an additional, alternative mechanism, in order to suppress cooling and quench star formation in massive galaxies. One possible solution might be additionally taking into account gravitational heating (conversion of potential energy of infalling objects into kinetic energy of the stripped material and *thermal* energy of the intracluster medium), what is mostly neglected in SAMs due to missing direct gas-dynamical modeling as in hydrodynamical simulations. Gravitational heating may lead to similar efficiencies

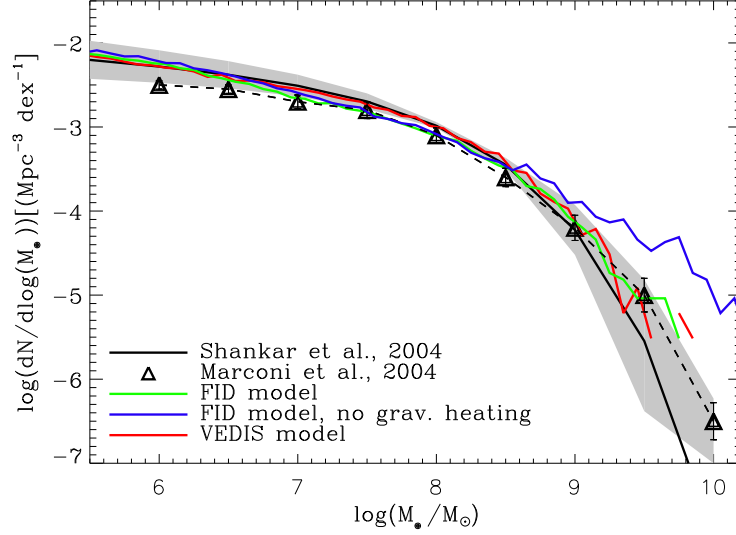


Figure 4.1: *Present-day black hole mass relation. The blue line illustrates the FID model, the green and the red line show the FID and the VEDIS model with gravitational heating and a reduced radio-mode accretion. Observations from Marconi et al. (2004); Shankar et al. (2004) are illustrated by the black solid lines with the grey shaded area and the black dashed lines with open triangles.*

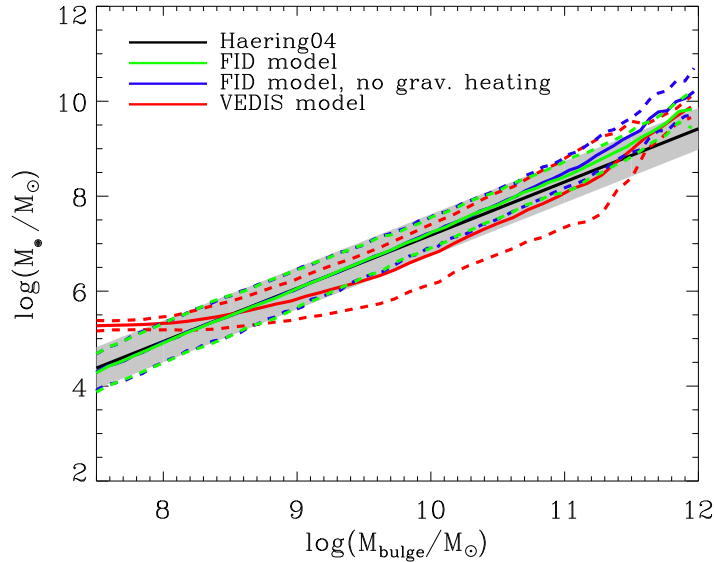


Figure 4.2: *Present-day black hole bulge mass relation. The blue line shows the FID model, the green and the red lines illustrate the FID and the VEDIS model including gravitational heating and a reduced radio-mode accretion. The black line corresponds to the observed, local relation (Häring & Rix, 2004). Dashed lines and the grey shaded area show the scatter in models and observations, respectively.*

as radio-mode feedback, as presented in a study of Khochfar & Ostriker (2008) and shows an almost linear dependence on halo mass ($\propto M_{\text{DM}}^{1.1}$). Following their results, a simplified approximation for an additional heating rate due to gravitational heating is now assumed in the model, parameterized as:

$$\dot{M}_{\text{heat,grav}} \propto f_{\text{grav}} \left(\frac{M_{\text{DM}} - M_{\text{DM,crit}}}{M_{\text{DM,crit}}} \right)^{1.1}, \quad (4.27)$$

where $M_{\text{DM,crit}}$ is the critical halo mass, above which gravitational heating may occur and f_{grav} is an additional free parameter (it is used $M_{\text{DM,crit}} = 10^{11} M_{\odot}$ and $f_{\text{grav}} = 1$).

The green and red solid lines in Fig. 4.1 illustrate the FID and the VEDIS model *including* the simplified approximation of gravitational heating together with a reduced value for the radio mode accretion efficiency by 25% ($\kappa_{\text{radio,new}} = 0.5 \times 10^{-3}$). Due to this change, both models can achieve a reasonably good agreement with the observed black hole mass function for the *whole* mass range with simultaneously satisfying the high mass end of the galaxy-dark matter halo relation (see Section 4.4.3). Moreover, the two SAMs show almost no deviation from each other, indicating that neither the growth of black holes by disk instabilities nor the lowered accretion rates at low redshifts are influencing the black hole mass function significantly.

4.4.2 Black hole-bulge mass relation

The present-day relation between black hole and bulge mass is shown in Fig. 4.2. The FID model is depicted by the blue line and the FID and VEDIS model predictions with gravitational heating and a reduced radio-mode accretion are illustrated by the green and red lines, respectively. The black solid line corresponds to the median of the observed black hole-bulge mass relation according to Häring & Rix (2004), the grey shaded area illustrates the $1 - \sigma$ range of the scatter. The FID models are in reasonably good agreement with the observations. The FID model without gravitational heating, however, results in slightly too massive black holes at the high mass end ($M_{\text{bulge}} > 10^{11.5} M_{\odot}$), what is again due to the excessive growth during the radio-mode what could have already been seen for the high-mass end of the the black hole mass function (see Section 4.4.1). Thus, lowering the radio-mode accretion reduces the growth of black holes and leads to a good agreement of the FID model with the observed relation for the *whole* mass range (see green line in Fig. 4.2). However, comparing the FID and the VEDIS models (both with gravitational heating and a reduced radio-mode accretion), shows that the modifications in the VEDIS model reveal a slightly worse match to the observed relation than the FID model. Only at the high mass end, $\log(M_{\text{bulge}}/M_{\odot}) > 11.5$, the VEDIS is still in good agreement with the FID model and the observations, but for $\log(M_{\text{bulge}}/M_{\odot}) < 8$, the black hole masses ($\approx 10^{7.5} M_{\odot}$) of the VEDIS model are found to be up to one order of magnitude larger compared to the FID model. This is a consequence of the heavy seeding scenario in the VEDIS model, where, by definition, no black holes smaller than $10^5 M_{\odot}$ can occur. Moreover,

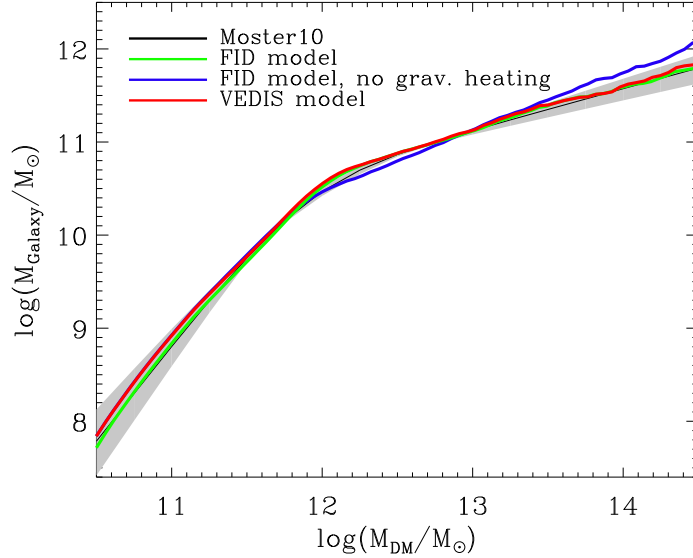


Figure 4.3: *The $M_{\text{galaxy}}-M_{\text{DM}}$ -relation at $z = 0$. The blue line illustrates the FID model, the green and the red line illustrate the FID and the VEDIS model including gravitational heating with a reduced radio-mode accretion. The black line corresponds to the halo occupation distribution of Moster et al. (2010) at $z = 0$ with a $1-\sigma$ -range shown by the grey shaded area.*

for $8.5 < \log(M_{\text{bulge}}/M_{\odot}) < 11$, the VEDIS model leads only to slightly smaller black hole masses than the FID model. This discrepancy is due to the slower growth of black holes as it is not allowed that the black holes accrete at the Eddington-rate at $z < 1$ anymore, but only at a decreasing fraction of it (sub-Eddington limit). This means it takes a longer time to reach the final black hole mass, which correlates with the spheroid mass in the used recipe, within one quasar accretion episode than in the FID model. Whether the modifications assumed in this study are still reasonable assumptions despite of the slightly worse agreement with the observed black hole-bulge mass relation, will be discussed in Section 4.10.

4.4.3 Galaxy-dark matter halo mass relation

Fig. 4.3 shows the $M_{\text{galaxy}}-M_{\text{DM}}$ -relation in the present-day Universe. The FID model without gravitational heating and the FID and the VEDIS models including gravitational heating are illustrated by the blue, green and red solid lines, respectively. The black solid line shows the halo occupation distribution function fit from Moster et al. (2010), where the stellar mass function from the SDSS-survey is combined with cosmological, dark matter N-body simulations. The grey shaded area depicts the corresponding $1 - \sigma$ range of the scatter. In the original FID model (blue line) can be seen that the galaxies with masses $M_{\text{galaxy}} > 10^{13}M_{\odot}$ are slightly over-predicted. In

S08, they suggest that this mass excess might be due to a significant underestimation of the observed luminosities and therefore, the stellar masses of the central galaxies in clusters (Desroches et al., 2007; Lauer et al., 2007; von der Linden et al., 2007) or due to scattering of stars out to large radii as a consequence of a merger event (diffuse stellar component, Gonzalez et al., 2005; Zibetti et al., 2005; Murante et al., 2004, 2007). However, including the simple approximation for an additional heating rate motivated by the physical process of gravitational heating, leads to a significant better agreement with the HOD model and thus, the observations even if the radio-mode accretion has been reduced resulting in a radio-mode feedback lowered by a factor of 4. Between the FID and the VEDIS model predictions (including gravitational heating), there is almost no discrepancy showing that the additional modifications do not influence the final distribution of the stellar masses significantly. Thus, one can conclude that both models (FID and VEDIS) are in reasonably good agreement with the observations for the whole mass range.

Note that the main results of this Chapter presented in Section 4.6 and 4.7 (the AGN number density evolution and the luminosity function) are only marginally influenced by reducing the radio-mode accretion and adding a gravitational heating source. However, for the following investigation, these modifications are always considered in the FID, VE, VEDI and VEDIS models.

4.5 Galaxy and black hole properties at higher redshift

Having shown that the statistical properties of nearby black holes and galaxies can be reproduced sufficiently well, in this Section the effect of the additional model extensions on the *high-redshift* evolution of galaxies and black holes is studied and the model predictions for high-redshift objects are compared to observations. Again, only a comparison of the FID and the VEDIS model is shown, as the VE and the VEDI models do not lead to stronger deviations from the FID model than the VEDIS model.

4.5.1 Black hole mass function

Fig. 4.4 shows the black hole mass function at different redshift steps illustrated by different colors ($z = 0, 0.5, 1, 2, 3, 4, 5, 6$). The upper panel depicts the FID model, lower one the VEDIS model (always with gravitational heating and a reduced radio-mode accretion rate). At redshifts $z < 3$, the evolution of the black holes is very similar in the FID and the VEDIS model showing that the modifications in the VEDIS model do not affect the black hole population at these redshifts. However, turning to higher redshift $z \geq 3$, the main difference between both models is the larger amount of black holes more massive than $M_{\bullet} > 10^6 M_{\odot}$. This can be explained on the one hand by the 'heavy' seeding scenario, on the other hand by the larger scatter in the accreted

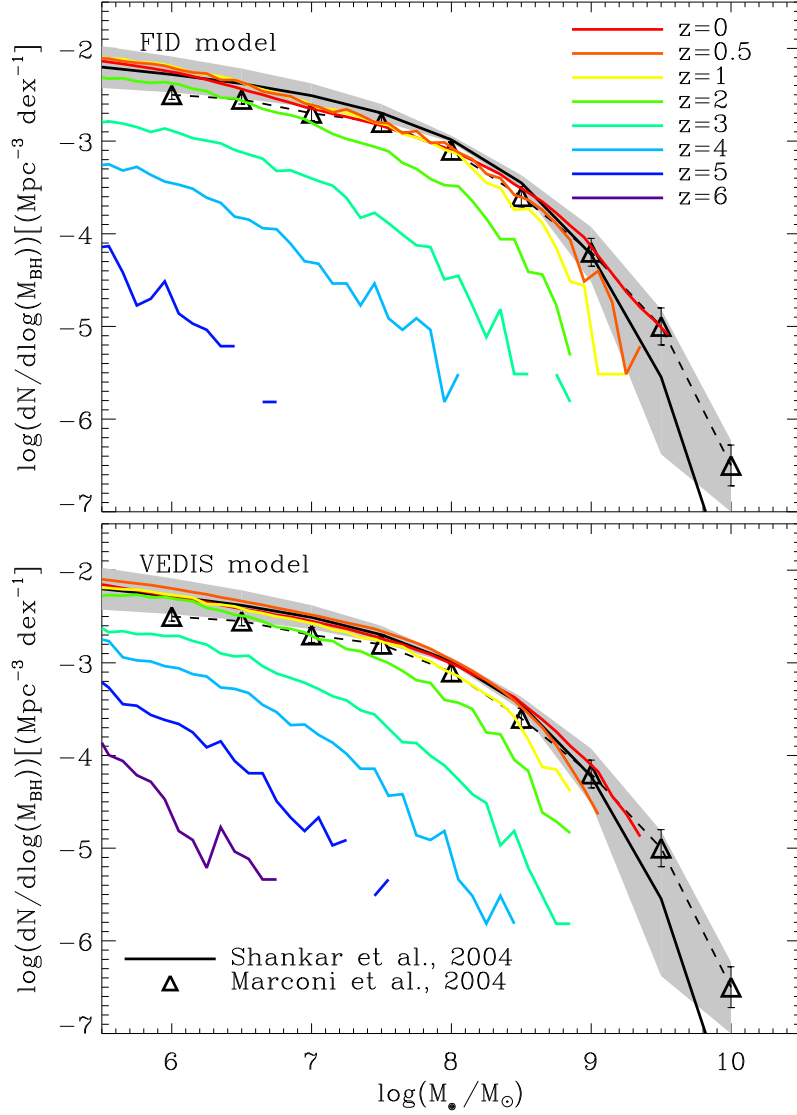


Figure 4.4: Evolution of the black hole mass function for the FID and the VEDIS models (upper and lower panel, respectively). The colored lines illustrate the SAM results at different redshifts, the black dashed and solid lines correspond to observations from Marconi et al. (2004) and Shankar et al. (2004). Adopting a “heavy”-seeding scenario leads to a larger amount of black holes with $M_{\bullet} > 10^6 M_{\odot}$ at high redshift $z > 3$.

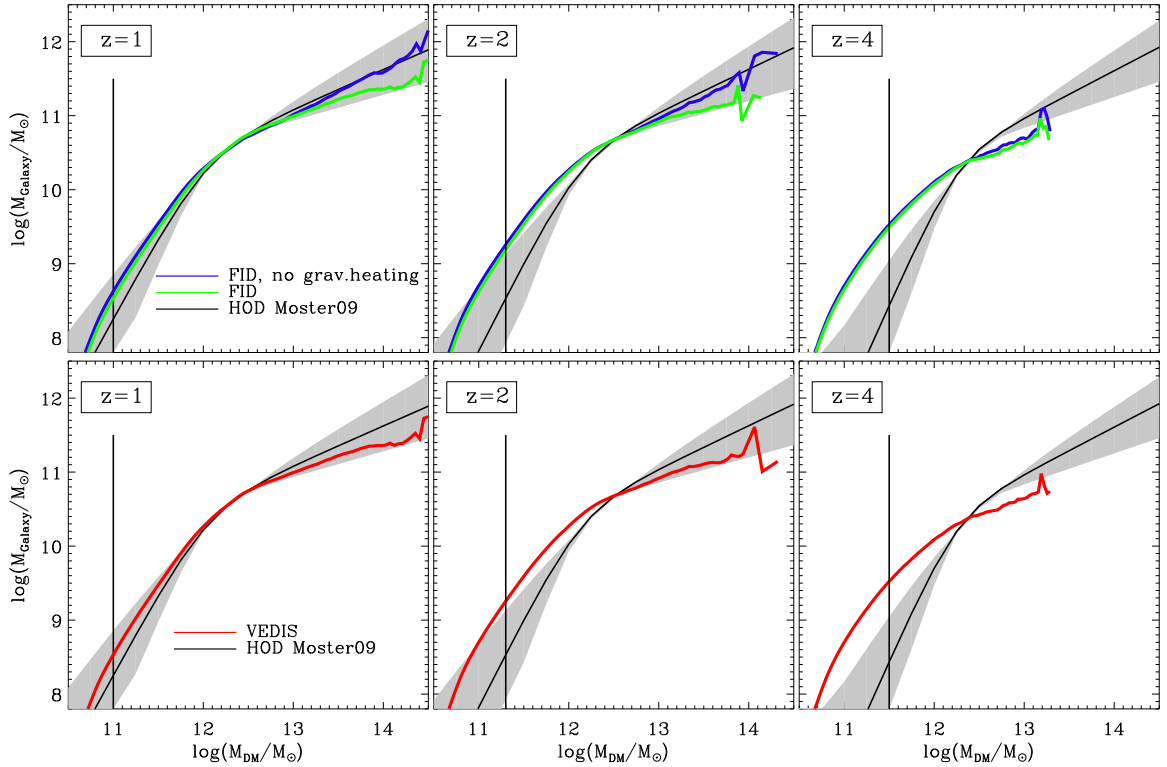


Figure 4.5: *The galaxy-halo mass relation for the FID (with and without gravitational heating, green and blue lines, upper row) and the VEDIS model (red line, lower row) at $z = 1$ (left column), $z = 2$ (middle column) and $z = 4$ (right column). The black solid line illustrates the HOD fit from Moster et al. (2010), the grey shaded area show the scatter. The thin, vertical lines depict the lower observational mass limit.*

gas mass onto the black hole at $z > 5$ leading to larger black hole masses and a faster growth at early redshift. Towards lower redshift, however, this effect can not be seen anymore as the subsequent growth by gas accretion is compensating the initial black hole masses by orders of magnitude. Compared to the study of Fanidakis et al. (2010) this trend is even more pronounced in their model as they allow the black holes to accrete at super-Eddington rates: e.g. at redshift $z = 6$, black holes with $M_{\bullet} = 10^6 M_{\odot}$ have a number density of $\log \Phi = -2.7 \text{ Mpc}^{-3} \text{ dex}^{-1}$, whereas in the VEDIS model a number density of only $\log \Phi = -4 \text{ Mpc}^{-3} \text{ dex}^{-1}$ is obtained.

4.5.2 Galaxy-dark matter halo relation

Fig. 4.5 depicts the galaxy-dark matter halo mass relation at $z = 1$, $z = 2$ and $z = 4$ (left, middle and right columns, respectively). The upper row corresponds to the FID model with and without gravitational heating (green and blue lines), while the lower panels illustrate the VEDIS model (including gravitational heating). The black, solid

lines and the grey shaded areas show the halo occupation distribution (HOD) fits from Moster et al. (2010). The black, thin vertical lines illustrate the observational mass limit for the HOD fitting. Generally, with increasing redshift the agreement of the model output, regarding the FID as well as the VEDIS models, to the HOD becomes worse than what could have been seen at $z = 0$. Similar to the results at $z = 0$, there is no difference between the FID and VEDIS models (with gravitational heating) at high redshift showing that the additional model extensions do not influence the stellar population significantly. At the high mass end, one can clearly see the effect of the additional gravitational heating source. Similar to what is found at $z = 0$, this results in smaller galaxy masses in the FID and the VEDIS model than in the FID model without gravitational heating. However, this results in a slightly worse fit to but still a sufficient agreement with the observations. Nevertheless, this may indicate that the simplified approximation of gravitational heating might have a too strong effect at high redshift and thus, an additional redshift dependence for calculating the gravitational heating rate might be required in the model used here. Turning to the low mass end, fairly good agreement of all model predictions can be obtained with the HOD at $z = 1$. However, at $z \geq 2$ the FID as well as the VEDIS model extensively overestimate the amount of galaxies with masses $\log(M_{\text{Galaxy}}/M_{\odot}) < 12.2$. At $z = 4$ and for halo masses $\log(M_{\text{DM}}/M_{\odot}) \approx 11$ the models predict a larger number of galaxies by almost two orders of magnitude. This extreme deviation is a well-known problem in most of the currently used semi-analytic models, e.g. Fontanot et al. (2009) showed this for the MORGANA, MUNICH and the S08 model, and Guo et al. (2011) found the same for the latest version of the MUNICH model. Moreover, the excess of low mass galaxies at high redshift could have been also verified by cosmological simulations in a study of Davé et al. (2011), showing that this problem is not peculiar to SAMs alone and the corresponding larger inaccuracies in the simplified analytic models. One may speculate that a stronger supernova feedback at high redshift might be required in order to overcome this problem (Caviglia & Somerville, in prep.). Another solution, which will be investigated in Caviglia & Somerville (in prep.), is that the star formation efficiency is lower in low mass galaxies at high redshift what might be due to the ability of forming molecular hydrogen.

4.6 Number density evolution of AGN

In this Section it is investigated whether the SAMs can account for the observed down-sizing behavior in black hole growth. Fig. 4.6 shows the different model predictions for the AGN number densities versus redshift, illustrated by the open squares and the solid lines. The AGN are divided into different bolometric luminosity classes and the different luminosity bins are indicated by different colors:

- black: $42.5 < \log(L_{\text{bol}}) < 43.5$
- dark blue: $43.5 < \log(L_{\text{bol}}) < 44.5$

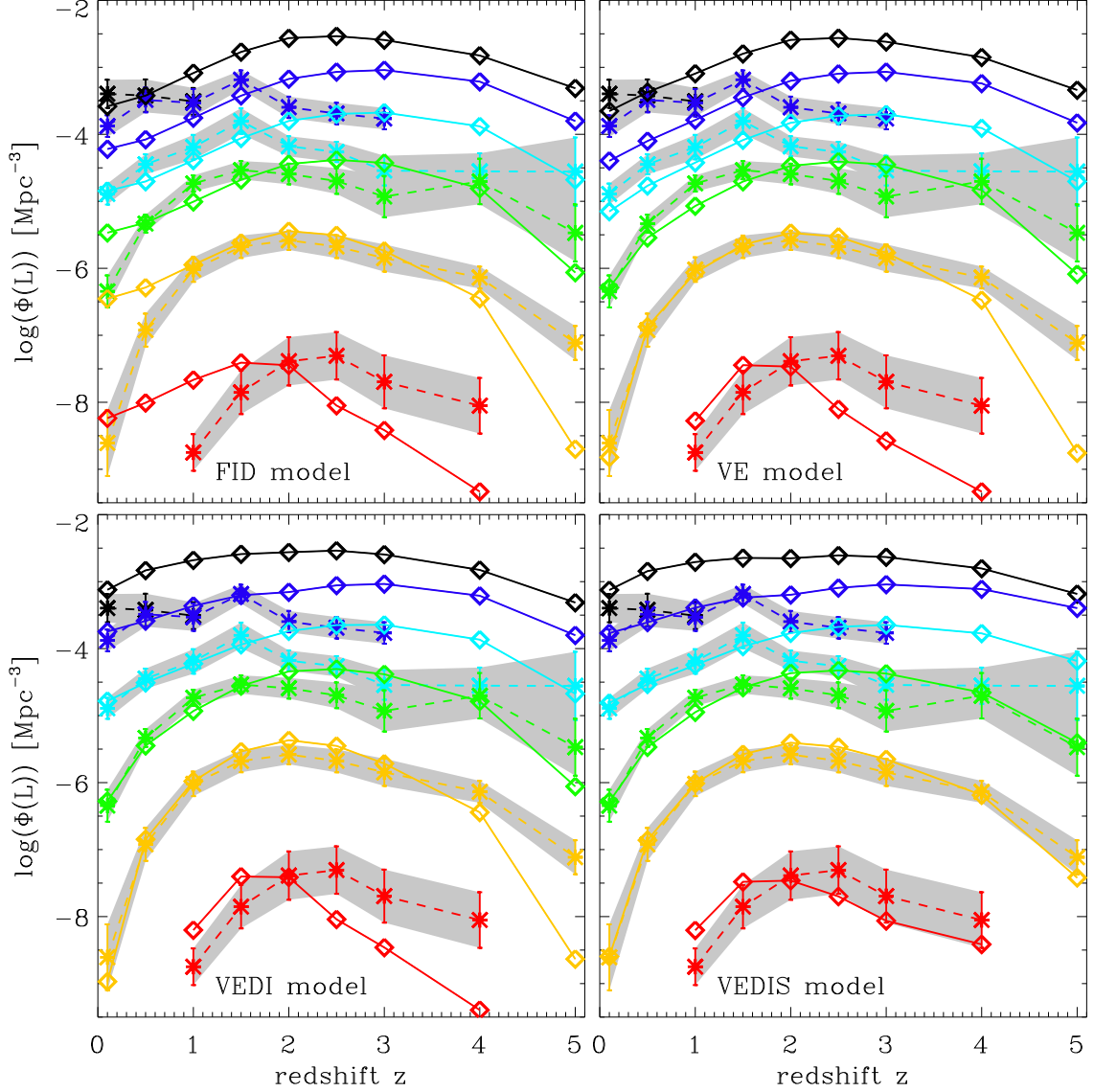


Figure 4.6: Number densities of AGN versus redshift for the four different SAM versions (FID, VE, VEDI and VEDIS). The different bolometric luminosity bins are indicated by different colors: red: $47.5 < \log(L_{\text{bol}})$, yellow: $46.5 < \log(L_{\text{bol}}) < 47.5$, green: $45.5 < \log(L_{\text{bol}}) < 46.5$, light blue: $44.5 < \log(L_{\text{bol}}) < 45.5$, dark blue: $43.5 < \log(L_{\text{bol}}) < 44.5$, black: $42.5 < \log(L_{\text{bol}}) < 43.5$. Solid lines and open squares illustrate the corresponding model output, dashed lines together with grey shaded areas visualize the observational compilation from Hopkins et al. (2007c). Whereas the FID model reveals typical downsizing problems, the best match with observations can be obtained for the VEDIS model.

- light blue: $44.5 < \log(L_{\text{bol}}) < 45.5$
- green: $45.5 < \log(L_{\text{bol}}) < 46.5$
- yellow: $46.5 < \log(L_{\text{bol}}) < 47.5$
- red: $47.5 < \log(L_{\text{bol}})$

In a first step, - as the basic output from the SAMs are *bolometric* luminosities - the SAM results are compared to the observational compilation from Hopkins et al. (2007c) for simplicity. In this study, they convert the AGN luminosities from different observational data sets and thus, from different wavebands (emission lines, NIR, optical, soft and hard X-ray) and from different redshift ranges into bolometric ones. They use a bolometric correction approximated by a double power-law:

$$\frac{L_{\text{bol}}}{L_{\text{band}}} = c_1 \left(\frac{L_{\text{bol}}}{10^{10} L_{\odot}} \right)^{k_1} + c_2 \left(\frac{L_{\text{bol}}}{10^{10} L_{\odot}} \right)^{k_2} \quad (4.28)$$

with different values for (c_1, k_1, c_2, k_2) depending on the considered waveband. Besides the bolometric correction, they also take into account a dust correction factor, in order to overcome the problem that obscured AGN are difficult to detect, in particular at high redshifts and for low luminosities. Note that this 'completeness' issue might be the simplest explanation for the low-luminous objects peaking at lower redshifts than high-luminous ones. In their study, they adopt a luminosity dependent observed column density distribution (no redshift dependence) from the hard and soft X-ray observations of Ueda et al. (2003). They also follow Ueda et al. (2003) and include an equal fraction of Compton-thick objects with $N_H > 10^{24} \text{ cm}^{-2}$ compared to that with $10^{23} \text{ cm}^{-2} < N_H < 10^{24} \text{ cm}^{-2}$. Altogether, using these observed column density distributions, they parameterize the observable fraction of AGNs in a certain waveband as a power-law:

$$f(L_{\text{bol}}) = \frac{\Phi(L_i)}{\Phi(L[L_i])} = f_{46} \left(\frac{L_{\text{bol}}}{10^{46} \text{ erg s}^{-1}} \right)^{\beta}, \quad (4.29)$$

where L_i is the luminosity in a certain band, L_{bol} is the corresponding bolometric luminosity and the parameters (f_{46}, β) vary for different wavebands. Even if these dust corrections lead to flattened curves of low luminous AGN ($L_{\text{bol}} < 10^{45} \text{ erg/s}$), they still find a clear, anti-hierarchical behavior in the evolution of AGN luminosities as illustrated in the four panels of Fig. 4.6 by the dashed lines together with the grey shaded areas.

The upper left panel shows the comparison of the FID model to the observational data. It can be seen that the number densities at the peak of each luminosity bin are in quantitative agreement with the observations. The maximum AGN number densities of each luminosity bin versus bolometric luminosities are directly plotted in

Fig. 4.7 (dashed line represents the observations, solid line corresponds to the FID model) showing that the FID model is able to produce automatically the correct order of magnitude of AGN number densities in the different luminosity bins. However, the observed time evolution of the peaks of the different luminosity classes cannot be successfully predicted by the FID model, where the luminosity curves peak all at a redshift of $z \approx 2$. This discrepancy points out the “typical” anti-hierarchical behavior within the framework of hierarchical structure formation as found by the majority of the current SAMs (e.g. Fontanot et al., 2006; Marulli et al., 2008). In particular, at low and high redshifts, the strongest deviations from observations are found, as follows:

1. $z < 2$: overprediction of AGN number densities with $\log(L_{\text{bol}}) > 46$
2. $z < 2$: underprediction of AGN number densities with $\log(L_{\text{bol}}) < 46$
3. $z > 3$: underprediction of AGN number densities with $\log(L_{\text{bol}}) > 46$
4. $z > 3$: overprediction of number densities with $\log(L_{\text{bol}}) < 45$

The first point suggests that at low redshifts either too massive black hole are accreting or that black holes accrete at too high rates. Assuming that activity is triggered by merger events implies that the natural decrease in the major merger rate is not sufficient in order to predict the observed steep decline in the AGN number densities. However, note that in earlier version of S08 it was shown that the SAM can reproduce the observed merger rate (Jogee et al., 2008), which is best constrained at $z \leq 1$, so that the excess in luminous quasars at low redshift is certainly not due to too many merger events. The low number densities of moderately luminous AGN (point 2) may indicate, however, that the AGN activity might not only be triggered by merger events, but also by secular evolution processes as suggested by different observational studies (Cisternas et al., 2010; Georgakakis et al., 2009; Pierce et al., 2007; Grogin et al., 2005). The deviations at high redshifts (points 3, 4) may be a consequence of a too late formation of massive black holes as well as of an over-prediction of number densities of less massive galaxies at high redshifts resulting in too many active galaxies with moderate luminosities. In particular the latter point, that SAMs overestimate the small mass galaxies at high redshift, was illustrated and discussed in Fig. 4.5 in Section 4.5.2.

In order to achieve a better reproduction of the observed downsizing with the FID model itself, in a first step the effect of solely changing several of the model parameters has been investigated, e.g. by varying the strength of Supernova and radio-mode feedback (as suggested in Fontanot et al., 2006). For stronger supernova feedback (doubling the efficiency for calculating the reheated gas mass ϵ_{SN}^0) a decrease in the amount of AGN can be found at *all* redshifts resulting in a mainly worse match to the observations. Even if the number density of moderately luminous objects ($L_{\text{bol}} < 10^{45}$ erg/s) at high redshifts decreases (towards the observational data), this is not sufficient in order to achieve a reasonably good match to observations in this range. Due to stronger supernova feedback, gas cooling and star formation is suppressed more

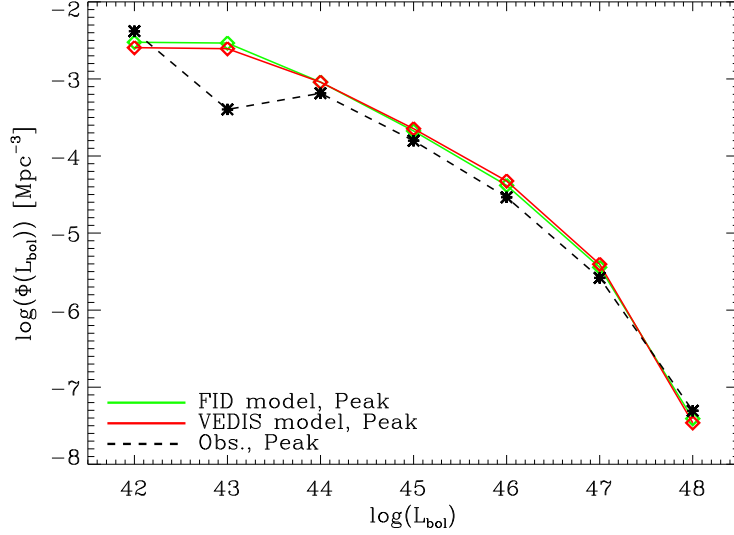


Figure 4.7: AGN number densities versus bolometric luminosities at the peak of each luminosity bin. The green solid line shows the FID model, the red solid line the VEDIS model and the dashed line the observational compilation. Both models can reproduce the right order of magnitude at the peak of each luminosity bin as observed (Hopkins et al., 2007c).

efficiently than in the FID model leading to a less efficient bulge and thus, black hole growth at all redshifts. Increasing the strength of the radio-mode feedback leads to a smaller amount of luminous AGN ($L_{\text{bol}} > 10^{45}$ erg/s) between redshifts $0 < z < 4$, as radio-mode feedback is very efficient in suppressing cooling and star formation in massive halos. This again results in a worse agreement with the observational compilation than the FID model itself. If 'halo quenching' is assumed instead of the radio-mode feedback, i.e. no cooling is allowed above a certain threshold halo mass ($M_{\text{halo,thres}} = 10^{12} M_{\odot}$), again, a decrease of the number of luminous AGN is obtained at *all* redshifts, but no redshift dependence as observed, similar to the case of a stronger radio-mode feedback. Moreover, in order to increase the number density of moderately luminous objects at low redshifts, the timescale (t_Q) in the power-law decline phase of a quasar episode has been varied. A study from Marulli et al., 2008 has shown that additionally assuming a power-law decline growth phase in their quasar mode *does* increase the number density of less luminous AGN at low redshift, resulting in a better agreement to observations. However, within this study it was found that varying t_Q did not help to get a better agreement with observations. Therefore, one can conclude that downsizing cannot be sufficiently reproduced by varying some of the parameters of the FID model. Instead, the influence of the additional modifications for black hole growth will be now studied as outlined in Section 4.3.3.

The result for the VE model (i.e. assuming a decreasing sub-Eddington accretion limit with decreasing redshift and increasing mass) is shown in the upper right panel of Fig. 4.6. For bolometric luminosities larger than 10^{46} erg/s (green, yellow and red curves), a mass and redshift dependent sub-Eddington limit leads to a reduced amount of AGN and thus, to a reasonably good reproduction of the observed steep decline in the number density of the luminous AGN at $z < 2$. This result can be seen as clear evidence that an upper limit for black hole accretion - decreasing with decreasing redshift and with increasing black hole mass - seems to be necessary in order to decrease the amount of luminous AGN at low z and to predict the observed decline in AGN number density. This would imply that massive black holes do exist at low redshifts, but they do not appear as luminous AGN anymore since they are less active and do not accrete at the Eddington-rate as at earlier times. The underlying reason might be due to the small amount of the available cold gas content in the host galaxies. One may speculate that low cold gas densities lead to smaller viscosity so that it takes longer for the gas to loose its angular momentum and thus, to be accreted onto the black hole. E.g. Hickox et al. (2009) show observationally that at higher redshifts galaxies contain on average a larger cold gas fraction than at low redshifts. Star formation and accretion onto the black hole is quenched when a halo mass of $10^{12} - 10^{13} M_{\odot}$ is reached. Therefore, massive ellipticals - hosting massive black holes - contain only a small amount of cold gas and show no quasar activity anymore.

Similar to the FID model, the VE model (see upper right panel in Fig. 4.6) still under-predicts the number densities of AGN which are less luminous than 10^{46} erg/s at $z < 1.5$. This failure might be due to missing trigger mechanisms for AGN activity, since so far, a quasar phase is only driven by major merger events. Thus, the lower left panel in Fig. 4.6 shows the AGN number density evolution for the VEDI model, including black hole accretion due to disk instabilities at $z \leq 2$. For a luminosity range of $43 < \log(L_{\text{bol}}) < 45$ (light and dark blue curves) it is found that accretion due to disk instabilities increases the number density of AGN, resulting in a reasonably good match with the observational compilation for $z < 1.5$. For the lowest luminosity bin, however, the amount of AGN is now over-predicted. Nevertheless, this additional accretion mechanism seems to play an important role for triggering AGN activity of moderately luminous objects. Compared to the GALFORM-model (e.g. Fanidakis et al., 2010), however, in the model of this study disk instabilities are only important for moderately luminous AGN whereas in their model, disk instabilities build up the major contribution for AGN number densities for *all* luminosities and at *all* redshift. Contrary, in the MUNICH-model, Marulli et al. (2008) and Bonoli et al. (2009) do not account for black hole accretion due to disk instabilities at all, but they are still slightly under-predicting the amount of moderately luminous AGN, even in their best-fit model (like in the FID and VE model).

Finally, the lower right panel of Fig. 4.6 shows the result for the VEDIS model. Here, a heavy seeding scenario is additionally assumed as well as a large scatter in the

accreted black hole mass at $z > 5$ resulting in larger AGN number densities for $z > 4$ than for the other three models, in particular for AGN with bolometric luminosities $L_{\text{bol}} > 10^{45} \text{erg/s}$. This shows clearly that black holes have to undergo at high redshifts ($z > 5$) a phase of very rapid growth, even if it is observationally still unknown and unconstrained whether and how such massive seed black holes can form out of a direct core-collapse or whether less massive seeds have to accrete at super-Eddington ratios. However, it is worth to point out that assuming even more massive black hole seeds with masses of $M_{\bullet, \text{seed}} = 10^6 M_{\odot}$ results in a too small amount of moderately luminous AGN at high redshift ($z \approx 5$) in the model. Note that the studies of Marulli et al. (2008) and Bonoli et al. (2009) assuming black hole seeds of $10^3 M_{\odot}$ cannot reproduce a large enough amount of luminous AGN at high redshift, whereas in the work of Fanidakis et al. (2010), they obtain a sufficiently large amount of luminous AGN at high redshift as they allow for super-Eddington accretion.

In the VEDIS model, the peak AGN number densities of the different luminosity bins still match the observed ones what can be seen by the red, solid line in Fig. 4.7. Moreover, in contrast to the FID model, the correct AGN number densities of high as well as of moderately luminous objects at low redshift can now additionally be reproduced and a reasonably good match for high-luminous objects at high redshift can be obtained. Thus, the VEDIS model is the current best-matching model for reproducing the downsizing trend in this work. However, in this model, there still exist deviations from observations in the lowest luminosity bin (black solid curve and light and dark blue curves at $z > 2$), where the number of objects is over-predicted. This might be due to the difficulty of detecting moderately luminous objects at high redshifts, being a consequence of obscuration by a dusty torus around the accreting black hole, which might eventually be modeled insufficiently for the dust correction factor applied to the observational compilation in the study of Hopkins et al. (2007c). Another possible explanation for the over-prediction of moderately luminous AGN at high redshift might be due to a not strong enough and/or different scalings for supernova feedback at high redshift (see discussion in Section 4.10).

4.7 The AGN luminosity function

4.7.1 Bolometric luminosities

Despite some minor shortcomings, the success of the VEDIS can also be explicitly seen in Fig. 4.8, where the bolometric quasar luminosity function (QLF) is plotted for different redshift bins in direct comparison to the FID model. Black symbols show the observational compilation from Hopkins et al. (2007c), the green lines correspond to the output of the FID model and the red lines illustrate the result from the VEDIS model, where a reasonably good agreement is achieved with observations for the whole redshift range. At redshift $z = 5$, a change in number density by about an order

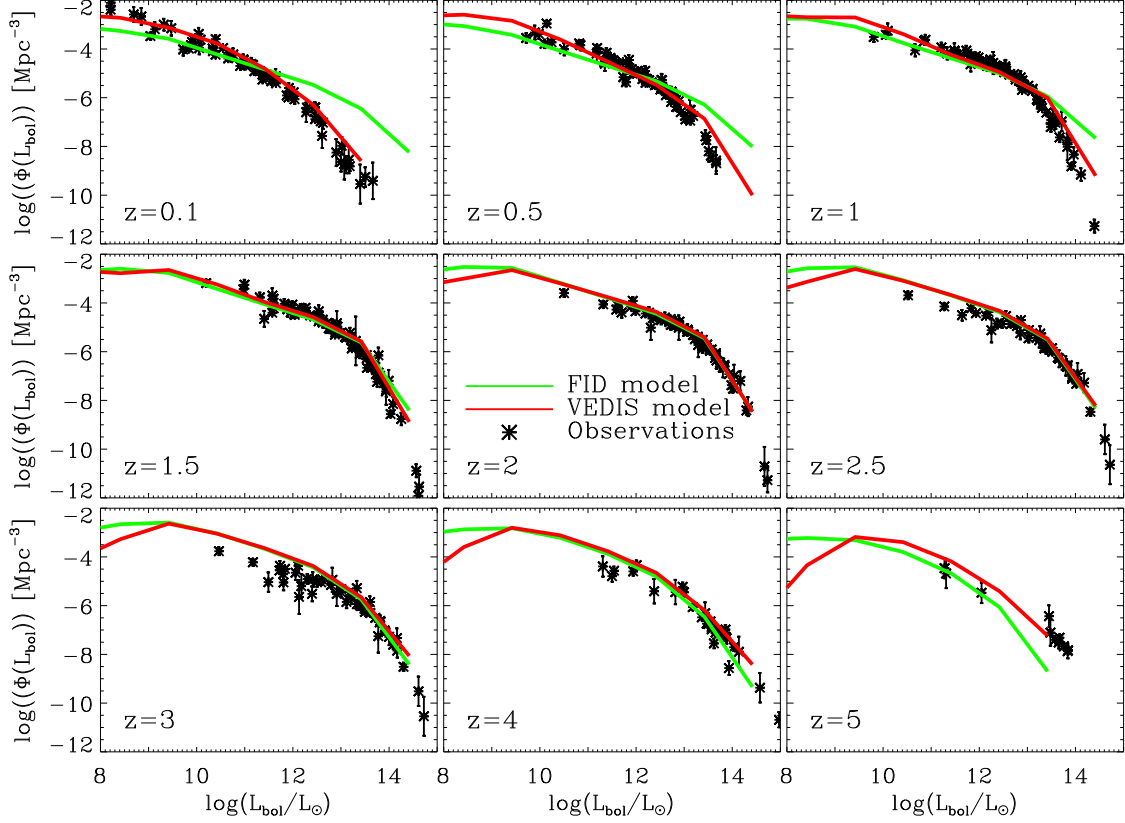


Figure 4.8: *Bolometric quasar luminosity functions for different redshifts. Black symbols show the observational compilation of Hopkins et al. (2007c), the green solid line corresponds to the output of the FID model and the red line illustrates the results from the VEDIS model. For the VEDIS model, a reasonably good agreement with observations can be obtained.*

of magnitude is obtained due to the heavy seeding scenario and the large scatter in the accreted black hole mass in the VEDIS model compared to the FID model. For the redshift range between 1.5 – 3, the additional model extensions do not cause any significant differences. However, for low redshifts, in particular at $z = 0.1$, the decreasing sub-Eddington limit leads to a discrepancy in AGN number densities at the high-luminous end by 2 – 3 orders of magnitude. Moreover, at the low-luminosity end, one can still see a change in VEDIS model by almost one order of magnitude as AGN are assumed to be additionally triggered by disk instabilities. One can conclude, owing to the better match to the observed QLF in the VEDIS model than in the FID model, that the additional assumptions might be important and non-negligible ingredients for galaxy formation and the connected black hole growth and, in particular, for the observed downsizing trend.

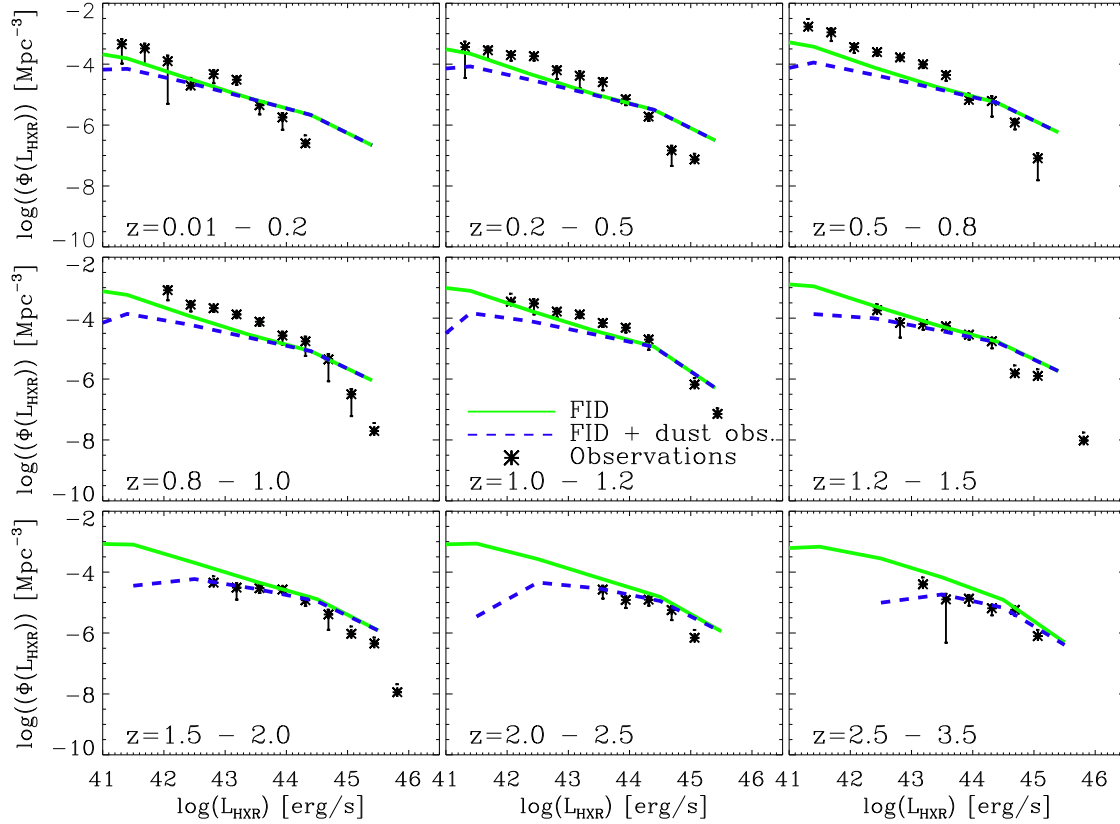


Figure 4.9: *Hard X-ray AGN luminosity function for different redshifts ranges. Black symbols show the observational compilation of Aird et al. (2010), the green solid lines correspond to the output of the FID model and the blue dashed lines illustrates the same results with dust correction.*

4.7.2 Hard X-ray luminosities

Besides comparing the model output to the bolometric luminosities from the observational compilations of Hopkins et al. (2007c), the predicted bolometric luminosities from the model are converted into hard X-ray luminosities in order to compare them directly to the observed hard X-ray luminosities of a recent observational study from Aird et al. (2010). In order to calculate the hard X-ray luminosities, we use the bolometric correction according to Marconi et al. (2004), where the hard X-ray luminosities are approximated by the following third-degree polynomial fit:

$$\log(L_{\text{HXR}}/L_{\text{bol}}) = -1.54 - 0.24\mathbb{L} - 0.012\mathbb{L}^2 + 0.0015\mathbb{L}^3 \quad (4.30)$$

with $\mathbb{L} = \log(L_{\text{bol}}/L_{\odot}) - 12$. These corrections are derived from template spectra, which are truncated at $\lambda > 1 \mu\text{m}$ in order to remove the IR bump and which, and hence the bolometric corrections, are assumed to be independent of redshift. Moreover, a dust correction for the model luminosities is additionally assumed, as suggested

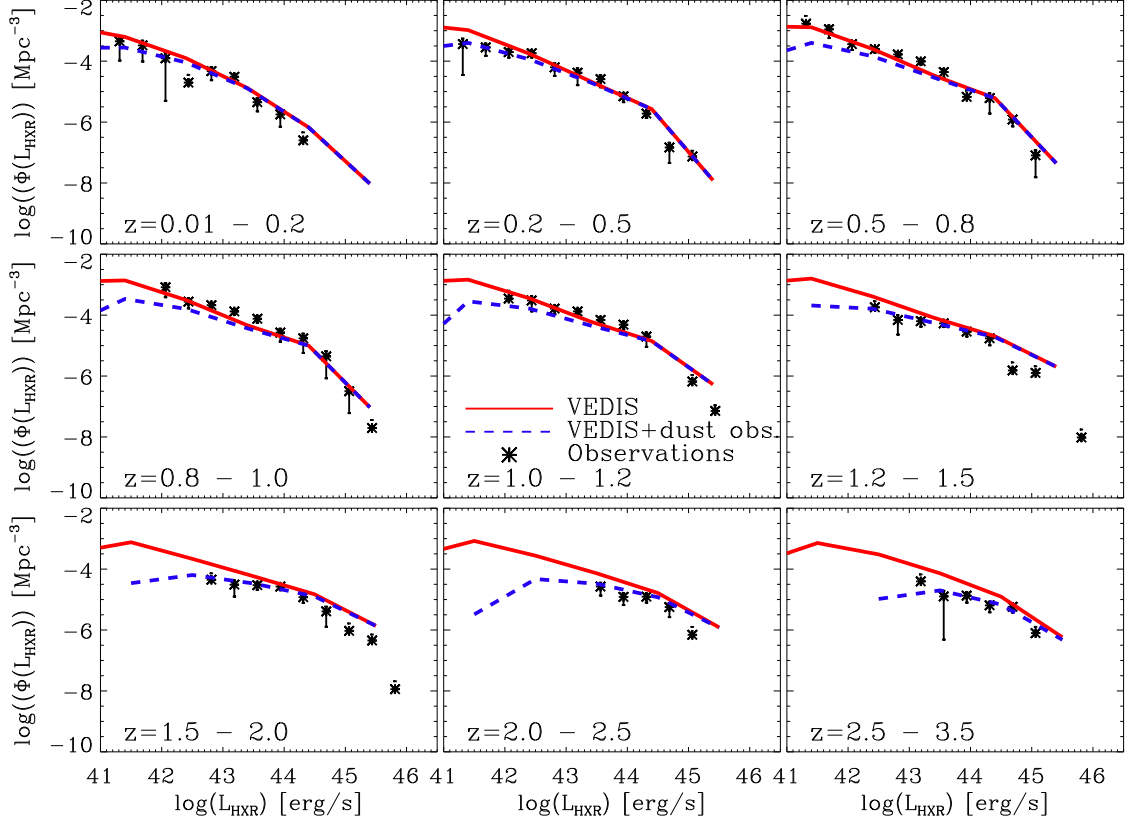


Figure 4.10: *Hard X-ray AGN luminosity function for different redshifts ranges. Black symbols show the observational compilation of Aird et al. (2010), the red solid lines correspond to the output of the VEDIS model and the blue dashed lines illustrates the same results with dust correction.*

by different observational studies (Ueda et al., 2003; Hasinger, 2004; La Franca et al., 2005), where they show that the fraction of obscured AGN is luminosity dependent and decreases with increasing luminosity. However, whether there exists an additional redshift dependence of the obscured fraction is under current, intense debate. Studies from Ballantyne et al. (2006) and Gilli et al. (2007) propose a strong evolution of the obscured AGN population (a relatively increasing fraction of obscured AGN with increasing redshift) to reproduce the properties of the X-ray background, whereas Ueda et al. (2003) and Steffen et al. (2003) do not find a clear dependence of the obscuration on redshift. In this thesis, I follow a recent observational study from Hasinger (2008), where they investigate a sample of X-ray selected AGN from ten independent samples. They find that the fraction of obscured AGN increases strongly with decreasing luminosity and increasing redshift. Following Hasinger (2008), the obscured fraction of AGN is modeled and approximated by this equation (see also Fanidakis et al. (2010)):

$$f_{\text{obsc}} = -0.281(\log(L_{\text{HXR}}) - 43.5) + 0.308(1 + z)^\alpha. \quad (4.31)$$

Fitting this equation to observations, as it is shown in Hasinger (2008), results in a value for the exponent of $\alpha = 0.62$. However, in this study, it is found that an even stronger redshift dependence is needed to be consistent with the observations ($\alpha \approx 0.8$). With calculating the obscured fraction of AGN in the hard X-ray band, the visible fraction of AGN $f_{\text{vis}} = 1 - f_{\text{obsc}}$ can be modeled, and thus the visible number density of AGN in the hard X-ray range can be approximated by:

$$\Phi_{\text{vis}}(L_{\text{HXR}}) = f_{\text{vis}} \times \Phi_{\text{total}}(L_{\text{HXR}}) \quad (4.32)$$

Fig. 4.9 shows the hard X-ray luminosity function for different redshift ranges. The black symbols illustrate the observations from Aird et al. (2010), the green lines show the predictions from the fiducial model without dust correction, whereas the blue dashed lines correspond to the number densities of visible AGN. At low redshift ($z = 0 - 1$), the fiducial model under-predicts moderately luminous AGN and over-predicts luminous AGN, as already seen for the bolometric luminosity functions in Fig. 4.8. As expected, in this redshift range, dust correction plays only a minor role and leads to small differences at the low luminosity end. Turning to higher redshift $z > 1.5$, the high luminosity end is only slightly overestimated anymore. However, at the low luminosity end the fiducial model without dust correction extremely over-predicts the number densities of these objects. Therefore, considering the number densities only of the visible fraction of AGN leads to a significantly better agreement with the observations at the low mass end. This shows clearly, that the model output confirms the observational finding of the existence of a strong redshift dependence in the obscured fraction of AGN. Besides, we can conclude that dust correction alone seems not to be a sufficient process in order to reproduce downsizing in the FID model, as at low redshift, the dust correction can account neither for the excess of luminous AGN nor for the lack of moderately luminous AGN. Considering the output of the VEDIS model, Fig. 4.10 illustrates the corresponding hard X-ray luminosities (solid, red lines) compared to the observations (black symbols). The blue, dashed lines show the results considering in addition the dust correction for the VEDIS model. Compared to the FID model, the predictions of the VEDIS model lead to a significant better agreement with the observations at redshifts $z \leq 1$ as through the additional modifications the number density of luminous AGN is reduced and the amount of moderately luminous AGN gets increased, as it was already shown for the bolometric luminosity function above. The results including dust obscuration show still a fairly good match with observations at this redshift range. Therefore, one can conclude that the best-fit VEDIS model combined with a redshift and luminosity dependent dust obscuration correction is successful in predicting the observed hard X-ray luminosity function for the whole, observed redshift range. Note that Fanidakis et al. (2010) use the same bolometric conversion for calculating hard X-ray luminosities and the almost the same dust obscuration correction (they use a smaller value for α). They show that they are able to match the hard X-ray luminosity functions from an observational study of Hasinger et al. (2005). However, their predictions are only illustrated for a comparatively small redshift range of $0.2 < z < 1.6$, where they have not applied any dust obscuration to

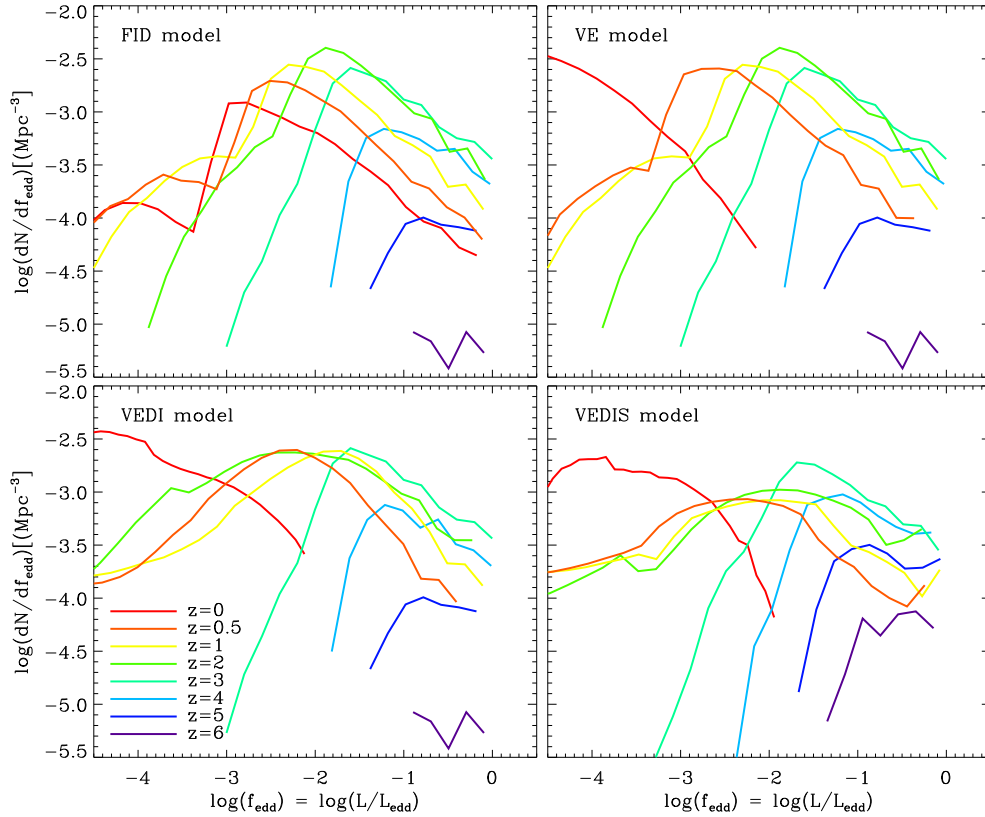


Figure 4.11: Eddington-ratio distributions for the FID, VE, VEDI and VEDIS models. Different colors correspond to different redshifts. It shows that most black holes are not radiating at the Eddington-limit. This is in qualitative agreement with observations (Vestergaard, 2003; Kollmeier et al., 2006; Kelly et al., 2010; Schulze & Wisotzki, 2010). Moreover, with decreasing redshift, the peak of the distribution is shifted towards smaller Eddington-ratios and the distributions are broadened.

their hard X-ray luminosities.

4.8 Eddington-ratio distributions

For a more fundamental understanding of the implications and consequences of the downsizing behavior for galaxy evolution and black hole growth caused by the additional model modifications, in this and the following Section, the Eddington-ratio distributions and the relation between black hole mass and bolometric AGN luminosity are investigated. The four panels in Fig. 4.11 show the Eddington-ratio distributions during the quasar phase for the four SAMs at different redshift steps, illustrated by different colors ($z = 0, 0.5, 1, 2, 3, 4, 5, 6$). In all models and at all redshift, the majority of AGN are found *not* to be radiating near or at the Eddington-limit as black

holes spend most of their time not in the first regime, accreting at the Eddington-rate but in the second regime, accreting in the power-law decline phase of the light curves. This is in qualitative agreement with different observational studies (Vestergaard, 2003; Kollmeier et al., 2006; Kelly et al., 2010; Schulze & Wisotzki, 2010). For example, Kelly et al., 2010 find that their Eddington-ratio distribution (using broad-line quasars between $z = 1 - 4$) peaks only at an Eddington-ratio of $f_{\text{edd}} = 0.05$.

In the FID model (upper left panel), one can see clearly that the peaks of the Eddington-ratio distributions emerge towards smaller ratios with decreasing redshift: at $z = 5$ the distribution peaks at $f_{\text{edd}} \approx 0.1$, whereas at $z = 0$ the peak is located around $f_{\text{edd}} \approx 10^{-3}$. This shows that with decreasing redshift an increasing number of black holes is accreting with smaller Eddington-ratios in the power-law decline phase of the light curves. These black holes are relicts from an earlier, more active phase with higher accretion. Moreover, the distributions are broadened with decreasing redshift. This qualitative trend of a shifted and broadened peak towards lower redshift with decreasing redshift is also qualitatively consistent with observational studies (see Vestergaard, 2003; Kollmeier et al., 2006; Netzer & Trakhtenbrot, 2007). In the VE model (see upper right panel), where it is additionally assumed that the black holes are not allowed anymore to accrete at the Eddington-rate in the first regime, but instead adopt an sub-Eddington limit decreasing with redshift and increasing black hole mass, the trend of the shifted peak towards smaller Eddington-ratios gets even amplified: by construction, there exist no larger Eddington-ratios than 0.01 at $z = 0$, and the distribution is shifted towards even smaller Eddington-ratios peaking at $f_{\text{edd}} \approx 10^{-4}$. However, in observations this shift is much less pronounced than in this theoretical study. This might eventually be due to observational flux limits only reaching Eddington-limits in excess of $f_{\text{edd}} = 10^{-3}$. Nevertheless, a stronger shift and smaller upper accretion limit (compared to the FID model) in the Eddington-ratio distribution, preventing especially massive quasars to accrete at the Eddington rate, might be necessary for reproducing the small, observed amount of luminous AGN at low redshift. Interestingly, with the GALFORM model (see Fanidakis et al., 2010), the Eddington-ratio distribution at $z = 0$ peaks also around $f_{\text{edd}} = 10^{-4}$ in agreement with this result even if their model is fundamentally different to the approach in this study. Using the VEDI model (see lower left panel), at redshifts $z \leq 2$, the distributions are additionally broadened compared to the FID and the VE models, mainly towards lower Eddington-ratios. This is due to the contribution of the black hole accretion following disk instabilities, which results in Eddington-ratios $f_{\text{edd}} \leq 0.01$. Finally, larger seed black hole masses in the VEDIS model (see lower right panel) lead to a much larger amount of accreting objects near to the Eddington-limit ($0.1 < f_{\text{edd}} < 1$) at $z > 3$. In particular, at redshift $z = 6$ the number density of accreting black holes in a quasar phase is increased by one order of magnitude ($\log(dN/df_{\text{edd}}) \approx -4.2$) compared to the other three models ($\log(dN/df_{\text{edd}}) \approx -5.2$). Note that in the study of Fanidakis et al., 2010, they obtain an even larger number density at $z = 6$ ($\log(dN/df_{\text{edd}}) = -3.4$) peaking at larger Eddington-ratios $f_{\text{edd}} = 0.5$ (allowing additionally for super-Eddington

accretion) than in this study.

4.9 Luminosity-black hole mass-relation

Fig. 4.12 shows the bolometric AGN luminosity versus black hole mass at $z = 0$ (left panels), $z = 2$ (middle panels) and $z = 4$ (right panels) for the four different SAMs (different rows). The different points correspond to the different objects in the sample with bolometric luminosities higher than $L_{\text{bol}} > 10^{43}$ erg/s. The red solid line illustrates accretion at the Eddington rate, the red dashed line depicts an Eddington-ratio of $f_{\text{edd}} = 0.1$ and the red dashed-dotted line an Eddington-ratio of $f_{\text{edd}} = 0.01$.

In all models, at $z = 4$ (right column in Fig. 4.12) an almost linear correlation between luminosity and black hole mass can be seen, indicating that the larger the black hole mass the more gas is accreted by black holes resulting in larger bolometric luminosities. Nearly all black holes at this redshift are accreting at Eddington-ratios larger than $f_{\text{edd}} < 0.01$ (see also Fig. 4.11). In the FID, VE and VEDI model black holes with masses $10^{4.5}M_{\odot} < M_{\bullet} < 10^8M_{\odot}$ are active, whereas in the VEDIS model, there exist no black holes accreting below $\log(M_{\bullet}/M_{\odot}) < 5.5$ due to the heavy black hole seeds. Moreover, in the VEDIS model, a larger amount of black holes with masses $10^6M_{\odot} < M_{\bullet} < 10^{7.5}M_{\odot}$ is actively accreting gas than in the other three models. Turning to redshift $z = 2$ (middle column Fig. 4.12), in all models, a larger number of active black holes exists than at $z = 4$, however, the relation between black hole mass and bolometric luminosity vanishes. E.g. black holes with masses $M_{\bullet} \approx 10^8M_{\odot}$ can now also power moderately luminous AGN with $L_{\text{bol}} \approx 10^{43}$ erg/s as they are accreting clearly with Eddington-ratios below $f_{\text{edd}} < 0.01$. Moreover, the probability for black holes with $M_{\bullet} > 10^7M_{\odot}$ to accrete at Eddington-ratios below $f_{\text{edd}} = 0.01$ is even higher than to accrete at larger Eddington-ratios (consistent with Fig. 4.11). This is due to the long power-law decline accretion phase, black holes are experiencing: massive black holes powering moderately luminous AGN are remnants of former, high-luminous AGN. Finally at redshift $z = 0$ (left column Fig. 4.12), the amount of actively accreting black holes is again clearly reduced compared to $z = 2$ and significant differences between the FID, the VE and the VEDI models appear. In the FID model (upper left panel), a few high-mass black holes ($M_{\bullet} \approx 10^9M_{\odot}$) are accreting close to the Eddington-limit, causing the high number densities of luminous AGN at low redshifts compared to the observations seen in Fig. 4.6 (yellow and red curve). This is, however, suppressed in the VE model, where the black holes are forced not to accrete above Eddington-ratios of $f_{\text{edd}} = 0.01$ resulting in a smaller amount of luminous AGN at low redshift. Furthermore, in the VEDI model, there exists an increased amount of active black holes with masses of $10^7M_{\odot} < M_{\bullet} < 10^8M_{\odot}$ due to the additional disk instabilities triggering a quasar phase. These black holes mainly contribute to the amount of AGN with bolometric luminosities between 10^{43} erg/s $< L_{\text{bol}} < 10^{45}$ erg/s. As Seyfert galaxies are mainly spiral galaxies with black hole masses in the range of

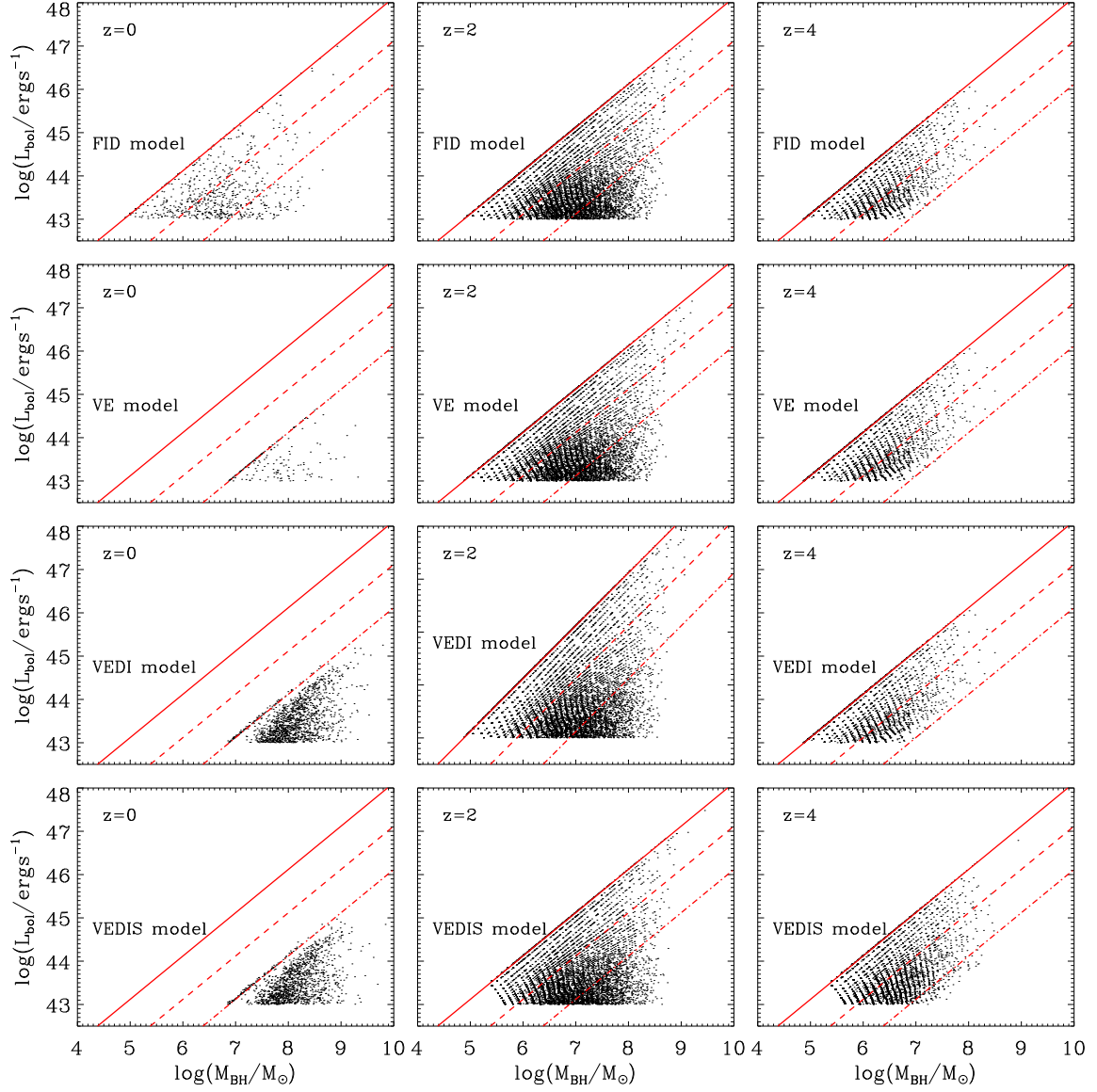


Figure 4.12: Bolometric luminosity versus black hole mass at $z = 0$ (left panels), $z = 1$ (middle panels) and $z = 2$ (right panels). The points correspond to the actively accreting black holes in the sample. The first row shows the results of the fiducial model, the second row for the VE model, the third row for the VEDI and the lower row corresponds to the results from the VEDIS model. The red solid line illustrates accretion at the Eddington-rate $f_{\text{edd}} = 1$, the red dashed and dotted dashed lines fractions of the Eddington-rate $f_{\text{edd}} = 0.1$ and $f_{\text{edd}} = 0.01$.

$10^7 M_\odot < M_\bullet < 10^8 M_\odot$ and are - compared to quasars - only moderately luminous, disk instabilities seem indeed to provide one of the most important underlying trigger mechanisms for their nuclear activity.

Note that in the study of Fanidakis et al. (2010), they obtain almost no evolution of their luminosity-black hole mass relation within a redshift range $0.5 < z < 2$. Black holes above $M_\bullet > 10^9 M_\odot$ accrete always below $f_{\text{edd}} = 0.01$ (ADAF regime), as in the VE, VEDI and VEDIS models. However, in clear contrast to this work, in this redshift range, they still have super-Eddington accretion, in particular for black hole masses between $10^8 M_\odot < M_\bullet < 10^9 M_\odot$ (resulting in $L_{\text{bol}} > 10^{46}$ erg/s). This is, however, in clear contrast to several observational studies, e.g. to Steinhardt & Elvis (2010), where they show that black holes with masses $M_\bullet > 10^7 M_\odot$ are *not* accreting near or at the Eddington-limit anymore at low redshifts $z = 0.2 - 0.4$.

Furthermore, Kollmeier et al. (2006) investigate a sample of 407 AGN from the AGES survey at $z \sim 0.3 - 4$ with bolometric luminosities between 10^{45} erg/s $< L_{\text{bol}} < 10^{47}$ erg/s. In their sample, black holes are mainly accreting between $f_{\text{edd}} \sim 0.1 - 1$. Massive black holes ($M_\bullet > 10^{8.5} M_\odot$) are found to be active at high redshift ($z = 3-4$), whereas at $z < 0.5$ mainly less massive objects are active ($M_\bullet < 10^8 M_\odot$). Such a mass dependence, however, cannot be reproduced by the four models so far.

4.10 Discussion and conclusion

In this Chapter, different mechanisms have been presented significantly influencing the co-evolution of galaxies and black holes, which may provide possible explanations for the observed anti-hierarchical trend in black hole growth. For this study, the semi-analytic model according to S08 has been used and three further modifications based on this fiducial model. The semi-analytic code is applied to the merging histories of the Millennium-simulation and contains most of the currently known physical processes which are important for galaxy formation. Moreover, the fiducial (FID) model includes an advanced prescription for black hole growth following the light curve models for AGN according to isolated merger simulations. Up to a critical mass limit, black holes are allowed to accrete at the Eddington-limit, whereas afterwards, in the power-law decline phase, they accrete only at fractions of the Eddington-rate. Black holes spend most of their time in the latter, low-Eddington-ratio regime. For the FID model it is found that the peaks of the distributions of Eddington-ratios move towards smaller values and the distributions get broadened with decreasing redshift in qualitative agreement with observational findings (Vestergaard, 2003; Kollmeier et al., 2006; Netzer & Trakhtenbrot, 2007; Kelly et al., 2010; Schulze & Wisotzki, 2010). Furthermore, the observed order of magnitude of AGN number densities at the *peak* of different luminosity bins can be reproduced. However, the FID model still reveals the characteristic anti-hierarchical failures within the framework of a hierarchical clustering scenario: at low redshift, the

FID model overproduces the number densities of luminous AGN and under-predicts the amount of moderately luminous AGN and at high redshift, this trend is reversed. By implementing the outlined modifications, a significantly improved match to the observations can be achieved, i.e. to the bolometric and hard X-ray AGN luminosity function showing the observed downsizing the trend:

1. A decreasing sub-Eddington limit with increasing mass and decreasing redshift reduces the amount of luminous AGN at low redshift (VE model).
2. Accretion onto the black hole due to disk instabilities is responsible for increasing the amount of moderately luminous AGN at low redshift (VEDI model).
3. A heavy seeding scenario together with a large scatter in the accreted gas mass results in a larger amount of luminous AGN at high redshift (VEDIS model).

Despite of these modifications, the observed galaxy and black hole properties of the present-day Universe in the VEDIS model, as the galaxy-halo mass relation and as the black hole mass function can be reproduced at $z = 0$. For the FID as well as for the VEDIS model it is found that an additional approximation for gravitational heating combined with a less efficient radio-mode accretion leads to a better agreement with the observed black hole mass function and the galaxy-halo mass relation at the *high* mass end balancing the stellar and black hole growth in a more physical way than by assuming a more efficient radio-mode accretion and feedback alone. However, turning to the present-day black hole-bulge mass relation, the modifications in the VEDIS model lead to a slightly worse agreement with the observations than the FID model. This is due to the decreasing upper limit of the Eddington-ratios resulting in a slower growth of black holes compared to the bulges and thus, in a smaller ratio of black hole to bulge mass than expected from observations. This shows clearly that in this respect, there is still need for improvement, even in the best-fit VEDIS model.

A sub-Eddington limit at low redshift (as suggested in observational studies by Netzer & Trakhtenbrot (2007); Steinhardt & Elvis (2010)), which is dependent on black hole mass and redshift, leads to a strikingly good agreement with the luminous AGN number density at low redshift as it prevents massive black hole to accrete near or at the Eddington-rate. As one may argue that the assumption of a sub-Eddington-limit at low redshift should be a *self-consistent* result from the model, a direct dependence of the gas accretion onto the black hole on the cold gas content, which is available in the galaxy, was tested. E.g. Hopkins et al. (2008a) have shown in simulations that allowing dry mergers to trigger quasar activity would overproduce the observed quasar luminosity density. Thus, a simple model was assumed, where the final black hole mass in the beginning of a quasar was linked directly to the cold gas mass $M_{\bullet, \text{final}} = 0.005 M_{\text{cold}}$ (note that in the FID model black hole accretion is related to the spheroid component of the merged system and thus, it is only indirectly linked to the cold gas content). Interestingly, this results in a natural downsizing behavior of the peaks of the curves: the peak positions evolve slightly towards lower redshifts with decreasing luminosity

of the AGN. This suggests that directly linking black hole accretion to the cold gas fraction may represent a promising way for modeling gas accretion onto black holes in SAMs. However, the quantitative shape of the curves, in particular the steep decline in number densities of luminous AGN at low redshifts (Fig. 4.6), is not in agreement with the observations so far, even if the simple approximation for gravitational heating has been adopted. Moreover, it seems reasonable to additionally scale the final black hole mass with the mass ratio of the two merging galaxies. In a study of Johansson et al. (2009a) it was shown that in isolated merger simulations the growth of a black hole during a merger event is extremely sensitive to the mass ratio (a smaller mass ratio leads to a reduced growth of the black hole). With the additional scaling of the final black hole mass with the mass ratio, indeed, the small number densities of luminous AGN at $z = 0$ can be reproduced. However, within the redshift range of $0 < z < 3$, this model would significantly under-predict the amount of luminous AGN resulting again in a wrong shape of the curves compared to the observations. This clearly shows that obtaining an evolving sub-Eddington limit with redshift for the Eddington-ratios in a self-consistent way from the FID model seems to be a pretty complex process. Thus, either the recipe for connecting black hole accretion to the cold gas content may have to be refined or the evolution of the cold gas content in the FID SAM may not be correctly modeled leading to a quantitatively wrong behavior. This might be due to incomplete prescriptions for feedback processes, in particular supernova feedback, or due to incorrect or simplified cooling recipes in the SAM. In Section 5.5.3 of the next Chapter, it will be shown that the cooling in SAMs compared to cosmological simulations seems to be insufficient, in particular for massive objects at high redshifts. One possibility for refining the cooling recipe in the SAM might be to assume in general cold gas infall and additionally to implement gravitational heating in a more self-consistent way than it is done so far (see e.g. Khochfar & Ostriker, 2008) in order to calculate the heated gas fraction (see also Chapter 5).

Additional gas accretion onto black holes due to disk instabilities is found to be a non-negligible trigger mechanism for moderately luminous AGN with black hole masses $10^7 M_\odot < M_\bullet < 10^8 M_\odot$ at low redshift. This increases the amount of AGN with bolometric luminosities $10^{43} \text{ erg/s} < L_{\text{bol}} < 10^{45} \text{ erg/s}$ by a factor of 2–4. This is in agreement with different observational studies (Cisternas et al., 2010; Georgakakis et al., 2009; Pierce et al., 2007; Grogin et al., 2005), where they show that in morphologies of nearby AGN galaxies, no stronger distortions can be seen, than in the ones of quiescent galaxies. This suggests that the nuclear activity cannot only be a consequence of major merger events, but also by secular evolution processes as disk instabilities. With the results in this Chapter, the current picture can be confirmed that disk instabilities are the main trigger mechanism to power moderately luminous Seyfert galaxies at low redshift, whereas major merger events are mostly driving the nuclear activity in high luminous quasars at high redshift (see e.g. Hopkins & Hernquist, 2009). Note that neither the MUNICH nor the GALFORM model come to similar conclusions (see below).

Heavy seeding mechanisms for black holes are found to provide one, straight-forward possibility in order to reproduce the observed amount of luminous AGN at high redshift. This is in agreement with the studies from Volonteri et al. (2008) and Volonteri (2010) showing that either massive black hole seeds are required or less massive seeds have to accrete at super-Eddington rates. Unfortunately, current observational constraints for such high redshift are not sufficient to favor one of these possibilities what will be, however, possible with the next generation of planned X-ray missions (as e.g. WFXTE, IXO).

Despite the success of the final VEDIS model in reproducing the bolometric AGN luminosity function fairly well, the amount of low luminous AGN is still over-estimated at high redshift $z > 2$. However, this is a common problem of most current SAMs (see e.g. Marulli et al., 2008; Fontanot et al., 2006). One possible explanation might be due to dust obscuration as even 2 – 10 keV X-ray surveys will miss a significant fraction of moderately obscured AGN (25% at $N_H = 10^{23} \text{ cm}^{-2}$) and nearly all Compton-thick AGN ($N_H > 10^{24} \text{ cm}^{-2}$, Treister et al., 2004; Ballantyne et al., 2006). From fits to the cosmic X-ray background, Gilli et al. (2007) predict that both moderately obscured and Compton-thick AGN are as numerous as unobscured AGN at luminosities higher than ($\log(L_{0.5-2\text{keV}}) > 43.5[\text{ergs/s}]$), and four times as numerous as unobscured AGN at smaller luminosities ($\log(L_{0.5-2\text{keV}}) < 43.5[\text{ergs/s}]$). The obscured and Compton-thick AGN missed in deep X-ray surveys, therefore, serve not only as important probes of SMBH/galaxy co-evolution, but likely constitute a significant fraction of the total AGN population at all luminosities, in particular of moderately luminous AGN at high redshift. The observational compilation of Hopkins et al. (2007c), which is used to be compared to the model output, does take into account a dust correction factor, where they assume a luminosity dependence of the obscured fraction (the less luminous the more obscured) and the same number of Compton-thick ($N_H > 10^{24} \text{ cm}^{-2}$) and Compton-thin ($10^{23} \text{ cm}^{-2} < N_H < 10^{24} \text{ cm}^{-2}$) AGN. However, due to insufficient observational constraints for obscuration of Compton-thick objects and of whether there exists an additional redshift dependence for the obscured fraction of AGN (see Hasinger, 2008), dust obscuration processes may be not sufficiently considered in Hopkins et al. (2007c) and thus, they may provide a possible explanation for the deviation between the modeled bolometric luminosities of moderately luminous AGN and the bolometric luminosities of the observational compilation at high redshift. This statement might be confirmed as the VEDIS model is in fairly good agreement with the low luminosity end of the observed hard X-ray luminosity function at high redshift, when a strong redshift dependence of the dust obscuration is assumed, even stronger as it is found in Hasinger (2008). From the latter point, one can conclude that dust correction indeed may provide a significant contribution in explaining the moderately luminous AGN number densities peaking at low redshift, but I want to emphasize that it cannot account for the observed downsizing completely on its own (see FID model and dust obscuration in Fig. 4.9).

Additionally, as a relatively strong redshift dependence for the dust obscuration is needed in order to be in agreement with observations, the over-estimation of low luminous AGN at high redshift might be also connected to the over-estimation of low mass galaxies at high redshift in SAMs (see Fig. 4.5). This is also found in other SAMs (Fontanot et al., 2009; Guo et al., 2011) as well as in simulations (Davé et al., 2011) showing that this problem is not only due to inaccuracies of SAMs. An additional or alternative explanation might be that in the SAM, feedback processes from supernova are not sufficiently accounted for at high redshift and the corresponding recipes might have to be refined (Somerville & Caviglia, in prep.). Apparently, there exists currently no trivial solution, as simply changing the corresponding parameters, which are responsible for supernova feedback, does not solve this problem.

When the results of this Chapter are compared to the findings of some previous studies (see Section 4.2), using the MUNICH and the GALFORM SAM, the following main points can be summarized: The best-fit model based on the MUNICH semi-analytic code presented in Marulli et al. (2008) and Bonoli et al. (2009) is able to reproduce the bolometric AGN luminosity function until at redshift $z = 3$. This is mainly due to the AGN light curves as well as an *explicit* redshift dependence of the accreted gas mass onto the black holes during the quasar phases, which is similar to the redshift dependence assumed for the upper limit of accretion in the model. Interestingly, even if in their model the black hole accretion is directly connected to the cold gas mass of the host galaxy, they still need this explicit redshift dependence for their best-fitting model. However, contrary to this thesis, they claim that they do not need AGN activity triggered by disk instabilities, what seems to be, however, not to be consistent with recent observations. Moreover, they fail to reproduce the AGN luminosity function at high redshift ($z > 3$), as they predict too few luminous AGN and too many low luminous AGN. At least the first point might be due to their assumption of black hole seeds to have masses of $M_{\bullet, \text{seed}} = 10^3 M_{\odot}$. I want to point out that their assumptions for the parametrization of black hole accretion in their best-fit model seem to be rather crude and ad-hoc and they do not seem to be physically motivated.

Compared to the Durham GALFORM model (Fanidakis et al., 2010) it should be emphasized that the main difference to the SAM in this study is the trigger mechanism for black hole activity: in their model, the major contribution originates from disk instabilities for *all* luminosities at *all* redshift. With their model they claim to reproduce the AGN luminosity function at all redshift: the low-luminosity end of the AGN luminosity function is mainly due to their ADAF model (cold gas accretion onto the black hole in a hot halo), whereas in the mode used here, it is due to accretion in the power-law decline regime as well as black hole accretion following disk instabilities. At high redshift, they predict that super-Eddington accretion is the major contribution for getting a large enough amount of luminous AGN. At this point, whether massive seed black holes (as assumed in this study) or super-Eddington accretion describe the correct

physical processes, the improvement of high-redshift AGN observations will be of crucial importance, both by enlarging the current high- z AGN samples and by reducing the current uncertainty originating from incompleteness problems. They mainly attribute the downsizing trend (that moderately luminous objects peak at smaller redshift than luminous objects) to dust obscuration effects and do not discuss any possible improvements for the supernova feedback and the connected reduction of low mass galaxies.

Altogether one can conclude that the model modifications presented in this Chapter state possible attempts in order to understand the origin and the underlying ingredients of the observed downsizing within hierarchical structure formation: at low redshift, very massive black holes do exist and have already assembled their mass at earlier times (mostly until $z \approx 2$), but they seem to accrete only at a small fraction of the Eddington-rate anymore and additionally, disk instabilities seem to become a more important mechanism with decreasing redshift for triggering the activity in moderately luminous Seyfert galaxies. In other words, downsizing *does not* necessarily imply that the growth of low-mass black holes is delayed to low redshift. At high redshift, massive black hole seeds together with a larger scatter in the accreted gas mass might be necessary in order to allow for a sufficiently large amount of luminous AGN. However, the remaining excess of moderately luminous AGN at high redshift might be partly explained by a redshift dependent dust obscuration (Hasinger (2008)). Additionally, a stronger supernova feedback required in the SAMs may also contribute to the reduction of moderately luminous AGN allowing for further improvements of the semi-analytic model.

Galaxy formation in semi-analytic models and zoom simulations

In this Chapter, a detailed comparison is presented between cosmological zoom simulations and semi-analytic models (SAMs) run within merger trees extracted from the simulations. The simulations represent 48 halos with virial masses in the range $2.4 \times 10^{11} M_{\odot} < M_{\text{Halo}} < 3.3 \times 10^{13} M_{\odot}$ with unprecedented resolution for a sample this large and covering such a broad range in halo mass. The simulations include radiative H & He cooling, photo-ionization, star formation and thermal SN feedback. Comparisons with different SAM versions are included. This analysis is focused on the cosmic evolution of the baryon content in galaxies and its division into various components (stars, cold gas, and hot gas). Also both the SAMs and simulations are compared with observational relations between halo mass and stellar mass, and between stellar mass and star formation rate, at low and high redshift. The simulations turn out to have much higher star formation efficiencies (by about a factor of ten) than the SAMs, despite nominally being both normalized to the same empirical Kennicutt relation at $z = 0$. Therefore the cold gas is consumed much more rapidly in the simulations and stars form much earlier. Also, simulations show a transition between stellar mass growth that is dominated by in-situ formation of stars to growth that is predominantly through accretion of stars formed in external galaxies. In SAMs, the stellar growth is always dominated by in-situ star formation, because they significantly under-predict the fraction of mass growth from accreted stars relative to the simulations. In addition, SAMs overestimate the fraction of “hot” relative to “cold” accretion. The reasons for these discrepancies are discussed, and several physical processes are identified that are currently missing in the SAM, but which should be included. This study has been submitted to MNRAS (Hirschmann et al., 2011).

5.1 Different approaches for modeling galaxy formation

The assembly of dark matter halos, which dominate the total matter content in the Universe, in large cosmological volumes can be followed with merger trees based on analytic approaches, e.g. by using Monte-Carlo methods based on the extended Press-Schechter formalism (EPS, Press & Schechter, 1974; Bower, 1991; Bond et al., 1991; Somerville & Primack, 1999b; Neistein & Dekel, 2008; Zhang et al., 2008; Angulo & White, 2010). Alternatively, as it was demonstrated in Chapter 3, the full dynamical evolution of dark matter can be accurately followed with collisionless particles in direct numerical simulations which are, by now, well resolved at the relevant scales (Frenk et al., 1988; Navarro et al., 1997; Moore et al., 1999; Klypin et al., 1999; Bode & Ostriker, 2003; Springel et al., 2005a, 2008; Diemand et al., 2008). Here the identification of dark matter halos and the construction of merger trees is considerably more demanding and various different approaches have been discussed (e.g. Davis et al., 1985; Kauffmann et al., 1993; Ghigna et al., 2000; Springel et al., 2001a; Weller et al., 2005; Genel et al., 2008; Fakhouri & Ma, 2008; Planelles & Quilis, 2010; Skory et al., 2010 and references therein). In particular, Springel et al. (2005a) constructed and analysed merger trees for the Millennium simulation, which were the basic input in Chapter 4, using the “Friends of Friends” (FOF) technique (Davis et al., 1985) to identify halos, and SUBFIND (Springel et al., 2001a) to identify sub-halos (bound objects within larger virialized dark matter halos).

Simulations of the formation and evolution of the galaxies which are believed to inhabit these dark matter halos are more demanding, theoretically as well as numerically. Additional gas-dynamical and radiative processes, such as the formation of stars and black holes as well as the respective feedback, have to be taken into account. To follow the evolution of galaxies two main approaches have been developed over the past decades: *Semi-analytic models (SAMs)* and *direct cosmological simulations*. SAMs, which have been the main tool of investigation in Chapter 4, use pre-calculated dark matter merger trees either from EPS or direct cosmological simulations and follow the formation of galaxies with simplified, physically and observationally motivated, analytic recipes (White & Frenk, 1991; Kauffmann et al., 1993; Cole et al., 1994; Kauffmann, 1996; Somerville & Primack, 1999b; Kauffmann et al., 1999; Kauffmann & Haehnelt, 2000; Cole et al., 2000; Springel et al., 2001a; Hatton et al., 2003; Kang et al., 2005; Baugh et al., 2005; Khochfar & Silk, 2006a; Croton, 2006; Bower et al., 2006; De Lucia & Blaizot, 2007; Somerville et al., 2008b; Font et al., 2008; Guo & White, 2009; Weinmann et al., 2009). The computational costs of this approach are typically low, and the influence of different physical mechanisms can be investigated separately in a straightforward way. Modern SAMs are quite successful at reproducing observed statistical properties of galaxies in large cosmological volumes over a large range of galaxy masses and redshifts (e.g. Somerville et al., 2008b; Guo et al., 2011), e.g. the downsizing behavior in black hole growth as it was demonstrated in Chapter 4. However, disad-

vantages of SAMs are that the dynamics of the baryonic component (gas and stars) and the interaction between baryonic matter and dark matter are not followed directly and that in many cases the assumed models are simplified and use a large number of free parameters to fit different observations simultaneously (Somerville et al., 2008b; Benson & Bower, 2010; Bower et al., 2010).

In contrast, direct cosmological, hydrodynamical galaxy formation simulations can follow the evolution of dark matter and gas explicitly. Even though they treat the underlying dynamics more correctly than SAMs, the spatial and mass resolution, at present, is not high enough to accurately simulate intermediate and low mass galaxies in large cosmological volumes. In addition, small scale processes like e.g. the formation of stars and black holes with the associated feedback has to be computed in a simplified manner with sub-grid/sub-resolution models (Cen & Ostriker, 1993; Davé et al., 2001; Springel & Hernquist, 2003; Maller & Bullock, 2004; Nagamine et al., 2005; Kereš et al., 2005; Navarro et al., 2009; Schaye et al., 2010b), which again require the introduction of additional free parameters. "Ab-initio" cosmological zoom simulations with proper cosmological boundary conditions enable direct simulations of the baryonic physics of certain regions of interest at higher resolution, either limited to small cosmological volumes (Crain et al., 2009) or, more popularly, individual halos (Navarro & Steinmetz, 1997; Governato et al., 2007; Naab et al., 2007; Brooks et al., 2009; Oser et al., 2010; Wadepuhl & Springel, 2011; Puchwein et al., 2010; Teyssier et al., 2010b; Sawala et al., 2010; Piontek & Steinmetz, 2011; Agertz et al., 2011). These simulations can attain very high resolution, and provide a way to resolve galaxies of very different masses with the appropriate resolution in each case. However they are very time consuming and therefore not currently feasible for representative studies of large populations of galaxies. In addition, the sub-resolution models are uncertain and it is still unclear how sensitive various results may depend on the details of these sub-grid models or the parameter values.

Both approaches make definite predictions for the evolution of galaxy properties at various masses over cosmic time. Because of their greater computational efficiency, SAMs generally include more models for physical processes than current numerical simulations, and because of their greater flexibility, it has been possible to tune them to obtain quite good agreement with a broad range of galaxy properties in the local Universe. SAMs have also been shown to reproduce the statistical properties (e.g. luminosity and stellar mass functions, star formation rates) of high redshift galaxies ($z \lesssim 6$) quite well, at least for massive galaxies ($m_{\text{star}} \gtrsim 10^{10} M_{\odot}$; e.g. Somerville et al. 2011; Fontanot et al. 2009). In particular, in the last Chapter was shown that applying some modifications to the model from Somerville et al. (2008b) the evolution of the quasar luminosity function (bolometric and hard X-ray) can be reproduced reasonably well. Therefore, one might expect SAMs to do a better job of reproducing the observed Universe than the simulations, but one might worry that they could do so for the wrong reasons. Because there is a great deal of uncertainty in many of the important pro-

cesses, and most of the physical recipes contain free parameters, if one physical process (e.g. gas cooling and accretion) is modeled inaccurately in the SAM, it is currently possible to compensate by tuning a competing process (such as feedback). By running SAMs within merger trees extracted from numerical simulations, in order to constrain the evolution of the dark matter component to be the same in both cases, various physical processes can be isolated and it can be attempted to improve the accuracy of the semi-analytic recipes. The consequences of improving and extending the often simplified physical prescriptions in SAMs might also be of special interest for studying the AGN galaxy population (see Chapter 4), in particular with respect to the recipes for gas cooling and the corresponding, possible change in the evolution of the cold gas content being available for black hole accretion. At the same time, by comparing the detailed predictions of the formation histories of galaxies in the simulations with the SAM predictions, one may gain insights into the origin of existing discrepancies between the simulations and the real Universe.

Various comparison studies between simulations and SAMs for large galaxy populations as well as individual halos have been discussed in the literature (these results are summarized in Section 5.2), following different philosophies. For some studies only individual physical processes, like cooling, were investigated (Lu et al., 2010; Benson & Bower, 2010), while others focused on the evolution of individual objects, such as a high-mass galaxy cluster (Saro et al., 2010) or a single disk galaxy (Stringer et al., 2010). The approach in this Chapter is new in many respects. The evolution of individual halos is compared but the, up to now, largest number of 48 high-resolution zoom simulations is used, as presented in Oser et al. (2010). The simulations cover dark matter halos in the mass range of $2.4 \times 10^{11} M_{\odot} < M_{\text{Halo}} < 3.3 \times 10^{13} M_{\odot}$. Although a limited complement of physical processes have been taken into account in the simulations, the more massive of these halos have been shown to represent fairly well the evolution of observed massive galaxies (Oser et al., 2010). These simulations are compared to results from the full Somerville et al. (2008b) SAM (as well as different stripped down versions), which was shown to reasonably well represent present-day galaxy properties over a wide range of masses. The SAMs are run within merger trees extracted directly from the numerical simulations. In addition, both model predictions are compared to observations at different redshifts and point out, where the respective models succeed or fail either to match each other and/or the observations.

This Chapter is organized as follows: In Section 5.2 results from previous comparisons between SAMs and simulations are discussed. The hydrodynamical simulations and the merger-tree construction method used for this study are discussed in Section 5.3 and the ingredients of the Somerville et al. (2008b) SAM is briefly reviewed in Section 5.4. The redshift evolution of the baryonic components in simulations and SAMs is compared in Section 5.5 followed by a comparison to observations in Section 5.6. Section 5.7 summarizes and discusses the main results of this Chapter. A resolution study for individual halos can be found in the Appendix A.

5.2 Previous comparison studies

Previous quantitative comparisons between simulations and SAMs have either focused on whole populations of galaxies (Benson et al., 2001; Yoshida et al., 2002; Helly et al., 2003; Cattaneo et al., 2007; Benson & Bower, 2010; Lu et al., 2010) or individual objects like a galaxy cluster (Saro et al., 2010) and a single disk galaxy (Stringer et al., 2010). Helly et al. (2003) compared the efficiency of gas cooling for different dark matter halos as a function of redshift between a $(50\text{Mpc}/h)^3$ SPH (Smoothed-Particle-Hydrodynamics) simulation (HYDRA, Pearce et al., 2001) excluding star formation, heating and feedback and a stripped down version – without star formation or feedback – of the GALFORM SAM (Cole et al., 2000). For $z = 0$ they find good agreement of the cold gas mass between the SPH simulation and the SAM. At high redshifts, however, more gas tends to cool in low-mass halos in the simulation due to the limited numerical resolution. Still, they conclude that simulations and SAMs give consistent results for the evolution of cooling galactic gas and confirm earlier findings of Benson et al. (2001) and Yoshida et al. (2002).

Cattaneo et al. (2007) considered star formation and supernova feedback for a similar comparison in a 34.19Mpc^3 volume. For the SPH-simulation they used the TreeSPH code (Dave et al., 1997) and as input for their SAM-code GalICS (Hatton et al., 2003) the merger trees were constructed from the dark matter component of the SPH-simulation. The SAM did not include a photo-ionising background but followed the cooling by metals, while the simulations did include a photo-ionizing background and assumed primordial composition of He and H. The star formation prescription in the SAM was quite standard (star formation occurs above a certain gas surface density, according to a Kennicutt-Schmidt-like relation), including also a simple recipe for SN-driven winds. In order to replicate AGN feedback, star formation is quenched when the bulge component of a galaxy reaches a critical mass. For the comparison they used two different SAM versions: one with no feedback and the ‘full’ model. In general, they found good agreement between the simulations and the no-feedback model for the baryonic mass functions at different redshifts and in different environments. Moreover, simulations and the no-feedback SAM made similar predictions for the ‘hot’ and ‘cold’ mode gas accretion histories of galaxies (e.g. Kereš et al., 2005). However, at low redshifts, much less gas was left over in the simulation than in the no-feedback SAM with both approaches over-predicting the observed baryonic mass function, in particular at the high mass end. The full SAM, on the other hand, matched the observations due to the inclusion of supernova-driven outflows and AGN feedback, which suppresses gas cooling in large halos. They concluded that the simulations and the no-feedback model failed as a consequence of missing physics rather than computational inaccuracies.

Saro et al. (2010) compared the galaxy populations within a massive cluster ($M_{\text{cl}} = 1.14 \times 10^{15} M_{\odot}$) using a high-resolution cosmological re-simulation run with GADGET2 (Dolag et al., 2009) and the SAM model of De Lucia & Blaizot (2007). They focused on

differences between the central and the satellite galaxies considering only gas cooling and star formation and neglecting any form of feedback. In general, they find similar *statistical properties* for the galaxy populations, e.g. the stellar mass function with a few remarkable *object by object* differences. The central galaxy in the simulation starts with a more intense and shorter initial burst of star formation at high redshift and forms fewer stars at low redshift than in the SAM. While in the SAM all stars in the central galaxy are formed in its progenitors, in the simulations the final stellar mass is larger than the sum of all progenitors. Satellite galaxies can lose up to 90 per cent of their stellar mass due to tidal stripping – a process, which is, however, not included in the De Lucia & Blaizot (2007) semi-analytic model, nor in most models discussed in the recent literature.

Moreover, Stringer et al. (2010) presented a comparison for the evolution of a single disk galaxy using the SPH-code GASOLINE (Wadsley et al., 2004) and the semi-analytic GALFORM model (Bower et al., 2006) based on the dark matter merger history of the simulation. They find that the two techniques show a *potential* consistency for the evolution of the stellar and gas components by assuming the same physics and the same initial conditions. They try to mimic in the SAM the ‘blast wave’ SN feedback implemented in the simulation, i.e. after a supernova explosion no cooling is allowed in a certain volume. However, using the GALFORM model as described in Bower et al. (2006) (including chemical enrichment, supernova and AGN feedback), the resulting system is not recognisably the same as the one predicted by the simulations. At all redshifts, the stellar mass is much larger and the hot gas fraction is much lower in the simulation than in the SAM.

Finally, Lu et al. (2010) and Benson & Bower (2010) focus on the algorithms for gas cooling in SAMs in great detail. Benson & Bower (2010) compare cold (rapid) and hot (slow) accretion rates in the GALFORM SAM and in simulations from Kereš et al. (2009) (50 Mpc/h, 2×288^3 particles). They used their ‘full’ model including feedback and metal cooling, although these processes are not included in the simulations. Moreover, they modified their SAM by adopting an updated calibration for the transition between the rapid and slow cooling regime following the methodology of Birnboim & Dekel (2003). They find reasonably good agreement for the hot and cold mode accretion fraction in the SAM and the simulations and thus, they conclude that the cold-mode physics is already adequately accounted for in SAMs. In the study of Lu et al. (2010) five different SAMs (‘Munich’ model: Croton, 2006, ‘Kang’ model: Kang et al., 2005, ‘GALFORM’ model: Cole et al., 2000, ‘GalICS’ model: Hatton et al., 2003 and the ‘Somerville’ model: Somerville & Primack, 1999b) are compared to the simulations of Kereš et al. (2009), without considering any feedback or metal enrichment in either method. They find a significant difference between hot and cold accretion rates: compared to the simulations, the cold mode accretion rates are lower and the hot mode accretion are higher in the SAMs. They construct a modified cooling recipe for the SAM to enable simultaneous hot and cold accretion, resulting in much better

agreement between the SAMs and the simulations.

Throughout the course of this Chapter, I will refer back to these studies and comment upon the similarities and differences with the results presented here.

5.3 The simulation and merger tree construction

5.3.1 Simulation setup

The cosmological zoom simulations presented in this Chapter are described in detail in Oser et al. (2010) and the simulation setup is briefly reviewed here. The dark matter halos for further refinement were selected from a dark matter only N-body simulation (GADGET-2, Springel et al., 2005a) with a comoving periodic box length of $L = 100$ Mpc and 512^3 particles (see also Moster et al., 2010). A Λ CDM cosmology is assumed based on the WMAP3 measurements (see e.g. Spergel et al., 2003) with $\sigma_8 = 0.77$, $\Omega_m = 0.26$, $\Omega_\Lambda = 0.74$, and $h = H_0/(100 \text{ kms}^{-1}) = 0.72$. The simulation starts at $z = 43$ and runs to $z = 0$ with a fixed comoving softening length of $2.52 h^{-1} \text{ kpc}$ and a dark matter particle mass of $M_{\text{DM}} = 2 \times 10^8 M_\odot/h$. Starting at an expansion factor of $a = 0.06$ halo catalogues are constructed for 94 snapshots until $z = 0$ separated by $\Delta a = 0.01$ in time. From this simulation, 48 halos were chosen identified with the halo finder algorithm *FOF* at $z = 0$. To construct the high-resolution initial conditions for the re-simulations, all particles are traced back in time that are closer than $2 \cdot r_{200}$ to the center of the halo in any snapshot and they are replaced with dark matter as well as gas particles at higher resolution ($\Omega_b = 0.044$, $\Omega_{\text{DM}} = 0.216$). In the high resolution region the dark matter particles have a mass resolution of $m_{\text{DM}} = 2.1 \cdot 10^7 M_\odot h^{-1}$, which is 8 times higher than in the original simulation, and the gas particle masses are $m_{\text{Gas}} = m_{\text{Star}} = 4.2 \cdot 10^6 M_\odot h^{-1}$. Individual cases were run at 64 times higher mass resolution and 4 times higher spatial resolution. The re-simulated halos cover a mass range of two orders of magnitude ($2.4 \times 10^{11} M_\odot < M_{\text{Halo}} < 3.3 \times 10^{13} M_\odot$).

For modeling the gas component the entropy conserving formulation of SPH is used (GADGET-2, Springel et al., 2005a). Star formation and cooling for a primordial composition of hydrogen and helium is included (Theuns et al., 1998). The cooling rates are computed under the assumption that the gas is optically thin and in ionization equilibrium. Furthermore, the simulations include a spatially uniform redshift dependent UV background radiation field according to Haardt & Madau (1996), where re-ionization takes place at $z \approx 6$ and the radiation field peaks at $z \approx 2 - 3$.

To model star formation and SN feedback the approach of Springel & Hernquist (2003) is used. In this model, the ISM is treated as a two-phase medium where clouds of cold gas form from cooling of hot gas and are embedded in the hot gas phase assuming pressure equilibrium. The hot gas is heated by supernovae and can evaporate the cold clouds. Stars form from the cold gas whenever the local density exceeds a threshold

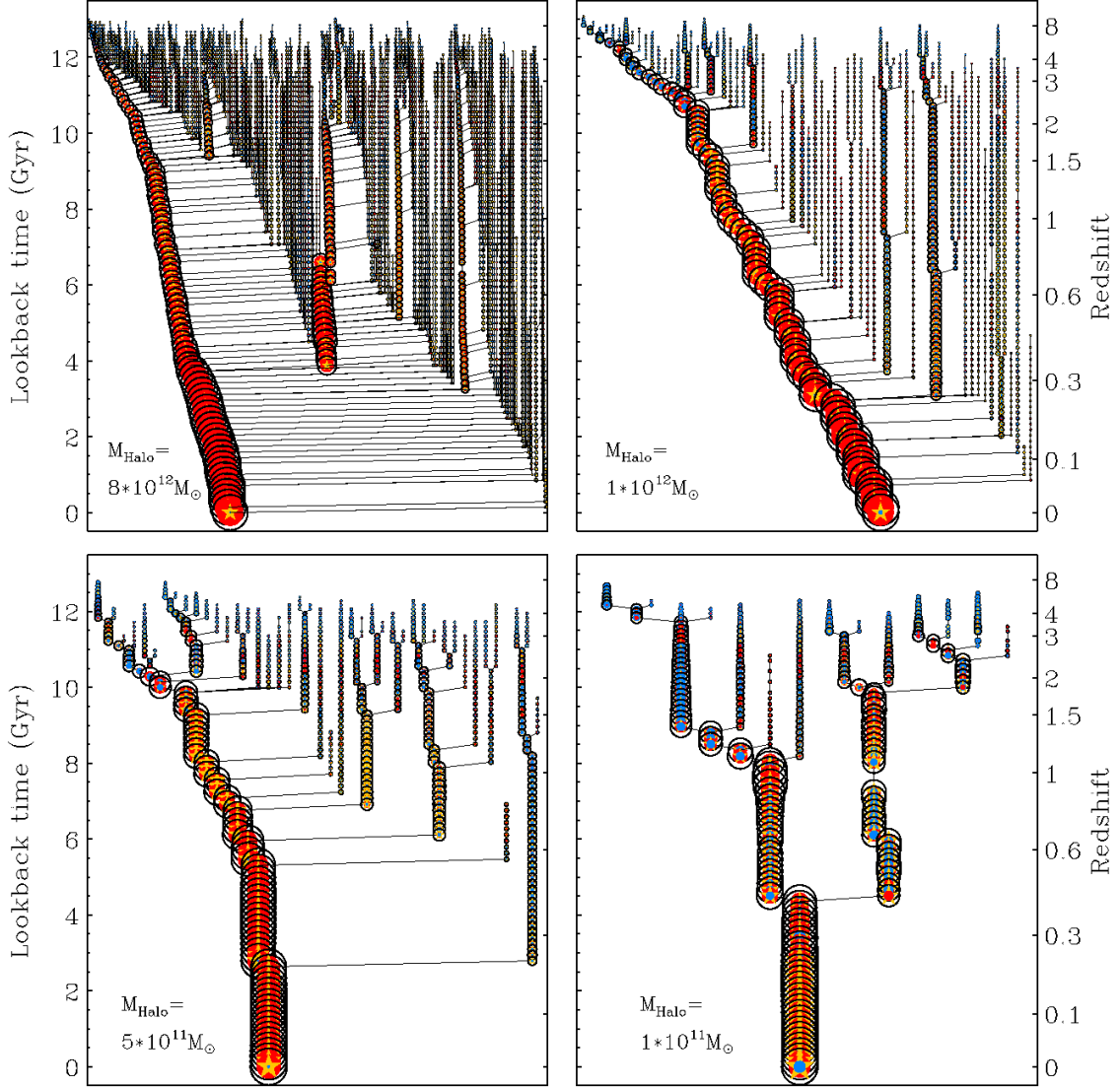


Figure 5.1: Visualisation of merger trees for four re-simulated halos with different masses: upper left: $M_{\text{vir}} = 8 \times 10^{12} M_{\odot}$ (M0162), upper right: $M_{\text{vir}} = 1 \times 10^{12} M_{\odot}$ (M1017), lower left: $M_{\text{vir}} = 5 \times 10^{11} M_{\odot}$ (M2665), lower right: $M_{\text{vir}} = 1 \times 10^{11} M_{\odot}$ (M6782). Black circles show the dark matter halo at every time-step of the simulations. The symbol size is proportional to the square root of the halo mass normalized to the halo mass at $z=0$. The yellow stars indicate the stellar mass, the blue and red filled circles the cold and hot gas mass within the virial radius of the dark matter halo. The symbol sizes for the baryons scale with the square root of the masses normalized to the maximum total baryonic mass at $z=0$.

density ($\rho > \rho_{\text{th}} = 0.205\text{cm}^{-3}$). The star formation rate is calculated by

$$\frac{d\rho_*}{dt} = (1 - \beta) \frac{\rho_c}{t_*} \quad (5.1)$$

Here, β is the mass fraction of massive stars, which is assumed to explode as supernovae type II, ρ_c is the density of cold gas and $t_* = t_*^0 (\rho/\rho_{\text{th}})^{-1/2}$ is the star formation time scale. The supernova explosions heat the surrounding gas with an energy input of 10^{51} ergs. Springel & Hernquist (2003) used an idealized, isolated disk galaxy simulation to set the free parameters ρ_{th} and t_*^0 , by adjusting them to obtain a match to the observed Schmidt-Kennicutt relation. The same values of these parameters are adopted here.

5.3.2 Merger trees

The merger trees of the dark matter component are constructed with the algorithm as described in Section 3.4.2. The minimum halo mass is set to 20 particles ($5 \times 10^8 M_\odot/h$). However, in the following, *isolated* merger trees are used without applying the split-algorithm of Genel et al. (2008), as the dark matter masses in the 'split-trees' are FOF masses, but virial masses are needed as input for the semi-analytic model.

Note that the tree-algorithm is only applied to the dark matter particles, star or gas particles are not separately traced back in time. They are assumed to follow the evolution of the dark matter. Therefore, to each dark matter halo in a tree, a hot/cold gas phase is assigned by counting hot/cold gas particles within the virial radius of the central dark matter halo. The stellar and cold gas particles within 1/10 of the virial radius are defined as the stellar and gas mass of the central galaxy. It is distinguished between hot and cold gas particles by using the following definitions (code units):

$$\log T < 0.3 \log \rho + 3.2 \rightarrow \text{cold} \quad (5.2)$$

$$\log T > 0.3 \log \rho + 3.2 \rightarrow \text{hot} \quad (5.3)$$

The above distinction was made by looking directly at the phase diagrams of the re-simulations, where it has been discriminated between the gas in the disk heated by SN feedback and the shock heated gas in order to capture the cold star-forming gas.

Fig. 5.1 shows a visualization of four merger trees of re-simulated halos with virial masses of $8 \times 10^{12} M_\odot$, $1 \times 10^{12} M_\odot$, $5 \times 10^{11} M_\odot$ and $1 \times 10^{11} M_\odot$. The sizes of the black circles approximate the dark matter halo masses, the yellow stars the stellar mass within the virial radius and the blue and red filled circles the cold and hot gas component, respectively. The symbol sizes scale with the square root of mass normalized to the final dark matter halo mass (dark matter component) and to the final baryonic mass (star, hot and cold gas mass). One can clearly see that galaxies at high redshift contain more cold gas, which either turns into stars or is heated towards lower

redshifts. In general, for more massive halos the fraction of cold gas and stars at $z = 0$ is lower.

To study the influence of numerical resolution on the evolution of the dark matter and the baryonic components, a few halos have been simulated with a $4 \times$ higher spatial resolution ($= 64 \times$ higher mass resolution) than the original dark matter simulation. A comparison of the results can be found in the Appendix. The overall mass assembly of the main halos and the number of major mergers do not show any significant variation, although the number of identified minor mergers increases due to the higher resolution. Overall, one can conclude that the results are well-converged and would not change significantly if the resolution is improved.

5.4 The semi-analytic model

The merger-trees constructed as described above are used as input for the semi-analytic model described in Chapter 4 and in Somerville et al. (2008b) (hereafter S08). The SAM makes use of merger trees for “isolated” halos only, and treats the evolution of sub-structure within virialized halos using semi-analytic approximations. The ‘full’ SAM version includes photo-ionization, gas cooling, star formation, SN feedback, metal enrichment, and black hole growth in a radio and quasar mode with corresponding feedback. However, to provide a more meaningful comparison to the simulations, I do not only consider the ‘full’ version, but also ‘stripped down’ models by separately switching off AGN feedback, metal cooling, Supernova-driven winds, and ‘thermal’ Supernova feedback. The following different versions are considered:

- **NF**: **N**o **F**eedback, primordial metallicity
- **SN**: thermal **S**N-feedback, primordial metallicity
- **SNWM**: thermal **S**N-feedback, **S**N-driven **W**inds, **M**etal cooling
- **FULL**: “full” version, including thermal SN-feedback, SN winds, metal cooling, and AGN feedback

In contrast to Section 4.3.2 and S08 - there is a small modification for limiting the hot gas content in the SAMs used in this Chapter. Note that in merger trees from N-body simulations it may happen that the total mass of two merging halos at the beginning of a merger event is larger than the mass of the merged object afterwards, since during the merger particles can become unbound through tidal forces. Therefore, in the SAM an upper limit is imposed on the hot halo mass of

$$M_{\text{hot}} = M_{\text{bar}} - M_{\text{star,tot}} - M_{\text{cold}} - M_{\text{eject}}. \quad (5.4)$$

Here, M_{eject} is the mass ejected by winds, $M_{\text{star,tot}}$ and M_{cold} are the total star and cold gas masses within the merged halo and M_{bar} is the expected baryonic fraction of the

halo. In this way, the sum of all baryonic components in the halo is prevented from exceeding the universal baryon fraction.

5.5 Redshift evolution of galaxy properties

In this Section, the cosmic evolution of the baryonic components of the galaxies and halos is compared from the direct cosmological simulations to the results from the SAMs using the dark matter merger trees constructed from the re-simulations. Here only the evolution of the central galaxy in the main branch of the merger tree (largest progenitor halo) is considered. The 48 halos are divided into three bins according to their halo mass at $z = 0$ (every bin contains 16 halos) with $4.5 \times 10^{12} M_{\odot} < M_{\text{halo}} < 4 \times 10^{13} M_{\odot}$ (high-mass), $1.2 \times 10^{12} M_{\odot} < M_{\text{halo}} < 4.5 \times 10^{12} M_{\odot}$ (intermediate-mass), and $2.4 \times 10^{11} M_{\odot} < M_{\text{halo}} < 1.2 \times 10^{12} M_{\odot}$ (low-mass). All comparisons in this Section make use of these bins.

Note also that a resolution study of the evolution of the baryonic component in SAMs based on $2 \times$ and $4 \times$ higher resolution simulations for a high- and a low mass halo can be found in the Appendix A. In both cases, the results based on the simulations with different resolution are consistent.

5.5.1 Baryon fraction

For a first comparison the total baryonic mass $M_{\text{bar}} = (M_{\text{star}} + M_{\text{cold}} + M_{\text{hot}})$ is computed within the virial radius of the main halo at every redshift for the simulations and the SAMs, respectively. In the re-simulations as well as in the SAMs, the hot gas mass is considered within the whole halo (i.e. within the virial radius), but the stars and the cold gas only of the central galaxy. Contributions from substructures are neglected, as diffuse stars and cold gas and satellite stars and cold gas. The baryonic mass is compared to the mass of available baryons within each halo, defined as $f_{\text{bar}} \times M_{\text{halo}}$, where $f_{\text{bar}} = 0.169$ is the cosmic baryon fraction.

Fig. 5.2 shows the average ratio of $M_{\text{bar}}/(f_{\text{bar}} \times M_{\text{halo}})$, as a function of redshift for the three mass bins. The simulations are compared to the four SAM variants: NF, SN, SNWM, and FULL (for details see Section 5.4). The simulations are expected to be most directly comparable to the NF or SN SAMs, as these SAMs include the same complement of physical processes as the simulations. Considering first the NF model, one can see that at low redshift, the SAM overestimates the baryon fraction in high mass halos, nearly agrees in intermediate mass halos, and slightly underestimates it in low mass halos. At high redshift, the NF SAM overestimates the baryon fraction at high redshift in high and intermediate mass halos, by a somewhat larger factor in the former. Turning next to the SN SAM, one can see that the SAM predicts baryon fractions that are everywhere higher than the simulation results, though much more so

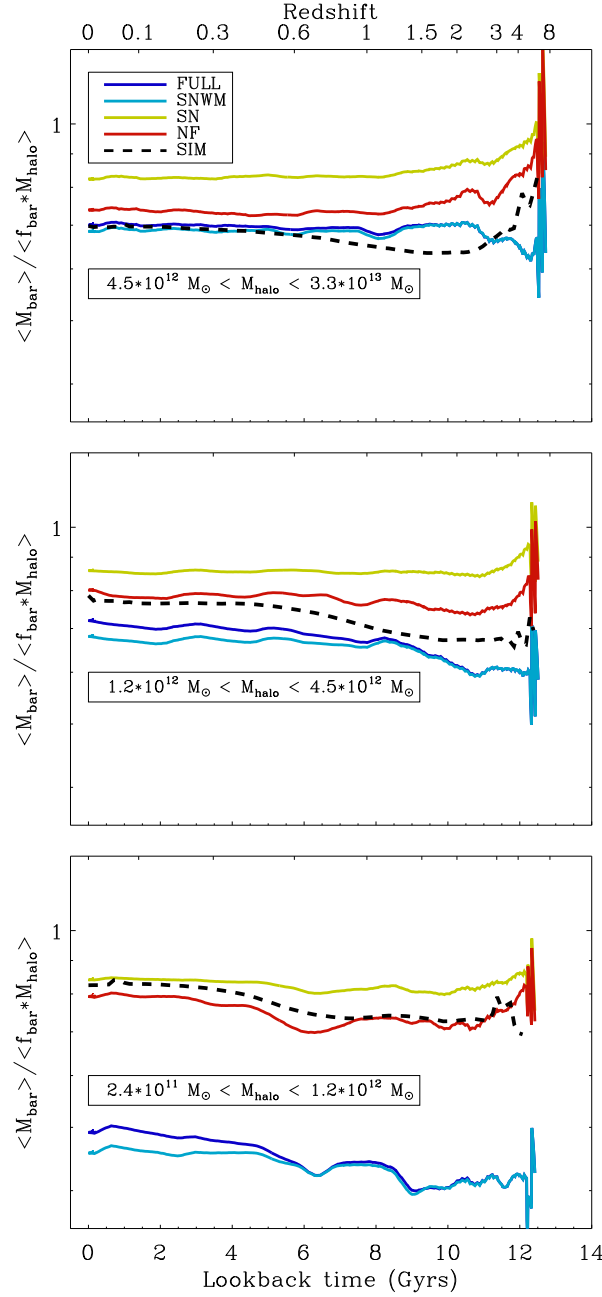


Figure 5.2: Fraction of baryonic mass, $M_{\text{bar}} = M_{\text{gas}} + M_*$, of the cosmic baryon fraction of the halo mass, $f_{\text{bar}} \times M_{\text{halo}}$, as function of lookback time for different semi-analytic models (red: no feedback - NF; green: thermal Supernova feedback - SN; blue: thermal Supernova feedback, SN-driven winds and metal cooling - SNWM; lila: 'full' model including feedback from black holes - FULL) and for the SPH-re-simulation (black lines). Upper panel: Average values for the high mass bin with $4.5 \times 10^{12} M_{\odot} < M_{\text{halo}} < 3.3 \times 10^{13} M_{\odot}$. Middle panel: Average values for the intermediate mass bin with $1.2 \times 10^{12} M_{\odot} < M_{\text{halo}} < 4.5 \times 10^{12} M_{\odot}$. Lower panel average values for halo masses between $2.4 \times 10^{11} M_{\odot} < M_{\text{halo}} < 1.2 \times 10^{12} M_{\odot}$. The best match to simulations is found in general for the NF model.

for the high and intermediate mass halos. This is because the “thermal” SN feedback removes baryons from satellite galaxies, which are not counted in this census, and deposits them in the hot gas component which is included here. In the SNWM and FULL model, the impact of the SN-driven winds can be clearly seen, which effectively remove baryons from the low-mass halos. AGN feedback mainly prevents hot gas from cooling, so does not affect the total baryon fraction significantly, but will be important for the fraction of stars and hot gas, which will be discussed later.

5.5.2 Cold gas and stars

Fig. 5.3 shows the evolution of the mass of condensed baryons (stars and cold gas, $M_* + M_{\text{cold}}$) as a fraction of the total baryon mass as a function of redshift for the three mass bins. There is fairly good agreement between the simulations and the NF model over the whole redshift range, although the SAM is a little low at high redshift and a bit high at low redshift, particularly in the high and intermediate mass bin. In the SN model, the condensed baryon fraction is lowered by an almost fixed factor relative to the NF model, and is significantly lower than the simulation results. This suggests that the “thermal feedback” implemented in the simulation is less effective than that included in the SAM. It may seem curious that the SNWM model results are *higher* than the SN model, in fact close to the NF model in the high and intermediate mass bin. This is because the SNWM includes metal cooling, while the SN model does not. The enhanced cooling rates partly compensate for the removal of cold gas via the SN-driven winds. Finally, one can see that in the FULL model, the AGN feedback begins to quench star formation in the massive halos after about $z \sim 2$, while it has little effect on the lower mass bins.

In Fig. 5.4 the evolution of the mean cold gas fraction of the central galaxy is plotted (note that in Fig. 5.3 cold gas plus stars is plotted). The efficiency of the conversion of cold gas to stars is clearly very different between the simulations and SAMs. In both cases (simulations and SAMs), the final cold gas fraction is increasing with decreasing halo mass. For the NF model, the SN and the SNWM model the cold gas fraction varies only slightly over time and is significantly higher (about an order of magnitude since $z = 2$) than for the simulations. This shows that the inclusion of SN feedback has little impact on the gas fractions of galaxies. Only the FULL model shows a much stronger decrease of the gas fraction with cosmic time for massive galaxies due to the radio mode feedback. The initial cold gas fraction, at high redshifts $4 < z < 8$, is almost the same for the simulations and SAMs. With evolving cosmic time the cold gas content decreases more rapidly in the simulations due to the more efficient conversion into stars. The cold gas in the simulations is already converted into stars at high redshift and there is almost no more cold gas left to turn into stars at lower redshifts. This is similar to the results found in the comparison of Cattaneo et al. (2007).

Fig. 5.5 shows the corresponding fraction of available baryons that are converted

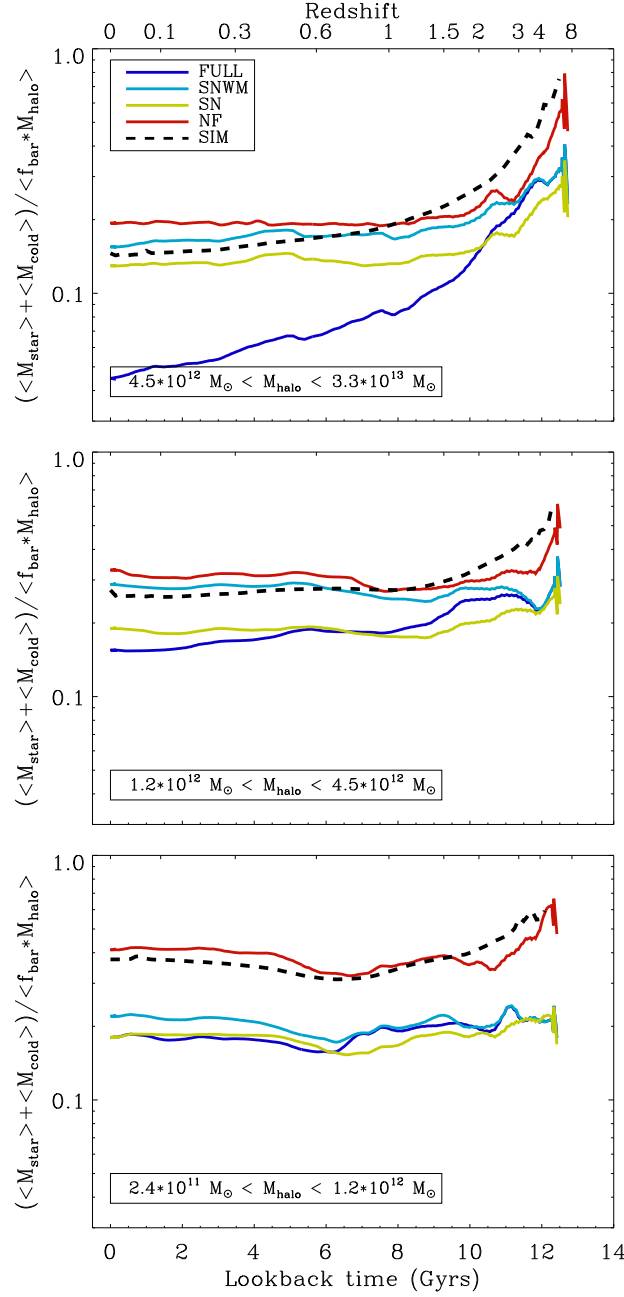


Figure 5.3: *The evolution of the fraction of the condensed baryons $M_* + M_{\text{cold}}$ of the total baryon mass as a function of redshift for the three mass bins. The condensed baryon fraction of all simulations is in reasonable agreement with the NF model at all redshifts. High-mass and intermediate-mass simulations agree well with the SNWM model. The effect of AGN feedback in the FULL model can be clearly seen in the high-mass bin. In the low-mass bin the SN wind feedback (SNWM) makes the biggest difference.*

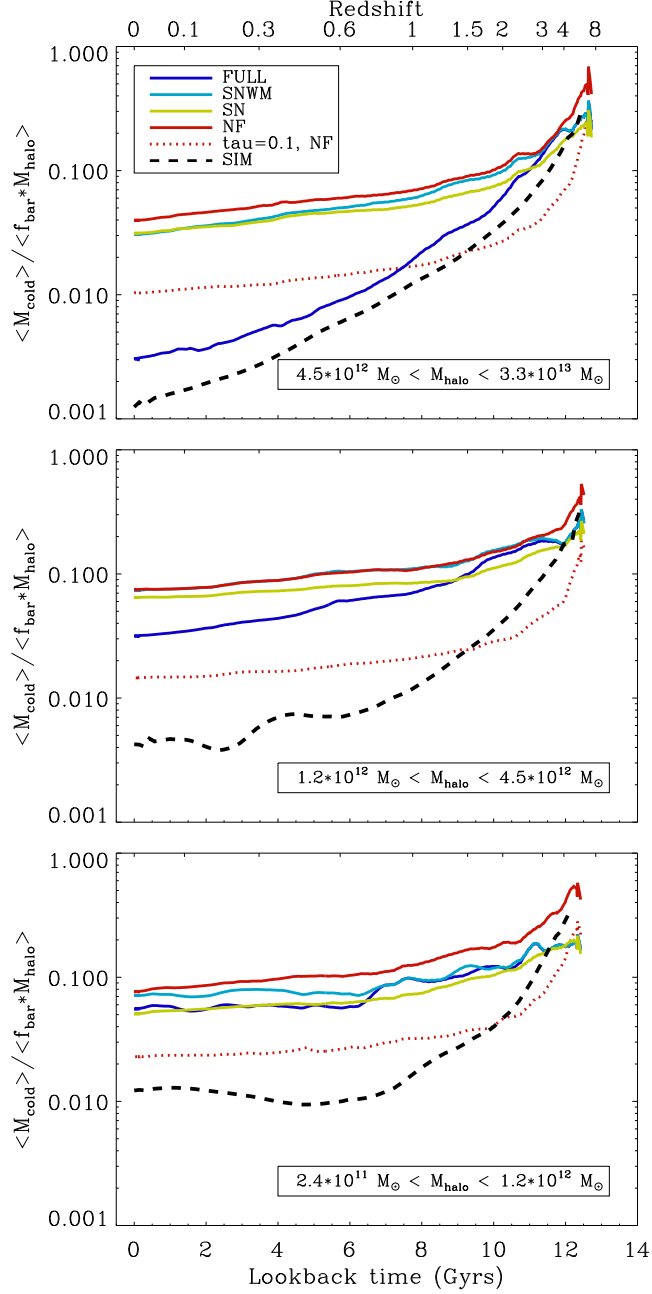


Figure 5.4: Evolution of mean cold gas fraction $M_{\text{cold}}/(f_{\text{bar}} \times M_{\text{halo}})$ of the central galaxies. Mass bins and colors are the same as in Fig. 5.2. In all simulations the cold gas is depleted more efficiently than in the SAMs due to the large star formation efficiency at high redshifts. The red dotted line shows the cold gas fraction assuming ten times higher efficiency for star formation in the NF model (see Eq. 5.5).

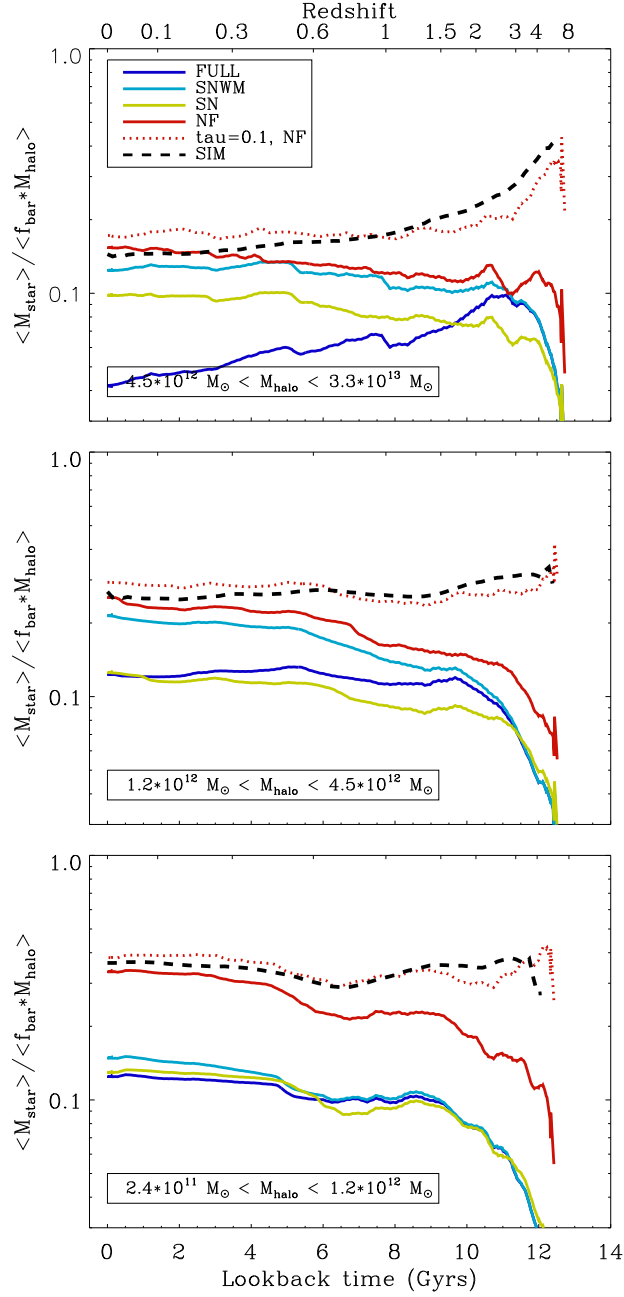


Figure 5.5: Comparison of the stellar baryon fraction of the central galaxy between simulations and SAMs. The mass bins and colors are the same as in Fig. 5.2. For all mass bins the simulations agree best with the NF SAM, but forming significantly more stars already higher redshifts $z > 1$. This discrepancy can be accounted for if the star formation efficiency parameter in the SAMs is increased by a factor 10 for the NF case (red dashed lines). At high masses the AGN feedback (FULL) and at the low masses the SN feedback (SN and SNWM) reduce the stellar baryon fractions in the SAMs.

into stars in the central galaxy $M_*/(f_{\text{bar}} \times M_{\text{halo}})$, sometimes termed ‘‘baryon conversion efficiency’’ (Guo & White, 2009; Moster et al., 2010). In general, all simulations predict a decreasing (high-mass) or almost constant (low-mass) conversion efficiency with redshift, whereas most SAMs predict increasing conversion efficiencies with the exception of high-mass galaxies in the FULL model with AGN feedback.

At low redshift $z < 0.6$ the conversion efficiencies agree well between the simulations and the NF model, with higher values for lower mass galaxies. However, at high redshifts $z > 1$ the conversion efficiencies are significantly higher for the simulations. This is in contrast to the results of Cattaneo et al. (2007), where the stellar masses agree at high redshift, but the SAM masses are larger than in simulations at low redshift. The difference in the behavior of the SAMs and the simulations can be explained in terms of star formation efficiency. We changed the normalization of the SK-relation in the SAM by introducing a factor τ_* in Eq. 4.4:

$$\Sigma_{\text{SFR}} = \frac{A_{\text{KS}}}{\tau_*} \Sigma_{\text{gas}}^{N_K}, \quad (5.5)$$

with $\tau_* \approx 0.1$. The results of the NF model with this elevated star formation efficiency for the stellar and cold gas mass evolution is shown in Figs. 5.4 and 5.5. At high redshift, gas is more efficiently depleted and converted into stars, resulting in a better agreement between this ‘high SFE’ model and the simulations. However, for the high-mass and intermediate-mass bin, the ‘high SFE’ model over-predicts the stellar fraction at low redshifts, suggesting that the Cattaneo et al. (2007) SAMs may also have had a higher SFE, and this could explain the discrepancy between their results and the initial results presented here. In all three mass bins, the NF model produces the most massive stellar components. Again, the more efficient cooling due to metals in the SNWM and the FULL model is cancelled by the effect of winds and, for massive galaxies, also by AGN feedback, resulting in lower stellar masses than in the NF model.

Star Formation Rates

To confirm the previous findings the star formation rates are compared in Fig. 5.6. At very high redshifts $z > 4$, the SFRs in the simulations are much higher than in the SAMs. Only by assuming more efficient star formation in the NF SAM ($\tau_* = 0.1$) a reasonable match to the simulations is obtained. However, at $z < 1.5$, the high SFE model results in similar SFRs as the original NF model, as the larger SF efficiencies at high redshift lead to a more rapid depletion of the cold gas. In the simulation, the cold gas is rapidly turned into stars, resulting in lower SFRs at low redshifts compared to SAMs because of gas depletion. Only the FULL model shows a strongly decreasing SFR with decreasing redshift due to radio mode feedback, which becomes especially important for low redshifts and large halo masses. This result is consistent with the study of Saro et al. (2010), who compared their stripped-down versions of SAMs (with no feedback) to simulations, and found higher SFRs in the simulations for all

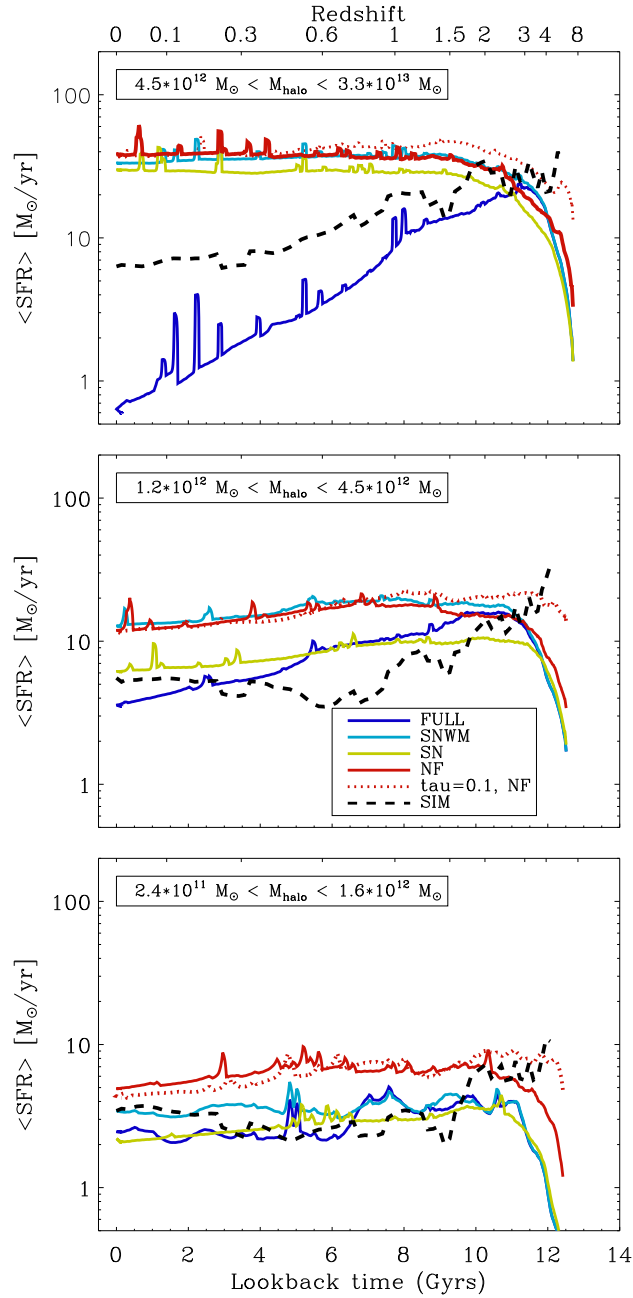


Figure 5.6: Evolution of the star formation rates in simulations and SAMs for three mass bins. The mass bins and colors are the same as in Fig. 5.2. At high redshifts, SFRs are higher in the simulations than in the SAMs leading to more rapid depletion of the cold gas with very low SFRs at low redshifts.

galaxies within a cluster (central and satellites) at high redshifts and lower SFRs at low redshifts. In addition, Stringer et al. (2010) find a similar discrepancy for the specific star formation rates at high redshifts (larger in simulations than in their SAM) and good agreement for low redshifts.

To better understand this discrepancy between simulations and SAMs we take a closer look at the respective implementations of star formation. According to Springel & Hernquist (2003), stars in the simulations are formed locally out of cold gas with the star formation rate density proportional to the local three-dimensional density of gas to the power of 1.5, $\rho_{\text{SF}} \propto \rho^{1.5}/t_*$. The star formation timescale t_* was set to approximate the observed local Schmidt-Kennicutt relation (SK) for a simulation of a smooth, isolated disk-dominated galaxy set up to resemble the Milky Way. In the SAMs, the cold gas is assumed to settle into smooth exponential disks and stars form according to the SK-relation, implemented in terms of surface densities.

In Fig. 5.7, the SFR surface density versus the surface density of the cold gas is plotted for the simulated galaxies at $z = 2$ and $z = 4$ within $1/10 r_{\text{vir}}$ for all re-simulations. The black dashed line is the SK-relation assuming a Salpeter IMF (Salpeter, 1955), as given in the original Kennicutt papers and as implemented in the simulations following Springel & Hernquist (2003). We would naively expect the simulations to follow this line. The red solid line shows the SK-relation for a Chabrier IMF (Chabrier, 2003), as assumed in the SAMs. At a given gas surface density, the SFR surface densities of the simulations lie mostly above the expected SK-relation. The change of normalization associated with converting from Salpeter to Chabrier cannot account for the increased star formation efficiency in the simulations. In general, star formation in the cosmological simulations is about a factor of five more efficient than for simulations of smooth isolated disks using the identical model (see Springel & Hernquist, 2003). This discrepancy is a consequence of the *clumpy* structure of cold gas in the cosmological simulations. In the clumps the gas can reach higher local densities than in the idealized smooth disks that have been used by Springel & Hernquist (2003) to calibrate the star formation timescale by matching the SK-relation. As the implemented SK-relation is not linear, the structure of the cold gas distribution plays an important role for the overall star formation efficiency within the galaxies (see Teyssier et al. (2010a) for a discussion on galaxy mergers). In other words, for any star formation model with a non-linear dependence on the local gas density (exponent larger than unity), a more clumpy gas distribution will effectively increase the star formation efficiency. These combined effects explain the much higher SF efficiencies at high redshift in the simulations relative to the SAMs.

Modes of Stellar Mass Growth

In the hierarchical picture, galaxies can grow their stellar masses in two ways: 1) by converting cold gas into stars in-situ and 2) by accreting already formed stars via

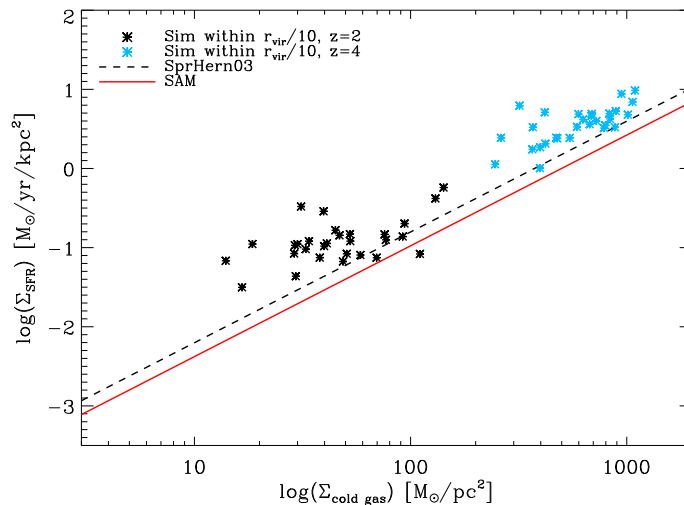


Figure 5.7: Star formation rate surface densities versus cold gas surface densities for the simulated galaxies within $1/10 r_{\text{vir}}$. Black and blue stars correspond to different re-simulations at $z = 2$ or $z = 4$, respectively. The red solid line illustrates the Kennicutt-relation implemented in the SAM assuming a Chabrier-IMF, the black dashed line the one in the simulations (Springel & Hernquist, 2003) assuming a Salpeter-IMF.

mergers. These two modes are referred to as “in-situ” and “accreted”. The simulations exhibit two phases of growth, with a rapid early phase at $z > 2$ during which stars are formed in-situ from infalling cold gas, followed by an extended phase at $z < 3$ during which the growth is primarily due to accretion of stars formed in external galaxies (Oser et al., 2010). It is now investigated whether the SAMs show the same behavior. Fig. 5.8 shows the fraction of cumulative in-situ over accreted stellar mass as a function of redshift for the three different mass bins. For the SAMs the qualitative trend of a decreasing fraction of in-situ growth is reproduced for the high mass bin. However, the fraction of in-situ formed stars dominates over accreted stars for all models, all masses, and at all redshifts. This is in contrast with the simulations, where accretion dominates over in-situ formation for massive systems at low redshifts as discussed in Oser et al. (2010).

I note several interesting trends in the in-situ to accreted fraction as vary the physics in the SAMs. Adding thermal SN feedback increases the in-situ fraction at all redshifts and in all mass bins. This is presumably because it suppresses star formation in low-mass satellites which are the source of accreted stars. Adding the SN-driven winds and metal cooling further increases the in-situ fraction, again at all redshifts below $z \sim 4$. Switching on AGN feedback increases the in-situ fraction at high redshift and decreases it at low redshift in the high mass bin (and to a lesser extent in the intermediate mass bin). This is because the radio mode feedback shuts off cooling at late times in massive

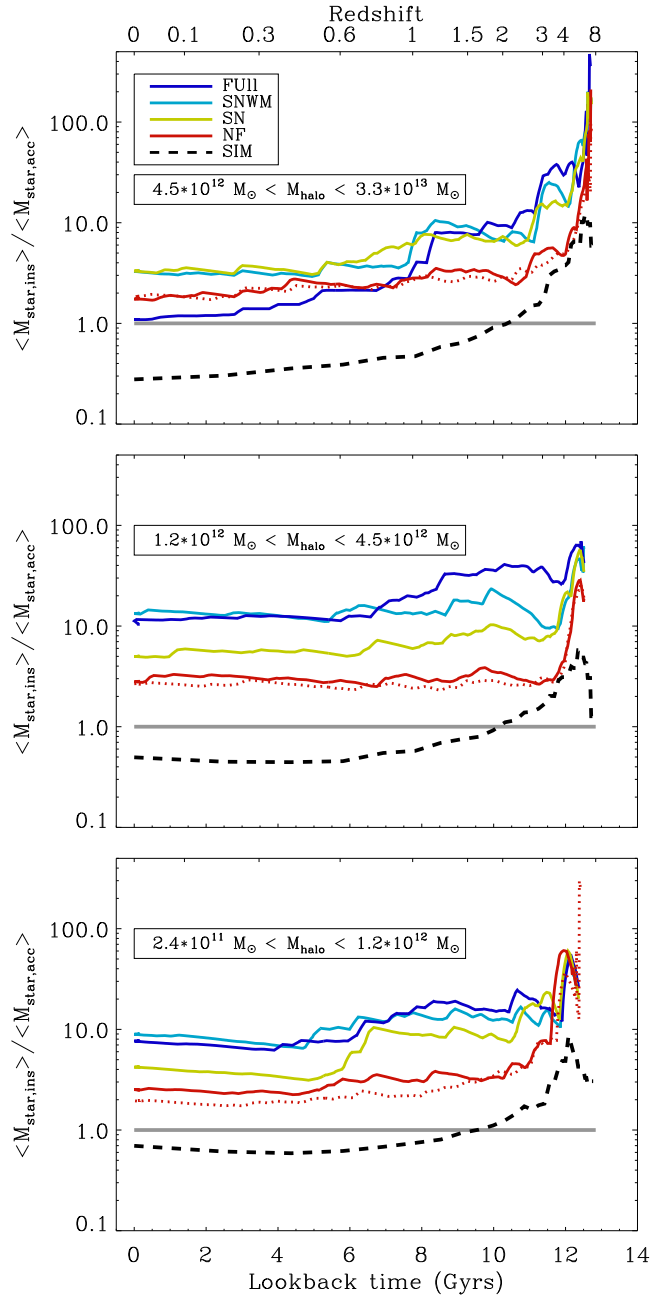


Figure 5.8: *Fraction of in-situ and accreted stellar mass versus redshift. The mass bins and colors are the same as in Fig. 5.2. The bimodal behavior as seen in simulations cannot be reproduced by the SAMs. Here, the in-situ star formation is dominating over accretion at all redshifts.*

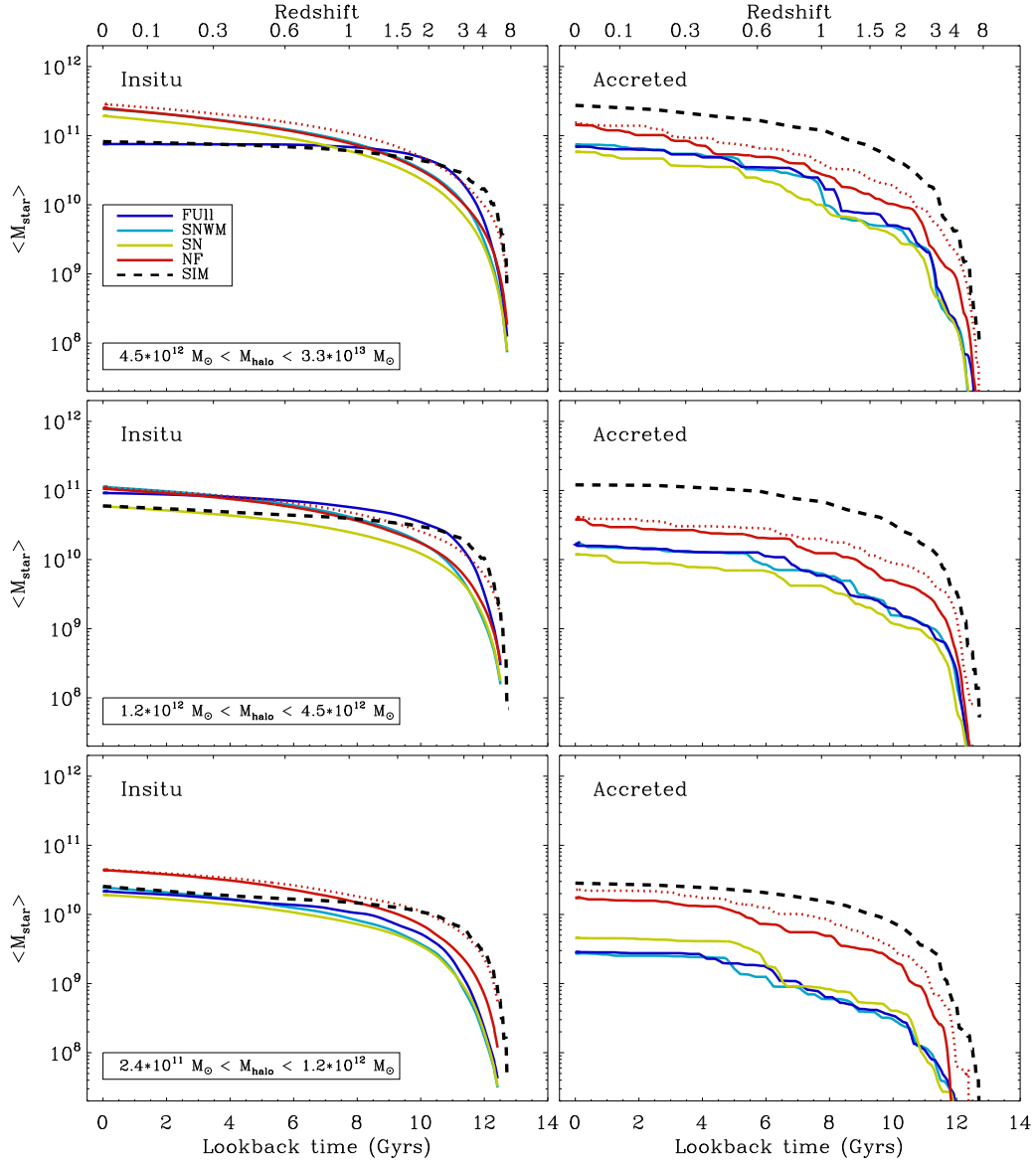


Figure 5.9: Comparison of the mean in-situ (left column) and accreted (right column) stellar masses. The mass bins and colors are the same as in Fig. 5.2. The in-situ stellar masses in the SAMs agree with the ones in the simulations reasonably well, whereas in the SAMs the accreted stellar mass is smaller than in the simulations.

halos, removing the supply of new gas needed to fuel ongoing in-situ star formation. Interestingly, increasing the star formation efficiency in the NF model has almost no effect on the in-situ to accreted fraction. This is presumably because the SF efficiency is increased in the central and (accreted) satellite galaxies alike. However, if the SFE were higher in high redshift galaxies than at low redshift, this would presumably increase the accreted fraction in present day galaxies. This may be part of the reason for the higher accreted fractions in the simulations.

Fig. 5.9 shows the evolution of the cumulative mass of in-situ and accreted stars separately for the simulations and the various SAM variants. Here one can see that the NF SAM actually reproduces the growth of *in-situ* stellar masses fairly well, though overproducing the in-situ mass at low redshift somewhat, especially in the highest mass bin. One can speculate that gravitational heating in the simulations may prevent some of the late cooling in the highest mass bin and leads to lower in-situ stellar mass than the NF SAM (Naab et al., 2007; Johansson et al., 2009b; Feldmann et al., 2010). The radio mode AGN feedback in the FULL model leads to a similar suppression of this in-situ mass growth in the massive halos. The NF model with increased SFE gives an even better match to the simulations at high redshift. The discrepancy arises from the much lower accreted masses in the SAM. Here again, the SF model with high SFE comes the closest to matching the simulation results, but it still falls short by a considerable amount.

Part of the reason for the lower predicted accreted masses in the SAMs is that the SAMs used here only allow for cooling onto the central galaxy in the halo, effectively assuming that the hot gas reservoir of a satellite galaxy is stripped as soon as it enters the virial radius of the host. This is known to result in satellites that are too red and have star formation rates that are too low compared with observations (Kimm et al., 2009). It will also truncate their star formation, resulting in a smaller amount of stellar mass that will eventually be accreted when they merge (Khochfar & Ostriker, 2008).

5.5.3 Hot halo gas

The evolution of the mean hot gas fraction is shown in the three panels of Fig. 5.10. In all but the SN SAM the hot gas fraction increases with increasing halo mass, which is qualitatively similar to the simulations. In the simulations this effect is caused by shock heating of infalling baryonic material which becomes more efficient for massive halos (e.g. Silk, 1977; Binney, 1977; White & Rees, 1978; Birnboim & Dekel, 2003; Birnboim et al., 2007; Kereš et al., 2005; Khochfar & Ostriker, 2008; Kereš et al., 2009; Johansson et al., 2009b). This trend is also seen by the SAMs, except for the SN model, where the supernova energy input heats most of the available gas to the virial temperature of the halos, keeping the hot gas fraction constant independent of halo mass. For the SNWM and FULL models the supernova winds drive some of the hot gas out of the low mass halos. The additional effect of Radio mode heating (FULL model), which

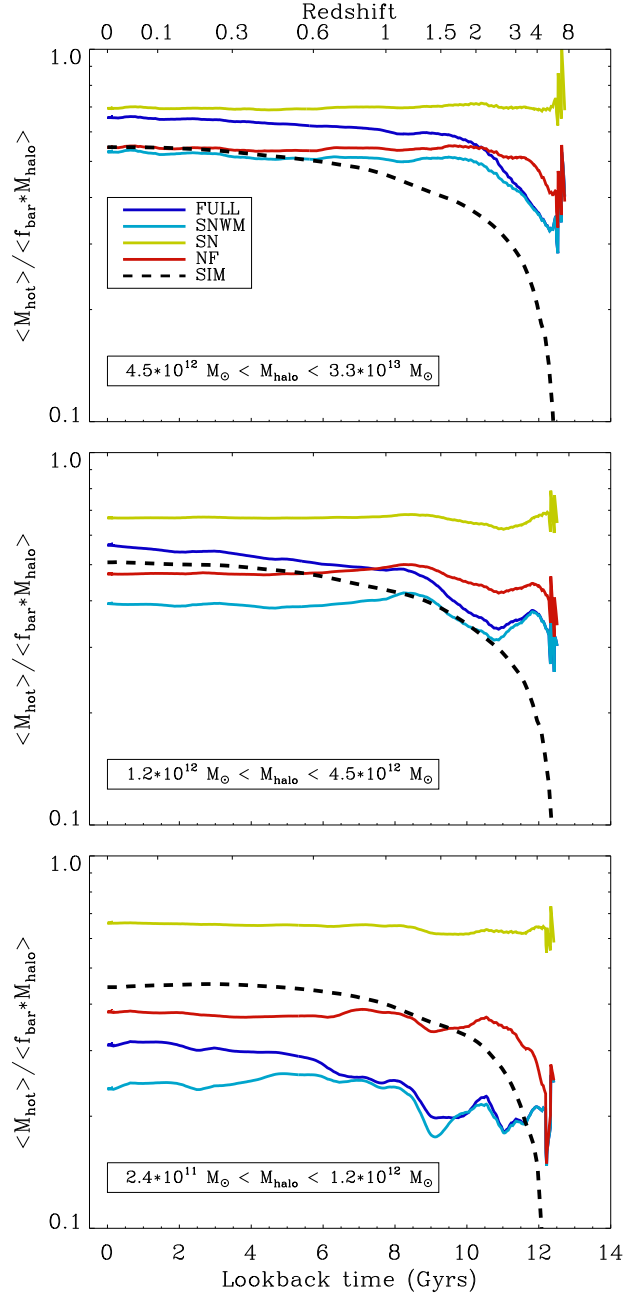


Figure 5.10: Evolution of the mass fraction of hot gas in simulations and SAMs normalized to the available mass in baryons. The mass bins and colors are the same as in Fig. 5.2. At low redshifts $z < 1.5$, simulations can be matched by the NF model. At high redshifts the hot gas content is significantly larger for the NF model. For $z > 3$, models including metal cooling provide a much better match to simulations which do not include metal cooling.

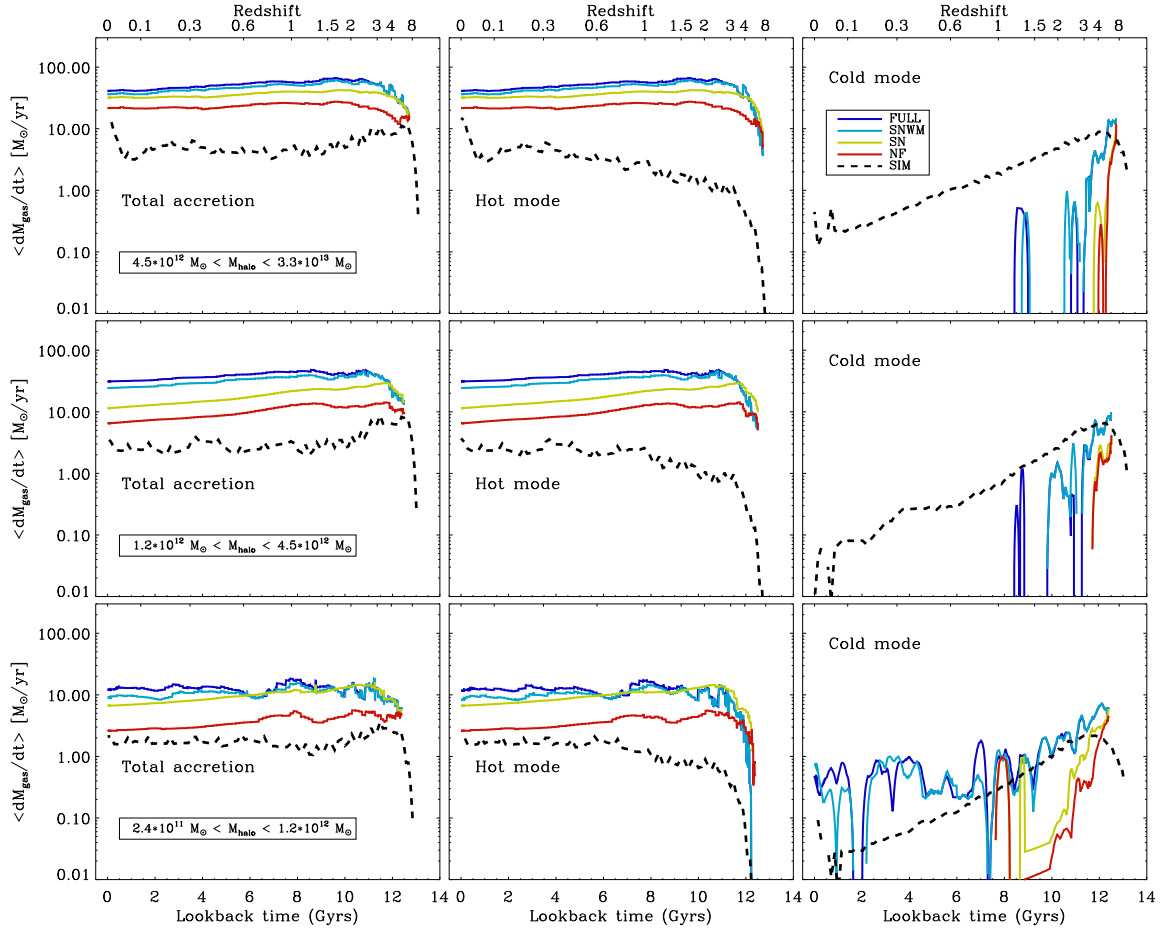


Figure 5.11: Comparison of the mean accretion rates of all gas (left column), hot (intermediate column) and cold (right column) mode accretion in simulations and SAMs. The mass bins and colors are the same as in Fig. 5.2. Compared to simulations, hot mode accretion is over-estimated in all SAMs, whereas cold mode accretion is in general under-estimated, particularly for SAMs without metal cooling.

prevents late cooling in massive halos and therefore leads to larger amounts of hot gas, is apparent for the intermediate and high mass galaxies. The NF model agrees fairly well with the simulations in all mass bins at $z \lesssim 1.5$ but substantially overpredicts the amount of hot gas at high redshift.

To understand the differences in the hot gas content at high redshift the gas accretion modes onto the central galaxies are investigated. For the simulations it is distinguished between hot and cold accretion by considering the highest temperature a gas particle had before it was accreted onto the galaxy, i.e. 1/10th of the virial radius. The same definition is used to distinguish between hot and cold gas as given by equation 5.2 (similar to Kereš et al., 2005). The SAMs distinguishes between hot and cold mode accretion (slow and rapid cooling) depending on whether the ratio of the cooling radius to the virial radius $r_{\text{cool}}/r_{\text{vir}}$ is larger (cold mode) or smaller (hot mode) than unity (White & Frenk, 1991). The distinction between hot and cold mode accretion approximately specifies whether the gas was heated to the virial temperature of the host halo before it was accreted onto the galaxy (hot mode) or was directly accreted without being heated (cold mode). The cold mode accretion is meant to represent the ‘cold flows’ recently discussed in the literature (Kereš et al., 2005, 2009; Oser et al., 2010; Dekel et al., 2009). Note that for the SNWM and FULL SAMs, the heating rates or rates of blown-out gas due to feedback processes are not subtracted from the accretion rates.

Fig. 5.11 shows the comparison of the total (left panels), hot (middle panels) and cold mode (right panels) gas accretion rates onto the central galaxies as a function of redshift. For all SAMs, the total gas accretion rates onto the galaxies are significantly higher than for the simulations. This is caused solely by higher hot mode accretion rates from the generally larger hot gas reservoir in particular at high redshift (middle panel in Fig. 5.11 and see Fig. 5.10). The cold mode accretion rates are much lower in the SAMs than in the simulations, and in the SAMs without metal cooling (which are more relevant to compare with the simulations), the cold mode is truncated at $z \lesssim 4$ for massive halos, $z \lesssim 1-1.5$ for low mass halos, while it declines smoothly until $z \sim 0$ in the simulations. However, the predicted rates of cold mode accretion are much higher in the SAMs that include metal cooling.

In contrast to the results presented here, Cattaneo et al. (2007) find a reasonably good match for the evolution of the hot gas content as well as for the hot and cold mode accretion rates in their SAM version without any feedback. However, they include metal cooling in their SAM, but not in their simulations. Benson & Bower (2010) compare cold and hot mode accretion rates from SAMs to simulations, varying the supernova feedback and conditions for the rapid cooling regime according to Birnboim & Dekel (2003). They concluded that cold-mode physics is already adequately accounted for in SAMs — but they also used simulations with only primordial H & He cooling, but included metal cooling in their SAMs. Lu et al. (2010) assume only H & He cooling

in their SAMs *as well as* in the simulations (like in this study) and find qualitatively similar results to ours: a discrepancy for the hot halo gas fraction at high redshift associated with larger hot mode and smaller cold mode accretion rates in the SAMs than in the simulations.

This suggests that the agreement presented in Cattaneo et al. (2007) and Benson & Bower (2010) is fortuitous, and arises because of the enhanced cold flows resulting from the metal cooling included in the SAMs. It is unclear whether this agreement would persist if metal cooling were included also in the simulations, but it appears that the agreement is not nearly so good as they claim when metal cooling is omitted from both techniques. In addition, the recipes for gas accretion in SAMs do not currently allow co-existing cold and hot gas accretion as seen in simulations. For this, Lu et al. (2010) proposed a new model that explicitly incorporates cold-mode accretion independent of the hot halo gas. By fitting the hot and cold gas fraction in simulations as a function of redshift and halo mass, and assuming accretion onto the galaxy within a free-fall time they calculate the accretion rate of the cold component and thus, achieve a better match of their SAMs to simulations.

5.6 Comparison to observations

In this Section, the results from the SAMs and simulations are compared to observational data and empirical constraints at different redshifts. It is focused on two key observational constraints: the relationship between halo mass and stellar mass (the $M_{\text{gal}} - M_{\text{halo}}$ -relation) and the relationship between stellar mass and star formation rates ($\dot{m}_{\text{star}} - M_{\text{gal}}$ -relation).

Fig. 5.12 shows the relation of galaxy mass and dark matter halo mass for $z = 0$ (left panels), $z = 1$ (middle panels), and $z = 2$ (right panels). The NF and FULL SAMs are shown, together with the simulations. One can also see the empirical constraints on the $M_{\text{gal}} - M_{\text{halo}}$ -relation from Moster et al. (2010), which were obtained by asking how halos and sub-halos in an N-body simulation must be populated in order to reproduce the observed stellar mass functions at different redshifts (halo abundance matching). The thin, black vertical lines illustrate the observational lower halo mass limit of the fit. Also shown are the similar constraints from Wake et al. (2011), which are derived using galaxy clustering data from the NEWFIRM Medium Band Survey between $1 < z < 2$ (see also Wechsler et al., 2006; Zheng et al., 2007; Conroy & Wechsler, 2009; Guo & White, 2009; Zehavi et al., 2010; Behroozi et al., 2010). Note that the fitting functions of Moster et al. (2010) and Wake et al. (2011) are somewhat different, in particular at the low mass end. This is not surprising, as they were derived using different methods and from different observational data sets. At all redshifts, the simulations over-predict the stellar masses at a given halo mass by about a factor of two for halos more massive than $10^{12} M_{\odot}$. At higher redshifts the progenitor galaxies have lower masses, and

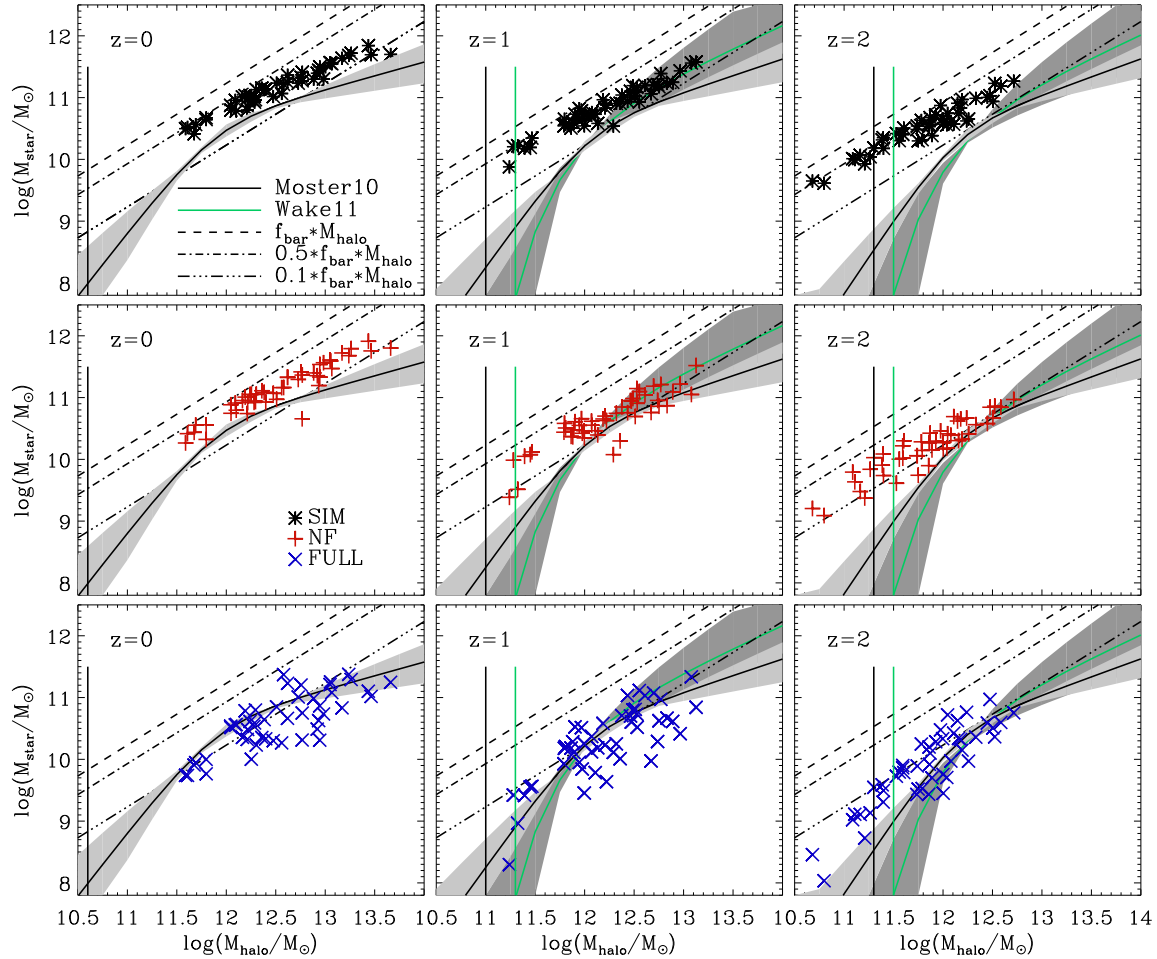


Figure 5.12: *Stellar mass versus dark matter halo mass for simulations (upper row), NF model (middle row) and the FULL model (lower row). The left column shows the dependence on halo mass for $z = 0$, the middle one for $z = 1$ and the right one for $z = 2$. The black lines show the fit for the halo occupation distribution from Moster et al. (2010). Thin black or green, vertical lines show the observational limit of the fits in Moster et al. (2010) or Wake et al. (2011), respectively. The dotted-dashed diagonal lines illustrate baryon fractions of $0.1 \times f_{\text{bar}}$, $0.5 \times f_{\text{bar}}$, and $1 \times f_{\text{bar}}$.*

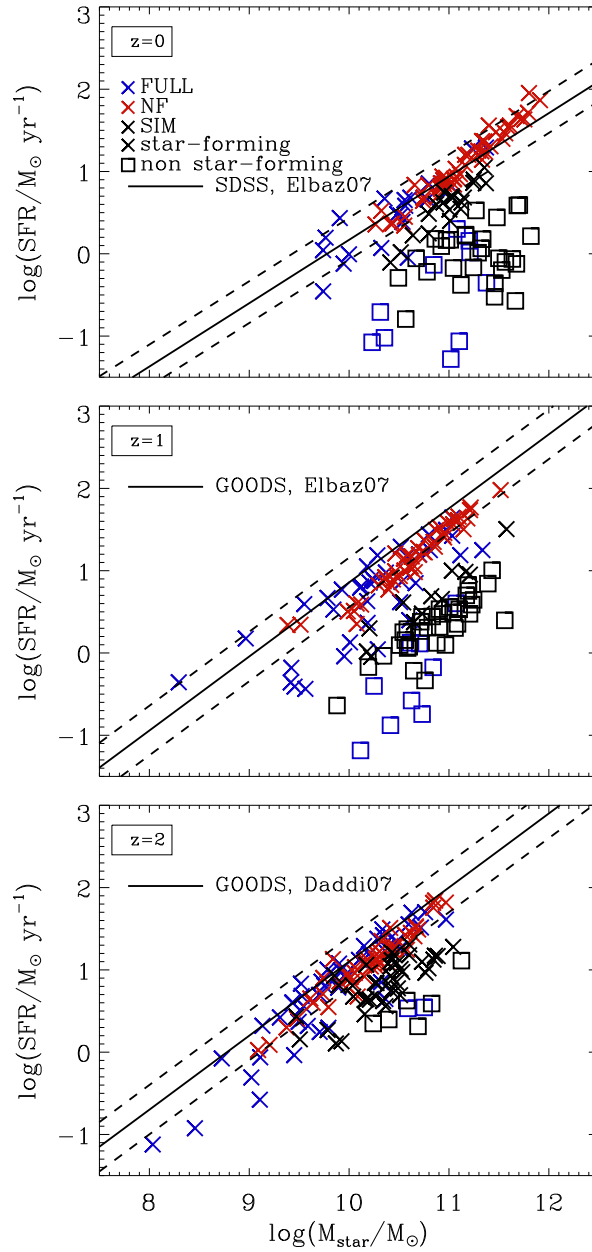


Figure 5.13: Star formation rate versus stellar mass for simulations and two different semi-analytic models (NF and FULL). Solid lines illustrate the observed relations at different redshifts: $z = 0, 1$: Elbaz et al. (2007), $z = 2$: Daddi et al. (2007). Note that following Herschel measurements the observed relation at $z = 2$ was re-normalized 0.3 dex downwards (see text).

deviate more from the expected distribution. At $z = 2$ the difference can be almost two orders of magnitude for halos of $\sim 10^{11}M_{\odot}$, in line with the findings of the previous Section — at high redshift, gas is very efficiently converted into stars in the simulations. Implementation of more efficient feedback from supernovae would help to solve this problem. Indeed it has been shown that simulations that do include effective SN feedback agree much better with expectations (see e.g. Scannapieco et al., 2009; Sawala et al., 2010; Genel et al., 2010; Governato et al., 2010 and references therein). In addition, it is apparent that the simulations require an additional process that can quench star formation at late times in massive halos, such as radio mode AGN feedback.

For high mass halos, the NF model (middle row) predicts galaxy masses close to the relation at $z = 1$ and $z = 2$ due to less efficient star formation at high redshifts (see Fig. 5.5), but, like the simulations, over-predicts the stellar masses in low mass halos. By $z = 0$ the offset is about as large as for the simulations. For the FULL SAM there is good agreement at $z = 0$, which is not surprising because the model was tuned to match the observed stellar mass function. However, the FULL model still predicts galaxy masses that are about a factor of two to three too high for low mass halos ($\log(M_{\text{halo}}) < 11.5$) at high redshift. This is related to the excess of low mass galaxies at high redshift and other connected problems discussed in Fontanot et al. (2009), and is seen in both SAMs and hydro simulations from several groups. It is likely that these problems are due to limitations in the current understanding or implementation of the physics of star formation and/or SN feedback.

The relation between the star formation rates and the galaxy stellar masses M_{star} is shown in Fig. 5.13 for redshifts $z = 0$, $z = 1$, and $z = 2$. It is distinguished between star-forming and non-star-forming galaxies (illustrated as crosses or open squares, respectively) using a criterion according to Franx et al. (2008): galaxies with specific star formation rates SFR/M_{star} smaller than $0.3 \times t_{\text{hubble}}^{-1}$, are considered to be quiescent, whereas galaxies with larger specific star formation rates are assumed to be star-forming. The black, solid lines always refer to the observed relation at the corresponding redshift ($z = 0$: SDSS, Elbaz et al. (2007); $z = 1$: GOODS, Elbaz et al. (2007); $z = 2$: GOODS, Daddi et al. (2007)) for star-forming galaxies. Note that the relation of Daddi et al. (2007) is shown at $z = 2$ re-normalised 0.3 dex downwards, following the re-calibration of SFR derived from 24 micron luminosity based on recent Herschel observations (Nordon et al., 2010).

In general, the simulations under-predict the star formation rates for star forming galaxies at all redshifts, but most notably at $z > 1$, due to the high star formation efficiencies at even higher redshifts and the resulting gas depletion (see Section 5.5.2). Once again, implementing more effective supernova feedback would presumably suppress star formation in the small, high redshift progenitors of these galaxies and result in higher SFR at these redshifts (see e.g. Oppenheimer & Davé, 2008; Genel et al., 2010). The NF SAMs fit the SF sequence at $z = 0$, but have too many high mass

galaxies with high SFR. In the FULL model, these galaxies are quenched by radio mode feedback, in agreement with observations (see Somerville et al., 2008b). Both the NF and FULL SAMs SF sequences are about a factor of two too low at $z \sim 1$ and 2. This also seems to be generic to many SAMs, as shown by Fontanot et al. (2009) and others. It is interesting to note that star forming galaxies in both the NF and FULL SAM galaxies all lie on the same SF sequence. This implies that SN feedback simply moves galaxies along the sequence, reducing both the stellar mass and the SFR such that the galaxies remain on the same relation, and is due to the self-regulating nature of SN feedback in the SAMs. In contrast, AGN feedback quenches star formation and moves massive galaxies off of the SF sequence (seen in the FULL model).

5.7 Discussion and conclusions

In this Chapter, a detailed comparison was presented between a set of 48 cosmological hydrodynamic zoom simulations and different stripped-down versions of semi-analytic models based on dark matter merger trees extracted from the simulations. The hydrodynamical simulations are run using the entropy-conserving formulation of SPH with the GADGET-2 code, and include atomic cooling assuming a primordial composition of H and He, a UV background radiation field, star formation, and supernova feedback. Results from a “no feedback” (NF) version of the SAM are presented which contains the same physical ingredients as the simulations, together with versions that include thermal feedback by supernovae (SN), a version that also includes large-scale SN-driven winds and metal cooling (SNWM), and the FULL version which includes all the previously mentioned ingredients as well as AGN feedback. With this approach the predictions of the two methods can be compared over two orders of magnitude in halo mass at unprecedented resolution.

The two approaches try to answer the same questions but differ in methodology. In the simulations the full dynamical and hydrodynamical evolution of the systems is followed by solving the equations of motion computationally. Additional physical processes like star formation and supernova feedback are included using sub-resolution models. The semi-analytic models are based on the computed dark matter accretion history and approximate the gas physics, star formation, and feedback processes with simplified recipes. The analysis is focused on the cosmic evolution of the baryon content in the central galaxies of the main branch of the merger trees and its division into various components (stars, cold gas, and hot gas), as well as how those galaxies acquired their gas — whether through “cold” or “hot” mode accretion — and their stellar mass (e.g. through in-situ star formation vs. accretion).

The results of the comparison are quite rich, with some surprising agreement and some striking disagreement. First, let me note that the results of the simulations are expected to lie somewhere in between the NF and the SN SAMs, since these SAMs

include the similar physical processes as the simulations. In most cases, the agreement is best between the simulations and the NF model, suggesting that the SN feedback implemented in the simulations has little effect. The NF SAMs produce very good agreement with the simulations for the mass of cold gas plus stars at all redshifts and for all halo masses. The SAMs slightly underestimate this “condensed baryon” fraction at high redshift ($z > 1$) and overestimate it at low redshift. This indicates that the overall cooling and accretion rates in the SAM and the simulations must be similar. The NF SAM also produces fairly good agreement (better than $\sim 20\%$ since $z \sim 4$) with the overall baryon fractions (i.e. hot gas plus cold gas and stars in the central galaxy) in the simulations, here overestimating the baryon fractions at high redshift in high and intermediate mass halos.

A striking difference is that when the evolution of the stellar and cold gas components is studied separately, the cold gas fractions are found to agree at very high redshifts, but the gas is consumed much more rapidly in the simulations, leading to cold gas fractions at all redshifts less than about $z \sim 3-4$, and in halos of all masses, being much lower (by up to two orders of magnitude) than in the NF SAM. Correspondingly, much higher stellar masses are found in the simulations than in the SAMs at high redshift, although they converge to almost the same value as the NF SAMs at $z = 0$. One can interpret this as an indication that the star formation efficiency is much higher in the simulations than in the SAMs, and the reason for the convergence in the stellar masses at low redshifts is because nearly all available gas has been consumed in the simulations. This conjecture is supported by the finding that if the star formation efficiency is boosted in the NF SAM by a factor of ten, excellent agreement is found with the stellar mass fraction evolution in the simulations, and improved agreement with the cold gas fraction evolution.

However, both the simulations and SAMs supposedly adopt the same empirical Schmidt-Kennicutt relation between cold gas density and star formation rate. How can the star formation efficiencies be so different? Let me note several differences in the implementation of the star formation recipe in the simulations and SAMs. In SAMs, the only available information about the structure of the star forming gas in galactic disks is an estimate of the scale radius of the total baryonic component of the disk, which comes from angular momentum conservation arguments (Mo et al., 1998; Somerville et al., 2008a). The SAMs then make a series of assumptions — that the gas is in a smooth, thin exponential disk with a radius that is a simple multiple of the stellar scale radius — and apply the Kennicutt relation in terms of the predicted gas surface density. Only gas above a critical surface density is allowed to form stars. In contrast, the simulations provide detailed 3D predictions for the structure of the cold gas in galaxies, and implement the SK relation in terms of 3D volume density (also applying a threshold for SF in terms of a critical volume density). It is well known that high redshift galaxy assembly in cosmological simulations is dominated by clumpy, high density, cold mode accretion. Disks may be more compact than in the idealized

case of perfect conservation of angular momentum, and are thick and clumpy. The adopted SF recipe is super-linear in the gas volume density (i.e. the exponent in the SK relation is larger than unity), and therefore star formation will be more efficient in a clumpy gas distribution than in a smooth one.

The appropriate values of the SF and SN feedback efficiency parameters for the simulations were obtained by tuning them to match the observed Kennicutt relation for an idealized, smooth thin exponential disk, designed to resemble a Milky Way-like galaxy at $z = 0$ (Springel & Hernquist, 2003). Using these same values for the parameters, the high redshift galaxies in the cosmological simulations are found to lie about a factor of five above the Kennicutt relation with the normalization adopted by Springel & Hernquist (2003). A second, minor issue, is that the SAMs were tuned to match a Kennicutt relation with a normalization a factor of two lower than the one used by Springel & Hernquist (2003), reflecting a different choice of IMF in the conversion from observed flux to SFR.

This seems to explain the reason for the factor of ~ 10 higher SFE in the simulations relative to the SAMs, but begs the question: is this a robust prediction of the simulations that should be taken seriously? Are these higher star formation efficiencies in high redshift galaxies really physical? There are several issues that are relevant here. First, the predicted “clumpiness” of the disks is highly sensitive to the assumed sub-grid recipes. For example, implementation of more effective SN feedback would reduce the clumpiness of the disks at high redshift, but might increase the clumpiness at $z \approx 2$ (e.g. Genel et al., 2010) in the simulations. Observed disks at high redshift are known to be more clumpy than nearby ones (Genzel et al., 2006, 2008, 2010; Förster Schreiber et al., 2009, 2011), but it remains highly uncertain which recipe for SN feedback will produce the “correct” degree of clumpiness and overall structure for statistical samples of high redshift galaxies while simultaneously reproducing the properties of local spirals (Piontek & Steinmetz, 2011; Governato et al., 2009; Scannapieco et al., 2009; Brooks et al., 2009). Moreover, recent observational studies indicate that star formation rate densities in local galaxies as well as at high redshift correlate linearly with the surface density of the *molecular gas*, with no evolution in the *molecular SK* relation (Bigiel et al., 2008; Daddi et al., 2010; Genzel et al., 2010). This is also true for galaxies with very clumpy star formation, as expected for a linear dependence with gas density. Only interacting galaxies undergoing a significant starburst seem to show an increased star formation efficiency (Daddi et al., 2010; Genzel et al., 2010). Neither the SAMs nor the simulations presented here include these effects.

A second major difference between the SAMs and the simulations is in the mode in which galaxies acquire most of their stellar mass. It is distinguished between “in-situ” growth, due to stars that form out of cold gas within the galaxy in question, and “accretion” of stars that formed in external galaxies and are accreted via mergers. This distinction is important because it may determine the characteristic size evolu-

tion of early type galaxies (Khochfar & Silk, 2006b; Naab et al., 2009; Guo et al., 2011; Covington et al., 2011). It has been shown previously that massive galaxies in the simulations and semi-analytic models have an early phase of growth dominated by the in-situ mode, and then switch over to a mode that is dominated by growth through accretion (De Lucia et al., 2006; Khochfar & Silk, 2006b; Guo & White, 2008; Oser et al., 2010; Feldmann et al., 2010; Zehavi et al., 2011). Although the ratio of in-situ to accreted stars always decreases with time in the SAMs, in qualitative agreement with the simulations, in the SAMs in-situ growth dominates over accretion in halos of all masses at all times. Examining the absolute mass in stars formed in situ or accreted, it is found that this is primarily because the SAMs predict much less mass growth through accretion — the in-situ mass evolution agrees fairly well with the simulation results. The comparison between SAMs including different physical processes gives us further insights into the origin of the discrepancy: 1) Increasing the efficiency of SN feedback (SN and SNWM SAMs) reduces the accreted mass because star formation is suppressed in the low-mass satellites that eventually get accreted. 2) Including radio mode AGN feedback (FULL SAM) reduces the in-situ growth in massive galaxies at late times, because it shuts off the fuel supply for in-situ star formation in these objects. Interestingly, increasing the SF efficiency in the SAM does not affect the fraction of in-situ versus accreted mass, presumably because all galaxies are boosted equally.

In summary, it is likely that the contributions from in-situ and accreted stars are currently incorrectly predicted in both the simulations and SAMs, for the following reasons. In order to match observations, the simulations presented here clearly require both a process that suppresses star formation in low mass objects at all redshifts (such as SN-driven winds) and one that can shut off residual cooling and quench star formation in massive galaxies at late times (such as radio mode AGN feedback). The former will reduce the accreted mass, while the latter will decrease the in-situ mass in massive objects at late times. In addition, if the SFE is higher in high redshift galaxies than at late times, this is likely to increase the accreted mass. On the other hand, the SAMs presented here, like many SAMs in the literature, make the assumption that hot gas from the halo can only be accreted onto the central galaxy. This rapidly truncates the star formation in satellite galaxies and is likely to artificially decrease the accreted mass fraction. In addition, the SAMs neglect gravitational heating, which is clearly important in the simulations and should reduce the in-situ growth in massive halos at late times. The recent study of Fontanot et al. (2011) has shown that the S08 SAM and other similar SAMs in which radio mode feedback is used to solve the overcooling problem over-predict the fraction of radio loud galaxies compared with observations, and the implemented dependence of radio luminosity on stellar and halo mass is too steep. Gravitational heating could play a similar role (Khochfar & Ostriker, 2008; Dekel & Birnboim, 2008; Birnboim & Dekel, 2010) and thereby reduce the need for such strong radio mode heating.

A third important result is that the cooling recipe implemented in these SAMs

(which is widely used in many SAMs) over-predicts the overall accretion rate of gas by a factor of 1.5 (in low mass halos) to four (in massive halos). If the accretion rates in the simulations are accurate, this implies that the SAMs that match present day galaxy properties are compensating for this “extra” accretion by artificially “tuning up” the feedback. Moreover, when the gas accretion is divided into “hot mode” and “cold mode” (Birnboim & Dekel, 2003; Kereš et al., 2005), the SAMs are found to systematically overestimate the hot mode growth (by up to an order of magnitude) and underestimate the cold mode. As well, in the SAMs without metal cooling, the cold mode shuts off completely at low redshifts (the shutoff redshift depends on halo mass), while in the simulations it declines smoothly but continues to low redshifts. This is likely to be a result of the fact that, in the SAMs, the criterion for discriminating between hot and cold mode accretion is based on the assumption of smooth, spherical halos, while in simulations cold gas can stream into halos along cold, dense filaments. In addition, in the SAMs, gas is assumed to accrete either in cold mode or hot mode, but simultaneous cold and hot mode accretion is not allowed. In the simulations, dense, cold streams can penetrate deep into the diffuse hot halos, allowing for both accretion modes occur within the same halo (Kereš et al., 2005, 2009; Brooks et al., 2009). Similar results were found in the study of Lu et al. (2010), who proposed a more accurate recipe for treating hot and cold mode accretion in SAMs. Here, I would like to point out that overcoming this weakness of cold and hot mode accretion in SAMs and thus, changing the amount of cold gas present in a galaxy may automatically result in a more self-consistent approach for modeling the downsizing in black hole growth. As shown in Chapter 4, so far, an explicit prescription for the evolution of a sub-Eddington limit of cold gas accretion onto the black hole is needed in order to obtain the observed decrease in number densities of luminous AGN at $z < 2$ and a direct connection of black hole accretion to the cold gas content failed in reproducing this decrease. Thus, it might be extremely interesting to see to what extent a more physical recipe for cold and hot gas cooling in SAMs might lead to a better agreement with the observed decrease in the amount of luminous AGN when black hole accretion is directly connected to the cold gas content.

Both the simulations and SAMs are compared to two key observational constraints at $z = 0, 1$, and 2: the relationship between dark matter halo mass and stellar mass, and the relationship between stellar mass and star formation rate. It is found that the simulations predict stellar masses that are too large for their halo masses at all redshifts. The stellar masses are too high by a factor of a few for massive halos ($\gtrsim 10^{12} M_{\odot}$), and by an order of magnitude or more for lower mass halos. The SAM results for the NF model are qualitatively similar, although the stellar masses at high redshift are lower, due to the lower star formation efficiencies, as already discussed. In the SAMs, the curvature in the empirical $M_{\text{gal}} - M_{\text{halo}}$ relation can be achieved by including supernova driven winds, which suppress star formation in low mass halos, and radio mode AGN feedback, which suppresses star formation in high mass halos. The SFRs at a given stellar mass are found to be too low in the simulations at all redshifts $z \lesssim 2$, proba-

bly because of the overly efficient star formation at higher redshifts and the resulting gas consumption. Star-forming galaxies in all SAMs were found to lie on the same relation, with supernova feedback shifting the galaxies along the relation. The SAMs (both FULL and NF) showed better agreement with the observed $\dot{m}_{\text{star}} - M_{\text{gal}}$ relation than the simulations, but have SFRs at a given stellar mass that are about a factor of ~ 2 lower at high redshifts.

In a final summary, I conclude that on the one hand, one can be encouraged by the robustness of SAMs as a tool for exploring the qualitative effects of varying the physical ingredients of galaxy formation. On the other hand, also several important areas have been identified where the quantitative accuracy of fundamental physical recipes in the SAMs should be improved, and several physical processes that are missing in the SAM but which should be included. Additionally, there is a tendency to treat numerical simulations as “truth”, but it has been shown that key predictions of these simulations are sensitive to uncertain sub-grid recipes. Also several physical processes have been highlighted that are neglected in the simulations studied here, but which appear to be crucial in order to understand the properties of real galaxies. These include more effective implementation of supernova-driven winds, chemical enrichment and metal cooling, and a self-consistent treatment of the growth of and feedback from black holes. Of course, these are hardly new suggestions, and considerable progress has been made recently in all of these areas (e.g. Di Matteo et al., 2005; Cattaneo et al., 2005; Sijacki et al., 2007; Oppenheimer & Davé, 2008; Booth & Schaye, 2009; Scannapieco et al., 2009; Governato et al., 2010; Schaye et al., 2010b; Sawala et al., 2010; Ostriker et al., 2010). In conclusion, I suggest that using these two complementary techniques (SAMs and hydrodynamic simulations) together in close coordination may provide the most powerful approach to understanding galaxy formation and evolution for the near future.

Conclusion and outlook

6.1 Summary

In our current picture of the joint evolution of galaxies and black holes, there exists a large number of exciting and puzzling questions, which are subject of intense debate. For example the origin of the black hole mass scaling relations, whether and how black hole mass scaling relations evolve at high redshift, trigger mechanisms and efficiency for black hole accretion and the origin of the observed downsizing in black hole growth. In this thesis, I used analytical and semi-analytical methods based on the merging history of cosmological N-body simulations in order to assess and understand some of the unanswered questions. As, however, semi-analytic models may be criticised due to their large degree of approximation combined with a huge parameter space compared to hydrodynamical simulations, the limitations of semi-analytic models were tested by a direct comparison to cosmological, hydrodynamical simulations. In summary, in this thesis, I focused on the following topics:

- The scatter evolution in black hole mass scaling relations (Chapter 3)
- The origin of the anti-hierarchical black hole growth (Chapter 4)
- Comparison of SAMs to cosmological zoom simulations (Chapter 5)

In the following, I will briefly summarize the most striking results of the different chapters. Chapter 3 concentrates on the influence of the merger-driven evolution of the black hole mass scaling relations and on the evolution of the intrinsic scatter in black hole mass. Several authors have found observational evidence that galaxies at high redshift have significantly higher or smaller $M_{\bullet}/M_{\text{bulge}}$ -ratios than ellipticals today (e.g. Treu et al., 2007 and Alexander et al., 2008). Some theoretical studies using merger simulations explain these observations by an evolution of the black hole-bulge mass relation with redshift as a consequence of the connected growth of galaxies and black holes via gas physical processes. However, in contrast to previous work, I have proposed a completely alternative scenario (Hirschmann et al., 2010) based on purely

statistical merging: the existence of a *larger intrinsic scatter in black hole mass at high redshifts*, even assuming no evolution of the mean relation with cosmic time and adopting no connected black hole and host galaxy growth by gas physical processes. In a purely merger-driven model for black hole growth (which becomes realistic for gas-poor, massive systems at low redshifts), it is found that *the scatter in black hole mass decreases with time*, the number of merger events and the black hole mass itself. This is a direct consequence of the statistical *Central-limit-theorem*, which might also state an alternative explanation for establishing a relation even if objects are uncorrelated initially and if their growth is not connected via gas-physical processes as AGN feedback (see also Peng, 2007; Jahnke & Maccio, 2010). The decrease of the scatter in black hole mass with time and merger number m can be approximated with $\sigma_{\text{merg}}(m) = \sigma_{\text{ini}} \times (m + 1)^{-a/2}$. This is valid for a range of analytical models assuming random merging of black holes in addition to growth scenarios based on the merging history of Λ CDM-simulations. I have created the merger trees for a cosmological simulation ($L = 100$ Mpc, $N_p = 512^3$, GADGET2), populated every newly occurring halo with black holes and galaxies by adding a certain 'seed' scatter and considered the subsequent evolution solely driven by merging events. Adopting a present-day scatter of $\sigma = 0.3$ dex, the results imply a scatter of $\sigma = 0.6$ dex at $z = 3$. Thus, a larger, intrinsic scatter in black hole mass is able to provide a possible scenario, which can account *simultaneously* for over- and under-massive black holes at high redshifts. Moreover, the result is also consistent with the observations of a study of Gültekin et al. (2009), where they find a smaller scatter for ellipticals (mainly massive objects) than for non-ellipticals (less massive objects). As a consequence of this study, I want to emphasize that *purely statistical, merging processes* of galaxies and black holes seem to be able to account for the emergence of the black hole scaling relations themselves as well as for the observed over- and under-massive black holes *without* a fundamental need for a connected growth of black holes and galaxies via gas physical processes.

However, besides the importance of merging processes, gas accretion onto black holes does represent a significant contribution to the over-all mass assembly, which will become especially important for explaining the puzzling question of the downsizing trend in black hole growth (Chapter 4). The anti-hierarchical trend is revealed in many observational studies of AGN (QSO) from different wavebands (IR, optical, soft and hard X-ray). They find that luminous AGN peak at higher redshifts than less luminous ones indicating that massive black holes are already in place early in the Universe whereas less massive black holes tend to form predominantly at later times - at least assuming that black holes are accreting at the Eddington rate (which is proportional to the black hole mass). At first sight, this might seem to be in contradiction with the currently favored hierarchical structure formation paradigm, where at early times low mass objects are assumed to form, while massive objects should assemble their mass only later-on. However, the downsizing trend is most likely caused by different accretion mechanisms onto black holes and their corresponding accretion efficiencies. Thus, for such an investigation, methods based on black hole growth purely due to merging

(as used in Chapter 3), are not sufficient anymore, as more complex gas accretion processes onto the black holes will play a crucial role. Therefore, I used instead a semi-analytic model according to Somerville et al. (2008b) and applied it for the first time to the merger histories of one of the largest currently existing dark matter N-body simulations, namely the Millennium simulation with a comoving box-length of 500 Mpc containing 10^{10} dark matter particles (this ensures good statistics). The original SAM includes an upgraded model for black hole growth following results of SPH-simulations of merging galaxies, by distinguishing between a luminous, Eddington-limited period (*Quasar-mode*) and a low Eddington-ratio accretion, radiatively very inefficient phase (*Radio-mode*). The quasar-mode is triggered by major mergers and black hole growth during this phase is divided into an accretion phase at the Eddington-limit followed by a blow-out phase with fading luminosity. Using this original SAM, the AGN number densities at the peaks of the luminosity curves can be reproduced. However, at low and high redshifts the characteristic anti-hierarchical behavior occurs: at low redshifts, the amount of luminous AGN is over-estimated, while moderately luminous AGN are under-estimated. At high redshifts this trend is reversed. However, I find that a combination of the following three modified and additional accretion mechanisms results in a significantly better agreement with the observed downsizing, in particular at low redshifts:

- A *decreasing sub-Eddington limit* with decreasing redshift and increasing black hole mass leads to a decrease in number densities of luminous AGN at low redshift.
- Secular evolution processes triggering additional accretion onto the black holes - *disk instabilities* - result in an increase of number densities of low luminous objects at low redshift.
- Assuming a *heavy seeding scenario* with $M_{\text{seed},\bullet} = 10^5 M_{\odot}$ and a larger scatter in accreted black hole mass at high redshift than at low ones increases the amount of luminous AGN at high redshift.

The greatest success of the best-fit model including these modifications is that it can reproduce the galaxy-halo mass relation as well as the black hole mass function at $z = 0$ and additionally its results are in fairly good agreement with the bolometric AGN luminosity function at $0 < z < 5$ from the observational compilation of Hopkins et al. (2007c). This indicates clearly that the outlined modifications might state important mechanisms in the picture of the co-evolution of galaxies and black holes: massive black holes can have assembled their mass until $z \approx 2$, but accrete only at a small fraction of the Eddington-rate at low redshifts so that they are hidden and do not occur as high luminous quasars in the present-day Universe. The large amount of moderately luminous AGN at low redshifts might be caused partly by the low-Eddington ratio accretion in the power-law decline phase, and partly by gas accretion triggered by secular evolution processes such as disk instabilities in agreement with observational results. Moreover, large seed black hole masses seem to be the most straight forward scenario to explain high luminous quasars at high redshifts. Current observational constraints,

however, are not sufficient in order to determine whether a heavy seeding scenario or a light seeding scenario with super-Eddington accretion is the correct process. Despite the success of the best-fit model, moderately luminous AGN at high redshifts are still over-estimated, even in the best-fit model. Insufficient treatment of obscuration effects in the observational compilation of Hopkins et al. (2007c) may account for this discrepancy. If namely a redshift dependent dust obscuration is additionally adopted in the best-fit model and the bolometric luminosities are converted into hard X-ray luminosities, then the observed hard X-ray luminosity function can be reproduced reasonably well by the best-fit model, as the dust obscuration mainly reduces the amount of moderately luminous AGN at high redshift. This shows that a redshift dependence in the dust obscuration might provide a further 'puzzle piece' for a complete understanding of downsizing.

Finally, even if semi-analytic models represent the best currently available method for investigating problems which demand large statistics, such as e.g. the downsizing problem, a main disadvantage of semi-analytic models is that there exists a great deal of uncertainty in many of the important processes and most of the physical recipes contain many free parameters (compared to simulations). The extent to which this actually matters has not yet been well assessed. Therefore, in particular in order to be critical against the results in Chapter 4 (which were based only on semi-analytic modeling) as well as to test their robustness and reliability, in Chapter 5, a detailed comparison of SAMs versus *cosmological zoom simulations* tries to reveal the degree of agreement in the evolution of the baryonic component (Hirschmann et al., 2011). Various physical processes can be isolated in order to improve the accuracy of the semi-analytic recipes and to assess the question which physical processes are missing in the simulations. I have created the merger trees for a large sample of ≈ 48 individual, re-simulated halos with unprecedented resolution providing the basic input for the SAMs. To make a fair comparison to the SPH-simulations, I use - besides the full SAM - three additional different stripped-down versions of the SAMs varying the SN feedback, metal enrichment and AGN feedback:

- No feedback, no metals (NF)
- Thermal SN-feedback, no metals (SN)
- Thermal SN-feedback with momentum-driven winds and metal evolution (SNWM)
- Additionally assuming feedback from black hole accretion (FULL)

Generally, SAMs and simulations reveal a better match at low redshift than at high ones. The best agreement to simulations is found for the 'no feedback' version (in particular for the total baryon mass and the condensed baryons), indicating the weak impact of the SN feedback in the simulations. However, a significant discrepancy occurs for the star formation efficiency at high redshift which is found to be much larger in simulations than in the SAMs due to a clumpy cold gas structure at high redshifts

found in the simulations. Moreover, in the framework of how galaxies assemble their stellar content, the bimodal behavior of the stellar evolution as it is found in the simulations by Oser et al. (2010) can not be reproduced by the SAMs. In all models, even including AGN feedback and metal cooling, in-situ star formation is dominating over accretion of stars at all redshifts, whereas in the simulations the fraction of accreted stars becomes larger than the one of in-situ formed stars with evolving time. This is due to a larger accreted stellar mass in the simulations than in the SAMs, probably a consequence of the extremely efficient star formation in simulations at high redshifts. Moreover, additional physical mechanisms in SAMs, as e.g. gravitational heating or delayed strangulation, might be necessary in order to balance the accreted and in-situ formed star fraction in the right way. Additionally, a striking discrepancy occurs for the high redshift evolution of the hot gas content, as the SAMs predict a larger hot gas content than simulations. This might be due to an overestimation of the heating rates in the SAMs, while cold flows are not sufficiently accounted for. For massive galaxies and in particular at high redshifts, accretion rates in the cold mode (= rapid cooling) are much larger in the simulations than in the SAMs, where cold flows occur only for very high redshifts. This points out that in the SAM a very simplified recipe for hot and cold mode accretion is used - depending on the ratio of the cooling radius to the virial radius, $r_{\text{cool}}/r_{\text{vir}}$. For this model, the recipes for cold and hot mode accretion should be improved significantly. A comparison of both model approaches to observations shows that only the full SAM reveals a reasonable good agreement with observations, whereas in simulations more physics, as e.g. a stronger supernova feedback (winds), has to be included. Here, I want to emphasize that it is very interesting to investigate, whether and how enhanced recipes in SAMs, e.g. gas cooling, might influence the black hole growth and thus, the evolution of the connected AGN population.

In final summary, this thesis points out that in order to explain the black hole mass scaling relations themselves and to be able to account for over- and under-massive black holes at high redshifts, solely statistical merging processes may be sufficient neglecting any connected growth between galaxies and black hole via *gas-physical* processes. However, a detailed understanding of gas accretion processes onto black holes, which states a significant contribution to the over-all black hole growth, seem to be of particular importance and the key ingredient for explaining of the evolution of differently luminous AGN number densities and thus, the corresponding downsizing trend. As for such an investigation large, statistical samples of galaxy populations have to be generated with semi-analytic models, a close coordination of these models, often including simplified approximations for galaxy formation, with cosmological, hydrodynamical simulations may provide one of the most powerful approaches to understand galaxy formation and evolution in more detail and thus, to enhance the recipes used in semi-analytic models.

6.2 Next steps

As pointed out in this work, in particular in the last Chapter, a well-known weakness of most semi-analytic models consists in the implementation of various, over-simplified recipes for galaxy formation, with a particular effect on the high-redshift evolution. Compared to results of detailed numerical studies, SAMs are often neglecting important physics, as e.g., most SAMs do not incorporate a sufficient model for describing cold flow physics yet and cannot account for the simulated bimodal behavior of the stellar evolution. In order to compete and keep up with numerical simulations in the future, a major task in the field of semi-analytics should be the extension and improvement of key physical ingredients by closely following the detailed knowledge of physics and from hydrodynamical simulations, with the particular aim to reproduce high-redshift observations. Thus, in future it might be useful to focus on more physical implementations and examine their importance for galaxy formation. In the following I list and describe some of the possible extensions to current models:

1. Missing cold flow physics: Self-consistent gas inflow and heating

In most of the SAMs, gas is accreted onto the halo either in the hot or in the cold mode (= slow and rapid cooling regime) depending on the ratio of cooling to virial radius. Typically, cold mode accretion occurs for low mass halos and for higher redshifts, hot mode accretion for high mass halos and for lower redshifts. However, simulations show a *simultaneous* infall of hot and cold gas onto the halo for all redshifts with a much larger fraction of cold infalling gas than in SAMs (assuming no metal enrichment in both methods). The simplified recipe in the SAMs does not account for the co-existence of cold and hot halo gas and the bimodal accretion seen in simulations. This influences strongly the evolution of galaxies, in particular at high redshifts. Thus, motivated by hydrodynamical simulations, implementing 'gravitational' heating seems to be a promising mechanism in order to treat gas inflow and heating in a self-consistent way. Following Khochfar & Ostriker (Khochfar & Ostriker, 2008), the heating of the intracluster medium (ICM) would be calculated by the net surplus of gravitational potential energy released from gas that has been stripped from infalling satellites. Note that the simplified approximation for an additional gravitational heating source as used in Chapter 4 can only be the start and has to be implemented in a more self-consistent way. Gravitational heating is found to be an efficient heating source for massive dark matter halos, where it prevents cooling, and becomes especially important at late times. Assuming in general cold infalling gas (no shock heating) and a fraction of hot accretion, which is only due to gravitational heating, would result in an automatic, less efficient heating at high redshifts and for low mass halos than in current SAMs. This should result naturally in larger cold accretion fractions for objects at high redshifts. As this new implementation might presumably mainly affect and change the high redshift evolution of the hot and cold gas content in galaxies, a direct comparison to new, observed data of high redshift luminosity functions ($z = 7 - 10$, Bouwens et al. (2008)) might provide a reasonable test for the success of this new model. A further advantage

of gravitational heating is - as the released energy can match the one of AGN feedback - less AGN feedback than currently assumed might be necessary to overcome the overcooling problem and to obtain a self-consistent black hole growth (this was already shown for the simplified approximation for gravitational heating in Chapter 4). In a recent study of Fontanot et al. (2011) it was shown that most of the currently used SAMs are extremely overestimating radio-mode accretion compared to observations. Moreover, due to the change of the cold gas content, gravitational heating might also influence the number densities of AGN, in particular at high redshifts, and thus, might reproduce the corresponding downsizing in a more self-consistent way than in the current model.

2. Bimodal behavior of the stellar evolution

Cosmological simulations of galaxy formation appear to show a two-phase character with a rapid early phase at $z > 2$ during which in-situ stars are formed within the galaxy from infalling cold gas followed by an extended phase since $z < 3$ during which ex-situ stars are primarily accreted. In the latter phase massive systems grow considerably in mass and radius by accretion of smaller satellite stellar systems formed at quite early times ($z > 3$) outside of the virial radius of the forming central galaxy. In contrast to that, in-situ star formation is found to be the dominating process in SAMs at *all* redshifts. This is because in SAMs less stars are produced in smaller, accreted galaxies. However, a well-known problem of many SAMs is that they often add excessive feedback from AGN to substitute for further important physics as gravitational heating. Therefore, due to physically not correct feedback processes, star formation might be prevented in small galaxies falling into larger ones. This might suggest that implementing gravitational heating - accounting for a physically motivated heating in galaxies - could be *again* a crucial ingredient in order to get an appropriate balance between accreted and in-situ star formation, and thereby, a bimodal stellar evolution as seen in simulations. Moreover, current SAMs are assuming instantaneous strangulation of the hot halo component of the accreted system. However, it might be more reasonable to adopt delayed strangulation in dependence on the halo potential. Besides, as accretion of stars is closely linked to the size evolution of galaxies, which, however, could not have been reproduced by current SAMs so far, the right fraction of in-situ and accreted stellar mass might also account for the observed size evolution.

3. AGN feedback from X-ray emission

As AGN are known to emit X-rays through their host galaxy, a step towards a more complex model of AGN feedback might be to take into account additional X-ray feedback from AGN. Implementing an observationally calibrated X-ray radiation field into hydrodynamical simulations, which emanates from black holes, shows that gas is heated out to large radii from the galactic center and thus, the effects which are reported from 'traditional' AGN feedback are enhanced: The 'new' feedback is found to be twice as effective at suppressing star formation (three times less SF in the last 6 Gyr) and lowers

the final black hole mass by 30%. Besides, less gas is accreted during major mergers (instead accretion happens more smoothly over the following several Gyr) and the baryonic conversion efficiency gets significantly reduced. Since one of the key strengths of the semi-analytic approach is the ability to easily investigate the influence of varying physical recipes on galaxy properties, an interesting issue might be to study the effect of X-ray feedback in a cosmological context by closely following the results from hydrodynamical simulations. Due to this additional heating process a major effect will presumably consist in the reduction of the star formation and the black hole accretion rates. Maybe, this might naturally result in a better reproduction of the observed downsizing without assuming a priori a decreasing upper limit for the Eddington-ratios.

4. Evolution of the stellar & AGN population due to stellar mass loss

In hydrodynamical simulations (see Ciotti & Ostriker, 2007) it is found that recycled gas from dying stars (stellar mass loss) causes important implications on galaxy formation. A typical stellar population - dependent on the adopted IMF - loses 30 – 40% of its mass over a Hubble time influencing star formation and metal enrichment. In addition, stellar mass loss provides an important source of fuel for the central SMBH, even in the absence of external phenomena such as galaxy merging. As gas from dying stars is flowing into the center, a nuclear starburst must occur coincident with an AGN flaring. Following the simulations of Ciotti & Ostriker (2007), roughly half of the recycled gas is ejected as galactic winds, half is consumed in central starbursts and only a small fraction of the order of $\simeq 1\%$ is accreted onto the central black hole inducing AGN activity. Most SAMs account for the mass-loss from Supernovae II explosions using the instantaneous recycling approximation so that recycled gas is available for cooling and star formation. However, many SAMs do not model *delayed* stellar mass loss from SNIa explosions and stellar winds from AGB stars and none of them do take into account associated AGN activity for the growth of black holes. Therefore, implementing such additional scenarios would provide a very suitable method to study how the over-all cosmological evolution of galaxies is affected, in particular the evolution of star formation rates, metals and the number density evolution of AGN over cosmic time compared to observations. Presumably, it would result in a significant contribution to the AGN number density in blue, star-forming and thus less massive host galaxies. Another interesting implication of gas recycling through star formation is that according to Martig & Bournaud (2010) the structural evolution of massive galaxies might strongly be affected by helping the disk growth and their survival in interactions and mergers. Taking this into account in SAMs may lead to a better reproduction of the observed bulge-to-disk ratio of massive galaxies at low redshifts.

Finally, I want to point out that it might be very reasonable and helpful if the improvements and changes as described above could always be accompanied by detailed comparison studies to simulations. Therefore, it would be of advantage to create cosmological, high-resolved SPH-simulations using up-to-date simulation codes including more enhanced physics as SNIa, metal enrichment, stellar mass loss or black hole

growth with feedback. Moreover, simulating large, cosmological volumes including sub-resolution models for gas, stars and black holes, would allow to make an overall, statistical comparison of the galaxy populations to SAMs, e.g. by investigating the evolution of the stellar or the black hole mass function and their dependence on environment.

To summarize, a desirable aim for the future might be to modify existing models of galaxy formation in several aspects - by improving the AGN feedback prescription (X-ray emission), cold gas accretion and stellar mass loss - so that it incorporates the majority of the current understanding of galaxy formation. After this implementation, it would be of great interest to explore the extent to which such additional physical processes would contribute to an over-all improvement of galaxy modeling by comparing to observational data, with the particular aim to achieve a deeper and more fundamental understanding for the exciting question of how galaxies and black holes are co-evolving, and thus, moving towards a more complete picture of the Universe we live in.

Effects of numerical resolution

A.1 Dark matter component

For one high and low mass halo with final masses of $M_{\text{halo}} = 3 \times 10^{12} M_{\odot}$ (M0501) and of $M_{\text{halo}} = 8 \times 10^{11} M_{\odot}$ (M1646), we have performed re-simulations with $4\times$ the original spatial resolution. We traced back the particles that are closer than $2 \times r_{200}$ to the center of the halo in any of our snapshots and replace them with dark matter and gas particles of higher resolution, achieving a $16\times$ better mass resolution in the high resolution region than in the original simulation: $m_{\text{DM}} = 2.5 \times 10^6 M_{\odot} h^{-1}$ and $m_{\text{Gas}} = m_{\text{Star}} = 5 \times 10^5 M_{\odot} h^{-1}$. The mass aggregation history of the dark matter component in both halos is very similar for the two different resolution limits as shown in the upper panel of Figs. A.1 and A.2. The red, dotted line corresponds to the $2\times$ resolution, the black solid line to the $4\times$ resolution. In the middle and lower panel of Figs. A.1 and A.2 one can see that the histograms of major ($> 1 : 10$) and minor mergers ($< 1 : 10$). The number of major mergers stays the almost the same, whereas halos are experiencing more minor merger events ($< 1 : 10$) in the higher resolution case, as more objects can be identified as substructure in the higher resolution case. This suggests that, since galaxy formation in the SAMs is mainly influenced by major merger events ($> 1 : 10$), the result from the SAMs is expected to be mostly independent of the resolution limit of the simulation.

A.2 Baryonic components

Figs. A.3 and A.4 show explicitly the evolution of the star, cold and hot gas mass in SAMs and simulations based on the trees of the two re-simulated individual halos for a $2 \times$ (dashed lines) and $4 \times$ (solid lines) resolution. As expected from the similar evolution of the dark matter component, for both, the low and the high mass halo re-simulations, we find between SAMs and simulation no significant difference in the evolution of the central galaxy/main halo. Therefore, due to computational costs, we restrict our study to $2\times$ re-simulations of 40 individual halos.

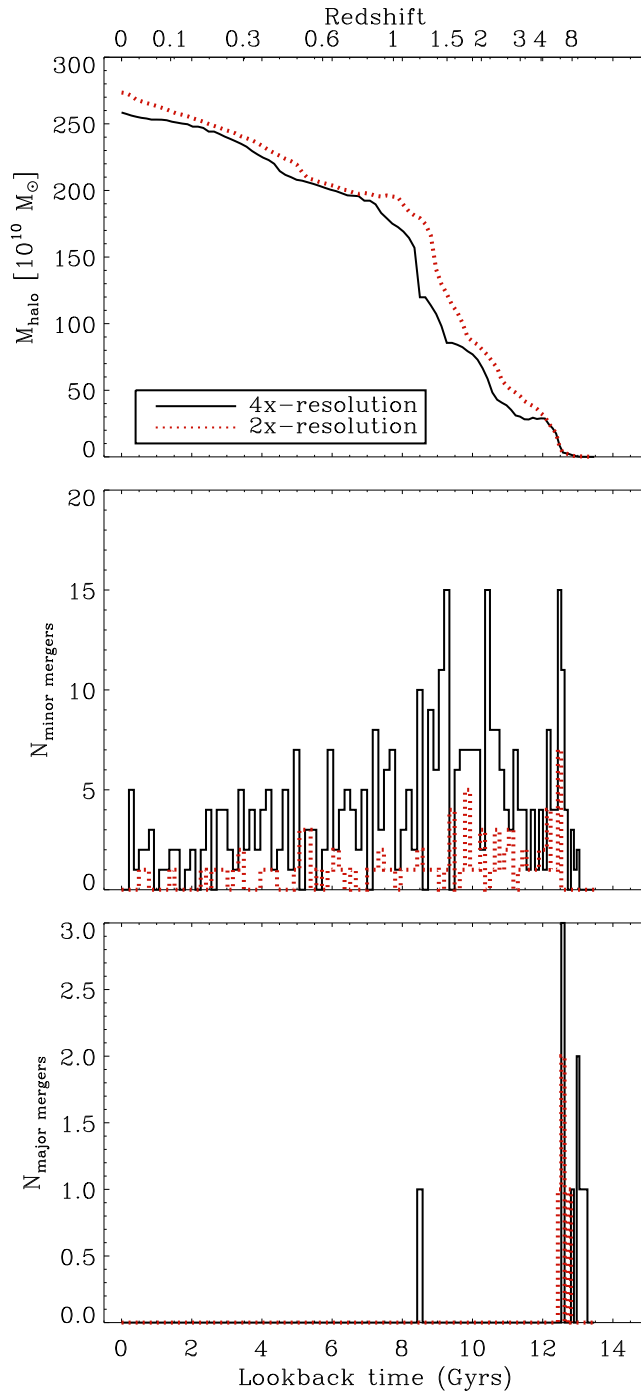


Figure A.1: *Upper panel: comparison of aggregation history (Resim M0501) of the halo mass for two different mass resolutions (2x: red, dotted line and 4x: black, solid line) in the SPH-re-simulations of a $3.0 \times 10^{12} M_{\odot}$ halo. Intermediate panel: Number of minor mergers ($> 10 : 1$) as a function of lookback time for the two different resolution limits. Lower panel: Number of major mergers ($< 10 : 1$) as a function of lookback time for the two different resolution limits.*

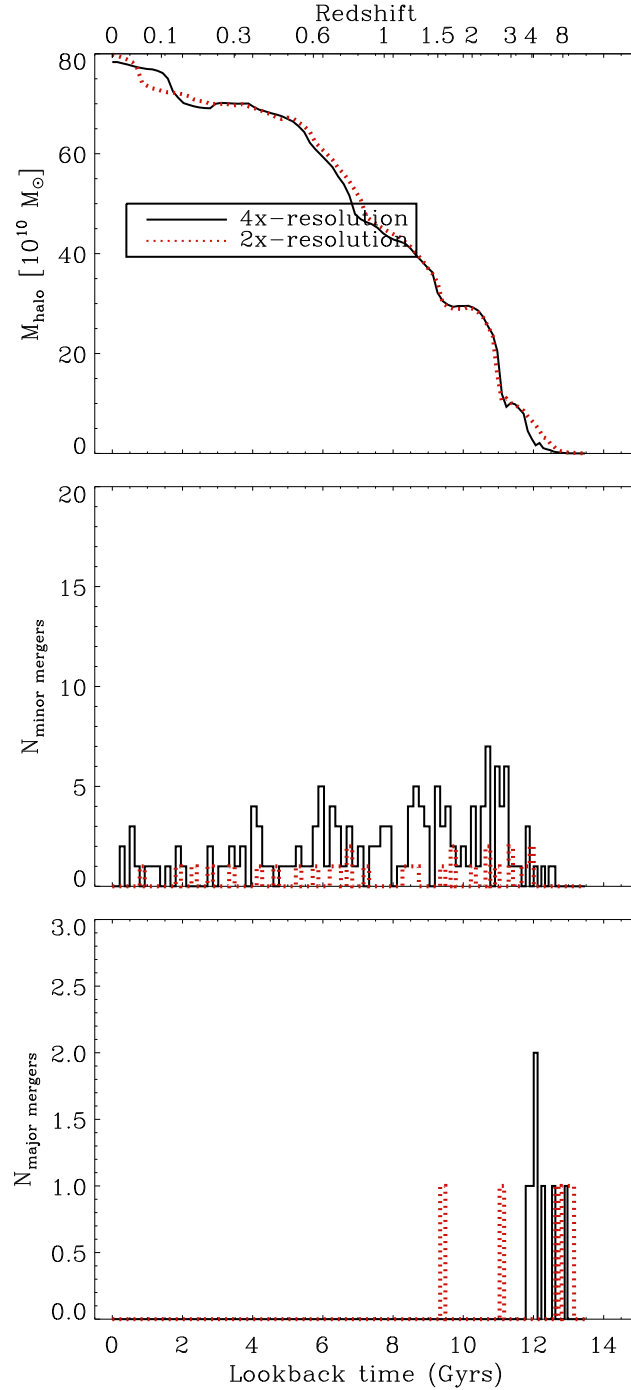


Figure A.2: Same as Fig. A.1, but for the halo M1646 with a smaller halo mass $8.0 \times 10^{11} M_{\odot}$.

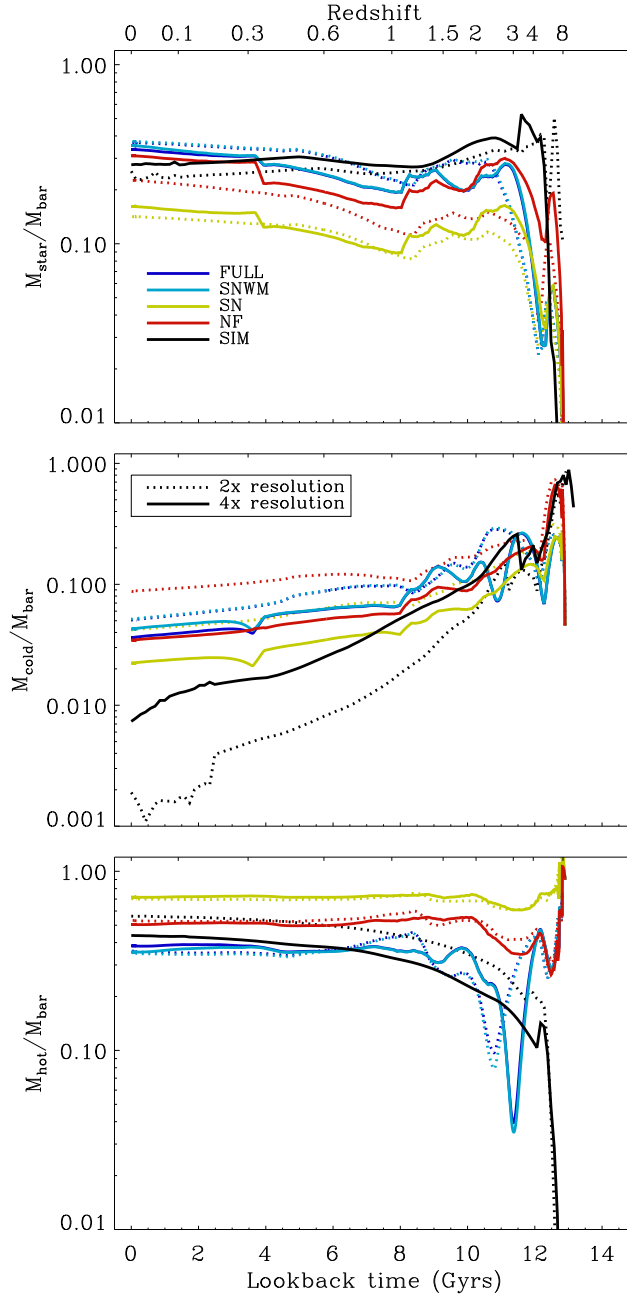


Figure A.3: Evolution of the baryonic components for two different mass resolutions (2x: dotted lines, 4x: solid lines) for the halo M0501. The upper panel shows the evolution of the stellar component, the middle panel the evolution of the cold gas fraction and the lower panel corresponds the hot halo gas component. Black lines illustrate the re-simulations, colored lines the different SAM versions.

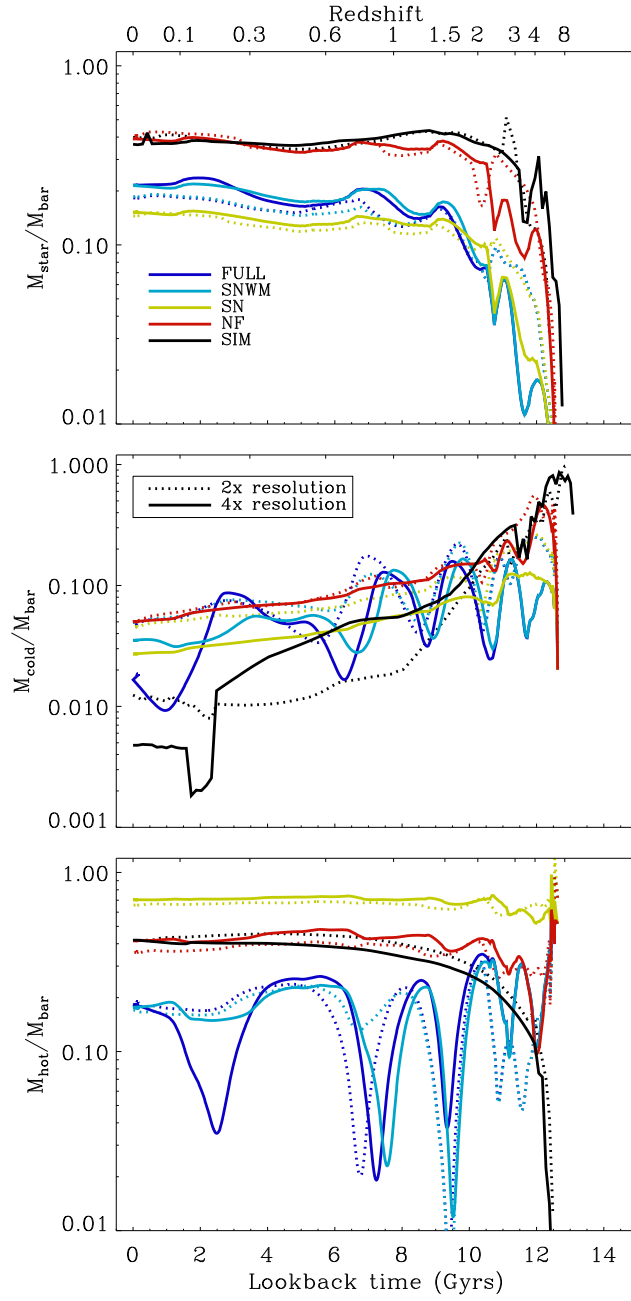


Figure A.4: Same as Fig. A.3, but for the halo M1646.

Bibliography

- AGERTZ, O., TEYSSIER, R., MOORE, B.: 2011. The formation of disc galaxies in a Λ CDM universe. *MNRAS*, **410**, 1391–1408.
- AIRD, J., NANDRA, K., LAIRD, E. S., GEORGAKAKIS, A., ASHBY, M. L. N., BARMBY, P., COIL, A. L., HUANG, J., KOEKEMOER, A. M., STEIDEL, C. C., WILLMER, C. N. A.: 2010. The evolution of the hard X-ray luminosity function of AGN. *MNRAS*, **401**, 2531–2551.
- ALBRECHT, A. STEINHARDT, P. J.: 1982. Cosmology for grand unified theories with radiatively induced symmetry breaking. *Physical Review Letters*, **48**, 1220–1223.
- ALEXANDER, D. M., BRANDT, W. N., SMAIL, I., SWINBANK, A. M., BAUER, F. E., BLAIN, A. W., CHAPMAN, S. C., COPPIN, K. E. K., IVISON, R. J., MENÉNDEZ-DELMESTRE, K.: 2008. Weighing the Black Holes in $z \approx 2$ Submillimeter-Emitting Galaxies Hosting Active Galactic Nuclei. *AJ*, **135**, 1968–1981.
- ANGULO, R. E. WHITE, S. D. M.: 2010. The birth and growth of neutralino haloes. *MNRAS*, **401**, 1796–1803.
- BALLANTYNE, D. R., SHI, Y., RIEKE, G. H., DONLEY, J. L., PAPOVICH, C., RIGBY, J. R.: 2006. Does the AGN Unified Model Evolve with Redshift? Using the X-Ray Background to Predict the Mid-Infrared Emission of AGNs. *ApJ*, **653**, 1070–1088.
- BARDEEN, J. M., STEINHARDT, P. J., TURNER, M. S.: 1983. Spontaneous creation of almost scale-free density perturbations in an inflationary universe. *Phys. Rev. D*, **28**, 679–693.
- BARGER, A. J. COWIE, L. L.: 2005. The Number Density of Intermediate- and High-Luminosity Active Galactic Nuclei at $z \sim 2-3$. *ApJ*, **635**, 115–122.
- BARGER, A. J., COWIE, L. L., CAPAK, P., ALEXANDER, D. M., BAUER, F. E., BRANDT, W. N., GARMIRE, G. P., HORNSCHEMEIER, A. E.: 2003. Very High

- Redshift X-Ray-selected Active Galactic Nuclei in the Chandra Deep Field-North. *ApJ*, **584**, L61–L64.
- BARNES, J. HUT, P.: 1986. A hierarchical $O(N \log N)$ force-calculation algorithm. *Nature*, **324**, 446–449.
- BAUGH, C. M., LACEY, C. G., FRENK, C. S., GRANATO, G. L., SILVA, L., BRESSAN, A., BENSON, A. J., COLE, S.: 2005. Can the faint submillimetre galaxies be explained in the Λ cold dark matter model? *MNRAS*, **356**, 1191–1200.
- BEHROOZI, P. S., CONROY, C., WECHSLER, R. H.: 2010. A Comprehensive Analysis of Uncertainties Affecting the Stellar Mass-Halo Mass Relation for $0 < z < 4$. *ApJ*, **717**, 379–403.
- BELL, E. F., MCINTOSH, D. H., KATZ, N., WEINBERG, M. D.: 2003. A First Estimate of the Baryonic Mass Function of Galaxies. *ApJ*, **585**, L117–L120.
- BENSON, A. J. BOWER, R.: 2010. Accretion shocks and cold filaments in galaxy formation. *MNRAS*, pages 1615–+.
- BENSON, A. J., DŽANOVIĆ, D., FRENK, C. S., SHARPLES, R.: 2007. Luminosity and stellar mass functions of discs and spheroids in the SDSS and the supermassive black hole mass function. *MNRAS*, **379**, 841–866.
- BENSON, A. J., PEARCE, F. R., FRENK, C. S., BAUGH, C. M., JENKINS, A.: 2001. A comparison of semi-analytic and smoothed particle hydrodynamics galaxy formation. *MNRAS*, **320**, 261–280.
- BENTZ, M. C., WALSH, J. L., BARTH, A. J., BALIBER, N., BENNERT, V. N., CANALIZO, G., FILIPPENKO, A. V., GANESHALINGAM, M., GATES, E. L., GREENE, J. E., HIDAS, M. G., HINER, K. D., LEE, N., LI, W., MALKAN, M. A., MINEZAKI, T., SAKATA, Y., SERDUKE, F. J. D., SILVERMAN, J. M., STEELE, T. N., STERN, D., STREET, R. A., THORNTON, C. E., TREU, T., WANG, X., WOO, J., YOSHII, Y.: 2009. The Lick AGN Monitoring Project: Broad-line Region Radii and Black Hole Masses from Reverberation Mapping of $H\beta$. *ApJ*, **705**, 199–217.
- BEST, P. N., VON DER LINDEN, A., KAUFFMANN, G., HECKMAN, T. M., KAISER, C. R.: 2007. On the prevalence of radio-loud active galactic nuclei in brightest cluster galaxies: implications for AGN heating of cooling flows. *MNRAS*, **379**, 894–908.
- BIGIEL, F., LEROY, A., WALTER, F., BRINKS, E., DE BLOK, W. J. G., MADORE, B., THORNLEY, M. D.: 2008. The Star Formation Law in Nearby Galaxies on Sub-Kpc Scales. *AJ*, **136**, 2846–2871.
- BINNEY, J.: 1977. The physics of dissipational galaxy formation. *ApJ*, **215**, 483–491.

- BIRNBOIM, Y. DEKEL, A.: 2003. Virial shocks in galactic haloes? *MNRAS*, **345**, 349–364.
- BIRNBOIM, Y. DEKEL, A.: 2010. Gravitational Quenching by Clumpy Accretion in Galaxies and Clusters II: Dynamical Response to Heating. *ArXiv:1008.1060*.
- BIRNBOIM, Y., DEKEL, A., NEISTEIN, E.: 2007. Bursting and quenching in massive galaxies without major mergers or AGNs. *MNRAS*, **380**, 339–352.
- BLANDFORD, R. D. MCKEE, C. F.: 1982. Reverberation mapping of the emission line regions of Seyfert galaxies and quasars. *ApJ*, **255**, 419–439.
- BLANTON, M. R., HOGG, D. W., BAHCALL, N. A., BRINKMANN, J., BRITTON, M., CONNOLLY, A. J., CSABAI, I., FUKUGITA, M., LOVEDAY, J., MEIKSIN, A., MUNN, J. A., NICHOL, R. C., OKAMURA, S., QUINN, T., SCHNEIDER, D. P., SHIMASAKU, K., STRAUSS, M. A., TEGMARK, M., VOGLEY, M. S., WEINBERG, D. H.: 2003. The Galaxy Luminosity Function and Luminosity Density at Redshift $z = 0.1$. *ApJ*, **592**, 819–838.
- BLUMENTHAL, G. R., PAGELS, H., PRIMACK, J. R.: 1982. Galaxy formation by dissipationless particles heavier than neutrinos. *Nature*, **299**, 37–+.
- BODE, P. OSTRIKER, J. P.: 2003. Tree Particle-Mesh: An Adaptive, Efficient, and Parallel Code for Collisionless Cosmological Simulation. *ApJS*, **145**, 1–13.
- BOLTON, C. T.: 1972. Dimensions of the Binary System HDE 226868 = Cygnus X-1. *Nature*, **240**, 124–+.
- BOND, J. R., COLE, S., EFSTATHIOU, G., KAISER, N.: 1991. Excursion set mass functions for hierarchical Gaussian fluctuations. *ApJ*, **379**, 440–460.
- BONDI, H.: 1952. On spherically symmetrical accretion. *MNRAS*, **112**, 195–+.
- BONOLI, S., MARULLI, F., SPRINGEL, V., WHITE, S. D. M., BRANCHINI, E., MOSCARDINI, L.: 2009. Modelling the cosmological co-evolution of supermassive black holes and galaxies - II. The clustering of quasars and their dark environment. *MNRAS*, **396**, 423–438.
- BOOTH, C. M. SCHAYE, J.: 2009. Cosmological simulations of the growth of supermassive black holes and feedback from active galactic nuclei: method and tests. *MNRAS*, **398**, 53–74.
- BOUWENS, R. J., ILLINGWORTH, G. D., FRANX, M., FORD, H.: 2008. $z \sim 7$ -10 Galaxies in the HUDF and GOODS Fields: UV Luminosity Functions. *ApJ*, **686**, 230–250.
- BOWER, R. G.: 1991. The evolution of groups of galaxies in the Press-Schechter formalism. *MNRAS*, **248**, 332–352.

- BOWER, R. G., BENSON, A. J., MALBON, R., HELLY, J. C., FRENK, C. S., BAUGH, C. M., COLE, S., LACEY, C. G.: 2006. Breaking the hierarchy of galaxy formation. *MNRAS*, **370**, 645–655.
- BOWER, R. G., VERNON, I., GOLDSTEIN, M., BENSON, A. J., LACEY, C. G., BAUGH, C. M., COLE, S., FRENK, C. S.: 2010. The parameter space of galaxy formation. *MNRAS*, **407**, 2017–2045.
- BOYLE, B. J., SHANKS, T., CROOM, S. M., SMITH, R. J., MILLER, L., LOARING, N., HEYMANS, C.: 2000. The 2dF QSO Redshift Survey - I. The optical luminosity function of quasi-stellar objects. *MNRAS*, **317**, 1014–1022.
- BOYLE, B. J., SHANKS, T., PETERSON, B. A.: 1988. The evolution of optically selected QSOs. II. *MNRAS*, **235**, 935–948.
- BROOKS, A. M., GOVERNATO, F., QUINN, T., BROOK, C. B., WADSLEY, J.: 2009. The Role of Cold Flows in the Assembly of Galaxy Disks. *ApJ*, **694**, 396–410.
- BRUCATO, R. J., KRISTIAN, J., WESTPHAL, J. A.: 1972. On the Optical Search for Centaurus X-3. *ApJ*, **175**, L137+.
- BRYAN, G. L. NORMAN, M. L.: 1998. Statistical Properties of X-Ray Clusters: Analytic and Numerical Comparisons. *ApJ*, **495**, 80+.
- BURKERT, A. SILK, J.: 2001. Star Formation-Regulated Growth of Black Holes in Protogalactic Spheroids. *ApJ*, **554**, L151–L154.
- BURKERT, A. TREMAINE, S.: 2010. A Correlation Between Central Supermassive Black Holes and the Globular Cluster Systems of Early-type Galaxies. *ApJ*, **720**, 516–521.
- CAPPELLARI, M., BACON, R., BUREAU, M., DAMEN, M. C., DAVIES, R. L., DE ZEEUW, P. T., EMSELLEM, E., FALCÓN-BARROSO, J., KRAJNOVIĆ, D., KUNTSCHNER, H., MCDERMID, R. M., PELETIER, R. F., SARZI, M., VAN DEN BOSCH, R. C. E., VAN DE VEN, G.: 2006. The SAURON project - IV. The mass-to-light ratio, the virial mass estimator and the Fundamental Plane of elliptical and lenticular galaxies. *MNRAS*, **366**, 1126–1150.
- CATTANEO, A., BLAIZOT, J., DEVRIENDT, J., GUIDERDONI, B.: 2005. Active Galactic Nuclei In Cosmological Simulations - I. Formation of black holes and spheroids through mergers. *MNRAS*, **364**, 407–423.
- CATTANEO, A., BLAIZOT, J., WEINBERG, D. H., KERES, D., COLOMBI, S., DAVÉ, R., DEVRIENDT, J., GUIDERDONI, B., KATZ, N.: 2007. Accretion, feedback and galaxy bimodality: a comparison of the GALICS semi-analytic model and cosmological SPH simulations. *MNRAS*, **377**, 63–76.

- CEN, R. OSTRIKER, J. P.: 1993. Cold Dark Matter Cosmogony with Hydrodynamics and Galaxy Formation: Galaxy Properties at Redshift Zero. *ApJ*, **417**, 415–+.
- CHABRIER, G.: 2003. Galactic Stellar and Substellar Initial Mass Function. *PASP*, **115**, 763–795.
- CHANDRASEKHAR, S.: 1931. The highly collapsed configurations of a stellar mass. *MNRAS*, **91**, 456–466.
- CIOTTI, L. OSTRIKER, J. P.: 2007. Radiative Feedback from Massive Black Holes in Elliptical Galaxies: AGN Flaring and Central Starburst Fueled by Recycled Gas. *ApJ*, **665**, 1038–1056.
- CIRASUOLO, M., MCLURE, R. J., DUNLOP, J. S., ALMAINI, O., FOUCAUD, S., SMAIL, I., SEKIGUCHI, K., SIMPSON, C., EALES, S., DYE, S., WATSON, M. G., PAGE, M. J., HIRST, P.: 2007. The evolution of the near-infrared galaxy luminosity function and colour bimodality up to $z \approx 2$ from the UKIDSS Ultra Deep Survey Early Data Release. *MNRAS*, **380**, 585–595.
- CISTERNAS, M., JAHNKE, K., INSKIP, K. J., INSKIP: 2010. Quasars Do Not Live in Merging Systems: No Enhanced Merger Rate at $z < 0.8$. In *IAU Symposium*, volume 267 of *IAU Symposium*, pages 326–326.
- COLE, S., ARAGON-SALAMANCA, A., FRENK, C. S., NAVARRO, J. F., ZEPF, S. E.: 1994. A Recipe for Galaxy Formation. *MNRAS*, **271**, 781–+.
- COLE, S., LACEY, C. G., BAUGH, C. M., FRENK, C. S.: 2000. Hierarchical galaxy formation. *MNRAS*, **319**, 168–204.
- COLPI, M., GORINI, V., HAARDT, F.: 2006. *Joint Evolution of Black Holes and Galaxies*.
- CONROY, C. WECHSLER, R. H.: 2009. Connecting Galaxies, Halos, and Star Formation Rates Across Cosmic Time. *ApJ*, **696**, 620–635.
- COVINGTON, M. D., PRIMACK, J. R., PORTER, L. A., CROTON, D. J., SOMERVILLE, R. S., DEKEL, A.: 2011. The Role of Dissipation in the Scaling Relations of Cosmological Merger Remnants. *ArXiv:1101.4225*.
- COWIE, L. L., BARGER, A. J., BAUTZ, M. W., BRANDT, W. N., GARMIRE, G. P.: 2003. The Redshift Evolution of the 2-8 keV X-Ray Luminosity Function. *ApJ*, **584**, L57–L60.
- COX, T. J., DUTTA, S. N., DI MATTEO, T., HERNQUIST, L., HOPKINS, P. F., ROBERTSON, B., SPRINGEL, V.: 2006. The Kinematic Structure of Merger Remnants. *ApJ*, **650**, 791–811.

- CRAIN, R. A., THEUNS, T., DALLA VECCHIA, C., EKE, V. R., FRENK, C. S., JENKINS, A., KAY, S. T., PEACOCK, J. A., PEARCE, F. R., SCHAYE, J., SPRINGEL, V., THOMAS, P. A., WHITE, S. D. M., WIERSMA, R. P. C.: 2009. Galaxies-intergalactic medium interaction calculation - I. Galaxy formation as a function of large-scale environment. *MNRAS*, **399**, 1773–1794.
- CRISTIANI, S., ALEXANDER, D. M., BAUER, F., BRANDT, W. N., CHATZICHRISTOU, E. T., FONTANOT, F., GRAZIAN, A., KOEKEMOER, A., LUCAS, R. A., MONACO, P., NONINO, M., PADOVANI, P., STERN, D., TOZZI, P., TREISTER, E., URRY, C. M., VANZELLA, E.: 2004. The Space Density of High-redshift QSOs in the Great Observatories Origins Deep Survey. *ApJ*, **600**, L119–L122.
- CROOM, S., FINE, S., MILLER, L., BABIC, A.: 2007. The Connection between Black Hole Mass and Dark Matter Halo Mass from 2QZ. In N. Metcalfe & T. Shanks, editor, *Cosmic Frontiers*, volume 379 of *Astronomical Society of the Pacific Conference Series*, pages 177–+.
- CROOM, S. M., SMITH, R. J., BOYLE, B. J., SHANKS, T., MILLER, L., OUTRAM, P. J., LOARING, N. S.: 2004. The 2dF QSO Redshift Survey - XII. The spectroscopic catalogue and luminosity function. *MNRAS*, **349**, 1397–1418.
- CROTON, D. J.: 2006. Evolution in the black hole mass-bulge mass relation: a theoretical perspective. *MNRAS*, **369**, 1808–1812.
- DADDI, E., DICKINSON, M., MORRISON, G., CHARY, R., CIMATTI, A., ELBAZ, D., FRAYER, D., RENZINI, A., POPE, A., ALEXANDER, D. M., BAUER, F. E., GIAVALISCO, M., HUYNH, M., KURK, J., MIGNOLI, M.: 2007. Multiwavelength Study of Massive Galaxies at $z \sim 2$. I. Star Formation and Galaxy Growth. *ApJ*, **670**, 156–172.
- DADDI, E., ELBAZ, D., WALTER, F., BOURNAUD, F., SALMI, F., CARILLI, C., DANNERBAUER, H., DICKINSON, M., MONACO, P., RIECHERS, D.: 2010. Different Star Formation Laws for Disks Versus Starbursts at Low and High Redshifts. *ApJ*, **714**, L118–L122.
- DAVÉ, R., CEN, R., OSTRICKER, J. P., BRYAN, G. L., HERNQUIST, L., KATZ, N., WEINBERG, D. H., NORMAN, M. L., O’SHEA, B.: 2001. Baryons in the Warm-Hot Intergalactic Medium. *ApJ*, **552**, 473–483.
- DAVE, R., DUBINSKI, J., HERNQUIST, L.: 1997. Parallel TreeSPH. *NewA*, **2**, 277–297.
- DAVÉ, R., OPPENHEIMER, B. D., FINLATOR, K.: 2011. Galaxy Evolution in Cosmological Simulations With Outflows I: Stellar Masses and Star Formation Rates. ArXiv:1103.3528.

- DAVIS, M., EFSTATHIOU, G., FRENK, C. S., WHITE, S. D. M.: 1985. The evolution of large-scale structure in a universe dominated by cold dark matter. *ApJ*, **292**, 371–394.
- DE BERNARDIS, P., ADE, P. A. R., BOCK, J. J., BOND, J. R., BORRILL, J., BOSCALERI, A., COBLE, K., CRILL, B. P., DE GASPERIS, G., FARESE, P. C., FERREIRA, P. G., GANGA, K., GIACOMETTI, M., HIVON, E., HRISTOV, V. V., IACOANGELI, A., JAFFE, A. H., LANGE, A. E., MARTINIS, L., MASI, S., MASON, P. V., MAUSKOPF, P. D., MELCHIORRI, A., MIGLIO, L., MONTROY, T., NETTERFIELD, C. B., PASCALE, E., PIACENTINI, F., POGOSYAN, D., PRUNET, S., RAO, S., ROMEO, G., RUHL, J. E., SCARAMUZZI, F., SFORNA, D., VITTORIO, N.: 2000. A flat Universe from high-resolution maps of the cosmic microwave background radiation. *Nature*, **404**, 955–959.
- DE LUCIA, G. BLAIZOT, J.: 2007. The hierarchical formation of the brightest cluster galaxies. *MNRAS*, **375**, 2–14.
- DE LUCIA, G., SPRINGEL, V., WHITE, S. D. M., CROTON, D., KAUFFMANN, G.: 2006. The formation history of elliptical galaxies. *MNRAS*, **366**, 499–509.
- DEKEL, A. BIRNBOIM, Y.: 2006. Galaxy bimodality due to cold flows and shock heating. *MNRAS*, **368**, 2–20.
- DEKEL, A. BIRNBOIM, Y.: 2008. Gravitational quenching in massive galaxies and clusters by clumpy accretion. *MNRAS*, **383**, 119–138.
- DEKEL, A., BIRNBOIM, Y., ENGEL, G., FREUNDLICH, J., GOERDT, T., MUMCUOGLU, M., NEISTEIN, E., PICHON, C., TEYSSIER, R., ZINGER, E.: 2009. Cold streams in early massive hot haloes as the main mode of galaxy formation. *Nature*, **457**, 451–454.
- DESROCHES, L., QUATAERT, E., MA, C., WEST, A. A.: 2007. Luminosity dependence in the Fundamental Plane projections of elliptical galaxies. *MNRAS*, **377**, 402–414.
- DI MATTEO, T., SPRINGEL, V., HERNQUIST, L.: 2005. Energy input from quasars regulates the growth and activity of black holes and their host galaxies. *Nature*, **433**, 604–607.
- DICKE, R. H., PEEBLES, P. J. E., ROLL, P. G., WILKINSON, D. T.: 1965. Cosmic Black-Body Radiation. *ApJ*, **142**, 414–419.
- DIEMAND, J., KUHLEN, M., MADAU, P., ZEMP, M., MOORE, B., POTTER, D., STADEL, J.: 2008. Clumps and streams in the local dark matter distribution. *Nature*, **454**, 735–738.

- DOLAG, K., BORGANI, S., MURANTE, G., SPRINGEL, V.: 2009. Substructures in hydrodynamical cluster simulations. *MNRAS*, **399**, 497–514.
- EFASTATHIOU, G., LAKE, G., NEGROPONTE, J.: 1982. The stability and masses of disc galaxies. *MNRAS*, **199**, 1069–1088.
- EFASTATHIOU, G., REES, M. J.: 1988. High-redshift quasars in the Cold Dark Matter cosmogony. *MNRAS*, **230**, 5P–+.
- EFASTATHIOU, G., SUTHERLAND, W. J., MADDOX, S. J.: 1990. The cosmological constant and cold dark matter. *Nature*, **348**, 705–707.
- EINASTO, J., KAASIK, A., SAAR, E.: 1974. Dynamic evidence on massive coronas of galaxies. *Nature*, **250**, 309–310.
- ELBAZ, D., DADDI, E., LE BORGNE, D., DICKINSON, M., ALEXANDER, D. M., CHARY, R., STARCK, J., BRANDT, W. N., KITZBICHLER, M., MACDONALD, E., NONINO, M., POPESSO, P., STERN, D., VANZELLA, E.: 2007. The reversal of the star formation-density relation in the distant universe. *A&A*, **468**, 33–48.
- FAKHOURI, O. MA, C.: 2008. The nearly universal merger rate of dark matter haloes in Λ CDM cosmology. *MNRAS*, **386**, 577–592.
- FAN, X., HENNAWI, J. F., RICHARDS, G. T., STRAUSS, M. A., SCHNEIDER, D. P., DONLEY, J. L., YOUNG, J. E., ANNIS, J., LIN, H., LAMPEITL, H., LUPTON, R. H., GUNN, J. E., KNAPP, G. R., BRANDT, W. N., ANDERSON, S., BAHCALL, N. A., BRINKMANN, J., BRUNNER, R. J., FUKUGITA, M., SZALAY, A. S., SZOKOLY, G. P., YORK, D. G.: 2004. A Survey of $z > 5.7$ Quasars in the Sloan Digital Sky Survey. III. Discovery of Five Additional Quasars. *AJ*, **128**, 515–522.
- FAN, X., NARAYANAN, V. K., LUPTON, R. H., STRAUSS, M. A., KNAPP, G. R., BECKER, R. H., WHITE, R. L., PENTERICCI, L., LEGGETT, S. K., HAIMAN, Z., GUNN, J. E., IVEZIĆ, Ž., SCHNEIDER, D. P., ANDERSON, S. F., BRINKMANN, J., BAHCALL, N. A., CONNOLLY, A. J., CSABAI, I., DOI, M., FUKUGITA, M., GEBALLE, T., GREBEL, E. K., HARBECK, D., HENNESSY, G., LAMB, D. Q., MIKNAITIS, G., MUNN, J. A., NICHOL, R., OKAMURA, S., PIER, J. R., PRADA, F., RICHARDS, G. T., SZALAY, A., YORK, D. G.: 2001. A Survey of $z > 5.8$ Quasars in the Sloan Digital Sky Survey. I. Discovery of Three New Quasars and the Spatial Density of Luminous Quasars at $z \sim 6$. *AJ*, **122**, 2833–2849.
- FAN, X., WHITE, R. L., DAVIS, M., BECKER, R. H., STRAUSS, M. A., HAIMAN, Z., SCHNEIDER, D. P., GREGG, M. D., GUNN, J. E., KNAPP, G. R., LUPTON, R. H., ANDERSON, JR., J. E., ANDERSON, S. F., ANNIS, J., BAHCALL, N. A., BOROSKI, W. N., BRUNNER, R. J., CHEN, B., CONNOLLY, A. J., CSABAI, I., DOI, M., FUKUGITA, M., HENNESSY, G. S., HINDSLEY, R. B., ICHIKAWA, T., IVEZIĆ, Ž., LOVEDAY, J., MEIKSIN, A., MCKAY, T. A., MUNN, J. A., NEWBERG,

- H. J., NICHOL, R., OKAMURA, S., PIER, J. R., SEKIGUCHI, M., SHIMASAKU, K., STOUGHTON, C., SZALAY, A. S., SZOKOLY, G. P., THAKAR, A. R., VOGLEY, M. S., YORK, D. G.: 2000. The Discovery of a Luminous $Z=5.80$ Quasar from the Sloan Digital Sky Survey. *AJ*, **120**, 1167–1174.
- FANIDAKIS, N., BAUGH, C. M., BENSON, A. J., BOWER, R. G., COLE, S., DONE, C., FRENK, C. S., HICKOX, R. C., LACEY, C., LAGOS, C. D. P.: 2010. The evolution of AGN across cosmic time: what is downsizing? *ArXiv:1011.5222*.
- FELDMANN, R., CAROLLO, C. M., MAYER, L., RENZINI, A., LAKE, G., QUINN, T., STINSON, G. S., YEPES, G.: 2010. The Evolution of Central Group Galaxies in Hydrodynamical Simulations. *ApJ*, **709**, 218–240.
- FERRARESE, L.: 2002. Beyond the Bulge: A Fundamental Relation between Supermassive Black Holes and Dark Matter Halos. *ApJ*, **578**, 90–97.
- FERRARESE, L. FORD, H.: 2005. Supermassive Black Holes in Galactic Nuclei: Past, Present and Future Research. *Space Science Reviews*, **116**, 523–624.
- FERRARESE, L. MERRITT, D.: 2000. A Fundamental Relation between Supermassive Black Holes and Their Host Galaxies. *ApJ*, **539**, L9–L12.
- FIGLIORE, F., BRUSA, M., COCCHIA, F., BALDI, A., CARANGELO, N., CILIEGI, P., COMASTRI, A., LA FRANCA, F., MAIOLINO, R., MATT, G., MOLENDI, S., MIGNOLI, M., PEROLA, G. C., SEVERGNINI, P., VIGNALI, C.: 2003. The HELLAS2XMM survey. IV. Optical identifications and the evolution of the accretion luminosity in the Universe. *A&A*, **409**, 79–90.
- FONT, A. S., BOWER, R. G., MCCARTHY, I. G., BENSON, A. J., FRENK, C. S., HELLY, J. C., LACEY, C. G., BAUGH, C. M., COLE, S.: 2008. The colours of satellite galaxies in groups and clusters. *MNRAS*, **389**, 1619–1629.
- FONTANOT, F., DE LUCIA, G., MONACO, P., SOMERVILLE, R. S., SANTINI, P.: 2009. The many manifestations of downsizing: hierarchical galaxy formation models confront observations. *MNRAS*, **397**, 1776–1790.
- FONTANOT, F., MONACO, P., CRISTIANI, S., TOZZI, P.: 2006. The effect of stellar feedback and quasar winds on the active galactic nucleus population. *MNRAS*, **373**, 1173–1187.
- FONTANOT, F., PASQUALI, A., DE LUCIA, G., VAN DEN BOSCH, F. C., SOMERVILLE, R. S., KANG, X.: 2011. The dependence of AGN activity on stellar and halo mass in semi-analytic models. *MNRAS*, pages 198–+.
- FÖRSTER SCHREIBER, N. M., GENZEL, R., BOUCHÉ, N., CRESCI, G., DAVIES, R., BUSCHKAMP, P., SHAPIRO, K., TACCONI, L. J., HICKS: 2009. The SINS Survey:

- SINFONI Integral Field Spectroscopy of $z \sim 2$ Star-forming Galaxies. *ApJ*, **706**, 1364–1428.
- FÖRSTER SCHREIBER, N. M., SHAPLEY, A. E., ERB, D. K., GENZEL, R., STEIDEL, C. C., BOUCHÉ, N., CRESCI, G., DAVIES, R.: 2011. Constraints on the Assembly and Dynamics of Galaxies. I. Detailed Rest-frame Optical Morphologies on Kiloparsec Scale of $z \sim 2$ Star-forming Galaxies. *ApJ*, **731**, 65–+.
- FRANX, M., VAN DOKKUM, P. G., SCHREIBER, N. M. F., WUYTS, S., LABBÉ, I., TOFT, S.: 2008. Structure and Star Formation in Galaxies out to $z = 3$: Evidence for Surface Density Dependent Evolution and Upsizing. *ApJ*, **688**, 770–788.
- FRENK, C. S., WHITE, S. D. M., DAVIS, M., EFSTATHIOU, G.: 1988. The formation of dark halos in a universe dominated by cold dark matter. *ApJ*, **327**, 507–525.
- GEBHARDT, K., BENDER, R., BOWER, G., DRESSLER, A., FABER, S. M., FILIPPENKO, A. V., GREEN, R., GRILLMAIR, C., HO, L. C., KORMENDY, J., LAUER, T. R., MAGORRIAN, J., PINKNEY, J., RICHSTONE, D., TREMAINE, S.: 2000. A Relationship between Nuclear Black Hole Mass and Galaxy Velocity Dispersion. *ApJ*, **539**, L13–L16.
- GENEL, S., GENZEL, R., BOUCHÉ, N., NAAB, T., STERNBERG, A.: 2009. The Halo Merger Rate in the Millennium Simulation and Implications for Observed Galaxy Merger Fractions. *ApJ*, **701**, 2002–2018.
- GENEL, S., GENZEL, R., BOUCHÉ, N., STERNBERG, A., NAAB, T., SCHREIBER, N. M. F., SHAPIRO, K. L., TACCONI, L. J., LUTZ, D., CRESCI, G., BUSCHKAMP, P., DAVIES, R. I., HICKS, E. K. S.: 2008. Mergers and Mass Accretion Rates in Galaxy Assembly: The Millennium Simulation Compared to Observations of $z \sim 2$ Galaxies. *ApJ*, **688**, 789–793.
- GENEL, S., NAAB, T., GENZEL, R., FÖRSTER SCHREIBER, N. M., STERNBERG, A., OSER, L., JOHANSSON, P. H., DAVÉ, R., OPPENHEIMER, B. D., BURKERT, A.: 2010. Short-lived star-forming giant clumps in cosmological simulations of $z \sim 2$ disks. ArXiv:1011.0433.
- GENZEL, R., BURKERT, A., BOUCHÉ, N., CRESCI, G., FÖRSTER SCHREIBER, N. M., SHAPLEY, A., SHAPIRO, K., TACCONI, L. J., BUSCHKAMP, P., CIMATTI, A.: 2008. From Rings to Bulges: Evidence for Rapid Secular Galaxy Evolution at $z \sim 2$ from Integral Field Spectroscopy in the SINS Survey. *ApJ*, **687**, 59–77.
- GENZEL, R., PICHON, C., ECKART, A., GERHARD, O. E., OTT, T.: 2000. Stellar dynamics in the Galactic Centre: proper motions and anisotropy. *MNRAS*, **317**, 348–374.

- GENZEL, R., TACCONI, L. J., EISENHAEUER, F., FÖRSTER SCHREIBER, N. M., CIMATTI, A., DADDI, E., BOUCHÉ, N.: 2006. The rapid formation of a large rotating disk galaxy three billion years after the Big Bang. *Nature*, **442**, 786–789.
- GENZEL, R., TACCONI, L. J., GRACIA-CARPIO, J., STERNBERG, A., COOPER, M. C., SHAPIRO, K., BOLATTO, A., BOUCHÉ, N., BOURNAUD, F., BURKERT, A., COMBES, F., COMERFORD, J., COX, P., DAVIS, M., SCHREIBER, N. M. F., GARCIA-BURILLO, S., LUTZ, D., NAAB, T., NERI, R., OMONT, A., SHAPLEY, A., WEINER, B.: 2010. A study of the gas-star formation relation over cosmic time. *MNRAS*, **407**, 2091–2108.
- GEORGAKAKIS, A., COIL, A. L., LAIRD, E. S., GRIFFITH, R. L., NANDRA, K., LOTZ, J. M., PIERCE, C. M., COOPER, M. C., NEWMAN, J. A., KOEKEMOER, A. M.: 2009. Host galaxy morphologies of X-ray selected AGN: assessing the significance of different black hole fuelling mechanisms to the accretion density of the Universe at $z \sim 1$. *MNRAS*, **397**, 623–633.
- GHEZ, A. M., HORNSTEIN, S. D., LU, J. R., BOUCHEZ, A., LE MIGNANT, D., VAN DAM, M. A., WIZINOWICH, P., MATTHEWS, K., MORRIS, M., BECKLIN, E. E., CAMPBELL, R. D., CHIN, J. C. Y., HARTMAN, S. K., JOHANSSON, E. M., LAFON, R. E., STOMSKI, P. J., SUMMERS, D. M.: 2005. The First Laser Guide Star Adaptive Optics Observations of the Galactic Center: Sgr A*’s Infrared Color and the Extended Red Emission in its Vicinity. *ApJ*, **635**, 1087–1094.
- GHIGNA, S., MOORE, B., GOVERNATO, F., LAKE, G., QUINN, T., STADEL, J.: 2000. Density Profiles and Substructure of Dark Matter Halos: Converging Results at Ultra-High Numerical Resolution. *ApJ*, **544**, 616–628.
- GILLI, R., COMASTRI, A., HASINGER, G.: 2007. The synthesis of the cosmic X-ray background in the Chandra and XMM-Newton era. *A&A*, **463**, 79–96.
- GILLI, R., TOZZI, P., ROSATI, P., PAOLILLO, M., BORGANI, S., BRUSA, M., COMASTRI, A., LUSSO, E., MARULLI, F., VIGNALI, C.: 2010. Demography of obscured and unobscured AGN: prospects for a Wide Field X-ray Telescope. ArXiv:1010.6024.
- GONZALEZ, A. H., ZABLUDOFF, A. I., ZARITSKY, D.: 2005. Intracluster Light in Nearby Galaxy Clusters: Relationship to the Halos of Brightest Cluster Galaxies. *ApJ*, **618**, 195–213.
- GOVERNATO, F., BROOK, C., MAYER, L., BROOKS, A., RHEE, G., WADSLEY, J., JONSSON, P., WILLMAN, B., STINSON, G., QUINN, T., MADAU, P.: 2010. Bulgeless dwarf galaxies and dark matter cores from supernova-driven outflows. *Nature*, **463**, 203–206.

- GOVERNATO, F., BROOK, C. B., BROOKS, A. M., MAYER, L., WILLMAN, B., JONSSON, P., STILP, A. M., POPE, L., CHRISTENSEN, C., WADSLEY, J., QUINN, T.: 2009. Forming a large disc galaxy from a $z < 1$ major merger. *MNRAS*, **398**, 312–320.
- GOVERNATO, F., WILLMAN, B., MAYER, L., BROOKS, A., STINSON, G., VALENZUELA, O., WADSLEY, J., QUINN, T.: 2007. Forming disc galaxies in Λ CDM simulations. *MNRAS*, **374**, 1479–1494.
- GRAHAM, A. W.: 2008a. Fundamental Planes and the Barless $M_{bh} - \sigma$ Relation for Supermassive Black Holes. *ApJ*, **680**, 143–153.
- GRAHAM, A. W.: 2008b. Populating the Galaxy Velocity Dispersion: Supermassive Black Hole Mass Diagram, A Catalogue of (M_{bh}, σ) Values. *Publications of the Astronomical Society of Australia*, **25**, 167–175.
- GRANATO, G. L., DE ZOTTI, G., SILVA, L., BRESSAN, A., DANESE, L.: 2004. A Physical Model for the Coevolution of QSOs and Their Spheroidal Hosts. *ApJ*, **600**, 580–594.
- GREENE, J. E. HO, L. C.: 2007. The Mass Function of Active Black Holes in the Local Universe. *ApJ*, **667**, 131–148.
- GREENE, J. E., PENG, C. Y., LUDWIG, R. R.: 2010. Redshift Evolution in Black Hole-Bulge Relations: Testing C IV-Based Black Hole Masses. *ApJ*, **709**, 937–949.
- GROGIN, N. A., CONSELICE, C. J., CHATZICHRISTOU, E., ALEXANDER, D. M., BAUER, F. E., HORNSCHEMEIER, A. E., JOGEE, S., KOEKEMOER, A. M., LAIDLER, V. G., LIVIO, M., LUCAS, R. A., PAOLILLO, M., RAVINDRANATH, S., SCHREIER, E. J., SIMMONS, B. D., URRY, C. M.: 2005. AGN Host Galaxies at $z \sim 0.4-1.3$: Bulge-dominated and Lacking Merger-AGN Connection. *ApJ*, **627**, L97–L100.
- GÜLTEKIN, K., RICHSTONE, D. O., GEBHARDT, K., LAUER, T. R., TREMAINE, S., ALLER, M. C., BENDER, R., DRESSLER, A., FABER, S. M., FILIPPENKO, A. V., GREEN, R., HO, L. C., KORMENDY, J., MAGORRIAN, J., PINKNEY, J., SIOPIS, C.: 2009. The $M - \sigma$ and $M - L$ Relations in Galactic Bulges, and Determinations of Their Intrinsic Scatter. *ApJ*, **698**, 198–221.
- GUO, Q., WHITE, S., BOYLAN-KOLCHIN, M., DE LUCIA, G., KAUFFMANN, G., LEMSON, G., LI, C., SPRINGEL, V., WEINMANN, S.: 2011. From dwarf spheroidals to cD galaxies: simulating the galaxy population in a Λ CDM cosmology. *MNRAS*, pages 164–+.
- GUO, Q. WHITE, S. D. M.: 2008. Galaxy growth in the concordance Λ CDM cosmology. *MNRAS*, **384**, 2–10.

- GUO, Q. WHITE, S. D. M.: 2009. High-redshift galaxy populations and their descendants. *MNRAS*, **396**, 39–52.
- GUTH, A. H.: 1981. Inflationary universe: A possible solution to the horizon and flatness problems. *Phys. Rev. D*, **23**, 347–356.
- GUTH, A. H. PI, S.: 1982. Fluctuations in the new inflationary universe. *Physical Review Letters*, **49**, 1110–1113.
- HAARDT, F. MADAU, P.: 1996. Radiative Transfer in a Clumpy Universe. II. The Ultraviolet Extragalactic Background. *ApJ*, **461**, 20–+.
- HAEHNELT, M. G. REES, M. J.: 1993. The formation of nuclei in newly formed galaxies and the evolution of the quasar population. *MNRAS*, **263**, 168–178.
- HAIMAN, Z.: 2010. The Origin and Detection of High-Redshift Supermassive Black Holes. In D. J. Whalen, V. Bromm, & N. Yoshida, editor, *American Institute of Physics Conference Series*, volume 1294 of *American Institute of Physics Conference Series*, pages 215–224.
- HAIMAN, Z. LOEB, A.: 1998. Observational Signatures of the First Quasars. *ApJ*, **503**, 505–+.
- HÄRING, N. RIX, H.-W.: 2004. On the Black Hole Mass-Bulge Mass Relation. *ApJ*, **604**, L89–L92.
- HASINGER, G.: 2004. The X-ray background and AGNs. *Nuclear Physics B Proceedings Supplements*, **132**, 86–96.
- HASINGER, G.: 2008. Absorption properties and evolution of active galactic nuclei. *A&A*, **490**, 905–922.
- HASINGER, G., MIYAJI, T., SCHMIDT, M.: 2005. Luminosity-dependent evolution of soft X-ray selected AGN. New Chandra and XMM-Newton surveys. *A&A*, **441**, 417–434.
- HATTON, S., DEVRIENDT, J. E. G., NININ, S., BOUCHET, F. R., GUIDERDONI, B., VIBERT, D.: 2003. GALICS- I. A hybrid N-body/semi-analytic model of hierarchical galaxy formation. *MNRAS*, **343**, 75–106.
- HAWKING, S. W.: 1982. The development of irregularities in a single bubble inflationary universe. *Physics Letters B*, **115**, 295–297.
- HEGER, A. WOOSLEY, S. E.: 2002. The Nucleosynthetic Signature of Population III. *ApJ*, **567**, 532–543.

- HELLY, J. C., COLE, S., FRENK, C. S., BAUGH, C. M., BENSON, A., LACEY, C., PEARCE, F. R.: 2003. A comparison of gas dynamics in smooth particle hydrodynamics and semi-analytic models of galaxy formation. *MNRAS*, **338**, 913–925.
- HEWETT, P. C., IRWIN, M. J., FOLTZ, C. B., HARDING, M. E., CORRIGAN, R. T., WEBSTER, R. L., DINSHAW, N.: 1994. The close-separation gravitational lens candidate Q1009-0252. *AJ*, **108**, 1534–1541.
- HICKOX, R. C., JONES, C., FORMAN, W. R., MURRAY, S. S., KOCHANNEK, C. S., EISENSTEIN, D., JANNUZI, B. T., DEY, A., BROWN, M. J. I., STERN, D., EISENHARDT, P. R., GORJIAN, V., BRODWIN, M., NARAYAN, R., COOL, R. J., KENTER, A., CALDWELL, N., ANDERSON, M. E.: 2009. Host Galaxies, Clustering, Eddington Ratios, and Evolution of Radio, X-Ray, and Infrared-Selected AGNs. *ApJ*, **696**, 891–919.
- HIRSCHMANN, M., KHOCHFAR, S., BURKERT, A., NAAB, T., GENEL, S., SOMERVILLE, R. S.: 2010. On the evolution of the intrinsic scatter in black hole versus galaxy mass relations. *MNRAS*, **407**, 1016–1032.
- HIRSCHMANN, M., NAAB, T., SOMERVILLE, R., BURKERT, A., OSER, L.: 2011. Galaxy formation in semi-analytic models and cosmological hydrodynamic zoom simulations. ArXiv:1104.1626.
- HOPKINS, P. F., COX, T. J., KEREŠ, D., HERNQUIST, L.: 2008a. A Cosmological Framework for the Co-evolution of Quasars, Supermassive Black Holes, and Elliptical Galaxies. II. Formation of Red Ellipticals. *ApJS*, **175**, 390–422.
- HOPKINS, P. F., HERNQUIST, L.: 2009. A Characteristic Division Between the Fueling of Quasars and Seyferts: Five Simple Tests. *ApJ*, **694**, 599–609.
- HOPKINS, P. F., HERNQUIST, L., COX, T. J., DUTTA, S. N., ROTHBERG, B.: 2008b. Dissipation and Extra Light in Galactic Nuclei. I. Gas-Rich Merger Remnants. *ApJ*, **679**, 156–181.
- HOPKINS, P. F., HERNQUIST, L., COX, T. J., KEREŠ, D.: 2008c. A Cosmological Framework for the Co-Evolution of Quasars, Supermassive Black Holes, and Elliptical Galaxies. I. Galaxy Mergers and Quasar Activity. *ApJS*, **175**, 356–389.
- HOPKINS, P. F., HERNQUIST, L., COX, T. J., ROBERTSON, B., DI MATTEO, T., SPRINGEL, V.: 2006a. The Evolution in the Faint-End Slope of the Quasar Luminosity Function. *ApJ*, **639**, 700–709.
- HOPKINS, P. F., HERNQUIST, L., COX, T. J., ROBERTSON, B., KRAUSE, E.: 2007a. A Theoretical Interpretation of the Black Hole Fundamental Plane. *ApJ*, **669**, 45–66.

- HOPKINS, P. F., HERNQUIST, L., COX, T. J., ROBERTSON, B., KRAUSE, E.: 2007b. An Observed Fundamental Plane Relation for Supermassive Black Holes. *ApJ*, **669**, 67–73.
- HOPKINS, P. F., RICHARDS, G. T., HERNQUIST, L.: 2007c. An Observational Determination of the Bolometric Quasar Luminosity Function. *ApJ*, **654**, 731–753.
- HOPKINS, P. F., ROBERTSON, B., KRAUSE, E., HERNQUIST, L., COX, T. J.: 2006b. An Upper Limit to the Degree of Evolution between Supermassive Black Holes and Their Host Galaxies. *ApJ*, **652**, 107–111.
- HUBBLE, E.: 1929. A Relation between Distance and Radial Velocity among Extra-Galactic Nebulae. *Proceedings of the National Academy of Science*, **15**, 168–173.
- HUBBLE, E. HUMASON, M. L.: 1931. The Velocity-Distance Relation among Extra-Galactic Nebulae. *ApJ*, **74**, 43–+.
- HUNT, M. P., STEIDEL, C. C., ADELBERGER, K. L., SHAPLEY, A. E.: 2004. The Faint End of the QSO Luminosity Function at $z=3$. *ApJ*, **605**, 625–630.
- JAHNKE, K. MACCIO, A.: 2010. The non-causal origin of the black hole-galaxy scaling relations. *ArXiv:1006.0482*.
- JOGEE, S., MILLER, S., PENNER, K., BELL, E. F., CONSELICE, C., SKELTON, R. E., SOMERVILLE, R. S., RIX, H., BARAZZA, F. D., BARDEN, M., BORCH, A., BECKWITH, S. V., CALDWELL, J. A. R., HÄUSSLER, B., HEYMANS, C., JAHNKE, K., MCINTOSH, D., MEISENHEIMER, K., PAPOVICH, C., PENG, C. Y., ROBAINA, A., SANCHEZ, S., WISOTZKI, L., WOLF, C.: 2008. Frequency and Impact of Galaxy Mergers and Interactions over the Last 7 Gyr. In J. G. Funes & E. M. Corsini, editor, *Formation and Evolution of Galaxy Disks*, volume 396 of *Astronomical Society of the Pacific Conference Series*, pages 337–+.
- JOHANSSON, P. H., BURKERT, A., NAAB, T.: 2009a. The Evolution of Black Hole Scaling Relations in Galaxy Mergers. *ApJ*, **707**, L184–L189.
- JOHANSSON, P. H., NAAB, T., OSTRICKER, J. P.: 2009b. Gravitational Heating Helps Make Massive Galaxies Red and Dead. *ApJ*, **697**, L38–L43.
- KANG, X., JING, Y. P., MO, H. J., BÖRNER, G.: 2005. Semianalytical Model of Galaxy Formation with High-Resolution N-Body Simulations. *ApJ*, **631**, 21–40.
- KAUFFMANN, G.: 1996. The age of elliptical galaxies and bulges in a merger model. *MNRAS*, **281**, 487–492.
- KAUFFMANN, G., COLBERG, J. M., DIAFERIO, A., WHITE, S. D. M.: 1999. Clustering of galaxies in a hierarchical universe - I. Methods and results at $z=0$. *MNRAS*, **303**, 188–206.

- KAUFFMANN, G. HAEBNELT, M.: 2000. A unified model for the evolution of galaxies and quasars. *MNRAS*, **311**, 576–588.
- KAUFFMANN, G., HECKMAN, T. M., BEST, P. N.: 2008. Radio jets in galaxies with actively accreting black holes: new insights from the SDSS. *MNRAS*, **384**, 953–971.
- KAUFFMANN, G., WHITE, S. D. M., GUIDERDONI, B.: 1993. The Formation and Evolution of Galaxies Within Merging Dark Matter Haloes. *MNRAS*, **264**, 201–+.
- KELLY, B. C., VESTERGAARD, M., FAN, X., HOPKINS, P., HERNQUIST, L., SIEMIGINOWSKA, A.: 2010. Constraints on Black Hole Growth, Quasar Lifetimes, and Eddington Ratio Distributions from the SDSS Broad-line Quasar Black Hole Mass Function. *ApJ*, **719**, 1315–1334.
- KENNICUTT, JR., R. C.: 1989. The star formation law in galactic disks. *ApJ*, **344**, 685–703.
- KENNICUTT, JR., R. C.: 1998. The Global Schmidt Law in Star-forming Galaxies. *ApJ*, **498**, 541–+.
- KEREŠ, D., KATZ, N., FARDAL, M., DAVÉ, R., WEINBERG, D. H.: 2009. Galaxies in a simulated Λ CDM Universe - I. Cold mode and hot cores. *MNRAS*, **395**, 160–179.
- KEREŠ, D., KATZ, N., WEINBERG, D. H., DAVÉ, R.: 2005. How do galaxies get their gas? *MNRAS*, **363**, 2–28.
- KHOCHFAR, S. BURKERT, A.: 2003. The Importance of Spheroidal and Mixed Mergers for Early-Type Galaxy Formation. *ApJ*, **597**, L117–L120.
- KHOCHFAR, S. OSTRICKER, J. P.: 2008. Adding Environmental Gas Physics to the Semianalytic Method for Galaxy Formation: Gravitational Heating. *ApJ*, **680**, 54–69.
- KHOCHFAR, S. SILK, J.: 2006a. A Simple Model for the Size Evolution of Elliptical Galaxies. *ApJ*, **648**, L21–L24.
- KHOCHFAR, S. SILK, J.: 2006b. On the origin of stars in bulges and elliptical galaxies. *MNRAS*, **370**, 902–910.
- KHOCHFAR, S. SILK, J.: 2009. Dry mergers: a crucial test for galaxy formation. *MNRAS*, **397**, 506–510.
- KIMM, T., SOMERVILLE, R. S., YI, S. K., VAN DEN BOSCH, F. C., SALIM, S., FONTANOT, F., MONACO, P., MO, H., PASQUALI, A., RICH, R. M., YANG, X.: 2009. The correlation of star formation quenching with internal galaxy properties and environment. *MNRAS*, **394**, 1131–1147.

- KLYPIN, A., KRAVTSOV, A. V., VALENZUELA, O., PRADA, F.: 1999. Where Are the Missing Galactic Satellites? *ApJ*, **522**, 82–92.
- KLYPIN, A., TRUJILLO-GOMEZ, S., PRIMACK, J.: 2010. Halos and galaxies in the standard cosmological model: results from the Bolshoi simulation. ArXiv:1002.3660.
- KOLLMEIER, J. A., ONKEN, C. A., KOCHANEK, C. S., GOULD, A., WEINBERG, D. H., DIETRICH, M., COOL, R., DEY, A., EISENSTEIN, D. J., JANNUZI, B. T., LE FLOC'H, E., STERN, D.: 2006. Black Hole Masses and Eddington Ratios at $0.3 < z < 4$. *ApJ*, **648**, 128–139.
- KOMATSU, E., DUNKLEY, J., NOLTA, M. R., BENNETT, C. L., GOLD, B., HINSHAW, G., JAROSIK, N., LARSON, D., LIMON, M., PAGE, L., SPERGEL, D. N., HALPERN, M., HILL, R. S., KOGUT, A., MEYER, S. S., TUCKER, G. S., WEILAND, J. L., WOLLACK, E., WRIGHT, E. L.: 2009. Five-Year Wilkinson Microwave Anisotropy Probe Observations: Cosmological Interpretation. *ApJS*, **180**, 330–376.
- KORMENDY, J. BENDER, R.: 2011. Supermassive black holes do not correlate with dark matter haloes of galaxies. *Nature*, **469**, 377–380.
- KORMENDY, J. RICHSTONE, D.: 1995. Inward Bound—The Search For Supermassive Black Holes In Galactic Nuclei. *ARA&A*, **33**, 581–+.
- KOUSHIAPPAS, S. M., BULLOCK, J. S., DEKEL, A.: 2004. Massive black hole seeds from low angular momentum material. *MNRAS*, **354**, 292–304.
- KOUSHIAPPAS, S. M. ZENTNER, A. R.: 2006. Testing Models of Supermassive Black Hole Seed Formation through Gravity Waves. *ApJ*, **639**, 7–22.
- LA FRANCA, F., FIORE, F., COMASTRI, A., PEROLA, G. C., SACCHI, N., BRUSA, M., COCCHIA, F., FERUGLIO, C., MATT, G., VIGNALI, C., CARANGELO, N., CILIEGI, P., LAMASTRA, A., MAIOLINO, R., MIGNOLI, M., MOLENDI, S., PUCETTI, S.: 2005. The HELLAS2XMM Survey. VII. The Hard X-Ray Luminosity Function of AGNs up to $z = 4$: More Absorbed AGNs at Low Luminosities and High Redshifts. *ApJ*, **635**, 864–879.
- LA FRANCA, F., MATUTE, I., FIORE, F., GRUPPIONI, C., POZZI, F., VIGNALI, C., THE HELLAS, ELAIS CONSORTII: 2002. The Evolution of AGNs in the Hard X-Rays and the Infrared. In R. Maiolino, A. Marconi, & N. Nagar, editor, *Issues in Unification of Active Galactic Nuclei*, volume 258 of *Astronomical Society of the Pacific Conference Series*, pages 241–+.
- LACEY, C. COLE, S.: 1993. Merger rates in hierarchical models of galaxy formation. *MNRAS*, **262**, 627–649.
- LANDAU, L.: 1938. Origin of Stellar Energy. *Nature*, **141**, 333–334.

- LAUER, T. R., TREMAINE, S., RICHTSTONE, D., FABER, S. M.: 2007. Selection Bias in Observing the Cosmological Evolution of the $M_{BH} - \sigma$ and $M_{BH} - L$ Relationships. *ApJ*, **670**, 249–260.
- LEMAÎTRE, G.: 1927. Un Univers homogène de masse constante et de rayon croissant rendant compte de la vitesse radiale des nébuleuses extra-galactiques. *Annales de la Societe Scietifique de Bruxelles*, **47**, 49–59.
- LI, Y., HERNQUIST, L., ROBERTSON, B., COX, T. J., HOPKINS, P. F., SPRINGEL, V., GAO, L., DI MATTEO, T., ZENTNER, A. R., JENKINS, A., YOSHIDA, N.: 2007. Formation of $z \sim 6$ Quasars from Hierarchical Galaxy Mergers. *ApJ*, **665**, 187–208.
- LINDE, A. D.: 1982. A new inflationary universe scenario: A possible solution of the horizon, flatness, homogeneity, isotropy and primordial monopole problems. *Physics Letters B*, **108**, 389–393.
- LOEB, A. RASIO, F. A.: 1994. Collapse of primordial gas clouds and the formation of quasar black holes. *ApJ*, **432**, 52–61.
- LU, Y., KEREŠ, D., KATZ, N., MO, H. J., FARDAL, M., WEINBERG, M. D.: 2010. On the algorithms of radiative cooling in semi-analytic models. *ArXiv:1008.1075*.
- LYNDEN-BELL, D.: 1969. Galactic Nuclei as Collapsed Old Quasars. *Nature*, **223**, 690–694.
- MADAU, P. REES, M. J.: 2001. Massive Black Holes as Population III Remnants. *ApJ*, **551**, L27–L30.
- MADDOX, S. J., EFSTATHIOU, G., SUTHERLAND, W. J., LOVEDAY, J.: 1990. Galaxy correlations on large scales. *MNRAS*, **242**, 43P–47P.
- MAGORRIAN, J., TREMAINE, S., RICHTSTONE, D., BENDER, R., BOWER, G., DRESSLER, A., FABER, S. M., GEBHARDT, K., GREEN, R., GRILLMAIR, C., KORMENDY, J., LAUER, T.: 1998. The Demography of Massive Dark Objects in Galaxy Centers. *AJ*, **115**, 2285–2305.
- MALBON, R. K., BAUGH, C. M., FRENK, C. S., LACEY, C. G.: 2007. Black hole growth in hierarchical galaxy formation. *MNRAS*, **382**, 1394–1414.
- MALLER, A. H. BULLOCK, J. S.: 2004. Multiphase galaxy formation: high-velocity clouds and the missing baryon problem. *MNRAS*, **355**, 694–712.
- MANDELBAUM, R., SELJAK, U., KAUFFMANN, G., HIRATA, C. M., BRINKMANN, J.: 2006. Galaxy halo masses and satellite fractions from galaxy-galaxy lensing in the Sloan Digital Sky Survey: stellar mass, luminosity, morphology and environment dependencies. *MNRAS*, **368**, 715–731.

- MARCONI, A. HUNT, L. K.: 2003. The Relation between Black Hole Mass, Bulge Mass, and Near-Infrared Luminosity. *ApJ*, **589**, L21–L24.
- MARCONI, A., RISALITI, G., GILLI, R., HUNT, L. K., MAIOLINO, R., SALVATI, M.: 2004. Local supermassive black holes, relics of active galactic nuclei and the X-ray background. *MNRAS*, **351**, 169–185.
- MARULLI, F., BONOLI, S., BRANCHINI, E., MOSCARDINI, L., SPRINGEL, V.: 2008. Modelling the cosmological co-evolution of supermassive black holes and galaxies - I. BH scaling relations and the AGN luminosity function. *MNRAS*, **385**, 1846–1858.
- MATUTE, I., LA FRANCA, F., POZZI, F., GRUPPIONI, C., LARI, C., ZAMORANI, G.: 2006. Active galactic nuclei in the mid-IR. Evolution and contribution to the cosmic infrared background. *A&A*, **451**, 443–456.
- MAULBETSCH, C., AVILA-REESE, V., COLÍN, P., GOTTLÖBER, S., KHALATYAN, A., STEINMETZ, M.: 2007. The Dependence of the Mass Assembly History of Cold Dark Matter Halos on Environment. *ApJ*, **654**, 53–65.
- MCLURE, R. J. DUNLOP, J. S.: 2001. The black hole masses of Seyfert galaxies and quasars. *MNRAS*, **327**, 199–207.
- MCLURE, R. J., JARVIS, M. J., TARGETT, T. A., DUNLOP, J. S., BEST, P. N.: 2006. On the evolution of the black-hole:spheroid mass ratio. *New Astronomy Review*, **50**, 782–785.
- MIHOS, J. C. HERNQUIST, L.: 1996. Gasdynamics and Starbursts in Major Mergers. *ApJ*, **464**, 641–+.
- MIYAJI, T., HASINGER, G., SCHMIDT, M.: 2000. Soft X-ray AGN luminosity function from it ROSAT surveys. I. Cosmological evolution and contribution to the soft X-ray background. *A&A*, **353**, 25–40.
- MIYOSHI, M., MORAN, J., HERRNSTEIN, J., GREENHILL, L., NAKAI, N., DIAMOND, P., INOUE, M.: 1995. Evidence for a black hole from high rotation velocities in a sub-parsec region of NGC4258. *Nature*, **373**, 127–129.
- MO, H., VAN DEN BOSCH, F. C., WHITE, S.: 2010. *Galaxy Formation and Evolution*.
- MO, H. J., MAO, S., WHITE, S. D. M.: 1998. The formation of galactic discs. *MNRAS*, **295**, 319–336.
- MONACO, P. FONTANOT, F.: 2005. Feedback from quasars in star-forming galaxies and the triggering of massive galactic winds. *MNRAS*, **359**, 283–294.
- MOORE, B., GHIGNA, S., GOVERNATO, F., LAKE, G., QUINN, T., STADEL, J., TOZZI, P.: 1999. Dark Matter Substructure within Galactic Halos. *ApJ*, **524**, L19–L22.

- MOSTER, B. P., SOMERVILLE, R. S., MAULBETSCH, C., VAN DEN BOSCH, F. C., MACCIÒ, A. V., NAAB, T., OSER, L.: 2010. Constraints on the Relationship between Stellar Mass and Halo Mass at Low and High Redshift. *ApJ*, **710**, 903–923.
- MURANTE, G., ARNABOLDI, M., GERHARD, O., BORGANI, S., CHENG, L. M., DIAFERIO, A., DOLAG, K., MOSCARDINI, L., TORMEN, G., TORNATORE, L., TOZZI, P.: 2004. The Diffuse Light in Simulations of Galaxy Clusters. *ApJ*, **607**, L83–L86.
- MURANTE, G., GIOVALLI, M., GERHARD, O., ARNABOLDI, M., BORGANI, S., DOLAG, K.: 2007. The importance of mergers for the origin of intracluster stars in cosmological simulations of galaxy clusters. *MNRAS*, **377**, 2–16.
- NAAB, T., JESSEIT, R., BURKERT, A.: 2006a. The influence of gas on the structure of merger remnants. *MNRAS*, **372**, 839–852.
- NAAB, T., JOHANSSON, P. H., OSTRICKER, J. P.: 2009. Minor Mergers and the Size Evolution of Elliptical Galaxies. *ApJ*, **699**, L178–L182.
- NAAB, T., JOHANSSON, P. H., OSTRICKER, J. P., EFSTATHIOU, G.: 2007. Formation of Early-Type Galaxies from Cosmological Initial Conditions. *ApJ*, **658**, 710–720.
- NAAB, T., KHOCHFAR, S., BURKERT, A.: 2006b. Properties of Early-Type, Dry Galaxy Mergers and the Origin of Massive Elliptical Galaxies. *ApJ*, **636**, L81–L84.
- NAAB, T., OSTRICKER, J. P.: 2009. Are Disk Galaxies the Progenitors of Giant Ellipticals? *ApJ*, **690**, 1452–1462.
- NAGAMINE, K., CEN, R., HERNQUIST, L., OSTRICKER, J. P., SPRINGEL, V.: 2005. Massive Galaxies and Extremely Red Objects at $z = 1-3$ in Cosmological Hydrodynamic Simulations: Near-Infrared Properties. *ApJ*, **627**, 608–620.
- NANDRA, K., LAIRD, E. S., STEIDEL, C. C.: 2005. The space density of moderate-luminosity active galaxies at $z = 3$. *MNRAS*, **360**, L39–L44.
- NATARAJAN, P., TREISTER, E.: 2009. Is there an upper limit to black hole masses? *MNRAS*, **393**, 838–845.
- NAVARRO, J. F., FRENK, C. S., WHITE, S. D. M.: 1997. A Universal Density Profile from Hierarchical Clustering. *ApJ*, **490**, 493–+.
- NAVARRO, J. F., SALES, L. V., OWLS TEAM: 2009. Disk Galaxies at $z=2$ in OWLS. In S. Jogee, I. Marinova, L. Hao, & G. A. Blanc, editor, *Astronomical Society of the Pacific Conference Series*, volume 419 of *Astronomical Society of the Pacific Conference Series*, pages 10–+.
- NAVARRO, J. F., STEINMETZ, M.: 1997. The Effects of a Photoionizing Ultraviolet Background on the Formation of Disk Galaxies. *ApJ*, **478**, 13–+.

- NEISTEIN, E. DEKEL, A.: 2008. Constructing merger trees that mimic N-body simulations. *MNRAS*, **383**, 615–626.
- NETZER, H. TRAKHTENBROT, B.: 2007. Cosmic Evolution of Mass Accretion Rate and Metallicity in Active Galactic Nuclei. *ApJ*, **654**, 754–763.
- NORDON, R., LUTZ, D., SHAO, L., MAGNELLI, B., BERTA, S., ALTIERI, B., ANDREANI, P., AUSSEL, H., BONGIOVANNI, A., CAVA, A., CEPHA, J., CIMATTI, A., DADDI, E., DOMINGUEZ, H., ELBAZ, D., FÖRSTER SCHREIBER, N. M., GENZEL, R., GRAZIAN, A., MAGDIS, G., MAIOLINO, R., PÉREZ GARCÍA, A. M., POGLITSCH, A., POPESSO, P., POZZI, F., RIGUCCINI, L., RODIGHIERO, G., SAINTONGE, A., SANCHEZ-PORTAL, M., SANTINI, P., STURM, E., TACCONI, L., VALTCHANOV, I., WETZSTEIN, M., WIEPRECHT, E.: 2010. The star-formation rates of $1.5 < z < 2.5$ massive galaxies. *A&A*, **518**, L24+.
- NOVAK, G. S., FABER, S. M., DEKEL, A.: 2006. On the Correlations of Massive Black Holes with Their Host Galaxies. *ApJ*, **637**, 96–103.
- NULSEN, P. E. J. FABIAN, A. C.: 2000. Fuelling quasars with hot gas. *MNRAS*, **311**, 346–356.
- OPPENHEIMER, B. D. DAVÉ, R.: 2008. Mass, metal, and energy feedback in cosmological simulations. *MNRAS*, **387**, 577–600.
- OPPENHEIMER, J. R. SERBER, R.: 1938. On the Stability of Stellar Neutron Cores. *Physical Review*, **54**, 540–540.
- OSER, L., OSTRIKER, J. P., NAAB, T., JOHANSSON, P. H., BURKERT, A.: 2010. The Two Phases of Galaxy Formation. *ApJ*, **725**, 2312–2323.
- OSTRIKER, J. P., CHOI, E., CIOTTI, L., NOVAK, G. S., PROGA, D.: 2010. Momentum Driving: Which Physical Processes Dominate Active Galactic Nucleus Feedback? *ApJ*, **722**, 642–652.
- OSTRIKER, J. P., PEEBLES, P. J. E., YAHIL, A.: 1974. The size and mass of galaxies, and the mass of the universe. *ApJ*, **193**, L1–L4.
- PADOVANI, P.: 1989. The evolution of the Eddington ratio for active galactic nuclei. *A&A*, **209**, 27–45.
- PEACOCK, J. A.: 1999. *Cosmological Physics*.
- PEARCE, F. R., JENKINS, A., FRENK, C. S., WHITE, S. D. M., THOMAS, P. A., COUCHMAN, H. M. P., PEACOCK, J. A., EFSTATHIOU, G.: 2001. Simulations of galaxy formation in a cosmological volume. *MNRAS*, **326**, 649–666.
- PEEBLES, P. J. E.: 1965. The Black-Body Radiation Content of the Universe and the Formation of Galaxies. *ApJ*, **142**, 1317–+.

- PEEBLES, P. J. E.: 1982. Large-scale background temperature and mass fluctuations due to scale-invariant primeval perturbations. *ApJ*, **263**, L1–L5.
- PENG, C. Y.: 2007. How Mergers May Affect the Mass Scaling Relation between Gravitationally Bound Systems. *ApJ*, **671**, 1098–1107.
- PENG, C. Y., IMPEY, C. D., HO, L. C., BARTON, E. J., RIX, H.-W.: 2006. Probing the Coevolution of Supermassive Black Holes and Quasar Host Galaxies. *ApJ*, **640**, 114–125.
- PENZIAS, A. A. WILSON, R. W.: 1965. A Measurement of Excess Antenna Temperature at 4080 Mc/s. *ApJ*, **142**, 419–421.
- PERLMUTTER, S., ALDERING, G., GOLDHABER, G., KNOP, R. A., NUGENT, P., CASTRO, P. G., DEUSTUA, S., FABBRO, S., GOOBAR, A., GROOM, D. E., HOOK, I. M., KIM, A. G., KIM, M. Y., LEE, J. C., NUNES, N. J., PAIN, R., PENNYPACKER, C. R., QUIMBY, R., LIDMAN, C., ELLIS, R. S., IRWIN, M., McMAHON, R. G., RUIZ-LAPUENTE, P., WALTON, N., SCHAEFER, B., BOYLE, B. J., FILIPPENKO, A. V., MATHESON, T., FRUCHTER, A. S., PANAGIA, N., NEWBERG, H. J. M., COUCH, W. J., THE SUPERNOVA COSMOLOGY PROJECT: 1999. Measurements of Omega and Lambda from 42 High-Redshift Supernovae. *ApJ*, **517**, 565–586.
- PETERSON, B. M.: 1993. Reverberation mapping of active galactic nuclei. *PASP*, **105**, 247–268.
- PIERCE, C. M., LOTZ, J. M., LAIRD, E. S., LIN, L., NANDRA, K., PRIMACK, J. R., FABER, S. M., BARMBY, P., PARK, S. Q., WILLNER, S. P., GWYN, S., KOO, D. C., COIL, A. L., COOPER, M. C., GEORGAKAKIS, A., KOEKEMOER, A. M., NOESKE, K. G., WEINER, B. J., WILLMER, C. N. A.: 2007. AEGIS: Host Galaxy Morphologies of X-Ray-selected and Infrared-selected Active Galactic Nuclei at $0.2 < z < 1.2$. *ApJ*, **660**, L19–L22.
- PIONTEK, F. STEINMETZ, M.: 2011. The modelling of feedback processes in cosmological simulations of disc galaxy formation. *MNRAS*, **410**, 2625–2642.
- PLANELLES, S. QUILIS, V.: 2010. ASOHF: a new adaptive spherical overdensity halo finder. *A&A*, **519**, A94+.
- PRESS, W. H. SCHECHTER, P.: 1974. Formation of Galaxies and Clusters of Galaxies by Self-Similar Gravitational Condensation. *ApJ*, **187**, 425–438.
- PUCHWEIN, E., SPRINGEL, V., SIJACKI, D., DOLAG, K.: 2010. Intracluster stars in simulations with active galactic nucleus feedback. *MNRAS*, **406**, 936–951.
- REES, M. J.: 1984. Black Hole Models for Active Galactic Nuclei. *ARA&A*, **22**, 471–506.

- REES, M. J. OSTRICKER, J. P.: 1977. Cooling, dynamics and fragmentation of massive gas clouds - Clues to the masses and radii of galaxies and clusters. *MNRAS*, **179**, 541–559.
- REINES, F., SOBEL, H. W., PASIERB, E.: 1980. Evidence for neutrino instability. *Physical Review Letters*, **45**, 1307–1311.
- RICHARDS, G. T., STRAUSS, M. A., FAN, X., HALL, P. B., JESTER, S., SCHNEIDER, D. P., VANDEN BERK, D. E., STOUGHTON, C., ANDERSON, S. F., BRUNNER, R. J., GRAY, J., GUNN, J. E., IVEZIĆ, Ž., KIRKLAND, M. K., KNAPP, G. R., LOVEDAY, J., MEIKSIN, A., POPE, A., SZALAY, A. S., THAKAR, A. R., YANNY, B., YORK, D. G., BARENTINE, J. C., BREWINGTON, H. J., BRINKMANN, J., FUKUGITA, M., HARVANEK, M., KENT, S. M., KLEINMAN, S. J., KRZESIŃSKI, J., LONG, D. C., LUPTON, R. H., NASH, T., NEILSEN, JR., E. H., NITTA, A., SCHLEGEL, D. J., SNEDDEN, S. A.: 2006. The Sloan Digital Sky Survey Quasar Survey: Quasar Luminosity Function from Data Release 3. *AJ*, **131**, 2766–2787.
- ROBERTS, M. S. ROTS, A. H.: 1973. Comparison of Rotation Curves of Different Galaxy Types. *A&A*, **26**, 483–485.
- ROBERTSON, B., BULLOCK, J. S., COX, T. J., DI MATTEO, T., HERNQUIST, L., SPRINGEL, V., YOSHIDA, N.: 2006a. A Merger-driven Scenario for Cosmological Disk Galaxy Formation. *ApJ*, **645**, 986–1000.
- ROBERTSON, B., COX, T. J., HERNQUIST, L., FRANX, M., HOPKINS, P. F., MARTINI, P., SPRINGEL, V.: 2006b. The Fundamental Scaling Relations of Elliptical Galaxies. *ApJ*, **641**, 21–40.
- ROBERTSON, B., HERNQUIST, L., COX, T. J., DI MATTEO, T., HOPKINS, P. F., MARTINI, P., SPRINGEL, V.: 2006c. The Evolution of the $M_{BH} - \sigma$ Relation. *ApJ*, **641**, 90–102.
- RUBIN, V. C., THONNARD, N., FORD, JR., W. K.: 1978. Extended rotation curves of high-luminosity spiral galaxies. IV - Systematic dynamical properties, SA through SC. *ApJ*, **225**, L107–L111.
- SALPETER, E. E.: 1955. The Luminosity Function and Stellar Evolution. *ApJ*, **121**, 161–+.
- SALPETER, E. E.: 1964. Accretion of Interstellar Matter by Massive Objects. *ApJ*, **140**, 796–800.
- SALVIANDER, S., SHIELDS, G. A., GEBHARDT, K., BONNING, E. W.: 2007. The Black Hole Mass-Galaxy Bulge Relationship for QSOs in the Sloan Digital Sky Survey Data Release 3. *ApJ*, **662**, 131–144.

- SARO, A., DE LUCIA, G., BORGANI, S., DOLAG, K.: 2010. Gas cooling in semi-analytic models and smoothed particle hydrodynamics simulations: are results consistent? *MNRAS*, **406**, 729–743.
- SAWALA, T., SCANNAPIECO, C., MAIO, U., WHITE, S.: 2010. Formation of isolated dwarf galaxies with feedback. *MNRAS*, **402**, 1599–1613.
- SAZONOV, S. Y. REVNIVTSEV, M. G.: 2004. Statistical properties of local active galactic nuclei inferred from the RXTE 3-20 keV all-sky survey. *A&A*, **423**, 469–480.
- SCANNAPIECO, C., WHITE, S. D. M., SPRINGEL, V., TISSERA, P. B.: 2009. The formation and survival of discs in a Λ CDM universe. *MNRAS*, **396**, 696–708.
- SCHAYE, J., DALLA VECCHIA, C., BOOTH, C. M., WIERSMA, R. P. C., THEUNS, T., HAAS, M. R., BERTONE, S., DUFFY, A. R., MCCARTHY, I. G., VAN DE VOORT, F.: 2010a. The physics driving the cosmic star formation history. *MNRAS*, **402**, 1536–1560.
- SCHAYE, J., DALLA VECCHIA, C., BOOTH, C. M., WIERSMA, R. P. C., THEUNS, T., HAAS, M. R., BERTONE, S., DUFFY, A. R., MCCARTHY, I. G., VAN DE VOORT, F.: 2010b. The physics driving the cosmic star formation history. *MNRAS*, **402**, 1536–1560.
- SCHMIDT, M. GREEN, R. F.: 1983. Quasar evolution derived from the Palomar bright quasar survey and other complete quasar surveys. *ApJ*, **269**, 352–374.
- SCHMIDT, M., SCHNEIDER, D. P., GUNN, J. E.: 1995. Spectroscopic CCD Surveys for Quasars at Large Redshift.IV.Evolution of the Luminosity Function from Quasars Detected by Their Lyman-Alpha Emission. *AJ*, **110**, 68–+.
- SCHÖDEL, R., OTT, T., GENZEL, R., ECKART, A., MOUAWAD, N., ALEXANDER, T.: 2003. Stellar Dynamics in the Central Arcsecond of Our Galaxy. *ApJ*, **596**, 1015–1034.
- SCHRAMM, M., WISOTZKI, L., JAHNKE, K.: 2008. Host galaxies of bright high redshift quasars: luminosities and colours. *A&A*, **478**, 311–319.
- SCHULZE, A. WISOTZKI, L.: 2010. Low redshift AGN in the Hamburg/ESO Survey . II. The active black hole mass function and the distribution function of Eddington ratios. *A&A*, **516**, A87+.
- SESANA, A., HAARDT, F., MADAU, P., VOLONTERI, M.: 2004. Low-Frequency Gravitational Radiation from Coalescing Massive Black Hole Binaries in Hierarchical Cosmologies. *ApJ*, **611**, 623–632.

- SESANA, A., HAARDT, F., MADAU, P., VOLONTERI, M.: 2005. The Gravitational Wave Signal from Massive Black Hole Binaries and Its Contribution to the LISA Data Stream. *ApJ*, **623**, 23–30.
- SHAKURA, N. I. SUNYAEV, R. A.: 1973. Black holes in binary systems. Observational appearance. *A&A*, **24**, 337–355.
- SHANKAR, F., SALUCCI, P., GRANATO, G. L., DE ZOTTI, G., DANESE, L.: 2004. Supermassive black hole demography: the match between the local and accreted mass functions. *MNRAS*, **354**, 1020–1030.
- SHANKAR, F., WEINBERG, D. H., SHEN, Y.: 2010. Constraints on black hole duty cycles and the black hole-halo relation from SDSS quasar clustering. *ArXiv:1004.1173*.
- SHAPIRO, K. L., GENZEL, R., QUATAERT, E., FÖRSTER SCHREIBER, N. M., DAVIES, R., TACCONI, L., ARMUS, L., BOUCHÉ, N., BUSCHKAMP, P., CIMATTI, A., CRESCI, G., DADDI, E., EISENHAUER, F., ERB, D. K., GENEL, S., HICKS, E. K. S., LILLY, S. J., LUTZ, D., RENZINI, A., SHAPLEY, A., STEIDEL, C. C., STERNBERG, A.: 2009. The SINS Survey: Broad Emission Lines in High-Redshift Star-Forming Galaxies. *ApJ*, **701**, 955–963.
- SHETH, R. K. LEMSON, G.: 1999. The forest of merger history trees associated with the formation of dark matter haloes. *MNRAS*, **305**, 946–956.
- SHIELDS, G. A., MENEZES, K. L., MASSART, C. A., VANDEN BOUT, P.: 2006. The Black Hole-Bulge Relationship for QSOs at High Redshift. *ApJ*, **641**, 683–688.
- SIJACKI, D., SPRINGEL, V., DI MATTEO, T., HERNQUIST, L.: 2007. A unified model for AGN feedback in cosmological simulations of structure formation. *MNRAS*, **380**, 877–900.
- SILK, J.: 1977. On the fragmentation of cosmic gas clouds. I - The formation of galaxies and the first generation of stars. *ApJ*, **211**, 638–648.
- SIVAKOFF, G. R., GILLI, R., BRANDT, W. N., HICKOX, R. C., MURRAY, S. S., PTAK, A., WIDE FIELD X-RAY TELESCOPE TEAM: 2010. Understanding The Growth And Evolution Of Super Massive Black Holes With The Wide Field X-ray Telescope. In *Bulletin of the American Astronomical Society*, volume 42 of *Bulletin of the American Astronomical Society*, pages 520–+.
- SKORY, S., TURK, M. J., NORMAN, M. L., COIL, A. L.: 2010. Parallel HOP: A Scalable Halo Finder for Massive Cosmological Data Sets. *ApJS*, **191**, 43–57.
- SOLTAN, A.: 1982. Masses of quasars. *MNRAS*, **200**, 115–122.

- SOMERVILLE, R. S., BARDEN, M., RIX, H., BELL, E. F., BECKWITH, S. V. W., BORCH, A., CALDWELL, J. A. R., HÄUSSLER, B., HEYMANS, C., JAHNKE, K., JOGEE, S., MCINTOSH, D. H., MEISENHEIMER, K., PENG, C. Y., SÁNCHEZ, S. F., WISOTZKI, L., WOLF, C.: 2008a. An Explanation for the Observed Weak Size Evolution of Disk Galaxies. *ApJ*, **672**, 776–786.
- SOMERVILLE, R. S., GILMORE, R., PRIMACK, J., DOMÍNGUEZ, A.: 2011. *MNRAS*. submitted.
- SOMERVILLE, R. S., HOPKINS, P. F., COX, T. J., ROBERTSON, B. E., HERNQUIST, L.: 2008b. A semi-analytic model for the co-evolution of galaxies, black holes and active galactic nuclei. *MNRAS*, **391**, 481–506.
- SOMERVILLE, R. S., LEMSON, G., KOLATT, T. S., DEKEL, A.: 2000. Evaluating approximations for halo merging histories. *MNRAS*, **316**, 479–490.
- SOMERVILLE, R. S. PRIMACK, J. R.: 1999a. Semi-analytic modelling of galaxy formation: the local Universe. *MNRAS*, **310**, 1087–1110.
- SOMERVILLE, R. S. PRIMACK, J. R.: 1999b. Semi-analytic modelling of galaxy formation: the local Universe. *MNRAS*, **310**, 1087–1110.
- SPERGEL, D. N., BEAN, R., DORÉ, O., NOLTA, M. R., BENNETT, C. L., DUNKLEY, J., HINSHAW, G., JAROSIK, N., KOMATSU, E., PAGE, L., PEIRIS, H. V., VERDE, L., HALPERN, M., HILL, R. S., KOGUT, A., LIMON, M., MEYER, S. S., ODEGARD, N., TUCKER, G. S., WEILAND, J. L., WOLLACK, E., WRIGHT, E. L.: 2007. Three-Year Wilkinson Microwave Anisotropy Probe (WMAP) Observations: Implications for Cosmology. *ApJS*, **170**, 377–408.
- SPERGEL, D. N., VERDE, L., PEIRIS, H. V., KOMATSU, E., NOLTA, M. R., BENNETT, C. L., HALPERN, M., HINSHAW, G., JAROSIK, N., KOGUT, A., LIMON, M., MEYER, S. S., PAGE, L., TUCKER, G. S., WEILAND, J. L., WOLLACK, E., WRIGHT, E. L.: 2003. First-Year Wilkinson Microwave Anisotropy Probe (WMAP) Observations: Determination of Cosmological Parameters. *ApJS*, **148**, 175–194.
- SPRINGEL, V., DI MATTEO, T., HERNQUIST, L.: 2005a. Black Holes in Galaxy Mergers: The Formation of Red Elliptical Galaxies. *ApJ*, **620**, L79–L82.
- SPRINGEL, V., DI MATTEO, T., HERNQUIST, L.: 2005b. Modelling feedback from stars and black holes in galaxy mergers. *MNRAS*, **361**, 776–794.
- SPRINGEL, V. HERNQUIST, L.: 2003. Cosmological smoothed particle hydrodynamics simulations: a hybrid multiphase model for star formation. *MNRAS*, **339**, 289–311.
- SPRINGEL, V., WANG, J., VOGELSBERGER, M., LUDLOW, A., JENKINS, A., HELMI, A., NAVARRO, J. F., FRENK, C. S., WHITE, S. D. M.: 2008. The Aquarius Project: the subhaloes of galactic haloes. *MNRAS*, **391**, 1685–1711.

- SPRINGEL, V., WHITE, S. D. M., JENKINS, A., FRENK, C. S., YOSHIDA, N., GAO, L., NAVARRO, J., THACKER, R., CROTON, D., HELLY, J., PEACOCK, J. A., COLE, S., THOMAS, P., COUCHMAN, H., EVRARD, A., COLBERG, J., PEARCE, F.: 2005c. Simulations of the formation, evolution and clustering of galaxies and quasars. *Nature*, **435**, 629–636.
- SPRINGEL, V., WHITE, S. D. M., TORMEN, G., KAUFFMANN, G.: 2001a. Populating a cluster of galaxies - I. Results at $z=0$. *MNRAS*, **328**, 726–750.
- SPRINGEL, V., YOSHIDA, N., WHITE, S. D. M.: 2001b. GADGET: a code for collisionless and gasdynamical cosmological simulations. *New Astronomy*, **6**, 79–117.
- STEFFEN, A. T., BARGER, A. J., COWIE, L. L., MUSHOTZKY, R. F., YANG, Y.: 2003. The Changing Active Galactic Nucleus Population. *ApJ*, **596**, L23–L26.
- STEINHARDT, C. L. ELVIS, M.: 2010. The quasar mass-luminosity plane - I. A sub-Eddington limit for quasars. *MNRAS*, **402**, 2637–2648.
- STRINGER, M. J., BROOKS, A. M., BENSON, A. J., GOVERNATO, F.: 2010. Analytic and numerical realizations of a disc galaxy. *MNRAS*, **407**, 632–644.
- TEYSSIER, R., CHAPON, D., BOURNAUD, F.: 2010a. The Driving Mechanism of Starbursts in Galaxy Mergers. *ApJ*, **720**, L149–L154.
- TEYSSIER, R., MOORE, B., MARTIZZI, D., DUBOIS, Y., MAYER, L.: 2010b. Mass Distribution in Galaxy Clusters: the Role of AGN Feedback. *ArXiv:1003.4744*.
- THEUNS, T., LEONARD, A., EFSTATHIOU, G., PEARCE, F. R., THOMAS, P. A.: 1998. P^3M -SPH simulations of the Ly α forest. *MNRAS*, **301**, 478–502.
- TOOMRE, A. TOOMRE, J.: 1972. Galactic Bridges and Tails. *ApJ*, **178**, 623–666.
- TREISTER, E., URRY, C. M., CHATZICHRISTOU, E., BAUER, F., ALEXANDER, D. M., KOEKEMOER, A., VAN DUYN, J., BRANDT, W. N., BERGERON, J., STERN, D., MOUSTAKAS, L. A., CHARY, R., CONSELICE, C., CRISTIANI, S., GROGIN, N.: 2004. Obscured Active Galactic Nuclei and the X-Ray, Optical, and Far-Infrared Number Counts of Active Galactic Nuclei in the GOODS Fields. *ApJ*, **616**, 123–135.
- TREMAINE, S., GEBHARDT, K., BENDER, R., BOWER, G., DRESSLER, A., FABER, S. M., FILIPPENKO, A. V., GREEN, R., GRILLMAIR, C., HO, L. C., KORMENDY, J., LAUER, T. R., MAGORRIAN, J., PINKNEY, J., RICHSTONE, D.: 2002. The Slope of the Black Hole Mass versus Velocity Dispersion Correlation. *ApJ*, **574**, 740–753.

- TREU, T., WOO, J.-H., MALKAN, M. A., BLANDFORD, R. D.: 2007. Cosmic Evolution of Black Holes and Spheroids. II. Scaling Relations at $z=0.36$. *ApJ*, **667**, 117–130.
- UEDA, Y.: 2006. AGN Evolution Revealed from X-ray Surveys. In A. Wilson, editor, *The X-ray Universe 2005*, volume 604 of *ESA Special Publication*, pages 763–+.
- UEDA, Y., AKIYAMA, M., OHTA, K., MIYAJI, T.: 2003. Cosmological Evolution of the Hard X-Ray Active Galactic Nucleus Luminosity Function and the Origin of the Hard X-Ray Background. *ApJ*, **598**, 886–908.
- VAN DEN BOSCH, F. C., YANG, X., MO, H. J.: 2003. Linking early- and late-type galaxies to their dark matter haloes. *MNRAS*, **340**, 771–792.
- VAN DEN BOSCH, F. C., YANG, X., MO, H. J., WEINMANN, S. M., MACCIÒ, A. V., MORE, S., CACCIATO, M., SKIBBA, R., KANG, X.: 2007. Towards a concordant model of halo occupation statistics. *MNRAS*, **376**, 841–860.
- VESTERGAARD, M.: 2003. Occurrence and Global Properties of Narrow C IV $\lambda 1549$ Å Absorption Lines in Moderate-Redshift Quasars. *ApJ*, **599**, 116–139.
- VESTERGAARD, M.: 2004. Early Growth and Efficient Accretion of Massive Black Holes at High Redshift. *ApJ*, **601**, 676–691.
- VOLONTERI, M.: 2010. Formation of supermassive black holes. *A&A Rev.*, **18**, 279–315.
- VOLONTERI, M., HAARDT, F., MADAU, P.: 2003. The Assembly and Merging History of Supermassive Black Holes in Hierarchical Models of Galaxy Formation. *ApJ*, **582**, 559–573.
- VOLONTERI, M., LODATO, G., NATARAJAN, P.: 2008. The evolution of massive black hole seeds. *MNRAS*, **383**, 1079–1088.
- VOLONTERI, M., NATARAJAN, P.: 2009. Journey to the $M_{BH} - \sigma$ relation: the fate of low-mass black holes in the Universe. *MNRAS*, **400**, 1911–1918.
- VON DER LINDEN, A., BEST, P. N., KAUFFMANN, G., WHITE, S. D. M.: 2007. How special are brightest group and cluster galaxies? *MNRAS*, **379**, 867–893.
- WADEPUHL, M., SPRINGEL, V.: 2011. Satellite galaxies in hydrodynamical simulations of Milky Way sized galaxies. *MNRAS*, **410**, 1975–1992.
- WADSLEY, J. W., STADEL, J., QUINN, T.: 2004. Gasoline: a flexible, parallel implementation of TreeSPH. *NewA*, **9**, 137–158.

- WAKE, D. A., WHITAKER, K. E., LABBÉ, I., VAN DOKKUM, P. G., FRANX, M., QUADRI, R., BRAMMER, G., KRIEK, M., LUNDGREN, B. F., MARCHESINI, D., MUZZIN, A.: 2011. Galaxy Clustering in the NEWFIRM Medium Band Survey: The Relationship Between Stellar Mass and Dark Matter Halo Mass at $1 < z < 2$. *ApJ*, **728**, 46–+.
- WALTER, F., CARILLI, C., BERTOLDI, F., MENTEN, K., COX, P., LO, K. Y., FAN, X., STRAUSS, M. A.: 2004. Resolved Molecular Gas in a Quasar Host Galaxy at Redshift $z=6.42$. *ApJ*, **615**, L17–L20.
- WARREN, S. J., HEWETT, P. C., OSMER, P. S.: 1994. A wide-field multicolor survey for high-redshift quasars, Z greater than or equal to 2.2. 3: The luminosity function. *ApJ*, **421**, 412–433.
- WECHSLER, R. H., ZENTNER, A. R., BULLOCK, J. S., KRAVTSOV, A. V., ALLGOOD, B.: 2006. The Dependence of Halo Clustering on Halo Formation History, Concentration, and Occupation. *ApJ*, **652**, 71–84.
- WEINMANN, S. M., KAUFFMANN, G., VAN DEN BOSCH, F. C., PASQUALI, A., MCINTOSH, D. H., MO, H., YANG, X., GUO, Y.: 2009. Environmental effects on satellite galaxies: the link between concentration, size and colour profile. *MNRAS*, **394**, 1213–1228.
- WELLER, J., OSTRIKER, J. P., BODE, P., SHAW, L.: 2005. Fast identification of bound structures in large N-body simulations. *MNRAS*, **364**, 823–732.
- WHITE, M., MARTINI, P., COHN, J. D.: 2008. Constraints on the correlation between QSO luminosity and host halo mass from high-redshift quasar clustering. *MNRAS*, **390**, 1179–1184.
- WHITE, S. D. M.: 1984. Angular momentum growth in protogalaxies. *ApJ*, **286**, 38–41.
- WHITE, S. D. M. FRENK, C. S.: 1991. Galaxy formation through hierarchical clustering. *ApJ*, **379**, 52–79.
- WHITE, S. D. M. REES, M. J.: 1978. Core condensation in heavy halos - A two-stage theory for galaxy formation and clustering. *MNRAS*, **183**, 341–358.
- WOLF, C., WISOTZKI, L., BORCH, A., DYE, S., KLEINHEINRICH, M., MEISENHEIMER, K.: 2003. The evolution of faint AGN between $z \approx 1$ and $z \approx 5$ from the COMBO-17 survey. *A&A*, **408**, 499–514.
- WOO, J.-H., TREU, T., MALKAN, M. A., BLANDFORD, R. D.: 2008. Cosmic Evolution of Black Holes and Spheroids. III. The $M_{BH} - \sigma_*$ Relation in the Last Six Billion Years. *ApJ*, **681**, 925–930.

- YANG, X., MO, H. J., VAN DEN BOSCH, F. C.: 2003. Constraining galaxy formation and cosmology with the conditional luminosity function of galaxies. *MNRAS*, **339**, 1057–1080.
- YOSHIDA, N., STOEHR, F., SPRINGEL, V., WHITE, S. D. M.: 2002. Gas cooling in simulations of the formation of the galaxy population. *MNRAS*, **335**, 762–772.
- YU, Q. LU, Y.: 2008. Toward Precise Constraints on the Growth of Massive Black Holes. *ApJ*, **689**, 732–754.
- ZEHAVI, E., LESHEM, A., LEVANDA, R., HAN, Z.: 2010. Weighted Max-Min Resource Allocation for Frequency Selective Channels. *ArXiv:1008.1372*.
- ZEHAVI, I., PATIRI, S., ZHENG, Z.: 2011. The Growth of Galaxy Stellar Mass Within Dark Matter Halos. *ArXiv:1104.0389*.
- ZEL'DOVICH, Y. B.: 1964. The Fate of a Star and the Evolution of Gravitational Energy Upon Accretion. *Soviet Physics Doklady*, **9**, 195–+.
- ZHANG, J., MA, C., FAKHOURI, O.: 2008. Conditional mass functions and merger rates of dark matter haloes in the ellipsoidal collapse model. *MNRAS*, **387**, L13–L17.
- ZHENG, Z., COIL, A. L., ZEHAVI, I.: 2007. Galaxy Evolution from Halo Occupation Distribution Modeling of DEEP2 and SDSS Galaxy Clustering. *ApJ*, **667**, 760–779.
- ZIBETTI, S., WHITE, S. D. M., SCHNEIDER, D. P., BRINKMANN, J.: 2005. Inter-galactic stars in $z \sim 0.25$ galaxy clusters: systematic properties from stacking of Sloan Digital Sky Survey imaging data. *MNRAS*, **358**, 949–967.

Curriculum Vitae

PERSONAL INFORMATION

Contact	Ruemannstrasse 53, 80804 München, Germany Tel. 0049 160 2608048 mhirsch@usm.uni-muenchen.de
Date of birth	April 7, 1981 in Nürnberg
Nationality	German

EDUCATION AND TRAINING

11/2006-pres.	PhD: research at University Observatory Munich, Munich <i>"Co-evolution of galaxies and black holes using analytic and semi-analytic methods"</i> Supervisor: Prof. Dr. Andreas Burkert
02/2006	Diploma in Physics, Friedrich-Alexander University Erlangen-Nürnberg (mark: 1.0, <i>with distinction</i>)
02/2005-02/2006	Diploma Thesis: research at the Friedrich-Alexander University, Chair for condensed matter: <i>"Scattering of electrons in image potential states on the Cu(001) surface at Co ad-atoms"</i> Supervisor: Prof. Dr. Thomas Fauster
10/2002-02/2005	Undergraduate and graduate studies in physics at the Friedrich-Alexander University of Erlangen-Nürnberg
09/1987 - 06/2000	Attendance at school. Final examination: Abitur (High School Degree, mark: 1.1), Ostendorfer Gymnasium, Neumarkt, Germany

AWARDS AND HONORS

07/2006: **Ohm-award** of the Max-Schaldach-Stiftung for one of the best diploma thesis during the academic year 2005/06

TALKS AT CONFERENCES AND WORKSHOPS

09/2010 12th Birmingham-Nottingham Extragalactic workshop, AGN: populations, parameters and power: *"Anti-hierarchical growth of black holes in the universe"*

08/2010 Santa Cruz Galaxy workshop 2010: *"Anti-hierarchical growth of black holes in the universe"*

06/2010 Puzzles of galactic nuclei, scientific workshop at MPE: *"Anti-hierarchical growth of black holes in the universe"*

09/2009 Collaborative workshop of the Φ GN-group at MPIA: *"The evolution of the intrinsic scatter of massive black holes"*

07/2009 Physics of galactic nuclei, scientific workshop at Ringberg Castle: *"The evolution of the intrinsic scatter of massive black holes"*

12/2007 Start-up workshop of the Φ GN group at MPE: *"Black hole growth in a hierarchical universe"*

03/2006 Annual conference of the DPG: *"Scattering of electrons in image-potential states on the Cu(001) surface at Co ad-atoms"*, Dresden

RESEARCH INTERESTS

Research fields: Cosmology, structure formation, galaxy evolution, scaling relations, co-evolution of galaxies and black holes, active galactic nuclei, comparison of semi-analytic models with simulations

Methods: Statistical methods (central-limit-theorem), semi-analytic models, cosmological SPH-simulations, construction of merger trees on basis of the halofinder FOF and SUBFIND

List of publications

REFEREED ARTICLES

- **Hirschmann, M.**, Fauster T. "*Scattering of electrons on the Cu(001) surface by Co adatoms*", Appl. Phys. A 88, 547 (2007)
- **Hirschmann, M.**, Khochfar, S., Burkert A., Naab, T., Genel S., Somerville R. "*On the evolution of the intrinsic scatter in black hole versus galaxy mass relations*", MNRAS 407, 1016-1032 (2010)
- **Hirschmann, M.**, Naab T., Somerville R., Burkert A., Oser L. "*Galaxy formation in semi-analytic models and cosmological hydrodynamic zoom simulations*", submitted to MNRAS

CONFERENCE PROCEEDINGS

- **Hirschmann, M.**, Khochfar, S., Burkert A., Naab T. "*The evolution of the intrinsic scatter of massive black holes*", proceedings of the Φ GN workshop

ARTICLES IN PREPARATION

- **Hirschmann, M.**, Somerville R., Naab T., Burkert A. "*Origin of the anti-hierarchical growth of black holes in the universe*", to be submitted
- Remus, R., Burkert A., **Hirschmann M.** et al. "*Galaxy groups*", in preparation
- Naab, T., Oser, L., **Hirschmann M.** et al. "*Assembly of massive galaxies*", in preparation

Danksagung

Ich danke...

- an erster Stelle meinem Doktorvater, **Prof. Dr. Andreas Burkert**, für die Möglichkeit an der Universitätssternwarte in München promovieren zu können, für seine ständige, engagierte Unterstützung dieser Arbeit, für die zahlreichen produktiven, wissenschaftlichen Diskussionen mit ihm genauso wie für seine kritische Anmerkungen mir mögliche Schwachstellen meiner Arbeit aufzuzeigen.
- **Dr. Thorsten Naab** für seinen unermüdlichen Einsatz für das Fortschreiten und Gelingen meiner Arbeit, seinen enormen Ideenreichtum, seine immerwährende Geduld (auch bei noch so “einfachen” Fragen) und seine aufbauenden und ermunternden Worte in den manchmal auch schwierigeren Zeiten meiner Promotion. Es war mir eine sehr grosse Freude mit ihm zu arbeiten.
- **Prof. Dr. Rachel Somerville** dafür, dass sie mich in die Geheimnisse der semianalytischen Modelle eingeweiht hat, mir dabei immer mit Rat und Tat zur Seite gestanden ist genauso wie für die zweimaligen USA Besuche an ihrem Institut (Space Telescope Science Institute). Ohne sie wäre diese Arbeit niemals das geworden, was sie ist.
- **Dr. Sadegh Khochfar** für seine engagierte Betreuung in den Fragen der Entwicklung der Streuung in der Masse des schwarzen Loches.
- der **CAST & ΦGN** Gruppe für interessante wissenschaftliche Diskussionen während der “group meetings”.
- den **Systemadministratoren** der USM, ganz besonders **Dr. Tadius Hoffmann**, der zu allen ‘Unzeiten’ auftretende Probleme immer schnellstmöglich behoben hat.
- den **Sekretärinnen** der USM, dafür, dass sie mir bei anfallendem “Verwaltungskram” behilflich waren.
- und ganz besonders meinen ‘Mitreitern’, **Hanna, Steffi und den ‘Jungs’, Ludwig, Simon, Michi und Matthias**, die mir die Zeit meiner Promotion sehr

'versüsst' haben während diverser Kaffeepausen, bei mittäglichen Kochgelagen und ganz besonders bei abendlichem Prosecco-Genuss. Die Zeit mit ihnen wird mir unvergesslich bleiben.

- meinem guten Freund **Ralf** für die exzellente "psychologische" Betreuung dieser Doktorarbeit und seine unerschöpfliche Geduld, die er mit mir hatte.
- meiner Freundin **Sabine** für die schönen und spassigen Zeiten, die wir in München zusammen hatten, in denen sie mich aus den 'wissenschaftlichen Gefilden' immer wieder auf den Boden Realität geholt hat.
- meinem Tanzpartner **Franz**, der mir gezeigt hat durchs Leben und durch die Promotion zu "tanzen". Das Training mit ihm war der perfekte Ausgleich zu meiner Doktorarbeit und ich werde es in Zukunft sehr vermissen.
- und nicht zuletzt meinen **Eltern**, mit deren ständiger Unterstützung ich es schaffen konnte, diese Doktorarbeit zu vollenden.

Ehrenwörtliche Versicherung und Erklärung

der Doktorandin

Michaela Hirschmann

Mit der Abgabe dieser Doktorarbeit versichere ich, dass ich die Arbeit selbständig verfasst und keine anderen als die angegebenen Quellen und Hilfsmittel benutzt habe.

Ort, Datum

Unterschrift